[FeFe]-Hydrogenase synthetic mimics based on *peri*-substituted dichalcogenides

by

Carlotta Figliola

A thesis submitted to
The University of Birmingham
For the degree of
DOCTOR OF PHILOSOPHY

School of Chemistry
College of Engineering and Physical Sciences
The University of Birmingham
July 2014

Acknowledgements

Here it is, the thesis! The big and final report concluding a long period full of victories and defeats, disappointments and gratifications, moments of sadness and immense joy. But mostly, a long period full of people, who made this adventure possible.

First of all, I would like to thank my supervisor Dr Richard Grainger for giving me the opportunity to work as PhD student in his group and, more important, for his constant and invaluable support during these four years.

I would like to thank Dr Sarah Horswell for introducing me to electrochemistry and helping me in the analysis of all the numbers, graphs and peaks, which fill these pages. A big thanks to the amazing analytical team: Dr Jonathan Snelling, Lianne Hill and Dr Neil Spencer. Thank you all for the time you have dedicated in answering my questions! I am very thankful to Dr Louise Male for her work in obtaining and refining my crystal structures. I also would like to thank Dr Chi Tsang for his fundamental help with gas chromatography.

Many thanks to all the past and present members of the Grainger group: Tom, Tyrone, Claire, Kevin, Marie, Matt, Mike, Pete, Sanaz, Rich and Fatima. Thank you all for sharing your chemistry knowledge, your support and, of course, all the funny moments in the lab. Among these precious colleagues, I am especially grateful to Marie for our long chats and detailed gossips, and to Kevin, always ready for brainstorming sessions on orbitals.

Thanks to the Tucker group, especially Gemma and Rosie, for lending me pipettes and cuvettes for my UV/vis experiments and, of course, for the wonderful after group meetings cakes and sweets! Thanks to the Davies and Fossey group for letting me steal many chemicals!

I could not have accomplished this work without the support of my friends, my family: Michou, Chris, Sallustrau, Andrea, Jack, Yanouk, Tom, Antoine and Alex. All our breaks in

the “corner” and Friday nights in the Staff House were not only a continuous consumption of nicotine and beer, but also a precious exchange of ideas, dreams, crazy life plans and fun. All mixed with endless discussions on how to solve daily chemistry-related problems. Knowing that you were there every day, even during weekends, helped me to face and, actually, enjoy these four years. And for this I will always be grateful. A special thanks to two (and a half) friends, Antoine and Myrto (and Kimi). Thanks for being always there to support me, for believing in me and pushing me to give the best in every situation, for proofreading this work and, in few words, for making me the luckiest person on Earth. Finally, I would like to thank the kindest person I have ever known, Manu. For your critical mind and wise questions, your careful and patient proofreading, your help and your support these last two years. For everything, thank you.

After all these names, finally thanks to my parents and my sister for always being on my side.

Abstract

[FeFe]-Hydrogenase plays an important role in the microbial energy metabolism, catalysing the reduction of protons into molecular hydrogen. The aim of this project is to synthesise and analyse *peri*-substituted dichalcogenide-based hexacarbonyl [FeFe]-complexes as model systems of the enzyme's active site and as catalysts for proton reduction/hydrogen production.

Chapter 1 describes the economic and environmental background which has promoted in-depth crystallographic, spectroscopy and mechanistic studies on the three major classes of hydrogenases: [Fe]-hydrogenase, [NiFe]-hydrogenase and [FeFe]-hydrogenase. Furthermore, it reviews the main strategies, which have been developed in order to synthesise [FeFe]-hydrogenase analogues, closely resembling both structure and function of the enzyme.

Chapter 2 reports the synthesis and analysis of [FeFe]-complexes based on the naphtho[1,8-*cd*][1,2]dithiole, naphtho[1,8-*cd*][1,2]diselenole and naphtho[1,8-*cd*][1,2]thiaselenole backbones, which incorporate substituents in the *ortho* position of the naphthalene ring (OMe, *t*Bu). Additionally, dichalcogenide-based [FeFe]-complexes, containing the conjugated aromatic phenanthrene and non-fused aromatic fluorene backbones are also discussed.

Chapter 3 describes the functionalization of the simple naphthalene-1,8-dithiole and diselenole with aromatic and alkyl amino/imino group on position 2 of the naphthalene ring. Spectroscopic and electrochemical studies of the corresponding [FeFe]-complexes show the expected protonation of the nitrogen, upon acid addition, and the remarkable effect on proton reduction catalysis.

In Chapter 4 the synthesis of a molecular dyad containing a zinc tetraphenylporphyrin covalently linked to a naphthalene-1,8-dithiolate-based [FeFe]-complex, via amino group, is discussed. Initial results on photoinduced hydrogen production catalysis are also described.

Abbreviations

A	Ampere
a.u.	arbitrary unit
Abs	absorbance
adt	azapropanedithiolate
Ar^F	pentafluorophenyl
BC	1,2-bisdiphenylphosphine-1,2-o-carborane
bdt	benzenedithiolate
BMC	Ballester, Molinet and Castaner
Boc	*tert*-butoxycarbonyl
bpy	bipyridine
Bz	benzoyl
Cp	cyclopentadienyl
CV	cyclic voltammetry
CyD	cyclodextrin
Cys	cysteine
Δ	heat under reflux
d (NMR)	doublet
δ	chemical shift
DCC	*N,N´*-dicyclohexylcarbodiimide
decomp.	decomposition
DFT	Density Functional Theory
DMF	dimethylformamide

DMI	1,3-dimethyl-2-imidazolidinone
DMSO	dimethyl sulfoxide
dppf	1,1′-bis(diphenylphosphino)ferrocene
dppr	1,1′-bis(diphenylphosphino)ruthenocene
dppv	1,2-bis(diphenylphosphino)ethylene
ε	extinction coefficient
E	potential
E°	standard potential
$E_{1/2}$	half-wave potential
EC	electrochemical
edt	ethanedithiolate
EI	electron impact
E_{pa}	anodic peak potential
E_{pc}	cathodic peak potential
EPR	electron paramagnetic resonance
ESI	electronspray ionization
EY	Eosin Y
Fc	ferrocene
Fmoc	fluorenylmethyloxycarbonyl
FT-IR	Fourier Transform Infrared
g	gram(s)
GC	gas chromatography
H_4MPT	methenyltetrahydromethanopterin
HBTU	*N*,*N*,*N*′,*N*′-tetramethyl-O-(benzotriazol)uranium hexafluorophosphate

heptd	heptet
Hmd	H_2-forming methylenetetrahydromethanopterin dehydrogenase
HOBt	1-hydroxybenzotriazole
HRMS	high resolution mass spectrometry
HYSCORE	hyperfine sublevel correlation
I_{pa}	anodic peak current
I_{pc}	cathodic peak current
IR	infrared
j	current density
J	coupling constant
K	Kelvin
λ	wavelength
Leu	leucine
LMCT	ligand metal charge transfer
m (NMR)	multiplet
m/z	mass/charge
MALDI	matrix-assisted laser desorption/ionization
*m*CPBA	meta-chloroperbenzoic acid
MLCT	metal-to-ligand charge transfer
mp	melting point
NBS	*N*-bromosuccinimide
NCS	*N*-chlorosuccinimide
NHE	normal hydrogen electrode
NMR	Nuclear Magnetic Resonance

[O]	oxidation
odt	oxopropanedithiolate
OECD	Organization for Economic Cooperation and Development
pdt	propanedithiolate
PEG	polyethylene glycol
PES	gas-phase photoelectron spectroscopy
PFV	protein film voltammetry
PMP	*para*-methoxyaniline
Pv	pivaloyl
Py	pyridine
Pyr	pyrrolyl
PPA	poly(acrylic acid)
ppm	part(s) per million
ppr	2-phenylpyridinato
*i*Pr	isopropyl
PS	photosensitizer
PVT	programmed temperature vaporizing
q	quartet
QD	quantum dot
RB	Rose Bengal
R_f	retention factor
s (NMR)	singlet
SEC	spectroelectrochemical
t	*tertiary*

t	triplet
t.l.c.	thin layer chromatography
TCD	thermal conductivity detector
tdt	thiapropanedithiolate
TFA	trifluoroacetic acid
THF	tetrahydrofuran
TMEDA	tetramethylethylenediamine
TOF	turnover frequency
TON	turnover number
TPP	tetraphenylporphyrin
TRIR	time-resolved infrared
UV/vis	ultraviolet/visible
V	volt
vic	*vicinal*
v	frequency
W	Watt

Table of content

Chapter 1: Bio-inspired systems towards hydrogen production

1.1 Hydrogen: sustainable energy carrier

1.1.1 Primary energy sources development

It has been estimated that worldwide economic growth will affect global energy consumption and demand with an increase of 56% and 85% respectively from 2010 to 2040. The countries outside the Organization for Economic Cooperation and Development (non-OECD), especially China and India, whose economies are among the fastest growing in the last few years, are the main actors in this urgent energy scenario. In contrast, the OECD nations, United States and Europe, already advanced in terms of economic development, show an uncertain economic growth and a slow recovery from the great recession in 2009.[1a)]

Total primary energy production is mainly based on fossil fuels, especially coal and oil, which continue to represent the first resources for industry and transportation.[1b)] However, the rising costs of oil have resulted in a significant increase in the demand and production of natural gases.[1a)]

In 2009 the Group of Eight (G8) highlighted the climate change emergency due to the impact of carbon dioxide emissions on the environment, and achieved an agreement with all the countries to reduce global emissions of 50% by the end of 2050. Nonetheless, it has been estimated that global carbon dioxide emissions will increase 3% every year from 2010 to 2040.[1a)]

As a consequence the development of renewable energy sources, such as hydropower, solar energy, wind and bio-fuels, has become necessary. In fact, recently their contribution to the global energy supply has expanded, covering 18% of total primary energy, thanks to new policies and initiatives in both OECD and non-OECD countries. Reasons for this rising attention are: security and variety in the energy supplies, a clear cut of carbon dioxide

emissions, sustainable economic development ("green growth") and an affordable access to energy services.[1c)]

Beside renewable energy sources, nuclear power represents an alternative to fossil fuels, but current issues of plant safety, the increase of disposable nuclear waste material and further the disaster in Fukushima Daiichi in 2011 have slowed down its future development.[1a)] Within this economic context, inclined towards sustainable and environmentally friendly energy sources, hydrogen plays an important role as a future energy carrier.

1.1.2 Hydrogen: advantages and disadvantages

Hydrogen, from the Greek υδωρ (= water) and γεννειν (= genesis), is the simplest element of the Periodic Table and the most abundant on Earth, in the form of water, hydrocarbons and biomass. Hydrogen is a colourless, tasteless and nontoxic gas, present in the air in a concentration of about 100 ppm.[2]

Interest in hydrogen began in 1785, when Lavoisier first discovered that splitting water gave oxygen and an "inflammable air", consequently called hydrogen.[3]At the beginning of the 20th century, the first commercial installation for water electrolysis was built in Canada for the production and the use of hydrogen as an energy carrier beside its usual applications in the synthesis of ammonia and methanol. During the Second World War, in Germany and England, hydrogen was used as fuel for delivery vans and trucks and, between 1950 and 1970, it was employed in the American aviation and space sector.[4] In 1954 the first hydrogen bomb was detonated on the Bikini Atoll in the Pacific Ocean, proving hydrogen to be a powerful airborne weapon.[3] It was during the decade 1970-1980 that hydrogen started to be conceived as a promising alternative to liquid fuels in all types of transport. The idea of a "hydrogen economy" came from John Bockris, electrochemist and consultant in General Motors, who

wrote the first book about hydrogen as a potential energy carrier (*Energy: The Solar Hydrogen Alternative*, 1975) thus leading to the foundation of The International Association for Hydrogen Energy.[5]

The advantages of using hydrogen as an energy carrier are: [4]

- ✓ Significant reduction of carbon dioxide emissions: hydrogen combines with oxygen producing energy in the form of electricity and water as by-product.
- ✓ Variety of production systems: hydrogen can be obtained by many primary energy sources (section 1.1.3).
- ✓ Sustainability: renewable energies sources, such as hydro, wind and solar, can be used to power the electrolysis of water, providing a sustainable system, independent from fossil fuel.

In contrast, the disadvantages related to a hydrogen-based economy are: [4]

- ✓ High cost and low efficiency: hydrogen is an energy carrier, which needs primary energy for its production, storage, distribution and use. The amount of energy generated by hydrogen is much lower than that currently needed to produce it and, additionally, expensive infrastructures are required for hydrogen production.
- ✓ Storage and transport: hydrogen is difficult to store on board and it requires suitable infrastructures for large scale distribution, which are currently missing.
- ✓ Large amounts of water required: water is needed to produce hydrogen from renewable energy sources and consequently it has become a resource at risk.
- ✓ Safety: hydrogen is the lightest among all the gases and it quickly disperses and leaks easily through cracks and holes. However, due to its volatility, it does not accumulate in the air, and causes explosions and, additionally, hydrogen is much less dangerous than, for example, gasoline, whose gas is 20 times more reactive than hydrogen. The

temperature for hydrogen auto-ignition is about 580 °C at 1 atmosphere, while for gasoline it is 260 °C.[6]

Based on these elements, the idea of a hydrogen-based economy deals with the current debate over whether hydrogen is actually needed as energy carrier or, instead, new investments should be directed towards alternative primary energies, such as renewable fuels and electricity.

1.1.3 Hydrogen production: non-renewable and renewable

As mentioned in the previous section, one of the main advantages of using hydrogen as energy carrier is the variety of primary resources employed for its production and consequently the significant number of technologies developed. The first necessary distinction is in non-renewable hydrogen, which is produced from fossil fuels through a series of thermochemical processes (**Figure 1.1**, left), and renewable hydrogen, generated from renewable sources, such as biomass, wind, hydro, geothermal and solar energy (**Figure 1.1**, right).[4]

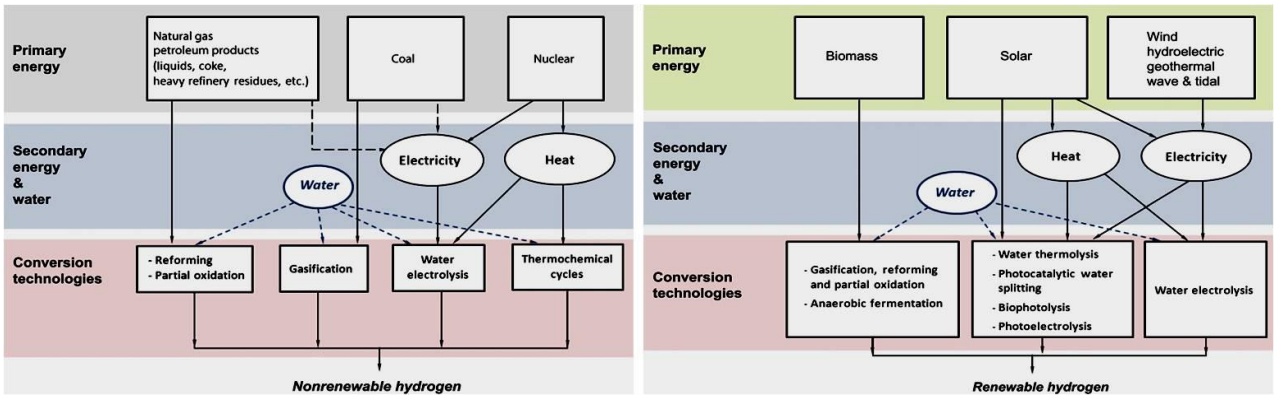

Figure 1.1 Methods converting non-renewable and renewable primary energies into hydrogen. This figure was used with permission from reference 4, copyright 2013 Elsevier Limited.

Non-renewable hydrogen currently covers 96% of total hydrogen production because of the high prices of renewable hydrogen and the requisite expensive infrastructures.[4] Even if initial installations costs are significant, the cheapest hydrogen is produced from coal, $1.05-1.83/kg versus $2.48-3.17/kg for hydrogen produced by natural gases (2010 prices).[7]

Steam reforming, partial oxidation and autothermal reforming are the main processes to produce hydrogen from fossil fuels (equation 1, 2, and 3 respectively).[8] They require high temperatures and catalysts (nickel, platinum and rhodium) to activate the substrate.

$$C_mH_n + mH_2O = mCO + (m + ½n)H_2 \quad \text{(eq. 1)}$$

$$C_mH_n + ½mO_2 = mCO + ½nH_2 \quad \text{(eq. 2)}$$

$$C_mH_n + ½mH_2O + ½mO_2 = mCO + (½m + ½n)H_2 \quad \text{(eq. 3)}$$

Among all the hydrocarbons available and tested to produce hydrogen by steam reforming, methanol and ethanol are the best candidates in terms of temperature, impact on the environment, availability, miscibility with water and because they do not suffer from sulfur contamination.[9]

Renewable hydrogen is mainly produced from water splitting through either electrolysis (from wind, hydro, geothermal, wave and tidal energies), thermolysis (from solar energy) or photolysis (from solar energy).[8] Water photolysis additionally requires catalysts (lead, platinum, iridium and gold) to decrease the activation energy of the reaction. In order to facilitate the process, water is combined with a sacrificial reducing agent and methanol, but the oxygen from water reacts with methanol releasing carbon dioxide, thus compromising the sustainability of the process.[4]

Biomass is a biological material, which derives from a significant variety of sources: animal, municipal and agriculture waste, corn, aquatic plants, grass etc. In order to produce hydrogen

from biomass the most common methods are biomass gasification and biological hydrogen production.[8,10]

Bio-hydrogen production derives from direct water photolysis by green algae or cyanobacteria and from fermentative processes of biomass, dark fermentation by anaerobic bacteria and photo-fermentation by purple non-sulfur bacteria.[8] Few microorganisms, suitable for bio-hydrogen production, are currently known and in many cases they have been modified to improve their performance.[11,12]

1.2 Hydrogenases

Hydrogen is an important energy source for many microorganisms, especially prokaryotes belonging to the Bacteria and Archaea domains. Similar to a "hydrogen-based micro-economy", hydrogen is released as a waste product and it is quickly absorbed and oxidized either by oxygen (aerobic organisms) or by fermentation of bioorganic molecules (anaerobic organism), yielding a large amount of chemical energy.[13]

The enzymes involved in the hydrogen metabolism are called hydrogenases and they catalyse reversible proton reduction (equation 4).

$$2\ H^+ + 2e^- \rightleftharpoons H_2 \qquad \text{(eq. 4)}$$

In the presence of an electron acceptor (water), the enzyme catalyses hydrogen uptake; on the other hand, if an electron donor is available, the reaction is driven towards hydrogen production.

Three classes of hydrogenases are known, [Fe]-hydrogenase, [NiFe]-hydrogenase and [FeFe]-hydrogenase, which are distinguished based on the nature of the metal involved in the catalytic cycle, the size, the structure and the types of electron donor and acceptor.[13]

1.2.1 [Fe]-Hydrogenase

[Fe]-Hydrogenase, also known as [FeS]-cluster free hydrogenase or H_2-forming methylenetetrahydromethanopterin dehydrogenase (Hmd), catalyses the reversible hydrogenation of methenyltetrahydromethanopterin (methenyl-H_4MPT$^+$) to methylenetetrahydromethanopterin (methylene-H_4MPT) (**Scheme 1.1**). This reaction is the key step in the synthesis of methane from carbon dioxide and hydrogen in methanogenic microorganisms. Unlike the other two classes of hydrogenases, [Fe]-hydrogenase is not involved in the reversible reduction of protons into hydrogen and the iron of the enzyme's cofactor does not have any redox role.[13]

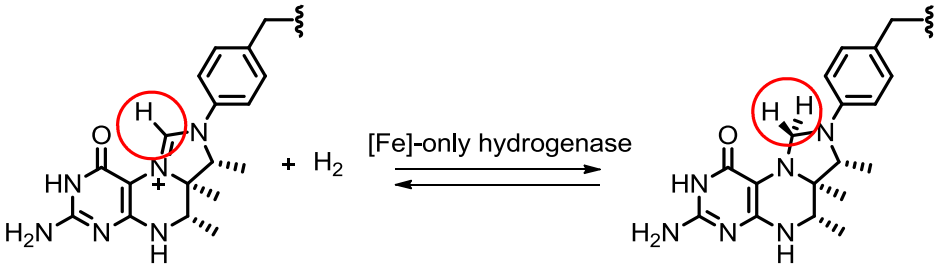

Scheme 1.1 Reversible hydrogenation of methenyl-H_4MPT$^+$ to methylene-H_4MPT catalysed by [Fe]-hydrogenase.[17]

[Fe]-Hydrogenase is a homodimeric protein with a central C-terminal globular subunit, linked linearly to two external N-terminal subunits.[14] The [Fe]-Hydrogenase cofactor is attached to the enzyme by a guanosine monophosphate and the iron is coordinated in a distorted octahedral geometry by the nitrogen and the acyl group of a guanylylpyridinol moiety, by two carbonyl groups and by a cysteinyl residue, thus forming the active site (**Figure 1.2**). The "open" coordination site, *trans* to the acyl group, has been identified as the hydrogen binding site. Furthermore, it has been proposed that the hydroxy group on the 2-pyridinone moiety acts as a base and hence favours the hydrogen binding to the iron.[15]

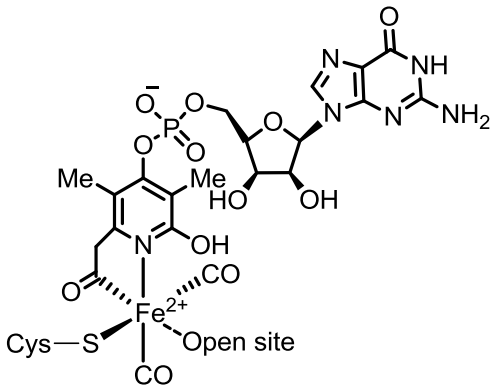

Figure 1.2 Structure of the [Fe]-hydrogenase cofactor.[14]

It has been suggested that the first step of the catalytic reaction involves the binding of methenyl-H_4MPT^+ to the active site inducing a transition from the closed to the open conformation of the enzyme. The iron, which acts as a Lewis acid, coordinates a molecule of hydrogen and then cleaves it with the participation of the deprotonated hydroxy group. By analogy with the mechanism of the [NiFe]-hydrogenase (Section 1.2.2), a cysteinyl thiolate has been also proposed as a base in the hydrogen cleavage. Finally the methenyl-H_4MPT^+ is reduced by the hydride bound to the iron and the proton is released (in the surrounding water).[16]

Prior the structure of the cofactor of the [Fe]-hydrogenase was clarified, [15h)] various approaches targeting the enzyme's active site have been developed based on spectroscopic and crystallographic analyses.[16–24] However, all the reported model systems react neither with hydrogen nor through hydride transfer. Some of the latest and significant [Fe]-hydrogenase synthetic mimics are discussed below.

Complex **1a** was the first synthetic mimic of the Hmd cofactor with iron in a distorted five-coordinated square planar geometry. The reactivity of **1a** towards strong and bulky electron-donating groups (*e.g.* PPh_3 and 2-mercapto-6-methylpyridine) and the absence of reaction with weak electron-donating nucleophiles (*e.g.* H_2O, CH_3CN, Py, NEt_3 etc.) suggest a strong

trans effect on the iron from the acyl group and no interference of the methoxy group with the vacant site (**Figure 1.3**).[20d] Compound **1b** is part of a new series of five-coordinated [Fe]-complexes, which have two dominant forms (monomeric and dimeric) both in solution and in solid state depending on the substituents of the aryl thiolate ligand.[20g] It has been observed that aryl thiolate ligands generally favour the monomeric form in solution, which is less stable than the dimeric form in the solid state, and that substitutions in *ortho* position on the aryl thiolate allows stable monomeric complexes in the solid state. Pickett and co-workers reported an easy synthetic approach to obtain mononuclear [Fe]-complexes (**2** and **3a-c**); the amino group on the pyridine ring in complex **3c** mimics the hydroxy group in the enzyme's cofactor and allowed investigation into the role of this functional group in the reaction mechanism.[21]

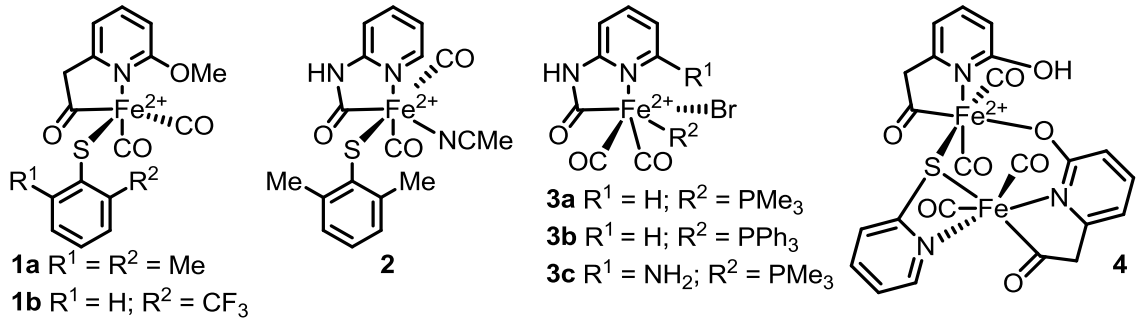

Figure 1.3 [Fe]-only hydrogenase synthetic models.[20d)g),21,24b)]

Song described the synthesis of a dinuclear [Fe]-hydrogenase analogue **4**, which derives from the dimerization of the deprotected hydroxy group in acidic conditions and which contains the pyridinol moiety of the natural system. X-ray crystallographic analysis showed that the iron centre has the same coordinating ligands as the enzyme's cofactor and the deprotonated hydroxy group is directly bound to the iron forming a hydrogen bond with the second hydroxy groups, similar to the interaction in the cofactor when hydrogen is activated.[24b)]

1.2.2 [NiFe]-Hydrogenase

[NiFe]-Hydrogenase is the most diversified and certainly the most studied protein among hydrogenases. It is a periplasmic protein, mainly expressed in bacteria and it catalyses hydrogen uptake (equation 4).[13]

The first crystal structure of a [NiFe]-hydrogenase, obtained from *Desulfovibrio gigas*, shows a globular heterodimeric protein. The active site of this enzyme is buried in the protein's core and it exchanges gases with the periplasm through a hydrophobic channel, which links the active site with the surface of the enzyme.[13] The [NiFe]-cluster is accommodated in the large subunit and is anchored to the enzyme by four cysteines forming a square planar coordination pattern around the nickel; two of the four cysteines are bridging ligands between the nickel and the iron centre, which is bound to an additional carbonyl and two cyanides (**Figure 1.4**).

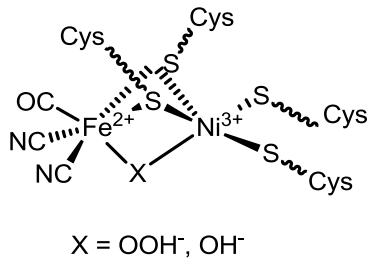

Figure 1.4 Proposed [NiFe]-hydrogenase active site. X = OOH^- for the inactive form Ni-A, while X = OH^- is for Ni-B.

The small subunit contains three [FeS]-cubane clusters: one [3Fe4S]-cluster in between one distal and one proximal [4Fe4S]-cluster. These three clusters form a straight channel, which delivers electrons to the catalytic [NiFe]-cluster for hydrogen activation. The proximal [4Fe4S]-cubane core plays a fundamental role for the enzyme's activity.[25]

Following the first crystal structure of the active site of the [NiFe]-hydrogenase from *Desulfovibrio gigas*, many other crystallographic studies have shown the variety of motifs that the active site assumes from a species of bacteria to another.[26] One example is the [NiFeSe]-hydrogenase isolated from *Desulfomicrobium baculatum* and from

Desulfomicrobium vulgaris.[27] When the cell is rich in selenium, the [NiFeSe]-hydrogenase, which contains a selenocysteine as ligand on the nickel and three [4Fe4S]-cubane clusters in the small subunit, is expressed in large quantity.

Advanced spectroscopic and crystallographic studies on [NiFe]-hydrogenase allowed the identification of the redox states of the nickel in the active site and elucidated the mechanism for hydrogen uptake.[26a)b)c),28] In the oxidised and inactive forms of the [NiFe]-cluster, Ni-A and Ni-B respectively, the nickel centre is bridged to the iron by either a peroxide or a hydroxy group (**Figure 1.4**). These two forms are converted by one-electron reduction (Ni(III)→Ni(II)) into the transition state of the active site, Ni-SI, which binds hydrogen to give Ni-R (**Scheme 1.2**). In this form the [NiFe]-cluster, upon one-electron oxidation, produces Ni-C bearing a bridging hydride between the nickel and the iron. It has been proposed that hydrogen cleavage by Ni-R occurs with the participation of one of the cysteinyl thiolates on the nickel.[28] Finally, upon a second one-electron oxidation, Ni-C releases the hydride and regenerates N-SI. It has been suggested that the binding site for the hydrogen in the Ni-SI is preferentially the nickel centre because of its position at the end of the hydrogen channel and because it binds CO, which inhibits the enzyme.[16] However, the iron centre might be the binding site as well, due the low spin d^6 transition metals' affinity for hydrogen (**Scheme 1.2**).[28] Since the iron has both filled d_π orbitals and empty d_σ orbitals, the H–H σ bond can fill the metal d_σ orbitals, while the d_π orbitals "back-donate" electrons into the empty H–H σ^* antibonding orbital. Electron-withdrawing groups or strong π-bonding acceptor (*i.e.* CO and CN^-) increase the acid character of the iron, reducing the iron-hydrogen back-donation, and favour the hydrogen binding to the iron.[29,30]

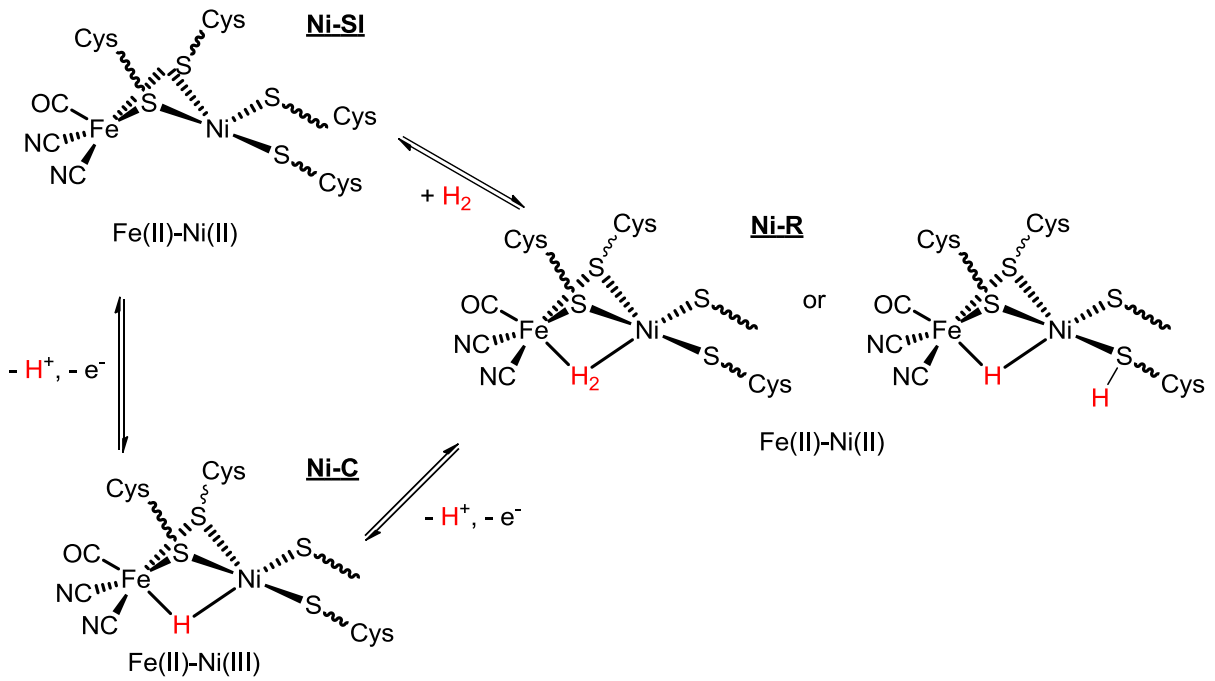

Scheme 1.2 Proposed mechanism for reversible hydrogen uptake by [NiFe]-hydrogenase.[16]

[NiFe]-Hydrogenase synthetic mimics, able to reproduce the structure of the enzyme as well as its function, still represent a challenge because of the complexity of the cluster and, additionally, the tendency of the nickel to form polynuclear clusters with bridging thiolates. Therefore, various strategies have been developed to overcome this synthetic issue.[16,17] [NiFe]-Hydrogenase analogues have been developed by coordinating nickel to electron-donating ligands, either S_2N_2 or S_2P_2, followed by the insertion of the iron, bound to an electron-withdrawing group.[16,17,31–34] Various thiolate ligands have also been employed to synthesise tetradentate nickel complexes, which facilitate the addition of a second transition metal (Fe, Ru, Mn etc.).[35] This latter group of [NiFe]-hydrogenase synthetic mimics exhibits a greater stability compared to the previous two, due to the chelation effect of the sulfur on the nickel. In addition, hindered substituents prevent metal aggregation and stabilise the complex during the catalytic cycle. Finally, polymetallic complexes with three or four transition metals have been employed to obtain [NiFe]-hydrogenase model systems.[36]

Some examples [NiFe]-hydrogenase analogues are shown in Figure 1.5.

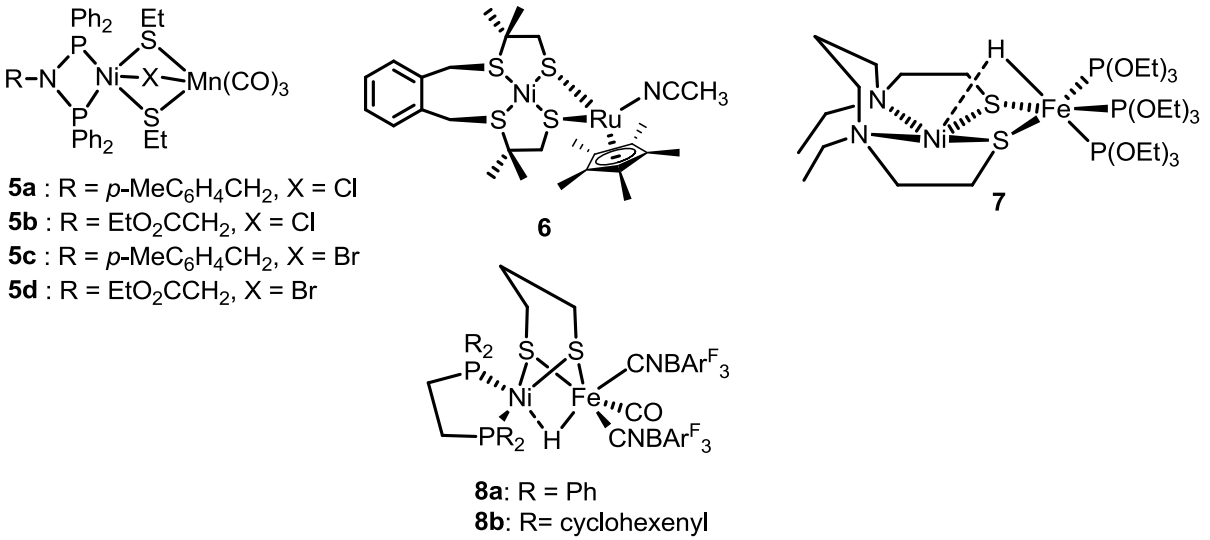

Figure 1.5 [NiFe]-Hydrogenase synthetic mimics reported by Song (**5a-d**), Artero (**6**), Ogo (**7**) and Rauchfuss (**8a-b**).[32c),33,34,35d)]

[NiMn]-complexes **5a-d** are the first examples of neutral dinuclear [NiMn]-clusters reproducing the active site of this class of hydrogenases. These compounds reflect the butterfly shaped core of the natural active site with the nickel centre in a distorted square planar geometry and they perform proton reduction catalysis in the presence of *para*-toluenesulfonic acid (*p*TsOH).[32c)] The [NiRu]-complex **6** is a stable and efficient [NiFe]-hydrogenase synthetic mimic and catalyst for proton reduction, converting more than 75% of triethylammonium chloride into hydrogen upon bulk electrolysis (**Figure 1.5**).[35d)]

Recently two examples of [NiFe]-hydrogenase synthetic mimics **7** and **8a-b**, active catalysts in both hydrogen oxidation and reduction, have been reported by Ogo and Rauchfuss respectively (**Figure 1.5**). However, both complexes perform hydrogen oxidation with very low efficiency using strong bases, while proton reduction requires strong acids and more negative potentials than the natural system.[33,34] Furthermore, the catalytic activity of complexes **8a-b** is based on the iron centre opposite to the actual active site's mechanism, which is based on the nickel. Bi-functional complexes **8a-b** contain a bridging hydride

between the nickel and the iron reproducing closely the NI-C state of the enzyme's active site. They derive from the corresponding non-bridging hydride complexes by hydrogen binding and consequent cleavage, similar to the transition from Ni-R to Ni-C (**Scheme 1.2**).[34]

1.3 [FeFe]-Hydrogenase

1.3.1 Structure and mechanism

[FeFe]-Hydrogenase catalyses the reversible reduction of protons into hydrogen (equation 4, Section 1.2) at high turnover rates (28,000 s^{-1} for hydrogen consumption and 6,000-9,000 s^{-1} for hydrogen production).[26e),37] It is either a periplasmic dimeric or a cytoplasmic monomeric enzyme, expressed in anaerobic prokaryotes, mainly clostridia and sulfate reducers, green algae, anaerobic fungi, trichomonads, ciliates and in lower eukaryotes, Although it is usually involved in hydrogen production, one sub-species of [FeFe]-hydrogenase, isolated from *Desulfovobrio vulgaris*, has been found to be a hydrogen uptake hydrogenase, which is up-regulated in order to protect the cell from oxidative stress.[13,38]

The first crystal structures of [FeFe]-hydrogenase were obtained independently from *Clostridium pasteurianum* and *Desulfovibrio desulfuricans* in 1998 and 1999 respectively.[39] The enzyme is composed by four non-overlapping domains; the largest domain contains the active site, which is positioned in the protein core and communicates with the enzyme's surface by a hydrophobic channel, [17,39a)] whereas the three smaller units consist of four auxiliary [FeS]-clusters. As mentioned for the [NiFe]-hydrogenase, the four auxiliary [FeS]-clusters include three [4Fe4S]-cubane cores and one [2Fe2S]-cluster and they form an electron channel to the active site. The active site of the enzyme, called the H-cluster, is composed of two sub-units, one [2Fe]-cluster and one [4Fe4S]-cubane core, reciprocally

linked by a cysteine. The [4Fe4S]-cubane core is attached to the protein by three cysteines and transfers electrons to the [2Fe]-subsite for catalytic proton reduction (**Figure 1.6**).

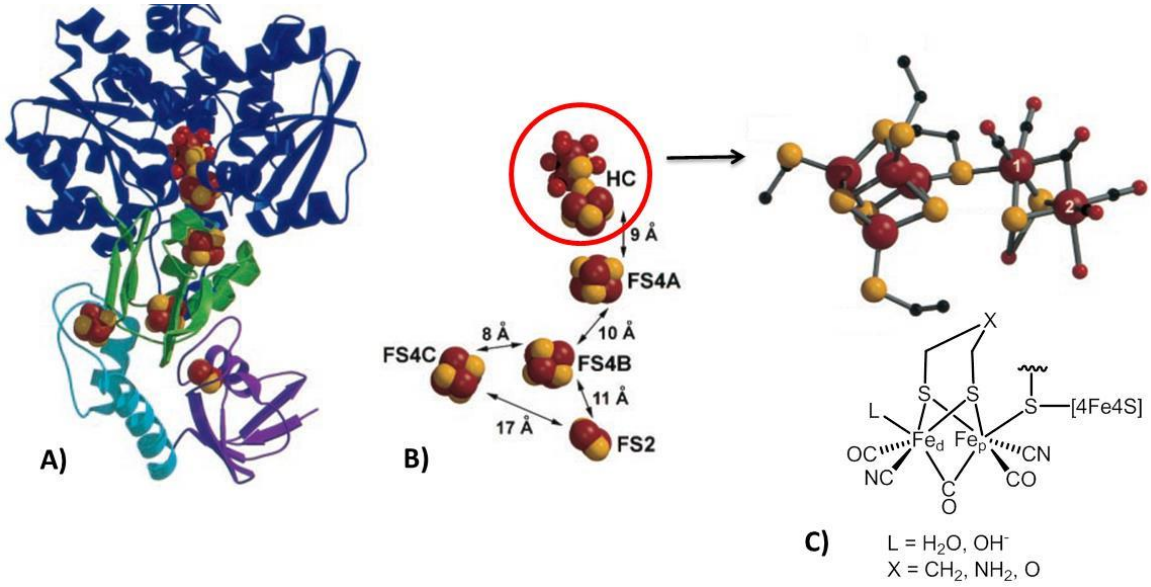

Figure 1.6 A) Crystal structure of [FeFe]-hydrogenase isolated from *Clostridium pasteurianum*. B) The four electrons transfer [FeS]-clusters (FS4A, FS4B, FS4C and FS2) and the H-cluster (HC). C) (Top) the active site of the [FeFe]-hydrogenase, (bottom) schematic structure of the [2Fe]-subunit; L is identified as either water or a hydroxy group, while X is either carbon, nitrogen or oxygen. This figure was adapted with permission from reference 39a), copyright 1998 The American Association for the Advancement of Science.

In the [2Fe]-cluster the two irons (distal, Fe_d, and proximal, Fe_p, to the [4F4S]-cubane core) are bound to biologically unusual cyanides and carbonyls (more specifically two cyanides and two carbonyls) and the Fe_d is also coordinated by either a molecule of water or a hydroxy group (**Figure 1.6**). [FeFe]-Hydrogenase, isolated from *Desulfovibrio desulfuricans*, contains an extra carbonyl group in place of the hydroxy/water ligand on Fe_d and it was confirmed as the inhibited form of the enzyme in *Clostridium pasteurianum*.[40] The two irons are also bridged by a carbonyl group and a propanedithiolate ligand, whose bridgehead atom (**Figure 1.6**) has been subject to numerous discussions. It was first thought to be carbon ($X = CH_2$),[39b)] but further crystallographic analysis and Density Functional Theory (DFT) optimizations, supported by advanced Electron Paramagnetic Resonance (EPR) analysis, proposed X to be a

secondary amine (X = NH).[41] Alternatively, the possibility of X being oxygen (X = O) was considered.[42] In a recent experiment a series of synthetic mimics with X = CH_2, NH an O, were employed during the expression of the enzyme. Out of the three mimics, only the azapropanedithiolate-bridged (X = NH) analogue displayed catalytic activity similar to the enzyme, thus strongly suggesting that the bridgehead atom in the natural active site is a secondary amine (Section 1.3.2.5).[16,43]

The [2Fe]-subsite requires activation before performing the catalytic cycle (**Scheme 1.3**).[44]

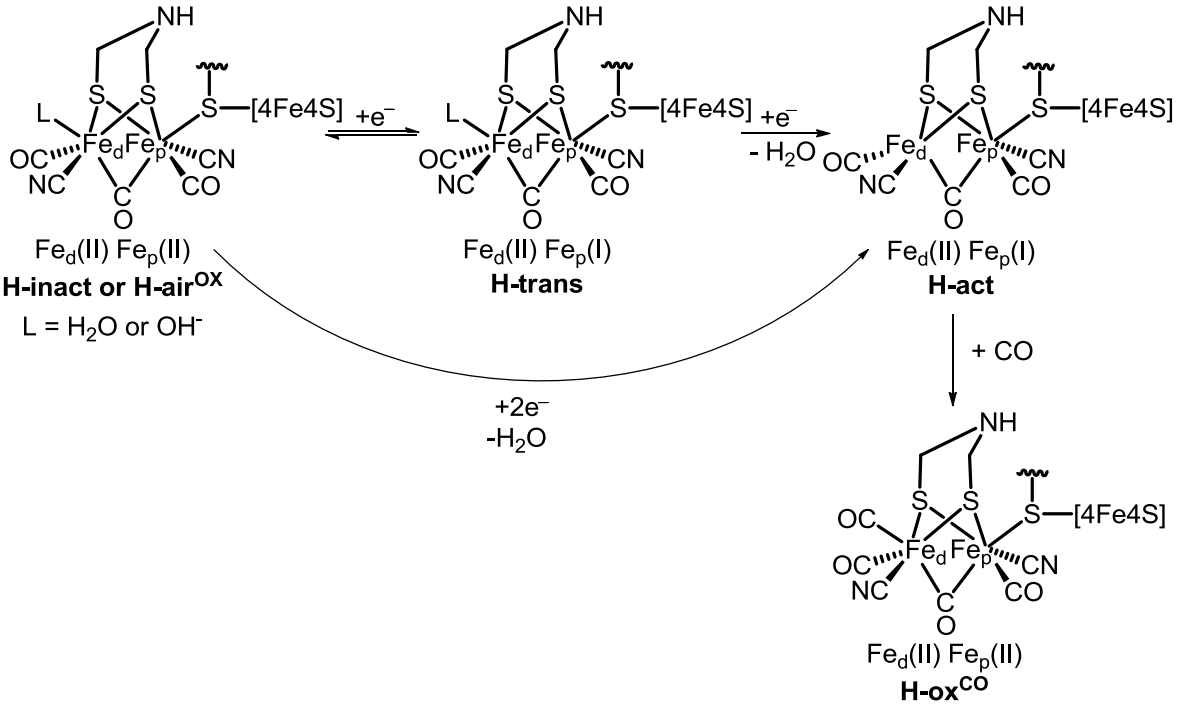

Scheme 1.3 Activation of the [FeFe]-hydrogenase H-cluster.

The inactive form, H-inact or H-air^{OX}, in which both Fe_d and Fe_p are Fe(II), is subject either to a reversible one-electron reduction to produce the transient form, H-trans, or to an irreversible two-electron reduction, recognized as activation step, to generate the active form of the [2Fe]-subsite, H-act. In the two-step process, the first electron reduces the Fe_p to Fe(I) and the second causes the loss of the ligand L, leaving a vacant site on the coordination sphere of Fe_d, which is five-coordinated in a square pyramidal geometry, the so-called "rotated state". In the

inhibited state, H-ox^{CO}, the vacant site on Fe_d is occupied by an extra carbonyl.[44,40] Recently an additional state of the H-cluster, H-sred ("super-reduced" state) has been observed experimentally and characterized; it contains a reduced [4Fe4S]-cubane core and it has been proposed as an intermediate in the catalytic cycle for proton reduction (**Scheme 1.4**).[16,45]

DFT calculations on [2Fe]-subsite synthetic models have been used to understand the mechanism of hydrogen production. The proposed mechanism takes into account the nature of the X atom on the dithiolate ligand, now revealed as NH, and the recently discovered third redox state, H-sred. After two consecutive one-electron reductions, H-sred is formed and the active site is able to reduce protons to hydrogen, regenerating the [2Fe]-subsite as H-act upon electron transfer from the reduced [4Fe4S]-cubane core to the Fe_d. The amino group on the dithiolate ligand is protonated during the catalytic cycle and forms a hydrogen bond with either Fe_d or the sulfur, thus decreasing the energy barrier of proton migration to Fe_d and the activation energy of the reaction. H-red is characterised by a partial shift of the bridging carbonyl which adopts a position *trans* to the vacant site. The semi-bridging conformation results in an increase of the nucleophilicity of the iron and promotes hydrogen bonding with the amino group and subsequent proton transfer (**Scheme 1.4**).[16,44] The semi-bridging carbonyl also has a steric effect and prevents protons from bridging the two irons. This mechanistic hypothesis has been supported by the first carbonyl-bridged diferrous synthetic mimic with a terminal hydride, which produces hydrogen upon reaction with acid; the corresponding hydride-bridged isomer with a terminal carbonyl does not catalyse this reaction, due to its high stability. However, synthetic mimics with a terminal hydride are unstable and could only be isolated at very low temperature (Section 1.3.2.2).[16,46,44] Therefore, it has also been proposed that catalytic hydrogen production involves a hydride-bridged intermediate.[28]

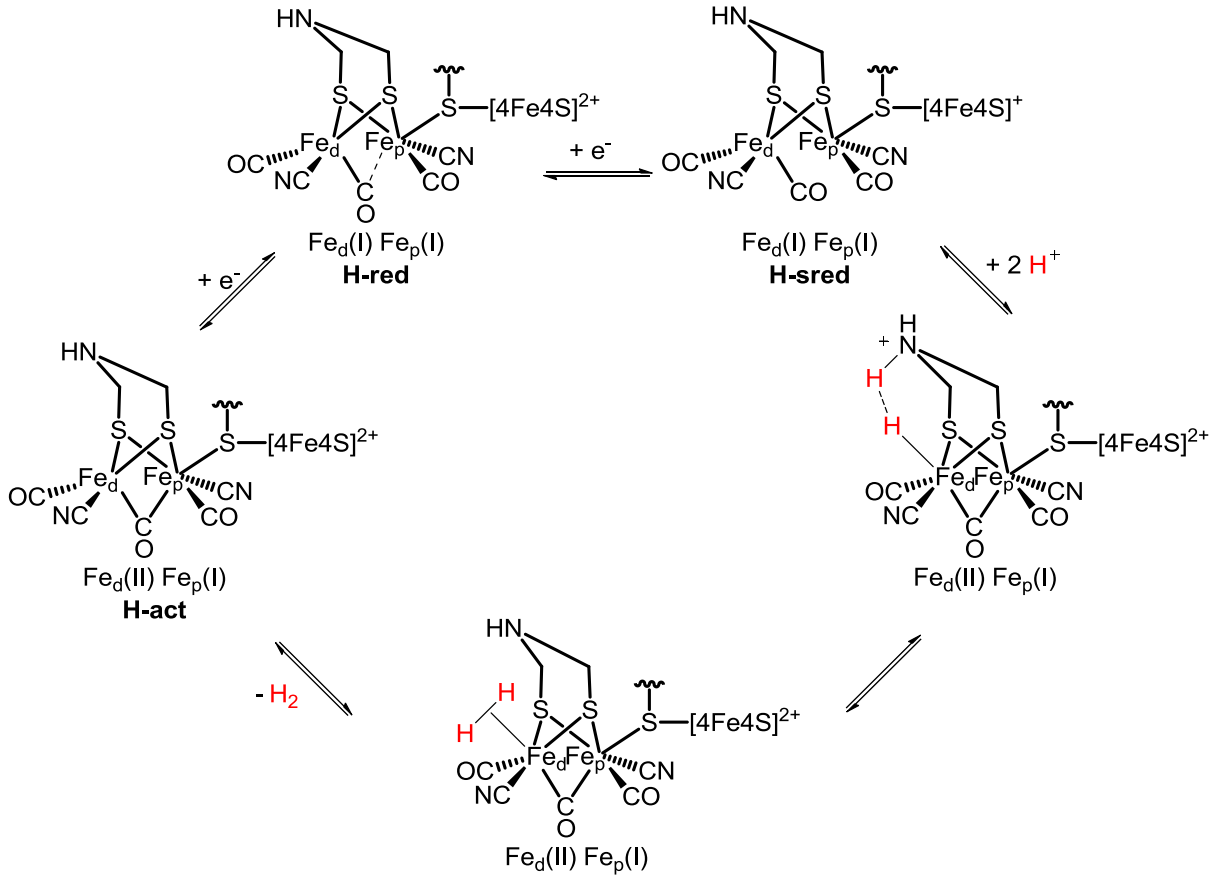

Scheme 1.4 Proposed catalytic cycle for proton reduction by the [2Fe]-subsite.[16]

1.3.2 [FeFe]-Hydrogenase synthetic mimics

Since the first crystal structure of the H-cluster was published in 1998 and 1999,[39] more than 300 [FeFe]-hydrogenase synthetic mimics have been reported and 100 in the last five years.[16,17,44,47,48]

After Reihlen first published in 1929 the synthesis of [(μ-SEt)$_2$Fe$_2$CO$_6$], [49] hexacarbonyl dithiolate-bridged [FeFe]-complexes, [(μ-SR)$_2$Fe$_2$CO$_6$], have been widely studied.[17] The structural similarity between the first crystal structure of [FeFe]-hydrogenase and the hexacarbonyl propanedithiolate-bridged (pdt) [FeFe]-complex **9**, [(μ-pdt)Fe$_2$CO$_6$], [50] became immediately inspirational for the chemistry targeting this enzyme (**Scheme 1.5**).

The first synthetic mimic **10**, $[(\mu\text{-pdt})Fe_3(CO)_4(CN)_2]^{2-}$, was reported independently by Rauchfuss, Pickett and Darensbourg in 1999. It derives from the reaction of **9** with the nucleophile Et_4NCN and it is a stable, water soluble dianion, containing one cyanide and two carbonyl groups on each iron (**Scheme 1.5**).[51]

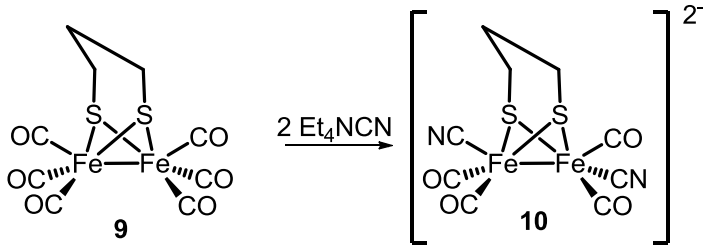

Scheme 1.5 Synthesis of the [FeFe]-hydrogenase mimic **10**.[51]

The nucleophilic substitution on the two iron centres was confirmed by infrared (IR) spectroscopy, which displayed a shift of the carbonyl bands towards lower wavenumbers compared to those of the hexacarbonyl [FeFe]-complex **9**. These values are lower than those reported for the enzyme, [40] but consistent with di-substituted cyanide [FeFe]-clusters.[51a)] X-ray crystallographic analysis of **10** displayed the butterfly-shaped [FeFe]-cluster, confirming its high similarity with the enzyme's active site.[51] Electrochemical studies showed an irreversible reduction wave at a more negative potential (–2.33 V) than the value required for the reduction of the H^+/H_2 couple (= 0.0 V) and catalytic activity towards the proton reduction was not observed.[51c)] However, in the presence of oxidising agents, such as iodine (I_2) and ammonium cerium nitrate ($(NH_4)_2Ce(NO_3)_6$), and triflic acid (TfOH), **10** is converted to a neutral polymeric form and traces of hydrogen are produced.[51b)]

Pickett and Best studied the reduction of the hexacarbonyl [FeFe]-complex **9** applying a wide range of electrochemical and spectroelectrochemical (SEC) techniques.[52] In a CO-saturated dried acetonitrile solution and at low and room temperature, **9** undergoes a reversible two-electron reduction at –1.60 V (vs Fc/Fc^+). Addition of water to the acetonitrile solution of **9**

causes, instead, the loss of the process reversibility and the formation of unstable by-products. It has been observed that the first one-electron reduction intermediate was identified as **9A**, which rapidly dimerises after electron and CO transfer to give **9B**. Protonation of the terminal sulfur and addition of CO causes the fragmentation of **9B** into **9C** and **9** (**Scheme 1.6**).[52a)]

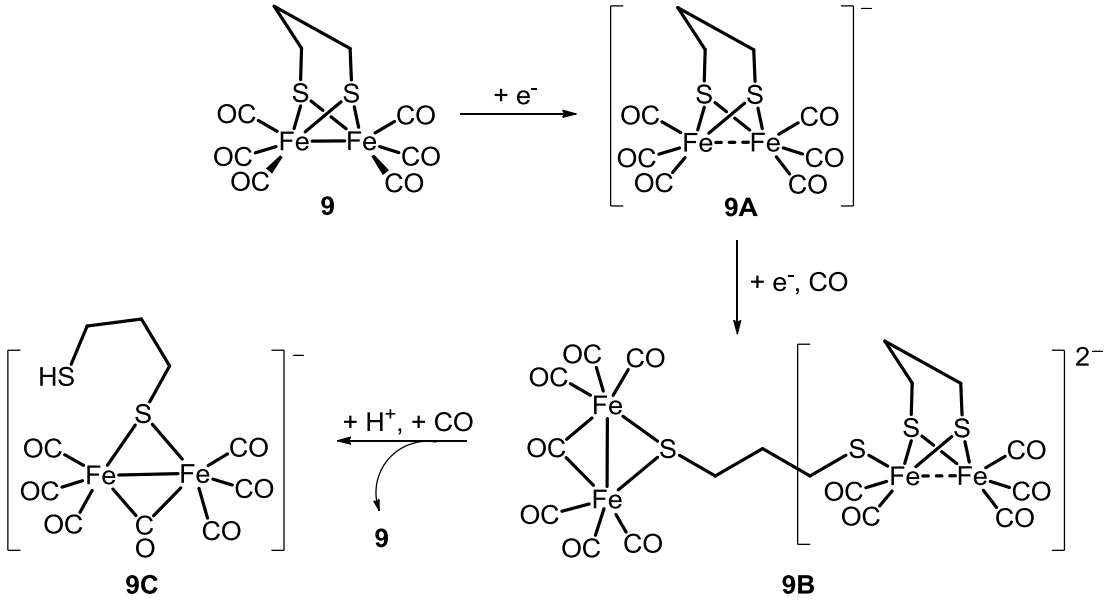

Scheme 1.6 Proposed electrochemical reduction products of hexacarbonyl pdt-bridged [FeFe]-complex **9**.

The suggestion that **9C** derived from the addition of two electrons and one proton to **9** were confirmed by spectroscopic analysis (IR and ^{1}H NMR) of the reaction product between **9** and hydride sources, Li(BHEt$_3$) and NaBH$_4$, in CO-saturated solutions. In the presence of *p*TsOH (pKa = 8 in CH$_3$CN), the Fe–Fe bond of **9A** is protonated causing a shift of the reduction potential towards a more positive value. The protonated intermediate is reduced by a second electron at potentials close to the reduction of **9** in the absence of acid, then protonated and further reduced leading to hydrogen evolution. In a CO-saturated solution the catalytic activity of **9** is significantly decreased by the formation of the intermediates (**9B** and **9C**), which lower the concentration of the catalytically active species from the solution.[52a)] This study provided important information about the stability and the chemistry following the

reduction of complex **9** and led to important structural changes, such as using aromatic dithiolate-based ligands, which will be discussed in Chapter 2.

1.3.2.1 Variation of the bridgehead atom

As mentioned in the previous section, the nature of the dithiolate bridgehead atom in the [2Fe]-subsite remained unclear for many years. Consequently a considerable number of [FeFe]-hydrogenase synthetic mimics were designed to solve this paradigm, incorporating CH_2, NH or O at the bridgehead.[17,44,47,48]

Rauchfuss and co-workers first published the synthesis of an azapropanedithiolate-containing (adt) [FeFe]-complex **12**, [*N*-Me(μ-adt)Fe_2CO_6], [53] and the corresponding disubstituted cyano complex **13**, [*N*-Me(μ-adt)$Fe_2(CO)_4(CN)_2]^{2-}$, both obtained from $S_2H_2Fe_2(CO)_6$ **11**.[51b),54a)] This work was soon followed by other [FeFe]-hydrogenase synthetic mimics **14a-d** with secondary/tertiary amines as the bridgehead group on the dithiolate ligand using a Mannich condensation-based approach (**Scheme 1.7**). X-ray crystallographic analysis of the corresponding dicyanide anion of complex **14a** confirmed its similarity to one of the proposed structures of the [2Fe]-subsite. IR spectroscopic analysis of the carbonyls stretches showed that, upon protonation with TfOH, the derived ammonium (pK_a = 2.3 in CH_3CN) species is easily deprotonated by water. Therefore, regarding the mechanism of [FeFe]-hydrogenase, the acidic proton of the ammonium intermediate is transferred to the hydride on Fe_d.[54b)] In contrast, tertiary amines on the apical position of the adt-bridge are less likely to be protonated ($7.6 \leq pKa \geq 10.6$ in CH_3CN) than the corresponding secondary amines. DFT calculation on complexes **12** and **14a** have suggested that a hyperconjugation effect between the lone pair of the nitrogen and the two C–S σ^* bond lowers the basicity of tertiary amines and increases the C–S bond length.[16,54a)]

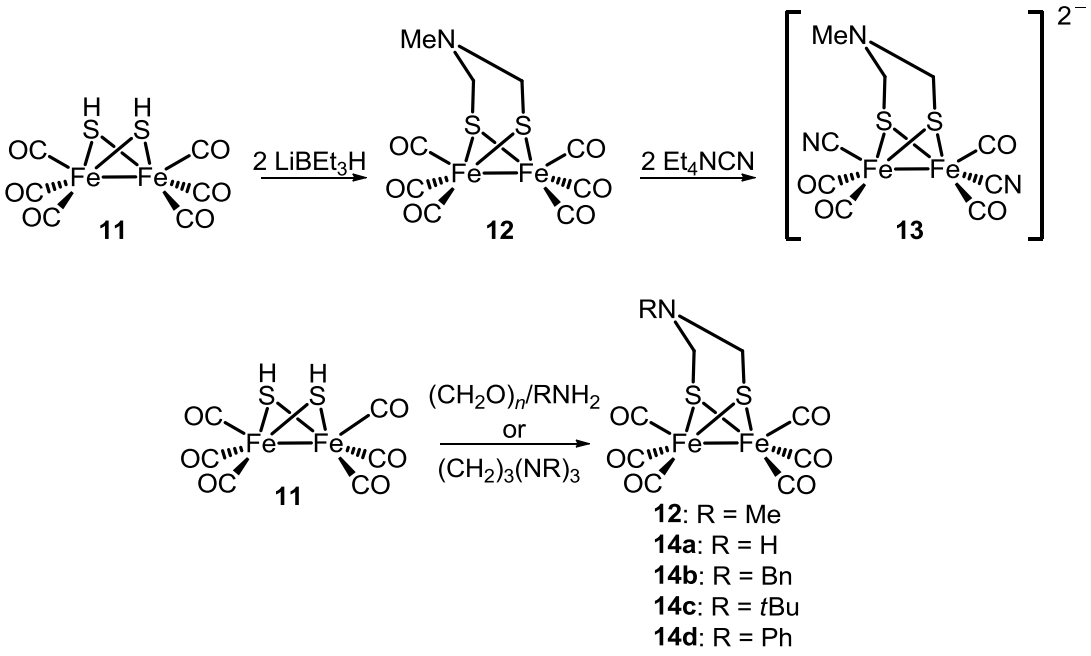

Scheme 1.7 Synthesis of adt-based [FeFe]-hydrogenase synthetic mimics **12** and **14a-d**.[54]

Although tertiary amines are weak bases, Ott demonstrated by IR and ^{1}H NMR spectroscopy that adt-based [FeFe]-complexes, [*N*-R(μ-adt)$Fe_2(CO)_6$], with *p*-bromobenzyl and *p*-methoxybenzyl groups on the nitrogen, are protonated at the apical nitrogen by strong acids. This causes a shift of the following reduction step towards more positive potentials and increases the catalytic efficiency, due to proton transfer from the apical position to bridging hydride on the Fe–Fe bond.[55]

Song and co-workers reported a series of oxapropanedithiolate-bridged (odt) [FeFe]-hydrogenase synthetic mimics **15-21** (**Figure 1.7**).[56] Nucleophilic substitution reactions on the hexacarbonyl odt-based analogue **15**, [(μ-odt)Fe_2CO_6], with Et_4NCN gave the mono and di-substituted cyanide derivatives **16** and **17**.[51b)] Using 1,1′-bis(diphenylphosphino)ferrocene (dppf) and 1,1′-bis(diphenylphosphino)ruthenocene (dppr) as nucleophiles allowed the synthesis of double [FeFe]-complex **18a-b** with ferrocene and ruthenocene as linkers.[56]

Besides dppf, other linkers, such aryl dicyanides, diphosphines and tetraphosphines, have been used to obtain the corresponding double [FeFe]-complexes **19-21** (**Figure 1.7**).[56b)]

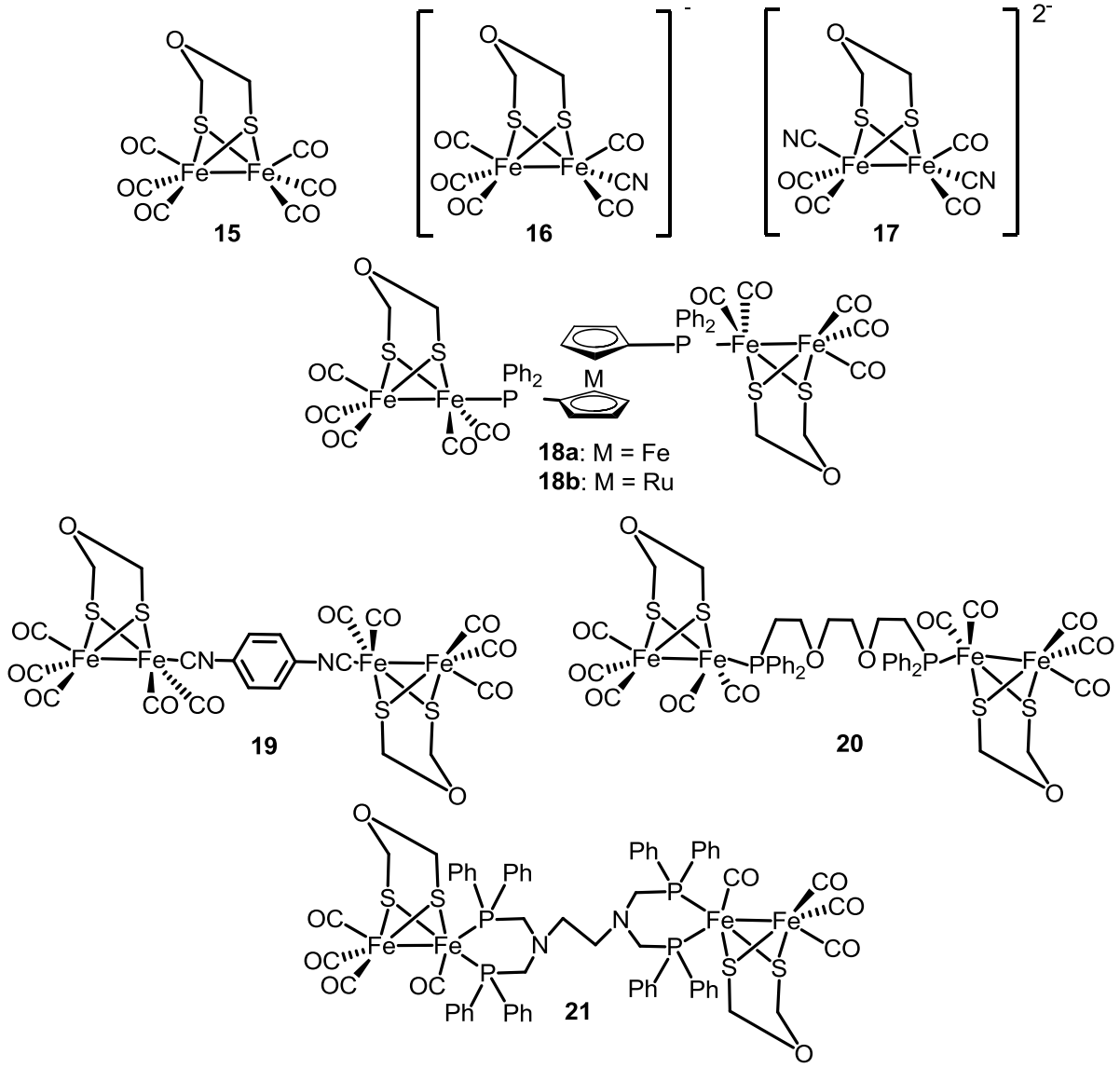

Figure 1.7 Odt-based [FeFe]-hydrogenase synthetic mimics **15-17**, **18a-b** and **19-21**.[56]

Crystal structures of [FeFe]-complexes **15-21** confirmed the analogy with the enzyme's active site, pdt and adt-based synthetic mimics. Electrochemical analysis of **15** showed two one-electron reduction events, Fe(I)Fe(I)→Fe(I)Fe(0) and Fe(I)Fe(0)→Fe(0)Fe(0), at more positive values (–1.59 V and –2.10 V respectively) than **10**, but still far from the natural

system. However, bulk electrocatalysis demonstrated hydrogen production upon treatment with acetic acid (AcOH).[56b)]

More recently, examples of thiapropanedithiolate-based (tdt) [FeFe]-hydrogenase mimics have been also reported. Song and co-workers described the synthesis of the hexacarbonyl tdt-bridged [FeFe]-complex **22**, [(μ-tdt)Fe_2CO_6], obtained by oxidative insertion of $Fe_3(CO)_{12}$ on the S–S bond of the 1,2,4-trithiolane (**Figure 1.8**).[57]

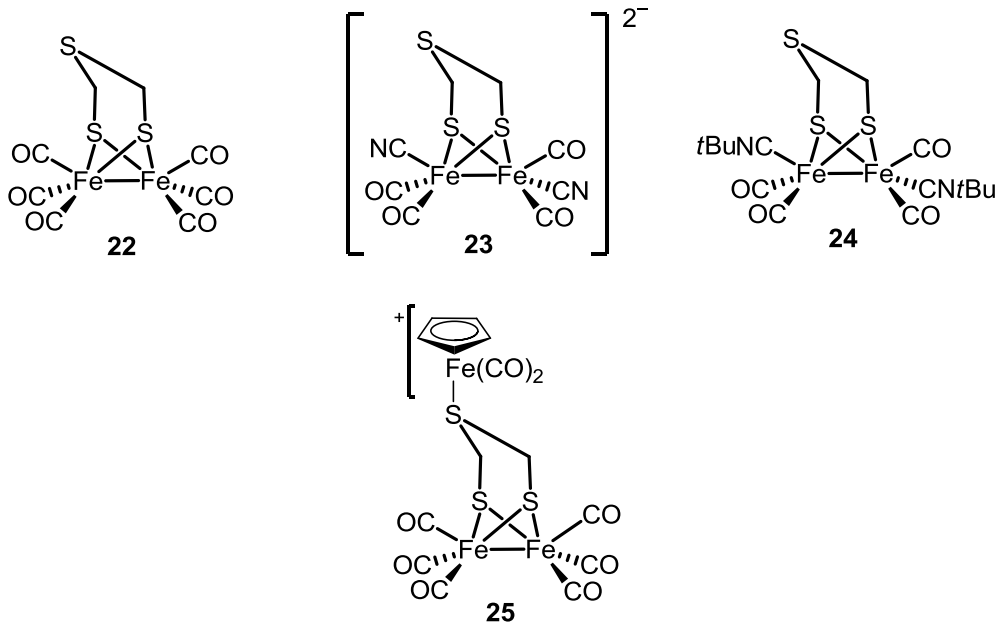

Figure 1.8 Tdt-based [FeFe]-hydrogenase synthetic mimics **22-25**.[57,58]

Its derivatives **23-25** were obtained by reaction of **22** with Et_4NCN and *t*BuCN and by coordination of the bridging sulfur to $CpFe(CO)_2BF_4$ (**Figure 1.8**).[51b,57] Synthesis, structure analysis and elecrochemical studies of complex **22** have also been reported independently by Weigand.[58]

Glass and co-workers reported the synthesis and spectroscopic studies of tin-bridged dithiolate-based [FeFe]-complexes **26** and **27** (**Figure 1.9**).[59] Gas-phase photoelectron spectroscopy (PES), supported by DFT studies, suggested that the energy required for the Fe–Fe bond cleavage, which is the crucial step in the catalytic mechanism of [FeFe]-hydrogenase,

is lowered by the presence of tin. In the case of complex **26**, the bridging dithiolate is positioned axially on the metal bond, inducing destabilization of the Fe–Fe σ bond by inductive interaction of the C–Sn σ bond and the sulfur lone pair. In contrast, the two substituents of the non-bridging thiolates in complex **27** assume the preferred equatorial position, causing the direct combination of the sulfur lone pair with the Fe–Fe σ bond, which is then destabilised.

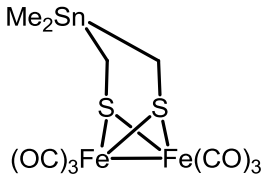

26

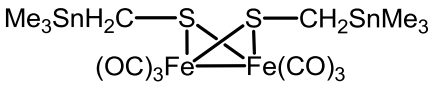

27

Figure 1.9 [FeFe]-Hydrogenase synthetic mimics based on bridging tin dithiolates **26** and **27**.[59]

Based on Glass' report, [59] Weigand investigated [FeFe]-hydrogenase synthetic mimics based on silicon-bridged propanedithiolates and reported the synthesis of complexes **28a-c** and **29** **(Figure 1.10**).[60a)] Substitution of the bridgehead carbon with silicon increases the electron-density on the dithiolate ligand by inductive interaction of the C–Si σ bond and the sulfur lone pair, as previously reported for **26** (**Figure 1.9**).

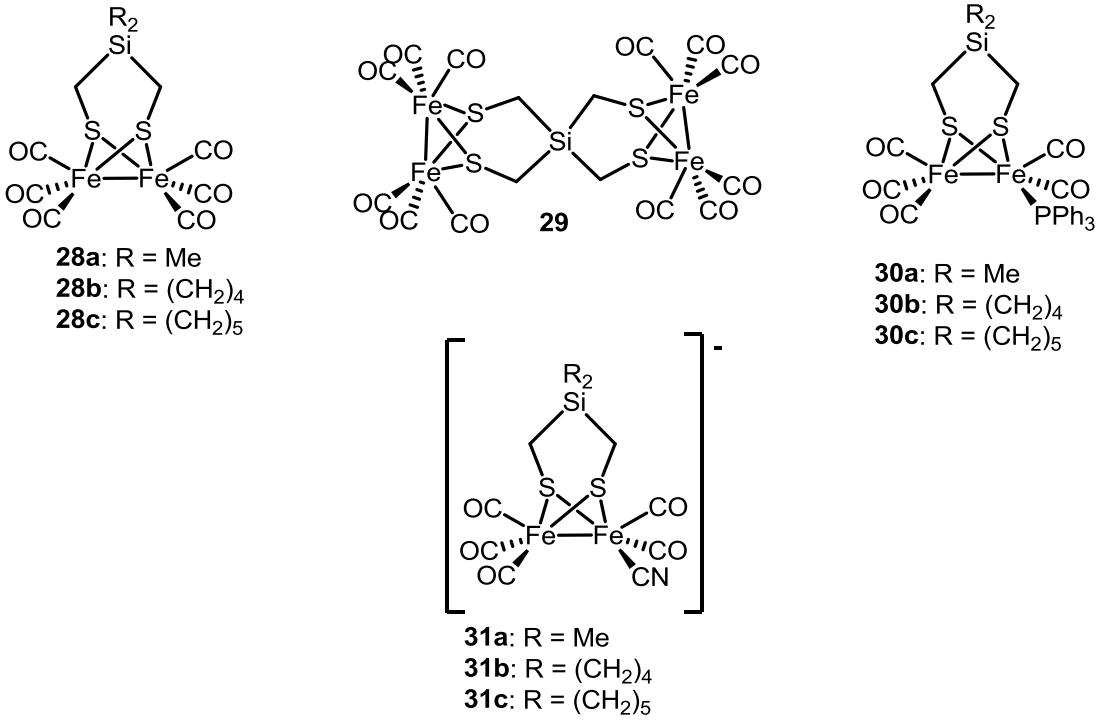

Figure 1.10 [FeFe]-Hydrogenase synthetic mimics based on silicon-bridged dithiolates **28a-c**, **29**, **30a-c** and **31a-c**.[60]

In order to increase the basicity of the Fe–Fe bond (Section 1.3.2.2), the same group described the synthesis of [FeFe]-complexes **30a-c** and **31a-c**, containing phosphines and cyanides on the iron centres, aimed at favouring the protonation of the Fe–Fe bond (**Figure 1.10**). The increase of the electron-density on the [FeFe]-cluster was confirmed by a more negative reduction potential than the parent compounds **28a-c**.[60b)]

[FeFe]-Hydrogenase synthetic mimics containing bridging selenium and phosphide oxide, **32** and **33**, were reported by Weigand and co-workers (**Figure 1.11**).[61,62]

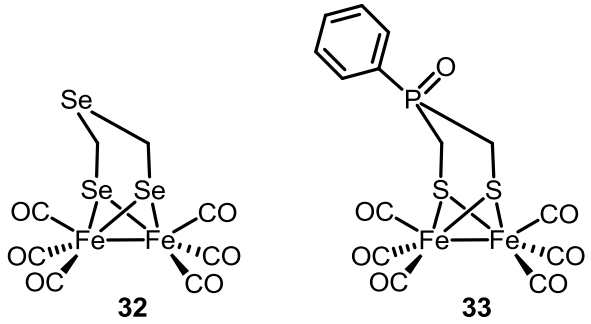

Figure 1.11 [FeFe]-Hydrogenase synthetic mimics with bridging selenium (**32**) and bridging phosphide oxide (**33**) on the dithiolate ligand.[61,62]

Protonation experiments on complex **33**, monitored by IR spectroscopy and ^{31}P NMR, showed the oxygen of the phosphide oxide as the most basic site of the molecule, mimicking the secondary amine function in the enzyme's active site and favouring the proton transfer to the iron centres.[62]

1.3.2.2 Variation of ligands on the iron centres

Most of the synthetic mimics discussed in the previous section contain the enzyme's structural feature of two cyanide ligands on the [FeFe]-cluster. Electrochemical studies on complex **10** (**Scheme 1.7**) revealed that the electron-rich cyanides ligands favours the reaction with acid and the protonation of the Fe–Fe bond. Hydrogen production was observed as well as the degradation of complex **10**, which is highly unstable and reactive towards acids.[51b),63] Consequently the use of alternatives ligands, with electron-donating properties similar to cyanides but lacking reactivity towards acid, has been developed, leading to a new class of bio-inspired catalysts for the hydrogen production. The most conventional alternatives to cyanides include isocyanides and phosphines, carbenes and amines.[16,17,44,47,48]

Rauchfuss reported the synthesis of a phosphine and cyano-substituted [FeFe]-complex, [(μ-pdt)(CN)$Fe_2(CO)_4(PMe_3)]^-$. This complex is protonated by an excess of aqueous sulfuric acid

(H_2SO_4) only at the Fe–Fe bond, producing a stable intermediate, which then, upon treatment with *p*TsOH, is protonated at the cyanide ligand. Although [(μ-pdt)(CN)$Fe_2(CO)_4(PMe_3)$]$^-$ is reduced at more negative potential than **10** (**Scheme 1.7**), it is more efficient and robust in proton reduction catalysis than the dicyano-substituted [FeFe]-complex.[64] The corresponding diphosphine-substituted complex, [(μ-pdt)$Fe_2(CO)_4(PMe_3)_2$], also catalyses proton reduction, but it is less efficient than the phosphine cyano-substituted parent compound.[65] The protonated cyanide in [(μ-pdt)(CN)$Fe_2(CO)_4(PMe_3)$]$^-$ is proposed to either interact with the bridging hydride on the Fe–Fe bond, relay protons to Fe–Fe bond, or increase their basic character favouring the [FeFe]-complex catalytic activity.

The use of isocyanides, phosphines, carbenes and amines allows to obtain stable carbonyl-bridged mixed-valent, Fe(II)–Fe(I), [FeFe]-complexes, which include an iron in a "rotated state", identical to the active site form H-act (Section 1.3). The stability of these [FeFe]-hydrogenase synthetic mimics strongly rely on the hindrance of the ligand substituents, which prevents the access to the vacant site of the five-coordinated iron, and on the ligand electron-donating properties, which stabilises the oxidized Fe(II).[17,48]

Following the initial studies on this class of synthetic mimics, [66,67] Gloaguen and co-workers have reported the synthesis and the study of new [FeFe]-hydrogenase analogues **34a-b**, [(μ-pdt)$Fe_2CO_4(\kappa^2$-LL)], obtained from the reaction of **9** (**Scheme 1.5**) with the chelating dicarbene (L = I_{Me}-CH_2-I_{Me}, where I_{Me} = 1-methylimidazol-1-ylidene), and diphosphine (L = dppe = 1,1′-bis(diphenylphosphino)ethane) respectively. The dicarbene ligand in complex **34a** favours the reaction of the corresponding oxidised mixed-valent [**34a**]$^+$, with nucleophilic substrates, such as $P(OMe)_3$, CH_3CN and CO. This is due to the strong electron-donating effect of the dicarbene ligand, confirmed by the IR carbonyl stretching bands shifted towards lower wavenumbers compared to the values reported for the diphosphine substituted complex.

Particularly, $P(OMe)_3$ binds the rotated iron centre in [**34a**]$^+$ and gives the diferrous carbonyl-bridged complex [**34a**]$^{2+}$ (**Figure 1.12**).[68]

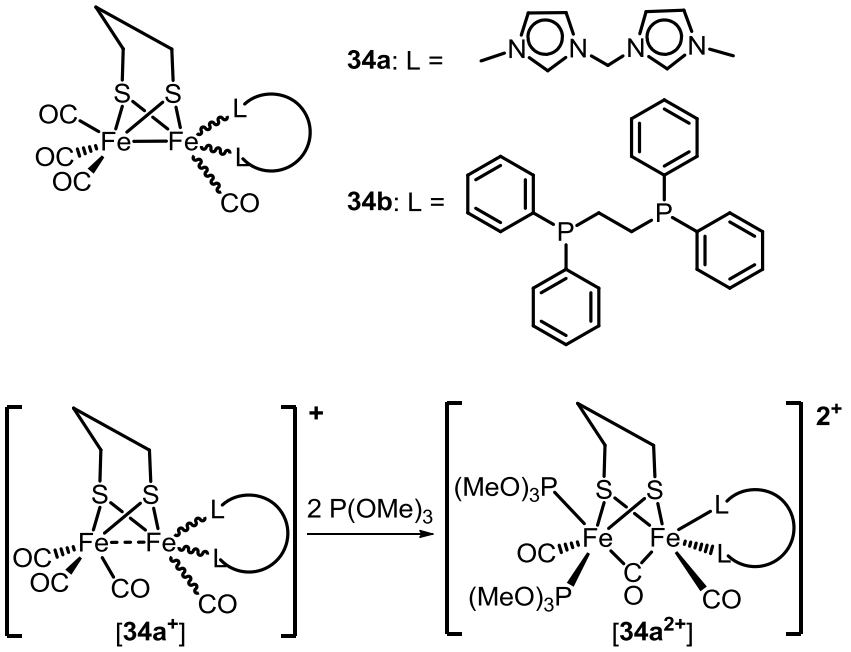

Figure 1.12 Dicarbene and diphosphine-chelated [FeFe]-complexes **34a-b**. The oxidized species [**34a**$^+$] reacts with $P(OMe)_3$ to give the diferrous carbonyl-bridged intermediate [**34a**$^{2+}$].[68]

Ott and co-workers reported the synthesis and the electrochemical analysis of the [FeFe]-hydrogenase synthetic mimics **35a-c**, [(μ-SR)Fe_2CO_4(κ^2-BC)] (BC = 1,2-bisdiphenylphosphine-1,2-*o*-carborane), containing three different types of bridging dithiolates, propanadithiolate (pdt), ethanedithiolate (edt) and 1,2-benzenedithiolate (bdt) respectively. The electron-deficient *o*-carborane diphosphine induces a weaker electron-donating effect to the iron compared to other chelating diphosphines, resulting in a pronounced shift of the carbonyl stretchings frequencies towards higher energies. In terms of electrochemical behaviour complexes, **35a-c** undergo one irreversible reduction event at more negative potential values than the corresponding hexacarbonyl complexes. However, the oxidation, Fe(I)Fe(I)→Fe(I)Fe(II), is reversible and the oxidised form of **35a-c** is stable for several minutes, allowing detailed spectroscopic analyses by EPR and Hyperfine Sublevel

Correlation Spectroscopy (HYSCORE). The electron-donating bridging pdt of complex **35a** induces the oxidation of the [FeFe]-cluster at lower potentials than **35b-c**, but the bridging dithiolates have a marginal effect on the reduction event compared to the chelating *o*-carborane diphosphine (**Figure 1.13**).[69]

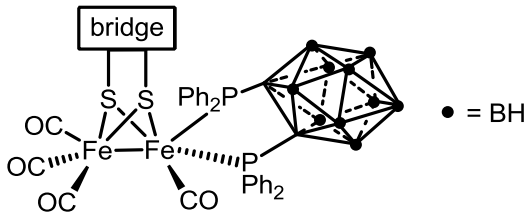

35a: bridge = pdt
35b: bridge = edt
35c: bridge = bdt

Figure 1.13 [FeFe]-complexes **35a-c** containing a chelating phosphine-1,2-*o*-carborane derivative, reported by Ott.[69]

The key step in the [FeFe]-hydrogenase mechanism is protonation of the vacant site on the five-coordinated Fe_d of H-act (**Scheme 1.4**). The first protonation of the [FeFe]-hydrogenase analogues Fe–Fe bond is achieved by either a chemical (C) or an electrochemical path (EC). The first path involves the direct protonation of the iron centres, whereas the second requires a reduction of the metal centre, followed by protonation (**Scheme 1.8**).[70]

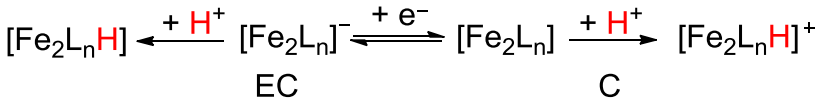

Scheme 1.8 Protonation of the Fe–Fe bond of [FeFe]-hydrogenase analogues through a chemical (C) and electrochemical (EC) pathway.

Due to the presence of weak electron-donating carbonyls, hexacarbonyl [FeFe]-hydrogenase analogues are protonated at the Fe–Fe bond mainly by strong acids and after one electron transfer, which increases the basicity of the iron centres (EC, **Scheme 1.8**). However, Darensbourg demonstrated that protonation of the Fe–Fe bond in complex **9** (**Scheme 1.5**) by weak acid (*e.g.* AcOH) occurs after two one-electron reductions, different from what Pickett

and Best observed (Section 1.3.1).[71] Replacing carbonyls with isocyanides, carbene and phosphines increases the electron-density of the iron centres and allows the direct protonation of the Fe–Fe bond (C, **Scheme 1.8**).[17,44,47]

Recently Liu and co-workers reported the synthesis of **36**, [(μ-bdt)$Fe_2(CO)_5PPh_2$], which, upon protonation with one equivalent of TfOH, resulted in a hydride-bridged intermediate on the Fe–Fe bond; further acid addition protonated of sulfur of the bdt bridge (**Scheme 1.9**). The protonated intermediates were characterised by IR spectroscopy and studied by DFT calculations.[72]

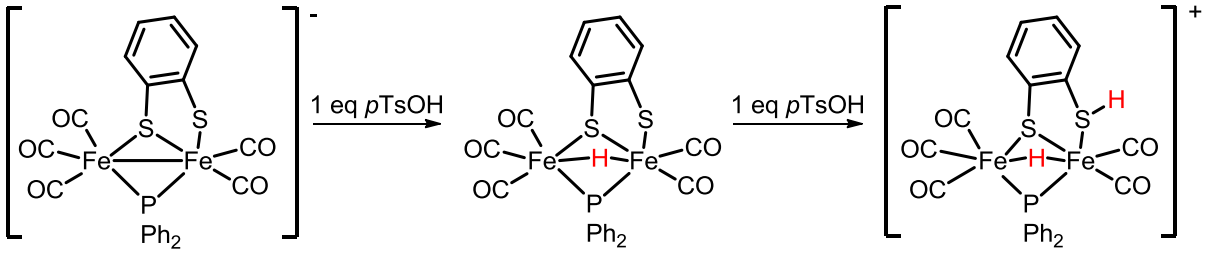

36

Scheme 1.9 [FeFe]-Hydrogenase synthetic mimic **36** reported by Liu, who showed the protonation sites upon increasing addition of acid.[72]

An additional strategy, first introduced by DuBois and later applied to [FeFe]-hydrogenase synthetic mimics, [73,74] is to control the first protonation site by using a pendant amine in the second coordination sphere of the iron centres.

Recently Ott and co-workers described the study on [FeFe]-complexes **37a-c**, which are identical in terms of electronic properties and differ only in the pendant group on the iron centres: **37a-b** contain a chelating diphosphine with tertiary amines respectively, **37c** features a CH_2 instead of the amino group (**Scheme 1.10**).

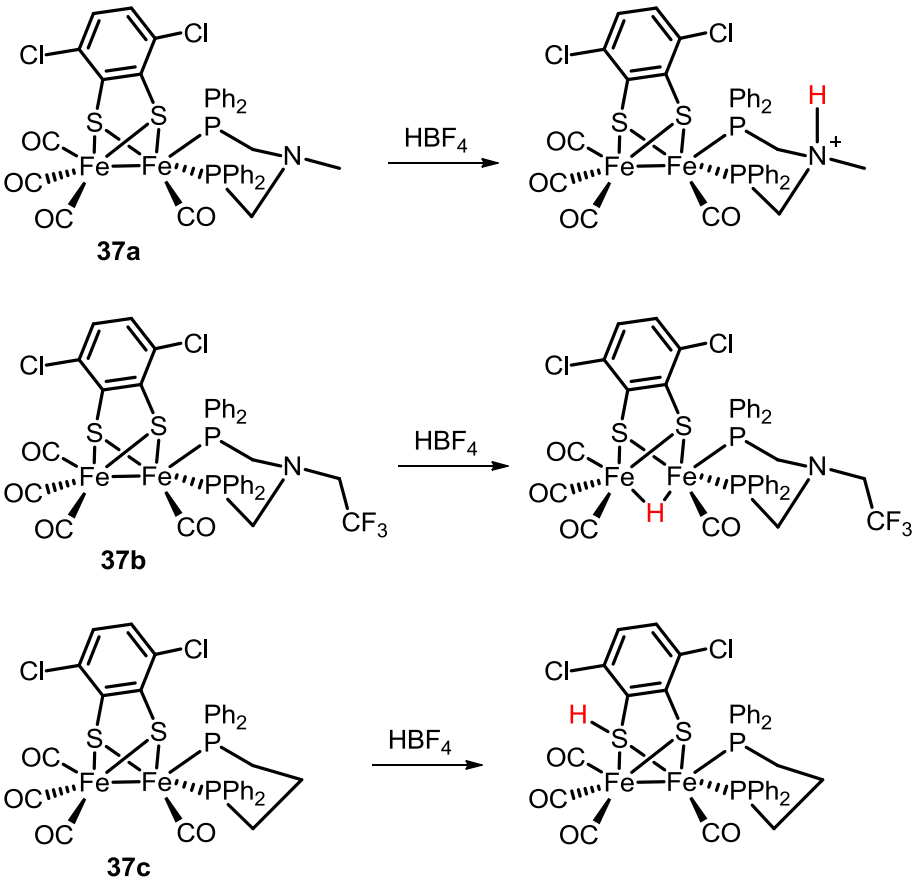

Scheme 1.10 Protonation studies on complexes **37a-c**.[75]

Spectroscopic analysis (IR, ^{1}H NMR and ^{31}P NMR) of **37a-c** revealed that the protonation site changes according to the presence of the pendant amine and that it is also affected by its substituents. An electron-rich amine (**37a**) favours protonation at the nitrogen, whereas in the presence of an electron-deficient amino group (**37b**) the Fe–Fe bond is protonated. In the absence of a pendant amine (**37c**), the most basic site is the sulfur of the dithiolate bridge (**Scheme 1.10**).[75]

Based on previous results by Darensbourg and Gloaguen, [76] Åkermark and co-workers introduced a new strategy for directing the protonation to the Fe–Fe bond by using carboxylic acids on the second coordination sphere of the iron centres. This work is based on the synthesis and electrochemical investigation of [FeFe]-hydrogenase synthetic mimics **38a-c**,

[*N*-R(μ-adt)$Fe_2(CO)_4(PMe_3)_2$], containing an adt bridge, functionalised with a carboxylic acids on the bridgehead nitrogen. Upon treatment of **38a-c** and **39a-c** with TfOH, complexes **38a** and **39a-c** undergo protonation only at the nitrogen. In contrast, the Fe–Fe bond of **38b-c** is the first to be protonated, followed by nitrogen at high concentration of acid. In the presence of an alkyl carboxylic acid group (**39b-c**), the nitrogen lone pair is involved in a hydrogen bond with the carboxylic acid, which allows protonation of the electron-rich Fe–Fe bond; the basicity of the nitrogen lone pair in complex **38a** is weakened by the electron-withdrawing aryl carboxylic acid. The absence of the electron-donating phosphine ligands on the iron centres in **39a-c** promoted the protonation of the nitrogen, which is the most basic site in the molecule. Interestingly complexes **38b-c** are active catalysts for proton reduction in water with the alkyl carboxylic acid moiety, which transfer proton to the amino group (**Figure 1.14**).[77]

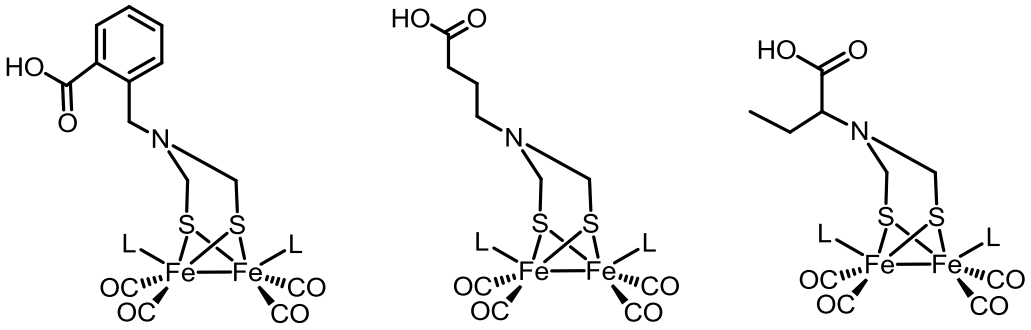

Figure 1.14 Carboxylic acid-functionalised [FeFe]-hydrogenase synthetic mimics **38a-c** and **39a-c**.[77]

Protonation of the vacant coordination site on the Fe_d produces a hydride-intermediate of the [2Fe]-subsite, but to date it has not been proved whether the hydride occupies a bridging or a terminal position on the Fe–Fe bond. Although, most of the [FeFe]-hydrogenase synthetic

mimics feature a bridging hydride, both isomers need to be studied to definitely elucidate the hydride's binding site on the Fe–Fe in the enzyme's mechanism.[78]

Poilblanc and co-workers reported that the protonation of symmetric diphosphine-substituted [FeFe]-complexes occurs at the Fe–Fe bond and produces a hydride intermediate, which was characterized by IR and ^{1}H NMR spectroscopy.[79] Based on this study, Rauchfuss published the first diferrous species with a terminal hydride **41**, which derived from the reaction at low temperature of **40** with $LiAlH_4$ or $NaBH_4$. At room temperature, complex **41** undergoes an intramolecular rearrangement to form the bridging hydride isomer **42** (**Scheme 1.11**). ^{1}H NMR analysis shows that **41** reacts with Brønsted acids to produce hydrogen, whereas the corresponding hydride-bridged isomer **42** is unreactive under the same conditions.[80]

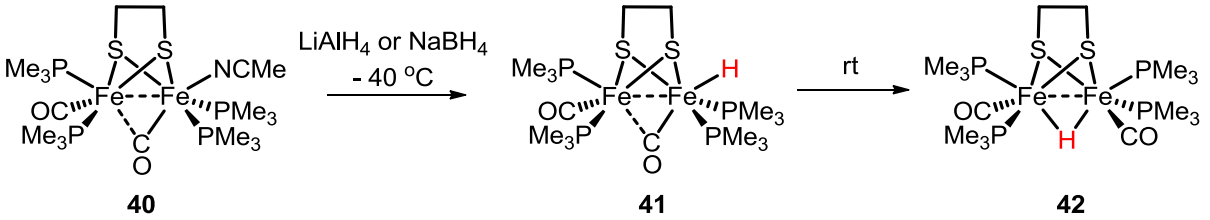

40 **41** **42**

Scheme 1.11 Formation of the terminal hydride **41** from complex **40** and its rearrangement into the bridged species **42**.[80]

Subsequently, many other terminal hydride species have been prepared and characterised by NMR spectroscopy.[81] Rauchfuss and co-workers reported the study of the electron-rich and sterically hindered complex **43**, [(μ-pdt)$Fe_2(CO)_2$(dppv)$_2$] (dppv = 1,2-bis(diphenylphosphino)ethylene), which upon protonation with strong acids gave the terminal hydride species **44**, stable at room temperature for several minutes, before isomerising slowly to the bridging hydride complex **45** (**Scheme 1.12**).[82] Electron transfer to complex **44** increases its hydridic character and leads to hydrogen production.

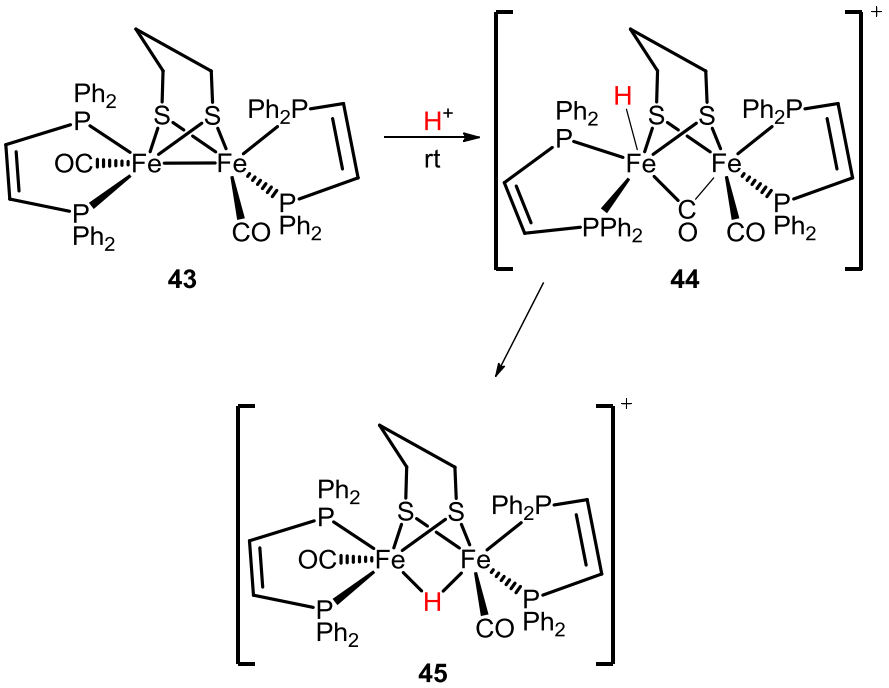

Scheme 1.12 Formation of the terminal hydride **44** upon strong acid protonation of **43** and its slow rearrangement into the bridged species **45**.[82]

In 2014 the same group isolated the first example of the [FeFe]-hydrogenase synthetic mimic **47** containing both a bridging and terminal hydride (**Scheme 1.13**).[83] The bridging hydride complex **45** (**Scheme 1.12**) [82] undergoes a displacement of a carbonyl group by a hydride from NBu_4BH_4, via a CH_3CN-complexed monosubstituted intermediate **46**. The structure of **47** was analysed spectroscopically and computationally (^1H and ^{31}P NMR, IR and DFT) and its hydridic character investigated. In presence of the strong and weak acids, $H(OEt_2)BAr^F{}_4$ ($BAr^F{}_4$ = tetrakis[3,5-bis(trifluoromethyl)phenyl]borate) and benzoic acid respectively, and mild oxidants, $FcBAr^F{}_4$, it produces hydrogen in high yield, unlike complex **43**, which requires an additional reduction step before reacting with even strong acids.[82]

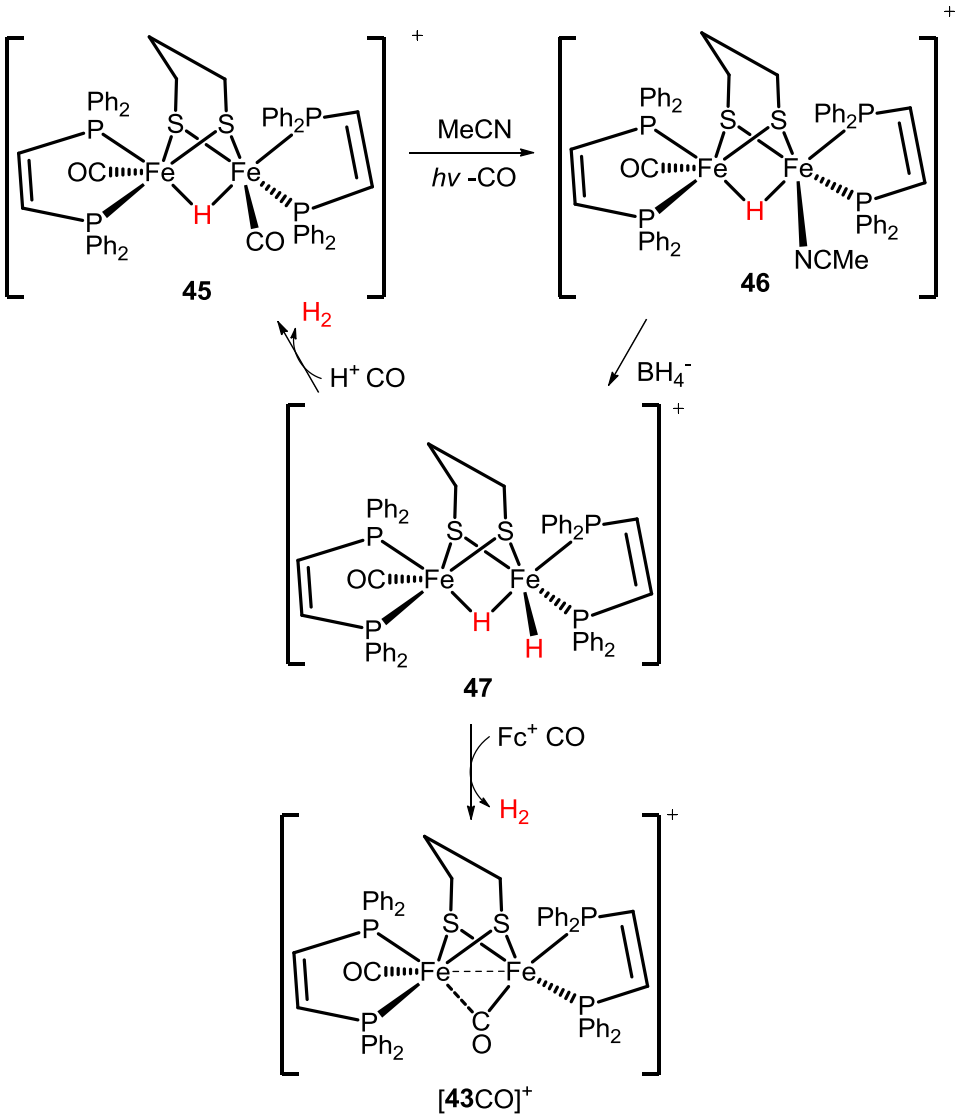

Scheme 1.13 Synthesis of the dihydride [FeFe]-complex **47** and hydrogen production upon treatment of **47** with acids and oxidants.[83]

Rauchfuss and co-workers studied the protonation of the adt-based [FeFe]-complex **48**, [(μ-adt)$Fe_2(CO)_2(dppv)_2$], and confirmed the results with IR and NMR spectroscopy and, additionally, with X-ray diffraction of the terminal hydride species. Protonation of the secondary amine in **48** at low temperature gave first the ammonium species **49**, which undergoes rapid proton transfer forming the terminal hydride intermediate **50**. The similarity of **50** with the protonated intermediate of the [2Fe]-subsite was shown by X-ray analysis, which also displays the short distance between the apical secondary amine and the terminal

hydride suggesting a hydrogen–bond interaction. However, when the temperature is raised to room temperature, compound **50** isomerises to the bridging hydride species **51** (**Scheme 1.14**).[84] Electrochemical analysis of the two species **50** and **51** confirmed the previous analysis: [82] the terminal hydride intermediate is easier to reduce and it catalyses proton reduction better than the corresponding hydride-bridged isomer. Furthermore, their acidities are different (**50**: pKa = 16 and **51**: pKa = 19 in CH_3CN), reinforcing the idea that the stronger acid (**50**) is easier to reduce and is more likely involved in the catalytic cycle, consistent with the higher reduction potential of **51**.

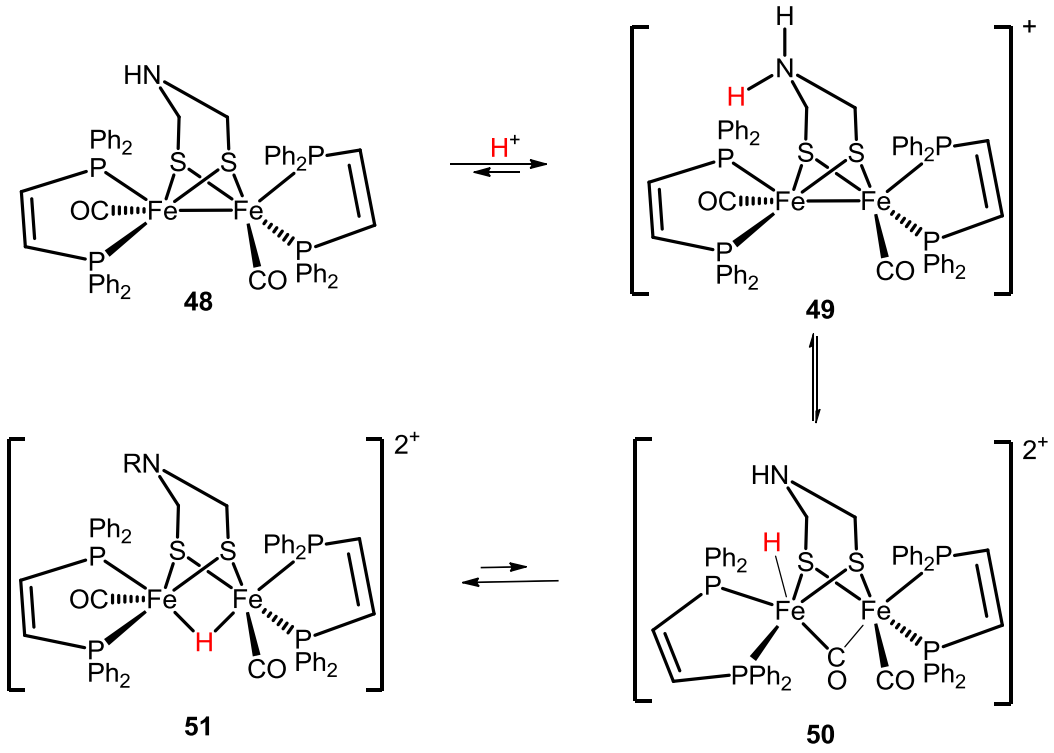

Scheme 1.14 Formation of first carbonyl-bridged terminal hydride intermediate **50** and its rearrangement to the bridged **51** after protonation of the [FeFe]-hydrogenase synthetic mimic **48**.[84]

1.3.2.3 Variation in the bridging dithiolate

Although most of the reported [FeFe]-hydrogenase synthetic mimics have shown electrocatalytic activity towards proton reduction, their efficiency is not comparable to that

reported for the enzyme (Section 1.3.1). This is mainly due to very negative reduction potentials and the iron centres oxidation states, which differ from the natural active site, (Fe(I)-Fe(I)/Fe(I)Fe(0) instead of Fe(II)Fe(I)/Fe(I)Fe(I)).[17,44] The redox properties of [FeFe]-hydrogenase analogues are modulated by replacing the sulfur atoms of the bridging dithiolate with the heavier chalcogen selenium.[16,17]

In the human body selenium is present in trace quantities and mainly in amino acids such as selonocysteines and selenomethionines, and in their metabolic precursors, where it replaces its isoelectronic atom, sulfur.[85] One example of selenoproteins, relative to the hydrogenases family, is the [NiFeSe]-hydrogenase, isolated in *Desulfomicrobium baculatum* and in the *Desulfomicrobium vulgaris* (Section 1.2.2).[27]

The strategy of replacing sulfur with selenium in the bridging linker was introduced first by Hou and co-workers, who described the synthesis of *N*-substituted azapropanediselenolate-based [FeFe]-complexes **52a-c**, [*N*-R(μ-ads)Fe_2CO_6], and a comparative study with the corresponding dithiolate-based [FeFe]-complexes **53a-c** (**Figure 1.15**).[86]

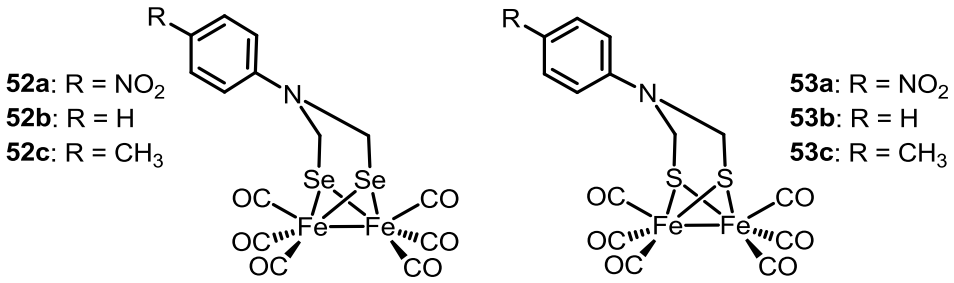

Figure 1.15 *N*-substituted azapropanediselenolates **52a-c** and the dithiolate-based [FeFe]-complexes **53a-c**.[86]

X-ray analysis showed the similarity of complexes **52a-c** with both the enzyme's [2Fe]-subsite and complexes **53a-c**, whereas IR spectroscopy displayed a bathochromic shift of the carbonyls bands of **52a-c**. The presence of selenium, less electronegative than sulfur, increases the electron-density on the iron and favours the π backbond donation from the metal

to the carbonyl lowering the carbonyl IR stretching frequencies. Electrochemical studies on **52a-c** confirmed the spectroscopic result: although there is no significant difference in terms of reduction potentials (typically 0.01 V), complexes **52a-c** are oxidised at less positive potentials (0.56–0.66 V) than **53a-c** (0.64–0.76 V) and, in terms of catalytic activity, **52a-c** are more efficient catalysts than the sulfur equivalents.[86] Following the initial work of Hou, Song published the synthesis of a series of propanediselenolates-bridged synthetic mimics **54a-d** (**Figure 1.16**). The electrochemical behaviour of **54a** was compared with the corresponding dithiolate **9**: it displayed lower reduction and oxidation potentials than **9** (**54a**: E_{pc} = –1.61 V, E_{pa} = 0.73 V; **9**: E_{pc} = –1.66 V, E_{pa} = 0.77 V) and was confirmed to be a better catalyst for proton reduction than **9**. Furthermore, complex **54a** showed the same reactivity of complex **9** in that it undergoes nucleophilic substitution at the iron centres giving the corresponding phosphine (**54b-c**) and dicarbene derivatives (**54d**) (**Figure 1.16**).[87]

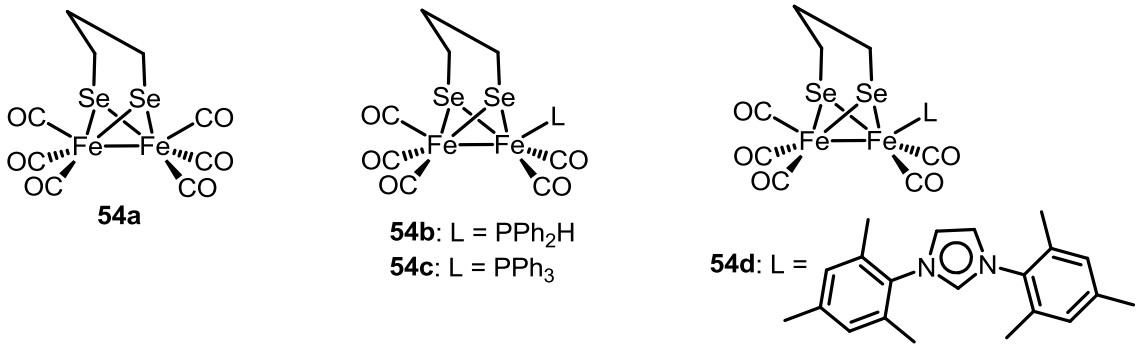

Figure 1.16 Propanediselenolate-bridged [FeFe]-hydrogenase synthetic mimic **54a** and the corresponding phosphine (**54b-c**) and dicarbene-substituted complexes (**54d**).[87]

Weigand described the synthesis and analysis of water-soluble sugar-based diselenolate-bridged [FeFe]-hydrogenase analogue **55** and the corresponding dithiolate **56** (**Figure 1.17**). Complex **55** has oxidation and reduction peaks at lower and higher potentials than complex **56** (**55**: E_{pc} = –1.50 V, E_{pa} = 0.97 V; **56**: E_{pc} = –1.46 V, E_{pa} = 1.09 V) and, additionally, it is more stable in water and a more efficient catalyst than the sulfur counterpart (**Figure 1.17**).[88]

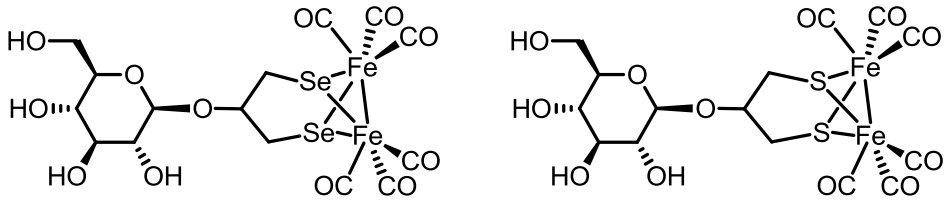

Figure 1.17 Water-soluble sugar-based diselenolate-bridged [FeFe]-complex **55** and the sulfur counterpart **56**.[88]

Additional studies reached similar conclusions on the benefit of replacing sulfur with selenium.[61,89]

Only few examples of ditellulorate-bridged [FeFe]-complexes have been reported.[90] In general these complexes display less negative reduction potentials than the corresponding diselenolate and dithiolate-bridged analogues, but the catalytic efficiency is similar to the diselenolate-based [FeFe]-complexes. Other alternatives to chalcogens have been prepared including bridging phosphines and amines.[91,92]

In order to modulate the redox properties of the enzyme analogues, another strategy is stabilising the reduced intermediates in the catalytic cycle by using aromatic bridging dithiolates, which will be discussed in Chapter 2.

1.3.2.4 Towards H-cluster synthetic mimics

Compared to the intensely developed chemistry of mimicking the [2Fe]-subsite, [17,44,47,48] very few synthetic strategies have been described to reproduce the complete H-cluster.[16] In the very early studies on [FeFe]-hydrogenase synthetic mimics, Pickett and co-workers reported the synthesis of functionalised pdt-based [FeFe]-complexes **57a-b** containing an appended thioether bound to one iron centre (**Scheme 1.15**).[93] The [2Fe3S]-core of these complexes reproduces closely the proposed structure of the H-cluster, where the Fe_p is linked by a cysteinyl residue to the [4Fe4S]-cubane core (**Figure 1.6**).

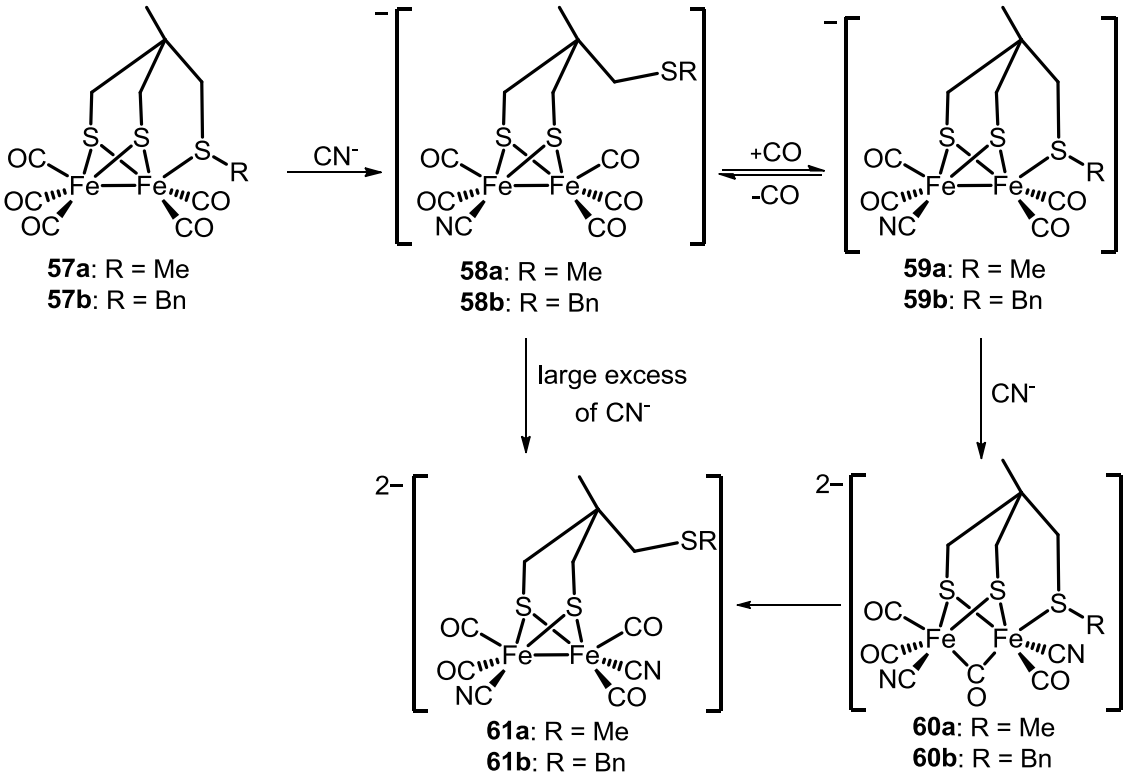

Scheme 1.15 Nucleophilic substitution on [2Fe3S]-core synthetic mimics **57a-b**.[93]

Nucleophilic substitution with one equivalent of cyanide is regioselective for the Fe_d and gave the stable complexes **59a-b**; excess of cyanide anion produced the unstable carbonyl-bridged species **60a-b**, which is slowly converted to compound **61a-b** (**Scheme 1.15**).[93]

Based on the same synthetic approach Pickett and co-workers reported the first H-cluster model systems **62a-b**, using $[4Fe4S(L)(SEt)]^{2-}$ (L = 1,3,5-tris-(4.6-dimethyl-3-mercaptophenylthio)-2,4,6-tris(*p*-tolyl-thio)benzene) and $[4Fe4S(SMe)_4][NBu_4]_2$ respectively) to reproduce the [4Fe4S]-cubane core of the natural system (**Figure 1.18**).[94] Although Pickett's work represented an important step for the future development of H-cluster model systems, proton reduction catalysis occurred at very negative potentials and hydrogen oxidation process was not observed.

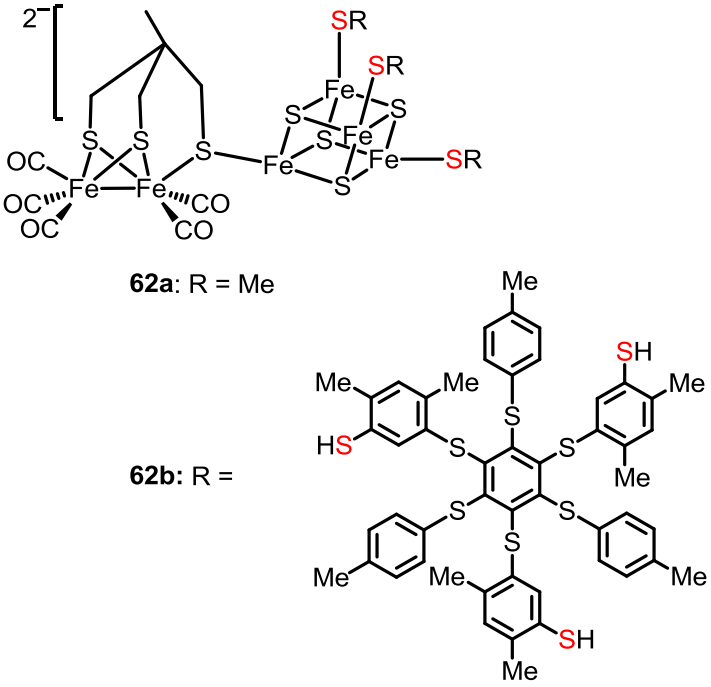

Figure 1.18 First H-cluster synthetic mimics **62a-b**.[94]

As previously described complexes **18a-b** (**Figure 1.7**, Section 1.3.2.1) contain the electron transfer moieties ferrocene/ruthacene, which is linked to the [2Fe]-core by a diphenylphosphine instead of thioether derivatives.[56b)] Nitrogen, silicon and oxygen-based [2Fe3S]-complexes **63**, **64** and **65** have been described by Rauchfuss, Song and Weigand respectively (**Figure 1.19**).[56a),60a),95] Despite the novelty of **18a-b**, **63** and **64**, the electrocatalytic activity towards protons reduction and the role of the electron transfer moiety has not been investigated. Complex **65** is structurally similar to **57a-b** (**Figure 1.18**), and it showed electrocatalytic activity towards protons reduction but without significant improvements in terms of reduction potentials and reversibility of the process.

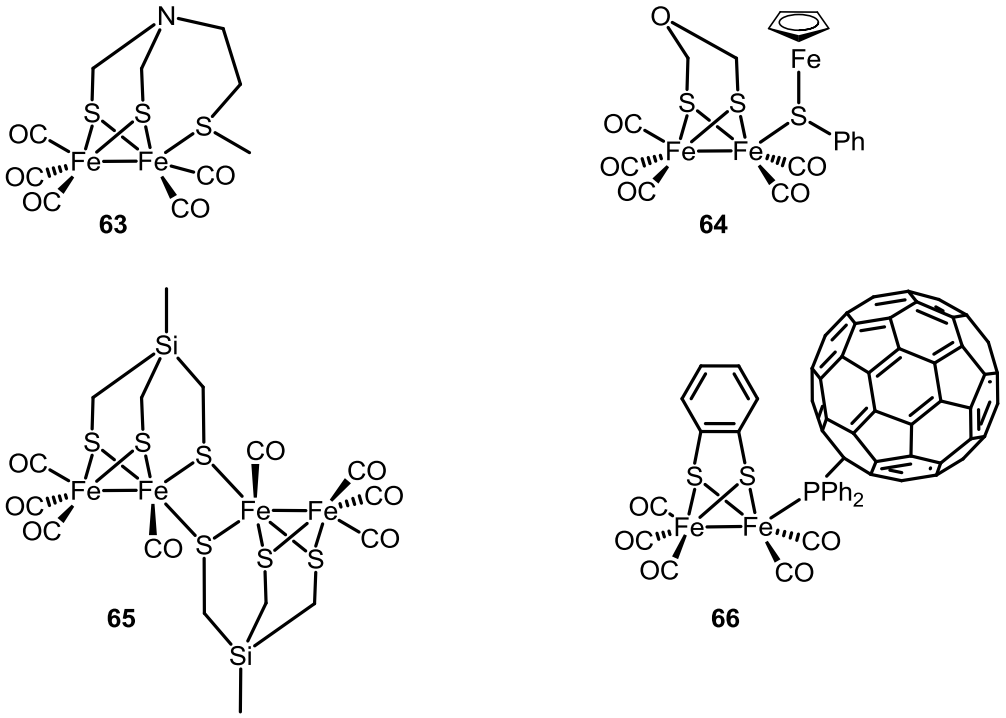

Figure 1.19 [2Fe3S]-core analogues **63** and **65** and H-cluster synthetic mimics **64** and **66**.[56a),60a)]

Recently ferrocene (Fc) derivatives have been used to mimic the H-cluster, but no electron transfer to the [2Fe]-subsite has been observed and the ferrocene component has been suggested to act as an internal standard in the electrochemical analysis.[96] In order to mimic the [4Fe4S]-cubane core, maleic anhydride, 2,2′-bipyridine and diphenylphosphine fullerene have been used; [97-99] however, only the latter example of a H-cluster synthetic mimic **66** (**Figure 1.19**) displayed an electron transfer from the fullerene to the [2Fe]-subsite moiety.

In general, a [4Fe4S]-cluster analogue needs to match the following features: oxidation potentials in the range (–0.3 V to 1.0 V vs Fc/Fc^+ couple) of the H_2/H^+ couple, strong affinity to the iron and chemical inactivity.[100] The only example of H-cluster model system in which the electron transfer component achieves all these requirements is **67**, reported by Rauchfuss and co-workers. It contains a $Cp^*Fe(C_5Me_4CH_2PEt_2)$ ($Cp^* = C_5Me_5$), as electron shuttle, an *N*-benzyl adt-based [FeFe]-complex with an amino group for proton transfer, and the strongly

electron-donating dppv ligand on one of the two irons. Electrochemical and spectroscopic analysis suggested that upon addition of one equivalent of oxidant the semi carbonyl-bridged mixed-valent intermediate [**67**]$^{+}$, bearing a vacant binding site on the Fe_d of the [2Fe]-subsite, is achieved. The second equivalent of oxidant involves the ferrocene component ($Fc \rightarrow Fc^{+}$), which is oxidised, thus producing the intermediate [**67**]$^{2+}$. In a hydrogen atmosphere, [**67**]$^{2+}$ binds hydrogen to form [**67**H_2]$^{2+}$ which through heterolytic cleavage by electron transfer from Fc^{+}, which is reduced back to Fc (**Scheme 1.16**).[100] In the presence of a base, **67** affords 0.4 turnovers of hydrogen oxidation in five hours (**Scheme 1.16**).

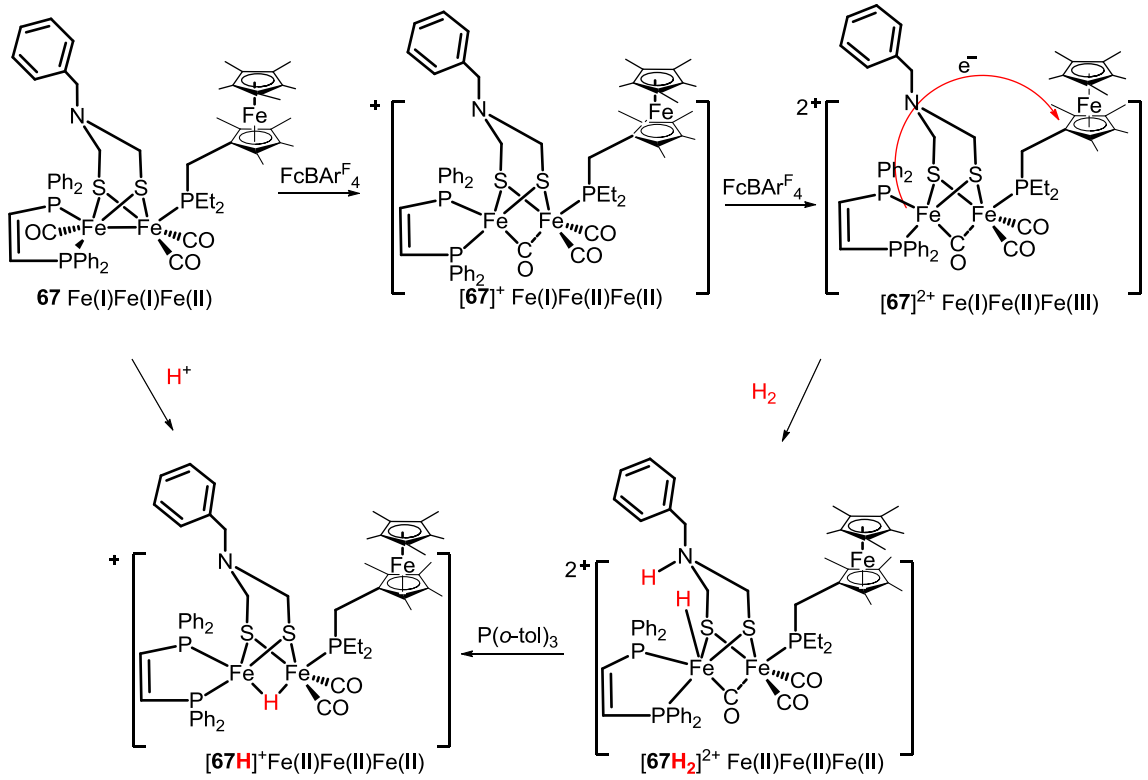

Scheme 1.16 Catalytic hydrogen activation cycle by the H-cluster synthetic mimic **67**.[100]

1.3.2.5 [FeFe]-Hydrogenase synthetic mimics in enzyme-like scaffolds

Although remarkable improvements have been achieved in understanding and reproducing synthetically the [FeFe]-hydrogenase active site, the difference in efficiency between model systems and enzyme is still significant. One of the reasons is the inability of the synthetic mimics to work in an aqueous medium and the absence of the enzymatic environment, which tunes the catalytic activity with hydrogen bonds and steric interactions. Furthermore, the protein environment protects the active site from undesired substrates and degradation.[16]

The first peptide-based synthetic mimics containing L-cysteine derivatives **68** and **69** were described by Sun and Metzler-Nolte respectively (**Figure 1.20**).

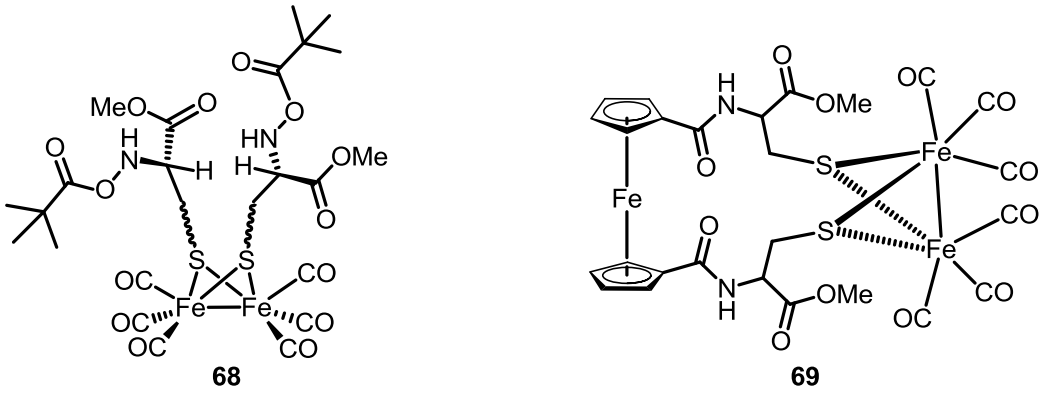

Figure 1.20 Cysteine-based [FeFe]-hydrogenase synthetic mimics **68** and **69**.[101,102]

Complex **68** contains an *N*-Boc (*tert*-butoxycarbonyl) L-cysteine methyl ester, which, however, is unstable in solution and undergoes intramolecular cyclisation.[101] Synthetic mimic **69** features a ferrocene-cysteine adduct bridging the two iron centres and is considered as H-cluster analogue due to the presence of the ferrocene as electrons transfer moiety (Section 1.3.2.4). However, electrochemical and spectroscopic measurements indicate no significant electronic interaction between the ferrocene and the [FeFe]-cluster.[102]

It has been reported that a lysine residue, which is 440 ppm distant from the [FeFe]-cluster, might act as proton source during the catalytic hydrogen evolution.[39b),103] In order to

understand whether proton transfer occurs, Weigand reported the first [FeFe]-hydrogenase synthetic mimic containing lysine derivatives **70-72** (**Figure 1.21**).

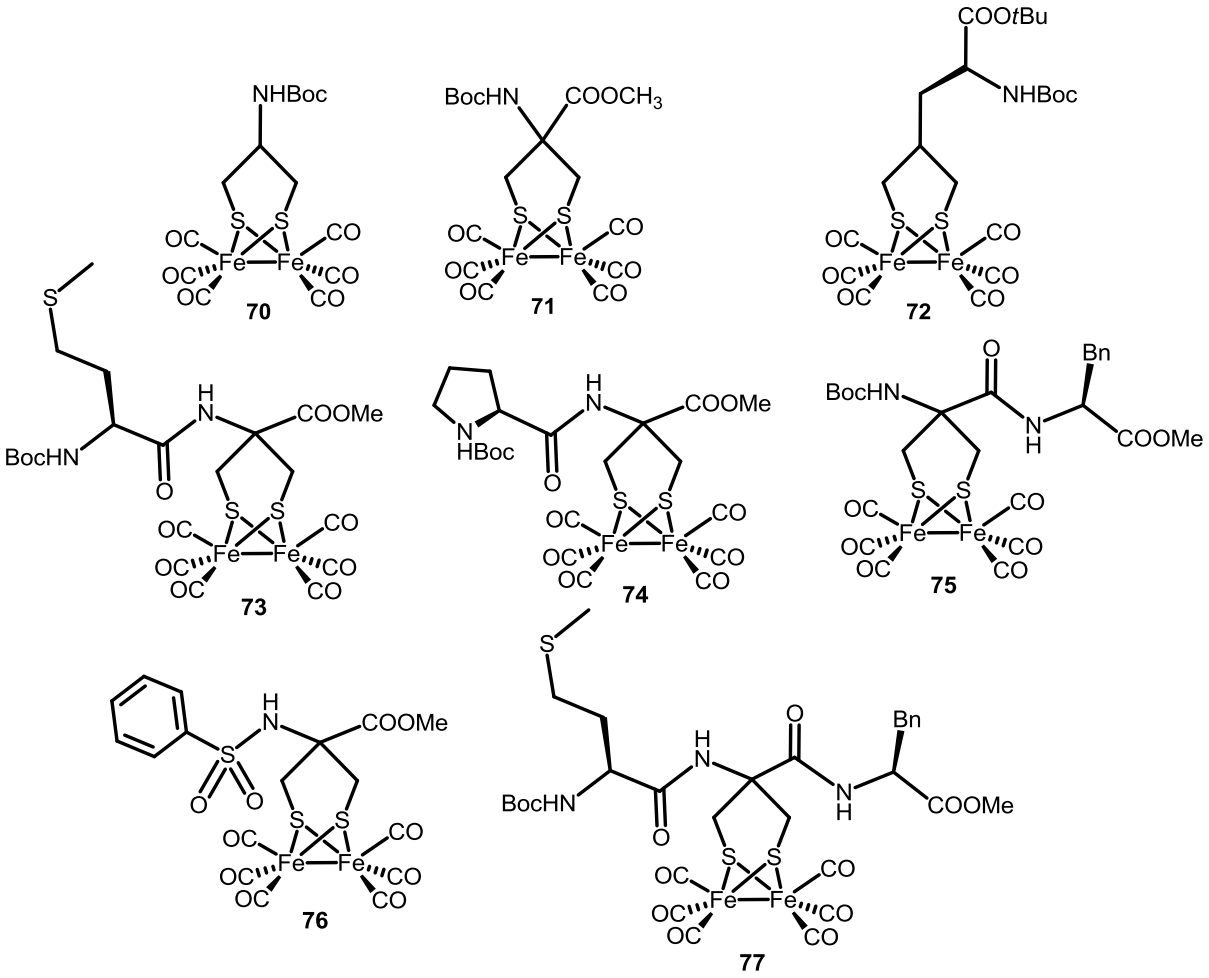

Figure 1.21 Amino acid-based [FeFe]-hydrogenase synthetic mimics **70-77**.[104]

However, although catalytic hydrogen evolution occurred, the weak acid AcOH did not protonate the amide nitrogen in complexes **70-72** and further attempts to remove the protecting group and synthesise analogues with the free amino group were unsuccessful.[104a)] Following these initial results the same group described a new series of model systems containing methionine and/or phenylalanine, **73-75**, proline, **76**, and *N*-sulfonyl moieties, **77**. However, electrochemical analysis on these complexes suggested no influence of the amino group on electrocatalytic proton reduction (**Figure 1.21**).[104b)]

Recently, the inclusion of [FeFe]-hydrogenase synthetic mimic into peptides and proteins has been developed.[16] Remarkably Jones and co-workers developed two methods to insert a hexacarbonyl [FeFe]-cluster in a peptidic scaffold. The first strategy involves the use of the *de novo* designed peptide, SynHyd1, with 32 amino acids, mainly alanines, and two cysteines in a Cys-X-X-Cys motif, necessary for bridging the iron centres. One disadvantage of this approach is that the formation of the [FeFe]-cluster is dependent on the right orientation of the two cysteines.[105a)] The second method is based on an artificial peptide with a lysine modified by a propanedithiol moiety, which reacts with $Fe_3(CO)_{12}$ giving the desired adduct.[105b)]

To identify the dithiolate bridgehead atom in the natural system, complexes **10**, **14a** and **17** (A, **Figure 1.22**) have been included into the HydF protein (from *T. maritima* expressed in *Escherichia coli*), which contains only the [4Fe4S]-cubane core (B, **Figure 1.22**) in order to complete the [FeFe]-hydrogenase maturation (C, **Figure 1.22**). The selected complexes share four carbonyls, two cyanides and the propanedithiolate backbone, but they differ in the nature of the bridgehead atom, CH_2 (**10**), NH (**14a**) and O (**17**). After the formation of the three hybrids, **10**/**14a**/**17**-HydF, only **14a**-HydF completes the enzyme's maturation and further it generates the [FeFe]-hydrogenase even when the HydF-maturase is not present (**Figure 1.22**).[43] The **14a**-enzyme hybrid displays catalytic activity towards hydrogen production in agreement with the natural system (D, **Figure 1.22**).

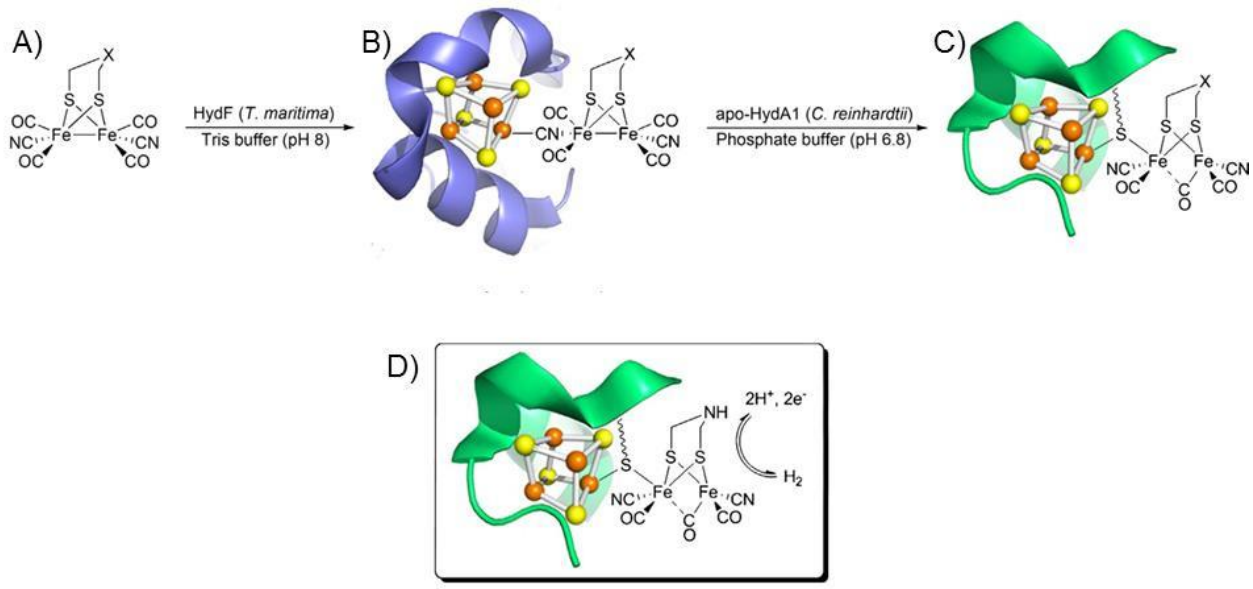

Figure 1.22 A) [FeFe]-hydrogenase synthetic mimics **10** (X = CH_2), **14a** (X = NH) and **17** (X = O); B) hybrid proteins, **10**/**14a**/**17**-HydF, containing the [4Fe4S]-cubane core; C) maturation of the fully active [FeFe]-hydrogenase; D) catalytic activity of the hybrid protein towards reversible proton reduction. The figure was used with permission from reference 43, copyright 2013 Nature Publishing Group.

Beside the use of peptides and proteins, other supramolecular scaffolds, such as gels, resins, polymers and micelles have been employed to reproduce the [FeFe]-hydrogenase active site surrounding. While the immobilization of [FeFe]-hydrogenase synthetic mimics on both gels and resins enables the design of future devices for hydrogen production, polymers and micelles increase the water solubility and provide an enzyme-like hydrophobic cavity with the same non-covalent interactions of the natural system, mainly hydrogen bonds.[16]

Following the strategy of modifying the electrode's surface and synthesising electropolymers by functionalised [FeFe]-hydrogenase synthetic mimics, reported by Gloaguen and Pickett respectively, [106,107] Darensbourg and co-workers described the use of Tentagel^{TM} resin beads as a solid support for [FeFe]-complexes. According to a previously developed procedure, [108] complex **9** (**Scheme 1.5**) was first functionalised with a carboxylic acid group then anchored

to functionalised polyethylene glycol (PEG) beads by an amide bond formation, giving the bio-inspired molecules **78-81** (**Figure 1.23**).

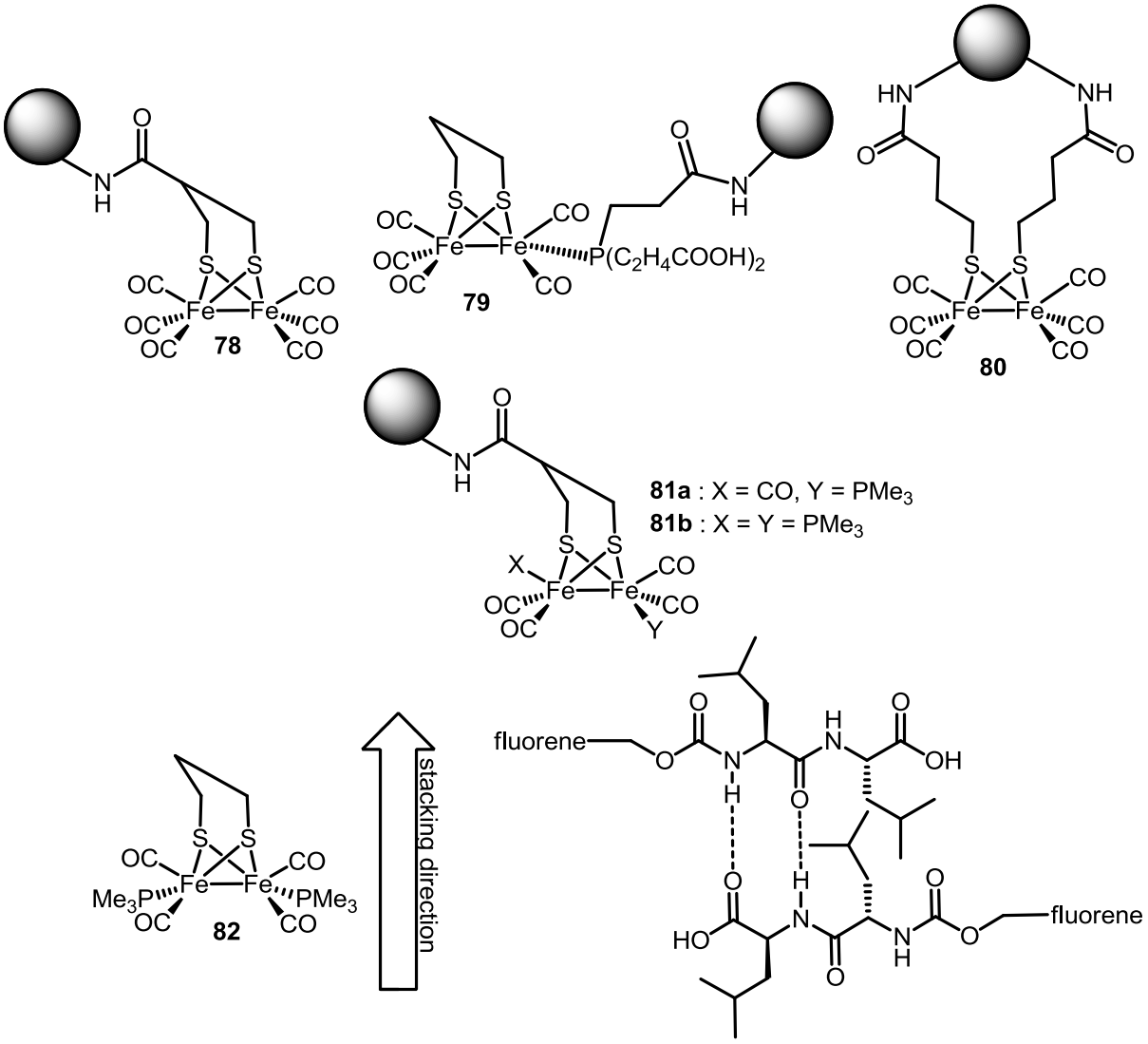

Figure 1.23 [FeFe]-synthetic mimics covalently attached to Tentagel™ resin beads **78-81**, and non-covalently attached to Fmoc-Leu-Leu dipeptide hydrogel **82**.[109,110]

The immobilised carboxylic acids-functionalised [FeFe]-complexes undergo to the same nucleophilic substitutions with phosphines and cyanides and display the same spectroscopic properties as the corresponding complexes in solution. However, the stability for the immobilised model systems is significantly decreased by the presence of PEG, which causes the loss of one carbonyl and degradation upon light exposure.[109] Pickett and co-workers

described the non-covalently insertion of [FeFe]-complex **82** into a Fmoc-Leu-Leu dipeptide hydrogel (Fmoc = fluorenyl-9-methoxycarbonyl, Leu = leucine) and studied its chemical properties by IR and ultrafast time-resolved infrared (TRIR) analysis. Complex **82** degrades in an aqueous medium, but, when it is incorporated in the hydrogel, is stable up to two weeks (**Figure 1.23**).[110]

Cyclodextrins (CyD) are widely used as scaffolds for bio-inspired synthetic models, because they possess a hydrophobic cavity to host organometallic molecules and hydrophilic hydroxy groups to provide stabilising hydrogen bonds. Darensbourg and co-workers described the insertion of **83**, [*N*-($C_6H_4SO_3^-$)-adt(Fe_2CO_6)], and the corresponding phosphine-substituted complexes **84-87** into β-CyD (**Figure 1.24**).[111] Although the water solubility of these complexes was greatly enhanced compared to the corresponding pdt-based [FeFe]-complexes, the catalytic activity towards proton reduction is dramatically affected by negative reduction potentials. Furthermore, the hydrophobic/hydrophilic character of the β-CyD results in the absorption onto the electrode surface thus complicating the electrochemical measurements.

However, the insertion of **83** along with organic dyes (Eosin Y, EY and Rose Bengal, RB), as photosensitizers, and triethylamine (NEt_3), as electron-donor, in cyclodextrins (β and γ) enhances the photocatalytic hydrogen production, due to the significant increase in water solubility and photostability. Furthermore, cyclodextrins favour electron transfer from the organic dye to the [FeFe]-cluster and enhance the efficiency of the system. Particularly, in the presence of EY in an excess of γ-CyD, complex **83** continuously generates hydrogen for 75 turnovers.[111c)]

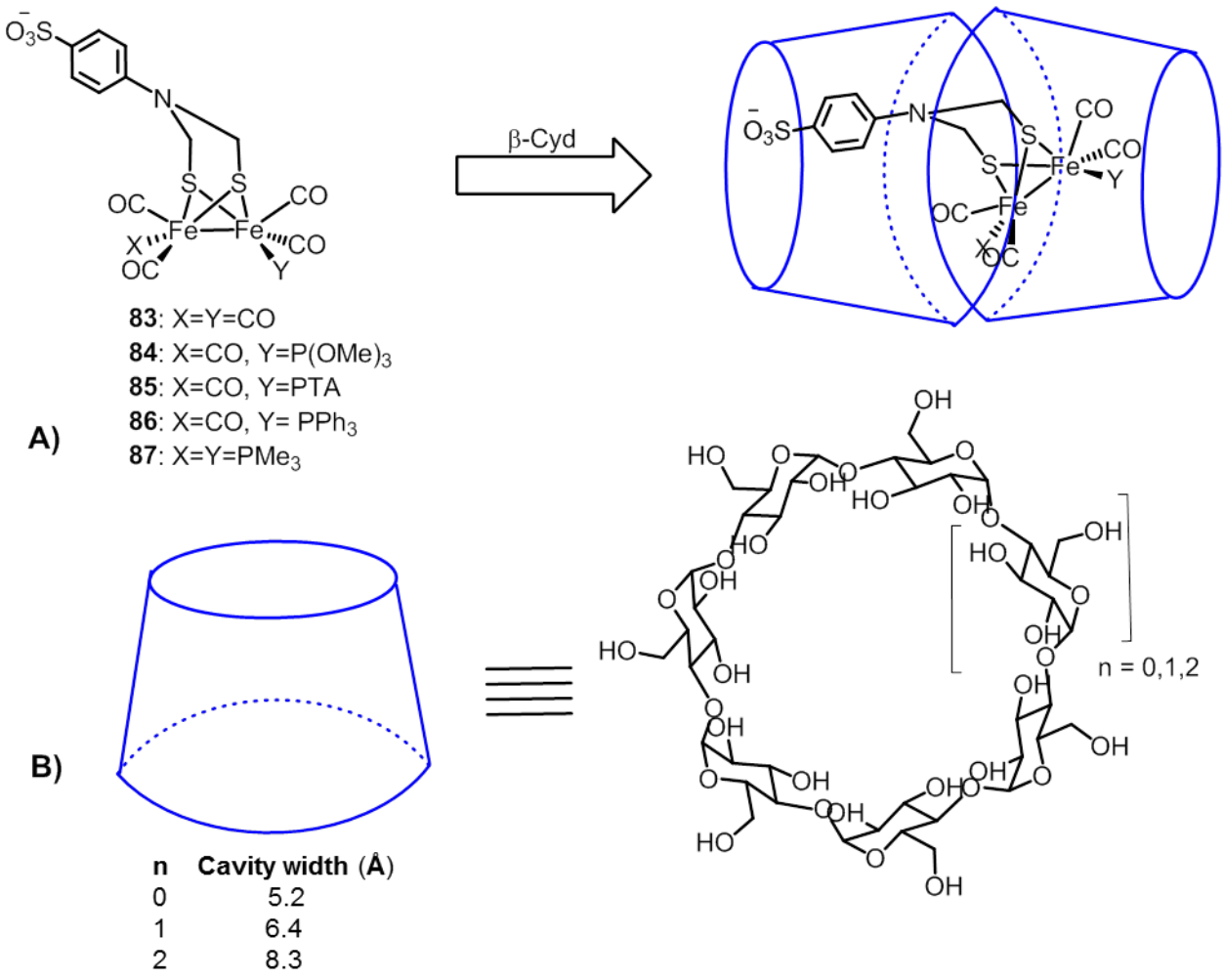

Figure 1.24 A) Insertion of *N*-benzenesulfonate-substituted [FeFe]-hydrogenase synthetic mimics **83-87** in β-CyD scaffold. B) According to the number of the extra sugar ring (n), cyclodextrins are classified as α-CyD (n = 0), β-CyD (n = 1) and γ-CyD (n = 2).

To summarise, in terms of structure similarity, remarkable progress has been achieved with the synthesis of [FeFe]-hydrogenase inspired systems, especially with the development of synthetic terminal hydrides and with carbonyl-bridged mixed valent synthetic intermediates. However, the reported analogues do not resemble the active site of the enzyme, because of their abiological iron ligands. Furthermore, not enough attention has been driven towards the inclusion of an electron transfer component. In terms of catalytic activity, many [FeFe]-hydrogenase synthetic mimics are active towards proton reduction, but the reaction efficiency and rate is not comparable to that reported for the enzyme. Furthermore most of the active site

analogues of the enzyme display electrocatalytic activity with very negative potentials and employ wrong redox states for the iron, Fe(I)Fe(I) instead of Fe(II)Fe(I) in the natural system. Moreover, [FeFe]-hydrogenase synthetic mimic, which perform both proton reduction and hydrogen oxidation are still rare and inefficient.

Chapter 2: Variation of chalcogens, aromatic backbone and *ortho* naphthalene substituent on ligands

2.1 Aromatic ligand-based [FeFe]-hydrogenase synthetic mimics

The hexacarbonyl pdt-based [FeFe]-complex **9** affords unstable intermediates under reducing conditions due to CO transfer and fragmentation, which reduce the proton reduction catalytic efficiency (**Scheme 1.6**, Chapter 1).[52] Accordingly, [FeFe]-hydrogenase synthetic mimics with unsaturated ligands have been introduced in order to enhance the stability of the reduced species by delocalization of the negative charge on the aromatic backbone.

The advantage of using aromatic ligands was first investigated by Gloaguen and co-workers, who reported the hexacarbonyl benzenedithiolate-bridged (bdt) [FeFe]-complexes, **88**, as viable [FeFe]-hydrogenase synthetic mimics (**Figure 2.1**).[112]

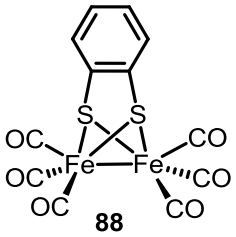

88

Figure 2.1 Bdt-based [FeFe]-complex **88**.[112]

Electrochemical analysis of complex **88** showed one reversible two electron-reduction, assigned to Fe(I)-Fe(I)→Fe(0)Fe(0), and it confirmed the aromaticity-induced stability of the reduced species. In addition, the electron-withdrawing benzene ring decreases the electron-density of the iron centres causing a shift towards less negative reduction potential, –1.44 V for **88** vs –1.60 V for **9**.[52,112] Upon treatment of [FeFe]-complex **88** with both fluoroboric acid (HBF_4) and *p*TsOH, the reversibility of the process was lost and the reduction wave was shifted to more positive potentials than –1.44 V, while the corresponding peak current increased with the acid concentration, confirming the reduced species, Fe(0)Fe(0), as a proton reduction catalyst.[112] Further electrochemical studies, in the presence of the weak AcOH (pKa = 22.3 in CH_3CN) and DFT calculations suggested a proton reduction mechanism for [FeFe]-

complex **88**.[113] The two electron-reduction promotes the cleavage of an Fe–S bond and the transfer of one carbonyl group from a terminal to a bridging position, generating the species [**88**]$^{2-}$. Reaction with AcOH produces the hydride-bridged species [**88**H]$^{-}$, which is further reduced and finally protonated to release hydrogen and the anion [**88**]$^{-}$ (**Scheme 2.1**).

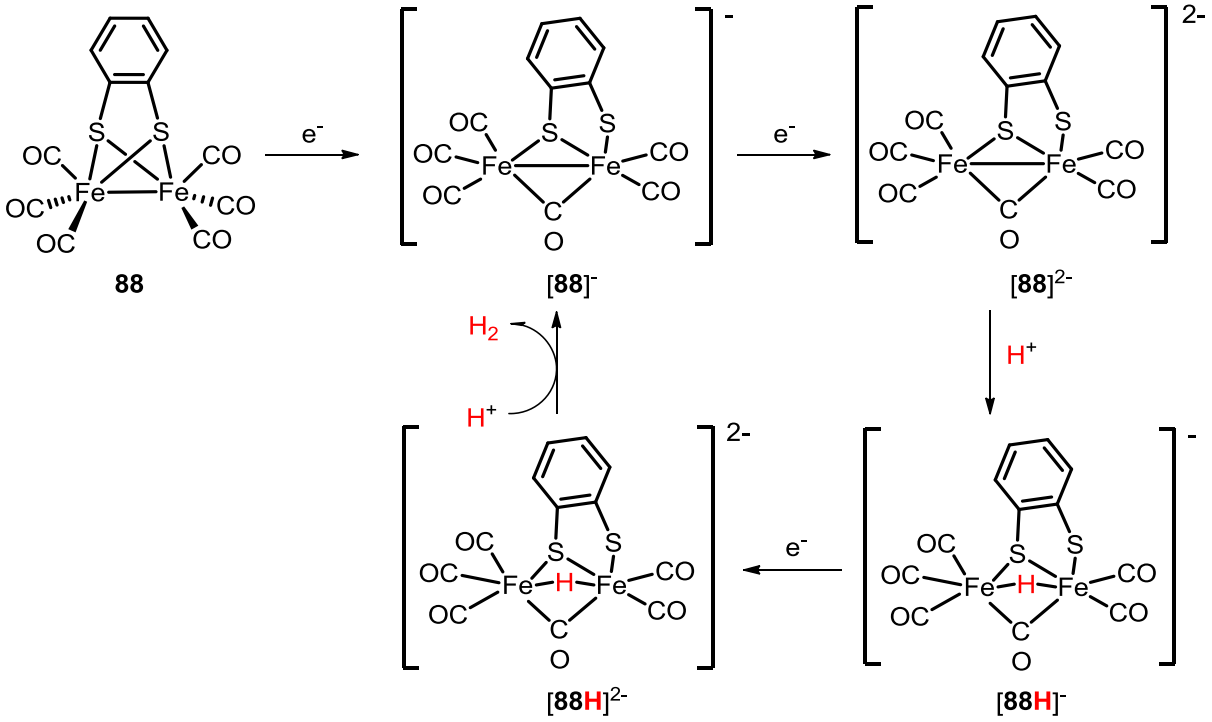

Scheme 2.1 Proposed proton reduction mechanism of [FeFe]-complex **88**.[113]

The above mechanism was confirmed by Tilley and co-workers, who obtained the X-ray crystal structure of the dianion [**88**]$^{2-}$ (**Scheme 2.1**). Additional spectroscopic analyses (^{1}H NMR, IR) gave further evidence of reaction of [**88**]$^{2-}$ with strong (TfOH) and weak (AcOH) acids and DFT calculations showed that the first protonation occurs at the iron centres in either a bridging or terminal position, while the second at the non-bridging thiolate.[114] Similar protonated intermediates were reported by Liu and co-workers, who replaced the bridging carbonyl with a diphenyl phosphine group.[115]

Electron-withdrawing substituents, particularly chlorines, in one or more positions on the benzene ring, promote the reduction of the [FeFe]-cluster at less negative potentials than the non-substituted complex **88**.[116,117] On the other hand, electron-donating groups in the *ortho* positions to the [FeFe]-cluster increase the proton reduction catalytic efficiency by enhancing the basicity of the dianion [**88**]$^{-}$ (**Scheme 2.1**) and the ability to bind protons.[118]

The synthesis of [FeFe]-hydrogenase analogues have been also achieved by using other aromatic backbones, such as *o*-carborane and biphenyl derivatives.[119,120]

Naphthalene *peri*-substituted dichalcogenides have been intensively employed in coordination chemistry with transition metals.[121] Among these studies, Tilley and co-workers, investigated the naphthalene-1,8-dithiole and derivatives as ligands for the [FeFe]-hydrogenase model systems and reported the synthesis and analysis of the [FeFe]-complexes **89a-c** (**Figure 2.2**).[122]

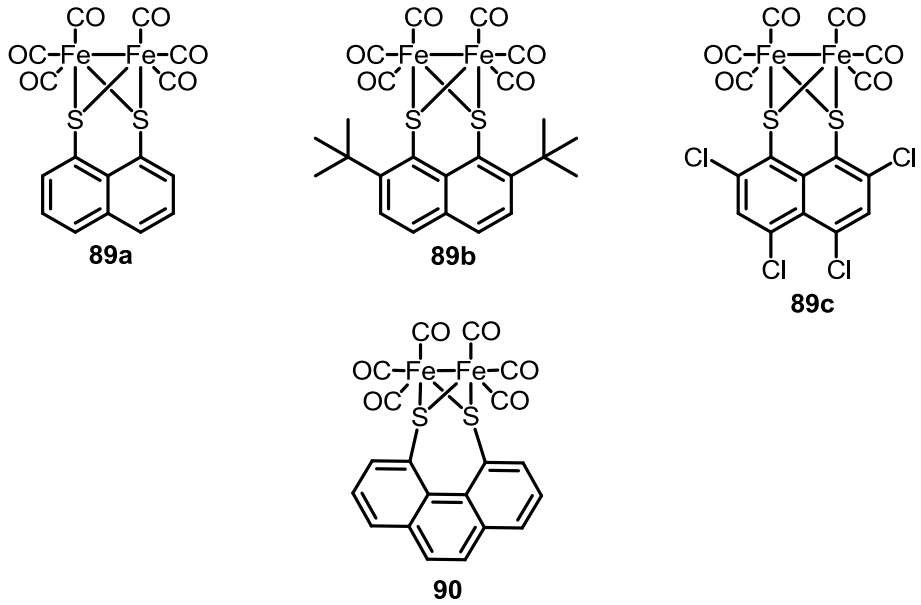

Figure 2.2 Naphthalene-1,8-dithioles and phenanthrene-4,5-dithiine-based [FeFe]-complexes **89a-c** and **90**.[122,125]

Cyclic voltammetry showed that the presence of the electron-withdrawing naphthalene shifts the reduction potential of complexes **89a-c** towards less negative values than the

hexacarbonyl pdt-based [FeFe]-complex **9** (**Scheme 1.6**, Chapter 1). In the case of **89a-b**, the rigid naphthalene backbone stabilises the corresponding reduced species (Section 2.3.3). The nature of the naphthalene ring substituents affects the [FeFe]-cluster redox properties. The electron-deficient complex **89c** is the easiest to reduce and the most efficient catalyst towards *p*TsOH reduction, confirming what has been previously observed for the chloro-substituted bdt-based [FeFe]-complexes.[116,117] However, the irreversibility of the two reduction processes for **89c** suggest decomposition of the corresponding reduced species.

Based on Tilley and co-workers work, other examples of naphthalene-based [FeFe]-hydrogenase synthetic mimics have been reported [123,124] and some of them have been investigated as photoactive proton reduction catalysts (Chapter 3).

Mebi and co-workers reported the only example of an [FeFe]-hydrogenase model system **90** based on the aromatic phenanthrene (**Figure 2.2**).[125] Electrochemical analysis of complex **90** showed a quasi-irreversible one electron-reduction at –1.27 V, which was assigned to the process Fe(I)-Fe(I)→Fe(0)Fe(I). Even though complex **90** appears to be less stable than **88** and **89a-c**, the electron-withdrawing effect of the phenanthrene is higher than that of the benzene and the naphthalene backbone, promoting a shift of 0.3 V towards less negative values compared to the reduction potential of complex **9**.[52]

2.2 Aims and objectives

This chapter describes the work on the synthesis and electrochemical analysis of a series of [FeFe]-hydrogenase synthetic mimics, based on *peri*-substituted naphthalene, **89d**, **91a-d** and **92a-d** (**Figure 2.3**).

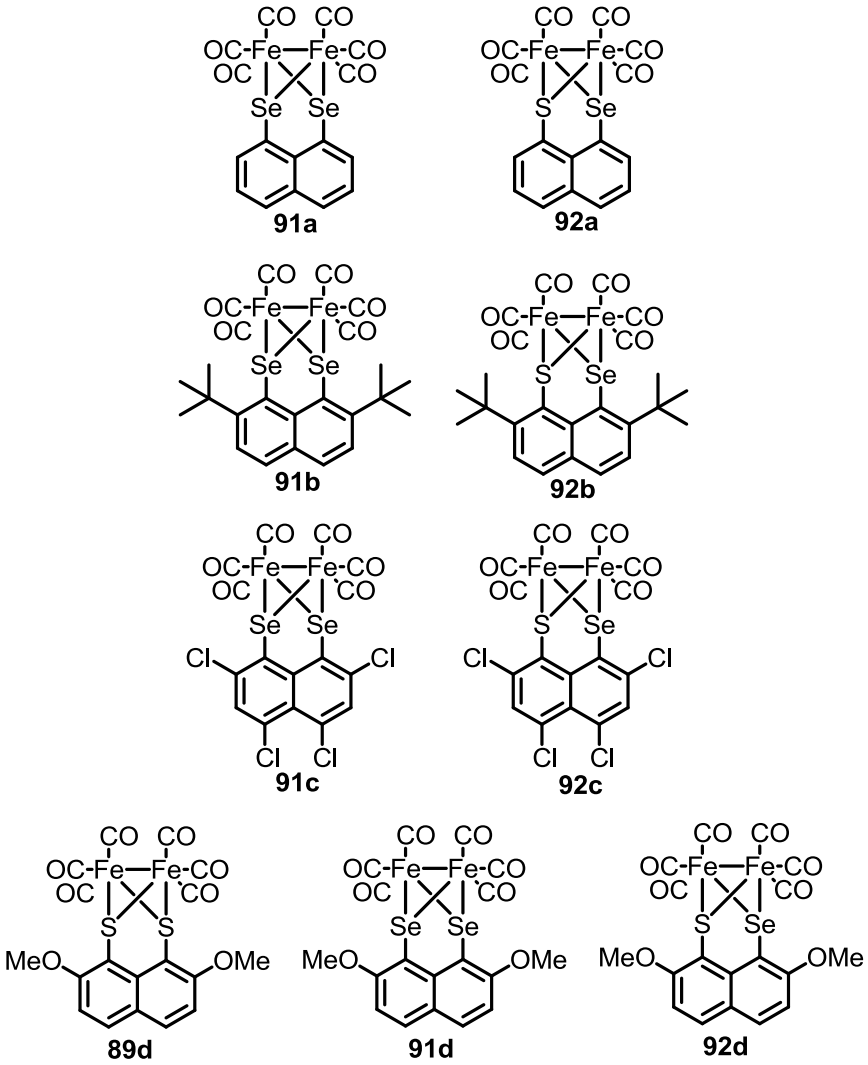

Figure 2.3 Target *peri*-substituted naphthalene-based [FeFe]-complexes **89d**, **91a-d** and **92a-d**.

Based on previous studies on diselenolate-bridged [FeFe]-complexes (Section 1.3.2.4, Chapter 1) and following Tilley's work (**Figure 2.2** , Section 1), [122] replacement of either both or a single sulfur from **89a-c** with selenium was proposed to give **91a-c** and **92a-c** (respectively) with the aim of studying the effect of the selenium on the electrochemical properties of the naphthalene-bridged [FeFe]-cluster. In addition to the *ortho tert*-butyl (*t*Bu) substituents of **89b**, methoxy groups (OMe) were proposed to further study the effect on the [FeFe]-cluster in complexes **89d**, **91d** and **92d**.

In the continuation of Mebi's work, [FeFe]-complexes **93** and **94**, based on phenathrene-1,10-dichalcogenides, and **95**, containing the linear conjugated system anthracene, were targeted. In addition, the synthesis of [FeFe]-complexes **96** and **97**, containing the non-fused fluorene, whose structure is comparable to that of a biphenyl system, [120] were envisioned (**Figure 2.4**).

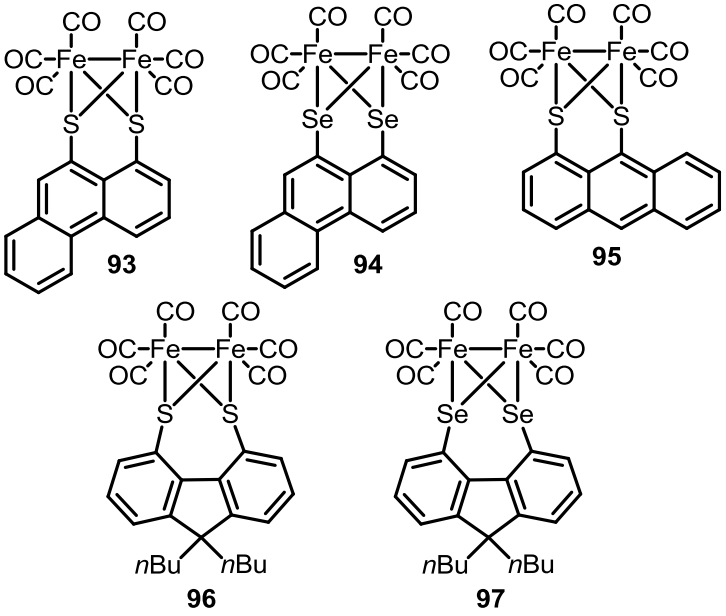

Figure 2.4 Proposed linear conjugated aromatic-based [FeFe]-complexes **93-95** and non-fused aromatic-based [FeFe]-complexes **96** and **97**.

2.3 Results and discussion

2.3.1 Synthesis of *peri*-substituted aromatic ligands

Following Woollins and co-workers procedure, [126] naphthalene-1,8-diselenole **99a** [127] was synthesised in moderate yield from the commercially available naphthalene **98**, via lithiation in position 1 and 8 on the aromatic ring with *n*butyl lithium (*n*BuLi) and subsequent quenching with elemental selenium (**Scheme 2.2**).[126]

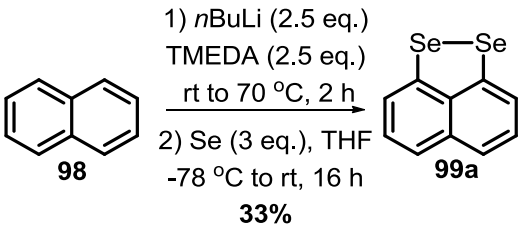

Scheme 2.2 Synthesis of diselenoles **99a**.

Previous studies in the Grainger group showed that Friedel-Craft *ortho* alkylation of naphthalene-1,8-dithiole **100a** using catalytic amount of iron trichloride ($FeCl_3$), instead of aluminium trichloride ($AlCl_3$), [128,129] and *tert*-butylbromide (*t*BuBr) gave the desired regioisomer **100b** in moderate yield and the reaction outcome was highly reproducible.[130] Accordingly, 2,7-di-*tert*-butylnaphthalene-1,8-diselenole **99b** was obtained by applying the same reaction conditions on compound **99a**. However, the equivalents of $FeCl_3$ were increased from 0.05 to 0.20 and the reaction yields improved (**Scheme 2.3**).

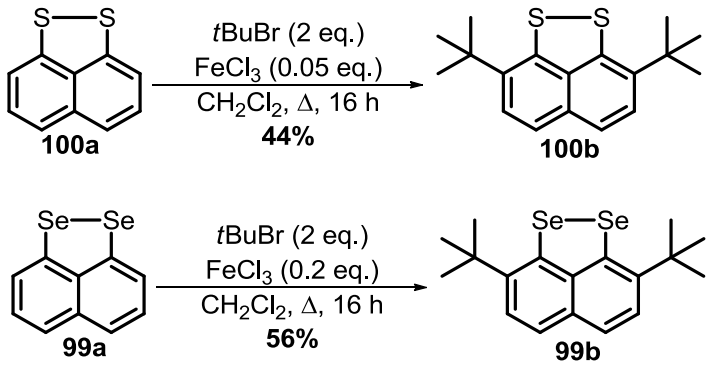

Scheme 2.3 Friedel-Craft *ortho* alkylation on dichalcogenides **99a** and **100a**.

Nucleophilic aromatic substitution on 1-bromonaphthalene **101** with sodium ethanethiolate (NaEtS) generated the naphthalene-1-thiol **102** (**Scheme 2.4**) as previously described in the literature.[131] Treatment of **102** with *n*BuLi in a mixture of TMEDA/hexane (1.1:1) resulted in deprotonation of the thiol and lithiation of position 8 on the naphthalene ring, which upon quenching with elemental selenium afforded the thiaselenole **103a** in comparable yield with

that in the literature.[132] The novel 2,7-di-*tert*-butylnaphthalene-1,8-thiaselenole **103b** was synthesised by applying the same reaction conditions described for compound **99b** (**Scheme 2.3**).

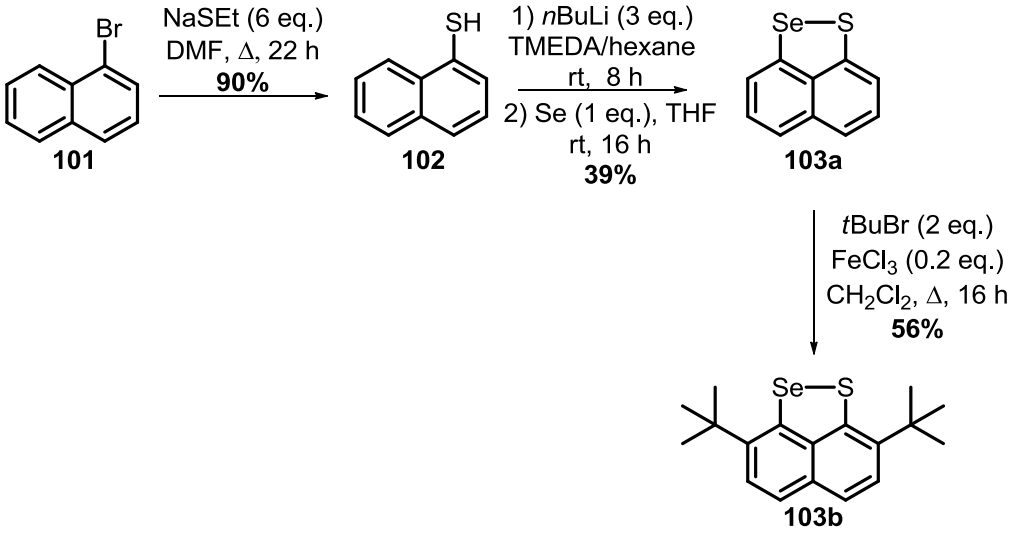

Scheme 2.4 Synthesis of thiaselenoles **103a-b**.

Tilley and co-workers showed that reaction of naphthalene-1,8-dithiole **100a** with an excess of chlorinating agent *N*-chlorosuccinimide (NCS) gave 2,4,5,7-tetrachloronaphthalene-1,8-dithiole **100c**.[122] The reaction was performed on the diselenole **99a** and the novel 2,4,5,7-tetrachloronaphthalene-1,8-diselenole **99c** was isolated, but in lower yield than the corresponding dithiole **100c**, 21% and 62% respectively. The low solubility of compound **99c** in common organic solvents made the isolation and purification of the desired product by column chromatography difficult. Attempt to synthesise 2,4,5,7-tetrachloronaphthalene-1,8-thiaselenole **103c** applying the same procedure, described for **99c** and **100c**, was unsuccessful and resulted in the formation of an unidentified insoluble compound possibly from decomposition of the starting material (**Scheme 2.5**).

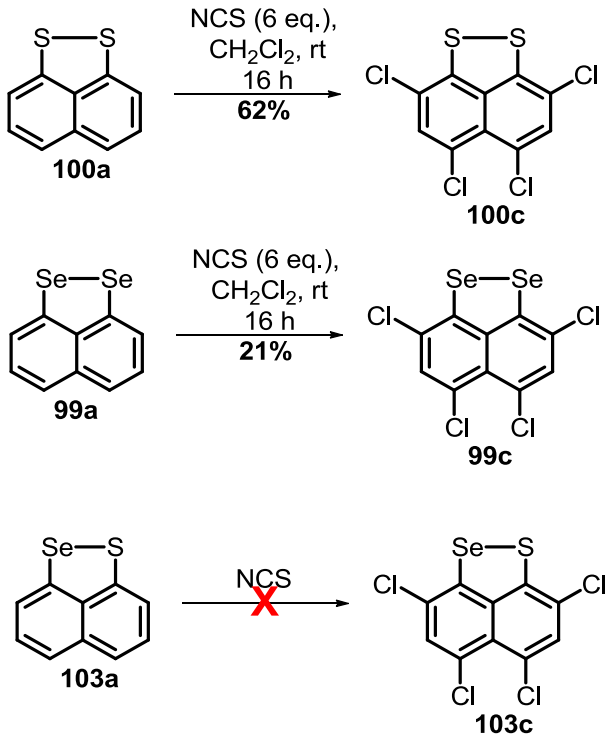

Scheme 2.5 Chlorination of dichalcogenides **99a**, **100a** and **103a**.

With the objective of synthesising [FeFe]-complexes **89d**, **91d** and **92d** (**Figure 2.3**, Section 2.2), the synthesis of dichalcogenides **99d**, **100d** and **103d** containing two OMe groups in the *ortho* positions on the naphthalene ring was investigated.

As previously described, methylation of 2,7-dihydroxynaphthalene **104** with dimethylsulfate (Me_2SO_4) gave 2,7-dimethoxynaphthalene **105**, [133] which reacted with a 1:1 mixture of an excess of pyridine (Py) and brominating agent *N*-bromosuccinimide (NBS) to give 1,8-dibromo-2,7-dimethoxynaphthalene **106** in high yield.[134] Lithiation of **106** with *n*BuLi and subsequent quenching with either recrystallized sulfur or elemental selenium afforded the dithiole **106d** and diselenole **99d** (respectively) in comparable yields to those reported in the literature (**Scheme 2.6**).[130,135]

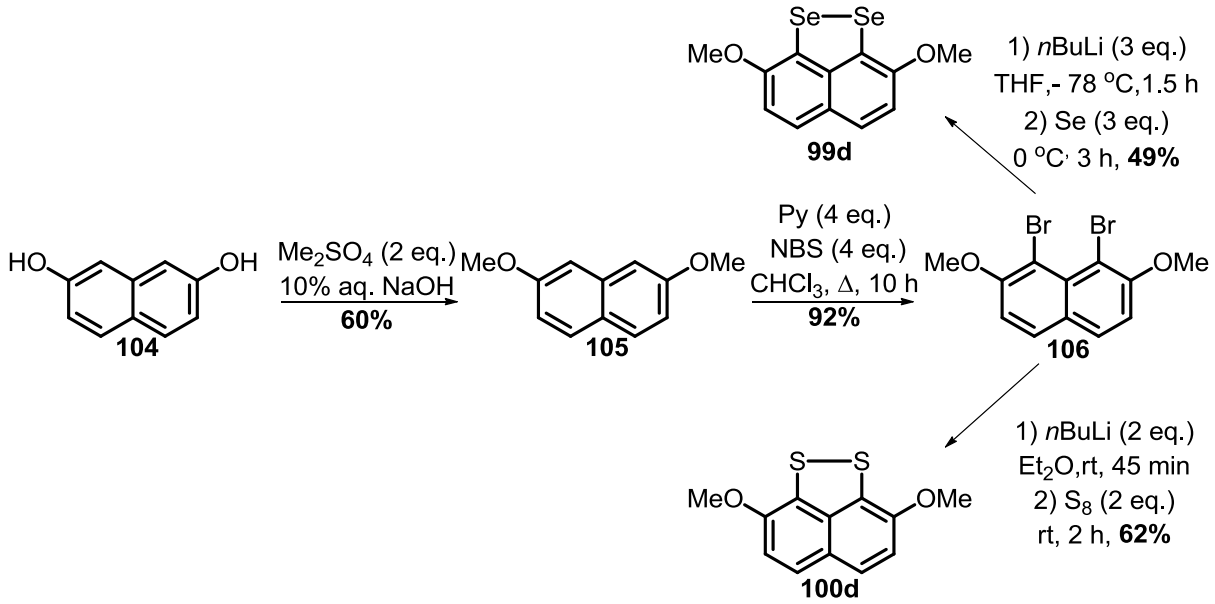

Scheme 2.6 Synthesis of 2,7-dimethoxynaphthalene-1,2-diselenole **99d** and dithiole **100d**.

Bromination of one *peri* position in **105**, using a 1:1 mixture of stoichiometric amount of Py and NBS, [130] afforded the novel 1-bromo-2,7-dimethoxynaphthalene **107** in high yield.

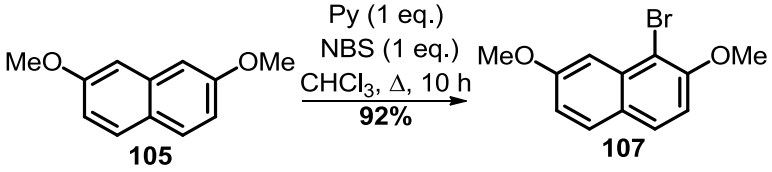

Scheme 2.7 Synthesis of 1-bromo-2,7-dimethoxynaphthalene **107**.

Following the literature procedure used for compound **99d** and **100d**, [130,135] lithiation of **107** with *n*BuLi and subsequent quenching with recrystallized sulfur gave the expected 2,7-dimethoxynaphthalene-1-thiol **108** in low yield (entries 2 and 4, **Table 2.1**). Variation of reaction time and equivalents of both *n*BuLi and sulfur did not improve the yields of the isolated **108** (entries 1, 5 and 6, **Table 2.1**). In order to exclude oxidation of the thiolate to disulfide (see below), reaction with a large excess of $LiAlH_4$ was performed after sulfur incorporation and before isolating the product; [136] however, thiol **108** was afforded in only 5%

yield (entry 3, **Table 2.1**). In all the attempts, the ^{1}H NMR analysis of purified **108** showed the presence of unidentified by-products and thus no further reactions were attempted.

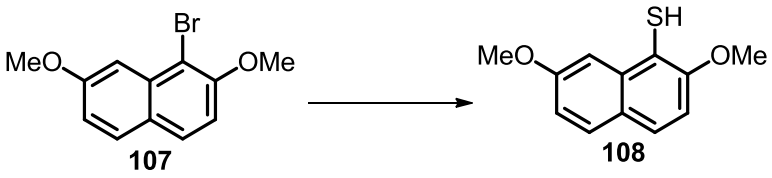

Table 2.1 Lithiation with *n*BuLi and consecutive substitution with sulfur to obtain **108**.

Entry	*n*BuLi/S_8 solvent	work-up	time 1st/2nd step	Reducing agent	% yield 108	References
1	1.4/1.4 eq. THF	aq. HCl	45min/3 h	-	19[a]	135
2	1.4/1.4 eq. THF	aq. HCl	1.5/3 h	-	14[a]	135
3	1.5/1.5 eq. THF	aq.NH_4Cl	1.5/12 h	$LiAlH_4$ (15.6 eq.)	5[a]	136
4	1.1/1.1 eq. Et_2O	aq.NH_4Cl	45min/2 h	-	23[a]	130
5	1.5/1.5 eq. THF	aq. HCl	1.5/12 h	-	-	135
6	1.5/1.1 eq Et_2O	aq. HCl	45min/2 h	-	16[a]	130

[a] Contamination shown by ^{1}H NMR spectroscopy.

Attempts to obtain 2,7-dimethoxynaphthalene-1,2-thiaselenole **103d** directly from **107** via formation of thiol **108** *in situ* was unsuccessful and a mixture of unidentified compounds was observed (**Scheme 2.8**).

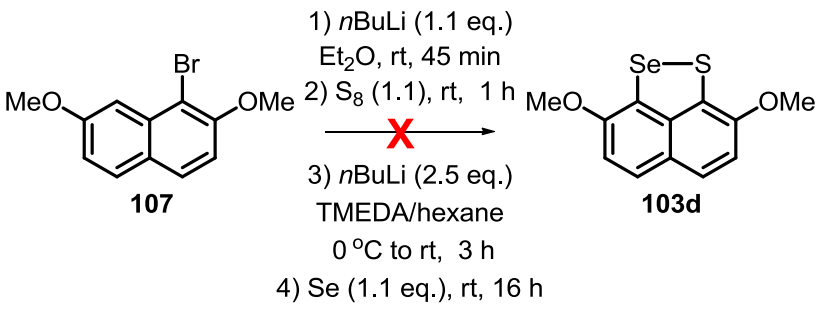

Scheme 2.8 Attempted synthesis of thiaselenole **103d** from **107**.

Dithiocarbamates can be considered as protected thiols and can be readily introduced into organic molecules by a variety of methods.[137] Reaction of **107** with *n*BuLi and subsequent substitution with bis(*N*,*N*-dimethylthiocarbamoyl)-disulfide generated the novel 2,7-dimethoxynaphthalne-1-dimethylcarbamodithioate **109** (**Scheme 2.9**).[137]

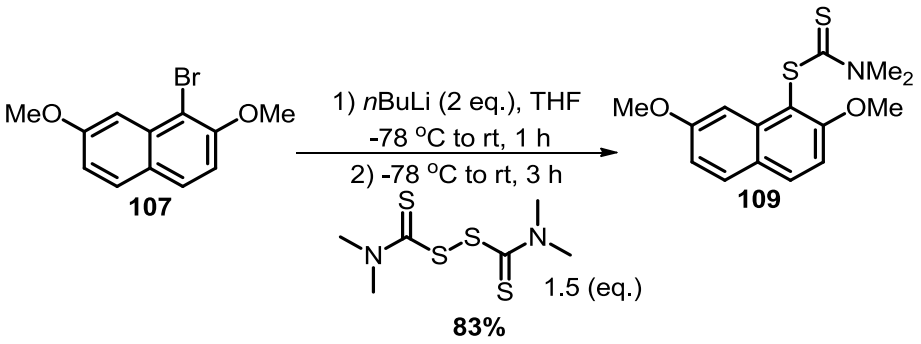

Scheme 2.9 Synthesis of the dithiocarbamate **109**.

Table 1.2 shows the attempted formation of thiol **108** by reduction with $LiAlH_4$ (entries 1-4), hydrolysis with KOH or NaOH (entries 5 and 6) and nucleophilic displacement with $N_2H_4{\cdot}H_2O$ and NaSEt (entries 7 and 8) of the dithiocarbamate **109**. It suggested that thiolate **110**, formed in the presence of an excess of base (in the reaction mixture and in the work-up) is oxidised to disulfide **111** (entries 2, 5 and 6, **Table 2.2**), whose structure was confirmed by mass spectrometry. However, compound **111** was also isolated in the absence of a base and even in degassed solvents (entries 7 and 8, **Table 2.2**). Under reducing conditions ($LiAlH_4$) the disulfide was not observed and thiol **108** was obtained either in low yield (entry 1, **Table 2.2**), contaminated as shown by ^{1}H NMR spectroscopy (entries 3 and 4) or it is not formed (entry 2).

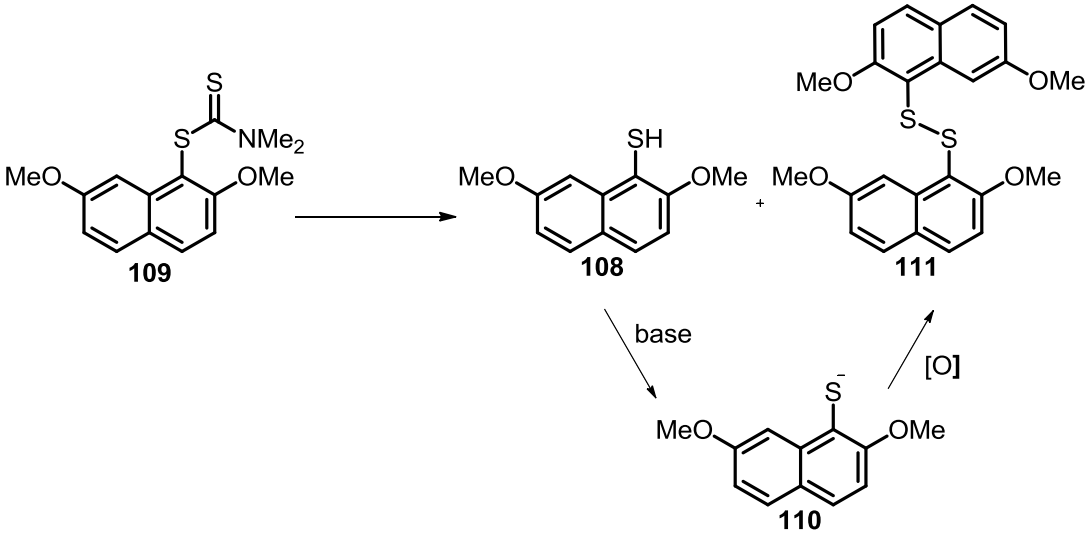

Table 2.2 Attempted reduction, hydrolysis and nucleophilic displacement of **109** to form the thiol **108**.

Entry	Reducing agent	Reaction conditions	%yield 109	%yield 108	%yield 111	References
1	$LiAlH_4$ (1 eq.)	THF, Δ, 1 h, aq. NH_4Cl	-	16	-	136
2	$LiAlH_4$ (5 eq.)	THF, 0→60°C, 8 h, 4 M NaOH	20	-	traces	138
3	$LiAlH_4$ (5 eq.)	Et_2O, 0°C→Δ, 4 h, 10% aq. HCl	-	14[a]	-	139
4	$LiAlH_4$ (8 eq.)	THF, 0→60°C, 2 h, 4 M NaOH	-	44[a]	-	
5	KOH (9 eq.)	MeOH, 0→60°C, 24 h	38	-	traces	140
6	NaOH (5 eq.)	H_2O/EtOH, Δ, 7 h	50	-	traces	141
7	$N_2H_4{\cdot}H_2O$	EtOH, Δ, 4 h	-	32	6	141
8	NaSEt (5 eq.)	EtOH, Δ, 6 h	-	28	11	141

[a] Contamination shown by ^{1}H NMR spectroscopy.

In a further attempt to obtain 2,7-dimethoxynaphthalene-1,8-thiaselenole **103d**, thiol **108** was reacted with *n*BuLi and elemental selenium. Directed deprotonation of 1-thiolnaphthalene **102**

at the 8-position has been previously described for the synthesis of analogous thiaselenole **103a** (**Scheme 2.4**).[132,130] However, this reaction resulted mainly in the recovery of the thiol **108** (41%) and in the isolation of the *n*butyl-substituted sulfide **112** (12%), whose structure was confirmed by ^{1}H and ^{13}C NMR spectroscopy and mass spectrometry. Traces of disulfide **111** (3%) were also present in the crude mixture (**Scheme 2.10**).

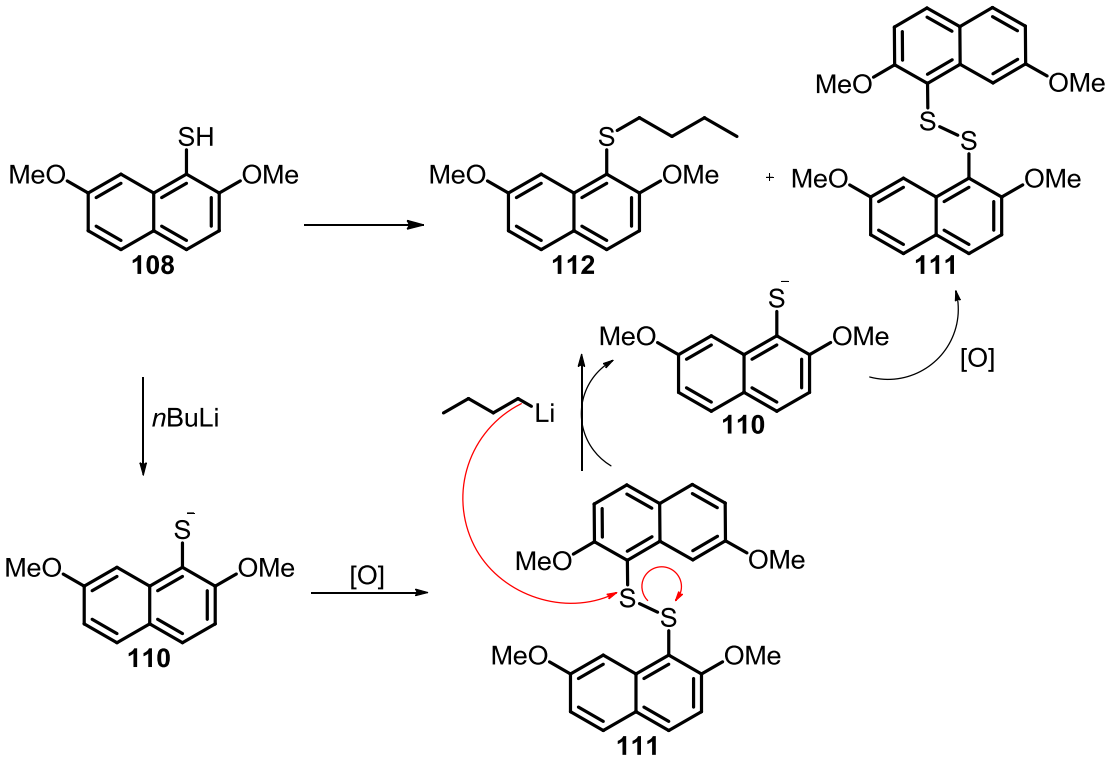

Scheme 2.10 Proposed mechanism for the formation of **111** and **112** upon lithiation of **108**.

Addition of D_2O to the reaction mixture of **108** and *n*BuLi suggested that lithiation of the *peri* position 8 does not occur. Disulfide **111** and the corresponding alkylated sulfide **112** were instead isolated in 5% and 40% yields respectively (**Scheme 2.10**). Quenching the reaction of **111** and *n*BuLi with D_2O gave a mixture of unidentified compounds. The proposed mechanism for the reaction of thiol **108** with *n*BuLi is shown in Scheme 2.10: *n*BuLi deprotonates thiol **108** to form thiolate **110**, which is oxidized *in situ* to the corresponding

disulfide **111**. Since *n*BuLi is present in excess in the reaction mixture, it reacts with **111** in a S_N2 reaction, forming the sulfide **112** and thiolate **110**, which is then re-oxidised.

In order to obtain [FeFe]-complexes **93** and **94** (**Figure 2.4**, Section 2.2) phenanthrene-1,10-dithiole **113** and the corresponding diselenole **114** were targeted.

Following Ashe and co-workers' procedure, [142] phenanthrene-1,10-dithiole **113** was obtained by lithiation of position 1 and 10 of 9-bromophenanthrene **115** and subsequent quenching with recrystallized sulfur in comparable yield with those reported in the literature. The same procedure was then applied to generate the novel diselenole **114**, but in lower yield than those described for compound **113** (**Scheme 2.11**).

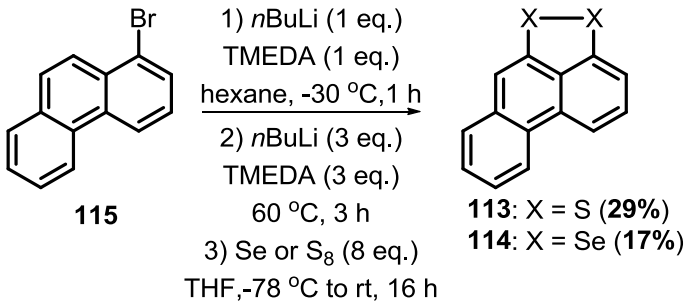

Scheme 2.11 Synthesis of phenanthrene-1,10-dithiole **113** and diselenole **114**.

The same synthetic approach was investigated in order to obtain the anthracene-1,9-dithiole **116** as ligand for [FeFe]-complex **95** (**Figure 2.4**, Section 2.2).[130,142] However, lithiation of 9-bromoanthracene **117** and subsequent addition of recrystallized sulfur gave a mixture of the expected dichalcogenide **116** (6%) and the *n*butyl-substituted anthracene **118** (7%), whose structure was confirmed by ^1H and ^{13}C NMR spectroscopy and mass spectrometry (**Scheme 2.12**). The mixture was difficult to separate by column chromatography, using either silica gel or alumina. Therefore, attempts to separate the mixture by either oxidation with *meta*-chloroperoxybenzoic acid (*m*CPBA) or reduction with $LiAlH_4$ of the S–S bond in **116** were performed, but unsuccessfully. The oxidative insertion of $Fe_3(CO)_{12}$ (Section 2.3.2) was also

attempted in order to obtain the [FeFe]-complex **95** (**Figure 2.5**) directly from the mixture of **116** and **118**, but the expected complex was not observed. Therefore, following the synthetic procedure described for **103a**, thiol **119** was obtained in comparable yield with the literature (**Scheme 2.12**).[131] Direct deprotonation of the known anthracene-1-thiol **119** at the *peri* position 9 with *n*BuLi was investigated. However, the reaction resulted, presumably, in the decomposition of the substrate.

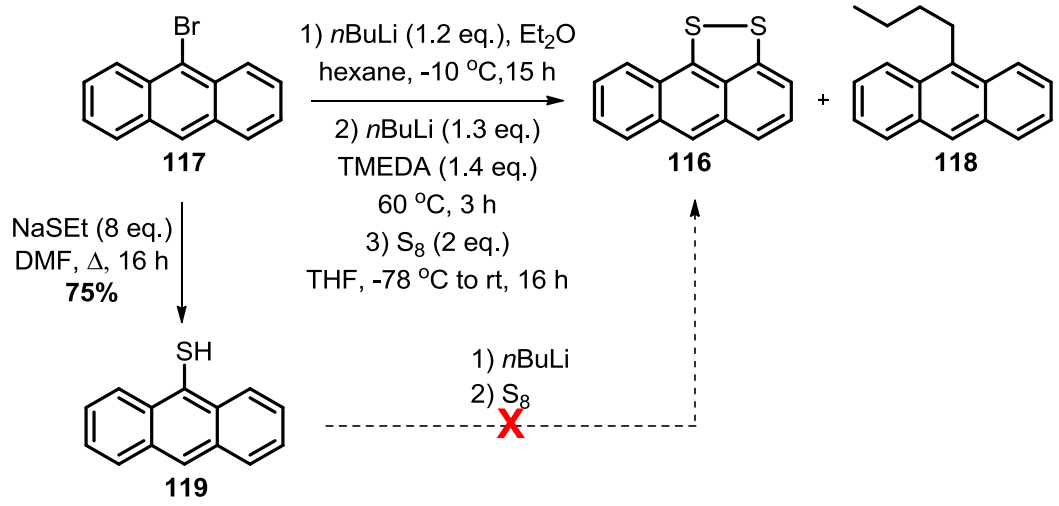

Scheme 2.12 Attempted synthesis of dithiole **116**.

In order to obtain [FeFe]-complexes **96** and **97**, fluorene-4,5-dithiine **120** was synthesised according to Bonifacio and co-workers' procedure.[143] The commercially available fluorene **122** was reacted first with *t*BuOK and *n*BuBr in order to obtain the novel di-alkylated substituted fluorene **123**.[143] Treatment of **123** with *n*BuLi and TMEDA, followed by the addition of recrystallized sulfur, afforded the expected dichalcogenides **122** in moderate yield.[143] The same synthetic procedure was then successfully applied to afford diselenine **121** in good yield (**Scheme 2.13**).

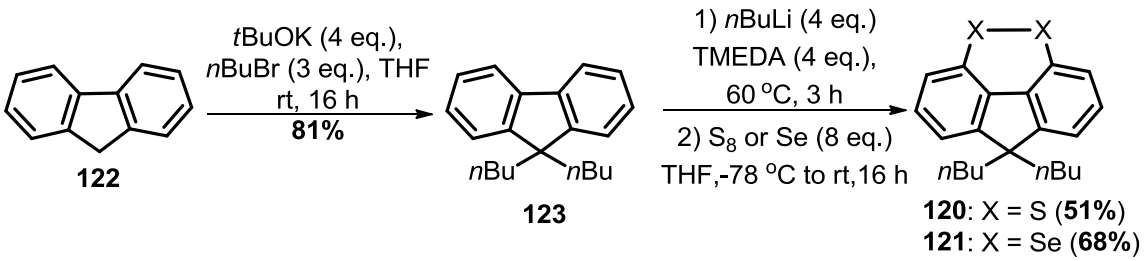

Scheme 2.13 Synthesis of fluorene-4,5-dithiine **120** and diselenine **121**.

2.3.2 Synthesis, spectroscopic analysis and X-ray diffraction of [FeFe]-complexes

Tilley and co-workers synthesised [FeFe]-complexes **89a-c** reacting $Fe_3(CO)_{12}$ with dithiols **124a-c** obtained by S–S bond reduction of the corresponding dithioles **100a-c** (**Scheme 2.14**).[122]

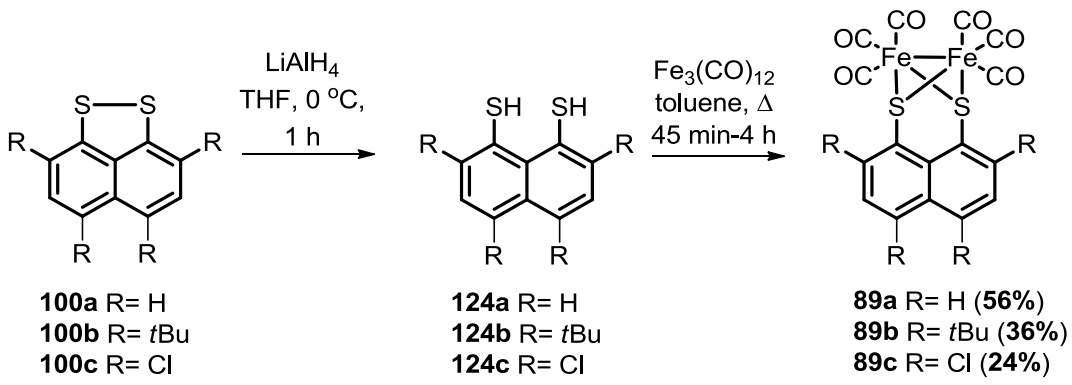

Scheme 2.14 Synthesis of naphthalene-1,8-dithiole-based [FeFe]-complexes **89a-c**.[122]

However, naphthalene-1,8-dithioles are known to react with transition metals by direct oxidative insertion of the metal into the S–S bond.[121] Consequently, the direct synthesis of [FeFe]-complexes **89a-b** was repeated by refluxing the dithioles **100a-b** with $Fe_3(CO)_{12}$ in toluene and the expected products were obtained in higher yields than those reported previously.[122] This procedure was then used to successfully synthesise [FeFe]-complexes **89d**, **91a**, **b** and **d**, **92a-b** and **93**, **94** and **96** (**Scheme 2.15**).

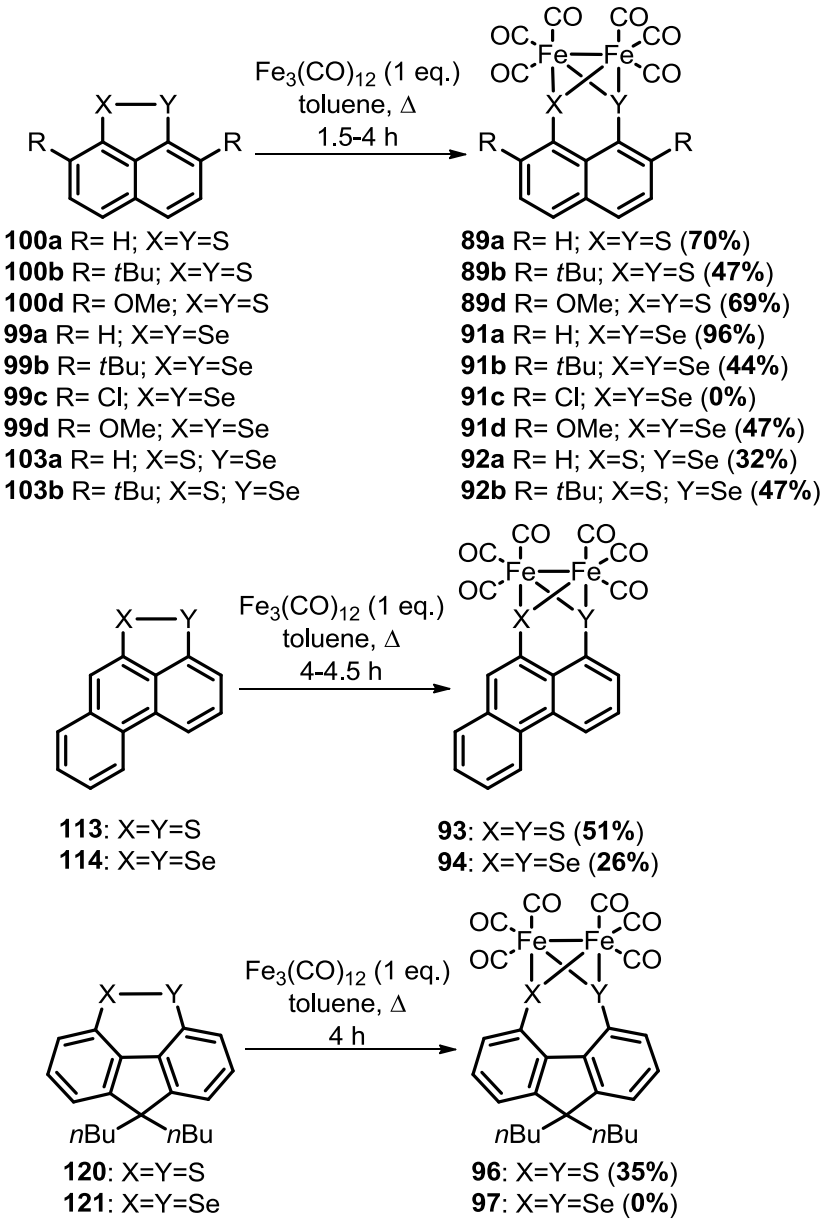

Scheme 2.15 Synthesis of [FeFe]-complexes **89d**, **91a**, **b** and **d**, **92a-b** and **93**, **94** and **96**.

Reaction of **99c** and **121** with $Fe_3(CO)_{12}$ in the same conditions did not give the expected [FeFe]-complexes **91c** and **97** (**Scheme 2.15**). The consumption of the starting material was observed by t.l.c. analysis, suggesting possible reaction between the Fe(0) and Se–Se bonds, followed by possible decomposition of the obtained complexes under these reaction conditions. The same reaction was also performed at lower temperature; however, both ligands were isolated together with the reagent $Fe_3(CO)_{12}$, due to the insolubility of the

chlorinated **99c** and the lack of reactivity of the Se–Se bond of **123** at room temperature. Presumably, in the case of **99c**, the electron-withdrawing effect of the naphthalene, enhanced by the chlorines, weakens the Se–Fe bond, already weaker than S–Fe bond of **100c** (see after X-ray analysis of dithiolate and diselenolate-based [FeFe]-complexes), and makes the corresponding [FeFe]-complex unstable. In the case of **122**, the presence of the selenium might shorten the distance between the two bay positions (4 and 5) on the fluorene, more than the sulfur in dithiine **121**, increasing the van der Waals repulsion between the two chalcogens and reducing the [FeFe]-complex stability.

[FeFe]-complexes **89d**, **91a**, **b** and **d**, **92a-b** and **93**, **94** and **96** (**Scheme 2.15**) were characterised by ^{1}H, ^{13}C NMR, IR and UV/vis spectroscopy and X-ray analysis (except for [FeFe]-complex **96**).

^{1}H NMR spectra shows the expected aromatic backbones peaks shifted to higher ppm values, due to the deshielding effect of the [FeFe]-cluster. Analogous to complexes **89a-c**, [122] ^{13}C NMR shows the expected peak at 207 and 208 ppm for sulfur and selenium-based [FeFe]-complexes respectively, which are assigned to the carbonyls on the iron centres.

The IR spectra of the metal-bound carbonyls of complexes **89d**, **91a**, **b** and **d**, **92a-b** and **93**, **94** and **96** provides information about the electron-density on the iron centres and, particularly, how it is affected by the nature of the chalcogens (sulfur and selenium), the *ortho* substituents (*t*Bu and OMe groups) and the aromatic ligands (naphthalene, phenanthrene and fluorene). The observed absorptions wavenumbers are consistent with those reported for the [FeFe]-complexes based on benzenedithiolate **88** and naphthalene-1,8-dithiolates **89a-c**, which are in the region 2070-1800 cm^{-1} (**Table 2.3**).[112,117,122]

Table 2.3 Carbonyl IR stretches of [FeFe]-complexes **89d**, **91a**, **b** and **d**, **91a-b**, **93**, **94** and **96**.

	Complex	v(CO)[cm^{-1}]
X= Y= S[a], naph[b], R= H[c]	**89a**[d]	2074, 2039, 2001
X= Y= S, naph, R= *t*Bu	**89b**[d]	2071, 2036, 1997
X= Y= S, naph, R= OMe	**89d**	2061, 2021, 1976, 1955, 1878
X= Y= Se, naph, R= H	**91a**	2058, 2016, 1996, 1979, 1822
X= Y= Se, naph, R= *t*Bu	**91b**	2057, 2015, 1979, 1970, 1956
X= Y= Se, naph, R= OMe	**91d**	2054, 2014, 1970, 1950, 1875
X= S,Y= Se, naph, R= H	**92a**	2061, 2020, 1999, 1982, 1958, 1822
X= S,Y= Se, naph, R= *t*Bu	**92b**	2061, 2017, 1980, 1972, 1961, 1940
X= Y= S, phen	**93**	2065, 2028, 1978, 1957, 1946, 1936
X= Y= Se, phen	**94**	2055, 2021, 1996, 1976, 1962, 1942
X= Y= S, fluorene	**96**	2072, 2030, 1990, 1986, 1974, 1952

[a] X,Y= chalcogen, [b] backbone (naph= naphthalene, phen= phenanthrene), [c] R= *ortho*-substituent on the naphthalene ring, [d] Data taken from reference [122].

The electron-density on the iron-centres is higher in the [FeFe]-complex **89b** than in the non-substituted **89a**, due to the presence of the electron-donating *t*Bu groups in the *ortho* positions.[122] Hence, the π backbond donation from the metal to the ligands is favoured, lowering the IR absorption energy of the carbonyls (**Table 2.3**). This effect is enhanced when the naphthalene ring is substituted by OMe groups (**89d**), which cause a shift of 13-18 cm^{-1} of the carbonyl stretching wavenumbers to lower energy. The same trend is observed in diselenole-based [FeFe]-complexes **91a**, **b** and **d**, in which, the presence of the selenium further increases the electron-density on the metal, consistent with previous reports (Section 1.3.2.3, Chapter 1). This selenium effect is confirmed by the IR carbonyls spectra recorded for the phenanthrene-based complexes **93** and **94**, but not for the lower four wavenumbers, which are higher for selenium than sulfur. Complexes **92a-b** show a lower energy shift of 10-13 cm^{-1} relative to **89a-b** and a higher energy shift of 3-4 cm^{-1} compared to **91a-b** (**Table 2.3**),

indicating that selenium has a stronger effect on the [FeFe]-cluster than the sulfur. In terms of *ortho* substituents, **92b** confirms what has been previously described for **89b** and **b**. A comparison of naphthalene dithiolate **89a** with phenanthrene-based dithiolate **93** shows that the additional conjugation in the phenanthrene ring causes a bathochromic shift in the IR stretching frequencies of the carbonyl groups. The effect in the selenium series is less clear cut, with comparative frequencies for diselenolate **91a** and phenathrene diselenolate **94** shifting to both higher and lower wavenumbers. Compared to **89a**,[122] the IR carbonyls absorptions of **96** are shifted towards lower wavenumbers, demonstrating a weaker electron-withdrawing effect on the iron centres from the two phenyl groups of the fluorene.

Complexes **89d**, **91a**, **b** and **d**, **92a-b** and **93**, **94** and **96** were further characterised by UV/vis spectroscopy. Figure 2.5 and Figure 2.6 show the absorption spectra of the [FeFe]-complexes and the corresponding dichalcogens; the calculated extinction coefficients are reported in Table 2.4.

Table 2.4 Absorption values of [FeFe]-complexes **89d**, **91a**, **b** and **d**, **91a-b**, **93**, **94** and **96**.

Complex	**λ / nm (ε / $M^{-1}cm^{-1}$)**
89a	249 ($\varepsilon = 3.5 \times 10^3$), 349 ($\varepsilon = 2.7 \times 10^4$)[a]
89b	261 ($\varepsilon = 3.5 \times 10^4$), 310 ($\varepsilon = 1.9 \times 10^4$), 352 ($\varepsilon = 2.1 \times 10^4$)[a]
89d	237 ($\varepsilon = 1.6 \times 10^4$), 327 ($\varepsilon = 6.1 \times 10^3$), 361 ($\varepsilon = 5.7 \times 10^3$)[b]
91a	253 ($\varepsilon = 6.2 \times 10^3$), 345 ($\varepsilon = 5.4 \times 10^3$)[b]
91b	265 ($\varepsilon = 1.7 \times 10^4$), 346 ($\varepsilon = 1.3 \times 10^4$)[a]
91d	240 ($\varepsilon = 8.8 \times 10^3$), 336 ($\varepsilon = 3.7 \times 10^3$), 358 ($\varepsilon = 3.1 \times 10^3$)[b]
92a	253 ($\varepsilon = 1.1 \times 10^4$), 348 ($\varepsilon = 8.5 \times 10^3$)[b]
92b	263 ($\varepsilon = 6.1 \times 10^3$), 309 ($\varepsilon = 3.7 \times 10^3$), 351 ($\varepsilon = 4.1 \times 10^3$)[b]
93	248 ($\varepsilon = 3.4 \times 10^4$), 346 ($\varepsilon = 6.3 \times 10^3$)[a]
94	251 ($\varepsilon = 3.1 \times 10^4$), 341 ($\varepsilon = 1.6 \times 10^3$)[a]
96	259 ($\varepsilon = 7.6 \times 10^3$), 330 ($\varepsilon = 3.1 \times 10^3$)[b]

[a] 2.5×10^{-5} or [b] 7.5×10^{-5} M.

The UV/vis spectra display the corresponding naphthalene/phenanthrene π-π^* transition band in the range 210-260 nm and an intense absorption band in the ultraviolet range 300-360 nm with a corresponding extinction coefficient (ε) of 10^3-10^4 M^{-1} cm^{-1}, which is then assigned either to the naphthalene/phenanthrene π-π^* transition or to the metal ligand charge transfer (MLCT) or ligand metal charge transfer (LMCT) from the iron centres to the carbonyls (**Figure 2.5** and **Figure 2.6**).[123,125,144] UV/vis spectra of complexes **89d**, **91b** and **91d** show a shoulder between 380 and 420 nm ($\varepsilon = 10^1$-10^2 M^{-1} cm^{-1}), which is assigned to each iron's d-d transition.[125,144]

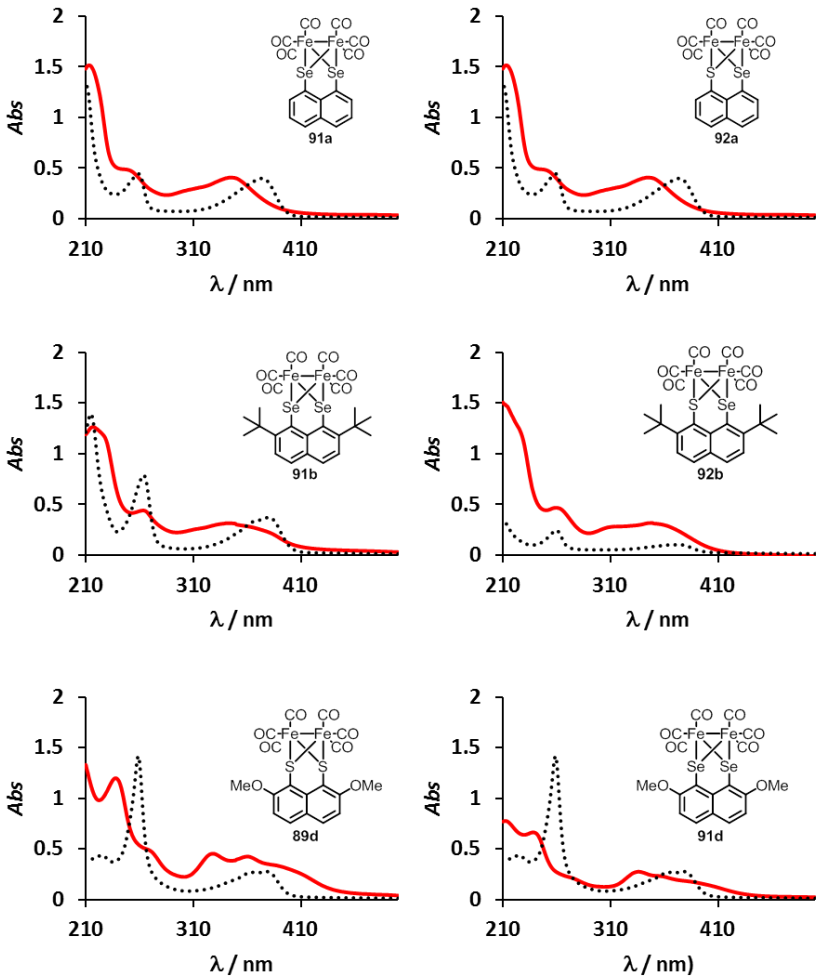

Figure 2.5 Absorption spectra of [FeFe]-complexes **89d**, **91a**, **b** and **d**, **92a-b** (—) and dichalcogens **99a**, **b** and **d**, **100d**, **103a-b** (•••).

In the case of the fluorene-based [FeFe]-complex **96**, the π-π* transition band, relative to the two benzene rings, is as intense as in the corresponding dichalcogen, while the MLCT or LMCT and d-d transition bands are the weakest (**Figure 2.6**).[123,125,144]

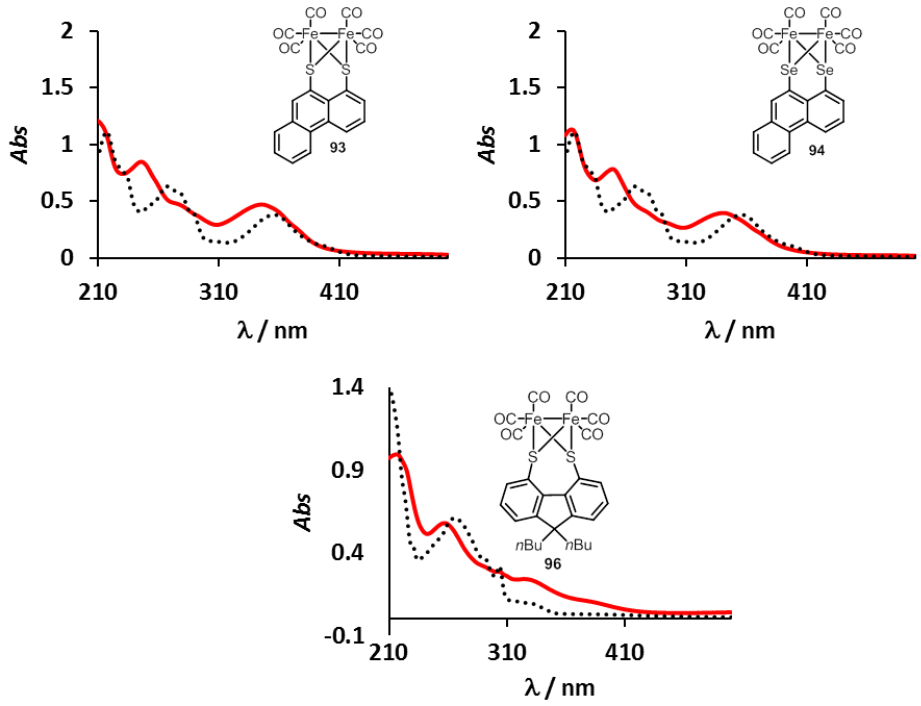

Figure 2.6 Absorption values of [FeFe]-complexes **93**, **94** and **96** (—) and dichalcogens **113**, **114d** and **120** (•••).

As previously reported, [123,144] UV/vis spectra of dichalcogens **99a-b** and **d**, **102a-b**, **106d**, **114**, **115** and **122** display broadened shapes and the absorption bands occur at lower energies than in the presence of the cluster.

Molecular structures of [FeFe]-complexes **89d**, **91a-b** and **d**, **92a-b**, **93** and **94** were confirmed by X-ray analysis. Suitable crystals of **89d**, **91a-b** and **d**, **92a-b**, **93** and **94** were obtained by slow evaporation of a concentrated solution of the complexes in dichloromethane (CH_2Cl_2) (Section 6.5 in Chapter 6 for experimental details). Recrystallization of [FeFe]-complex **96** was attempted several times without success. Crystal structures are shown in Figure 2.7; bond lengths and angles are listed in Table 2.5.

All the crystal structures possess a dichalcogenide-bridged [FeFe]-core which assumes the typical butterfly architecture and in which the two iron centres are linked to three carbonyl ligands in a distorted square-pyramidal geometry, as previously reported for **89a** and **89c**.[122] The Fe-Fe bond length for each complex is comparable with those reported in the literature for the active site of [FeFe]-hydrogenase (2.6 Å), as well as the bond length between each iron and each chalcogen (Fe1-S1 = Fe1-S2 = Fe2-S2 = Fe2-S2 = 2.3 Å in the enzyme).[39] As expected,[125] the crystal structure of phenanthrene-1,8-dithiolate based [FeFe]-complex **93** shows that the extra ring of the phenanthrene does not change the general structure and is comparable in bond lengths and angles with the data reported for the literature compound **89a** in Table 2.5.[122] Similarly the parameters in **91a** and **94** are comparable. The iron-chalcogen bond lengths are longer for selenium than sulfur (compare **89a**, **91a** and **92a**, **89d** and **91d,** and **93** and **94** in Table 2.5) as expected on electronegativity grounds.[86,87,88]

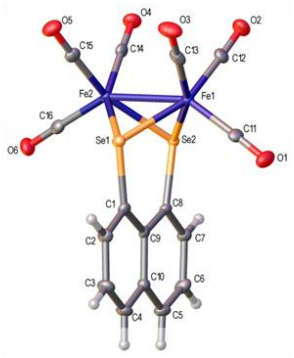

91a

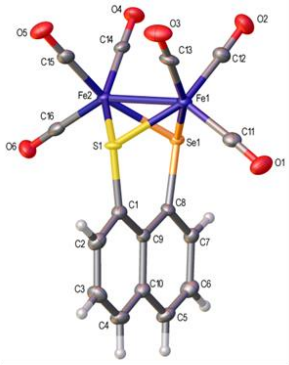

92a

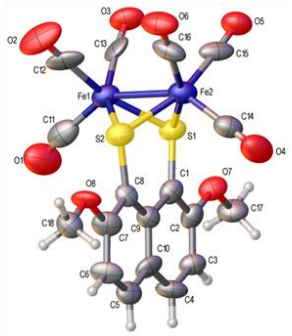

89d

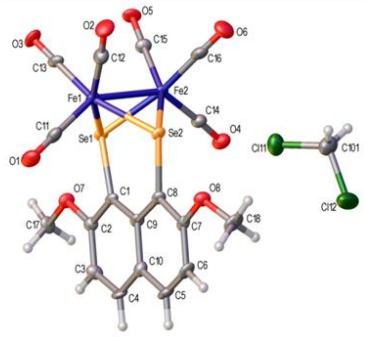

91d

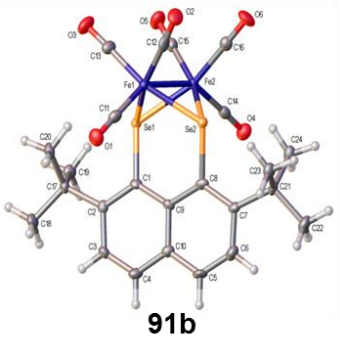

91b

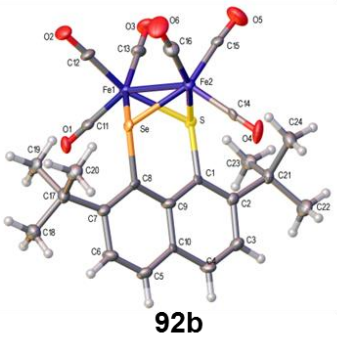

92b

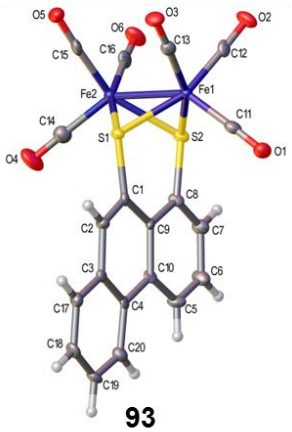

93

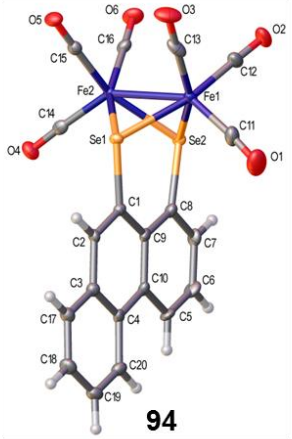

94

Figure 2.7 Crystal structure of [FeFe]-complexes **89d**, **91a**, **b** and **d**, **92a-b**, **93** and **94**.

Table 2.5 Selected bond lengths (Å) and angles (°) for compounds **89a** and **d**, **91a**, **b** and **d**, **92a-b**, **93** and **94**. Where there are two crystallographically-independent molecules (**92b**, **93** and **94**) only data from one molecule are given. Where there is disorder in the X and Y groups (**92a-b**) only the parameters from the major component are given.

	89a[a] **X= S(1)**[b] **Y= S(2)**[b] **Naph**[c] **R= H**[d]	**89d** **X= S(1)** **Y= S(2)** **Naph** **R= *t*Bu**	**91a** **X= Se(1)** **Y= Se(2)** **Naph** **R= H**	**91b** **X= Se(1)** **Y= Se(2)** **Naph** **R= *t*Bu**	**91d** **X= Se(1)** **Y= Se(2)** **Naph** **R= OMe**	**92a** **X= S(1)** **Y= Se(1)** **Naph** **R= H**	**91b** **X= S** **Y= Se** **Naph** **R= *t*Bu**	**93** **X= S(1)** **Y= S(2)** **Phen**	**94** **X= Se(1)** **Y= Se(2)** **Phen**
Fe(1)-Fe(2)	2.506(1)	2.536(3)	2.5482(8)	2.5617(13)	2.5734(17)	2.5270(10)	2.545(3)	2.5094(15)	2.5575(9)
Fe(1)-X	2.254(1)	2.252(4)	2.3606(7)	2.3484(12)	2.3513(15)	2.271(5)	2.28(6)	2.2444(18)	2.3584(7)
Fe(1)-Y	2.248(1)	2.237(4)	2.3632(7)	2.3668(11)	2.3621(14)	2.377(3)	2.338(14)	2.241(2)	2.3555(8)
Fe(2)-X	2.255(1)	2.247(4)	2.3601(7)	2.3556(12)	2.3573(15)	2.215(5)	2.21(4)	2.249(2)	2.3509(7)
Fe(2)-Y	2.249(1)	2.253(5)	2.3664(7)	2.3500(12)	2.3584(14)	2.367(3)	2.334(13)	2.246(2)	2.3514(7)
Fe(1)-C(11)	1.788(3)	1.85(2)	1.804(4)	1.803(8)	1.807(10)	1.799(5)	1.805(14)	1.802(7)	1.789(5)
Fe(1)-C(12)	1,797(3)	1.809(15)	1.803(4)	1.812(7)	1.802(10)	1.796(5)	1.792(14)	1.802(7)	1.802(4)
Fe(1)-C(13)	1.805(3)	1.819(16)	1.793(4)	1.799(7)	1.793(9)	1.805(5)	1.797(14)	1.805(7)	1.797(5)
Fe(2)-C(14)	1.801(3)	1.815(16)	1.798(4)	1.796(8)	1.788(9)	1.795(5)	1.843(14)	1.815(7)	1.807(5)
Fe(2)-C(15)	1.801(3)	1.791(16)	1.791(4)	1.811(8)	1.784(9)	1.790(5)	1.791(14)	1.805(7)	1.800(4)
Fe(2)-C(16)	1.805(4)	1.803(15)	1.800(4)	1.803(7)	1.798(10)	1.814(6)	1.820(15)	1.792(7)	1.803(4)
X-C(1)	1.777(3)	1.774(14)	1.911(4)	1.936(6)	1.924(8)	1.796(6)	1.83(6)	1.790(6)	1.917(4)
Y-C(8)	1.778(3)	1.774(12)	1.921(4)	1.955(7)	1.920(8)	1.886(5)	1.902(19)	1.769(6)	1.921(4)

X-Fe(1)-Y	84.12(3)	84.34(15)	85.08(2)	83.43(4)	85.85(5)	83.80(14)	83.1(12)	84.24(7)	84.97(3)
X-Fe(2)-Y	84.08(3)	84.09(14)	85.02(2)	83.63(4)	85.80(5)	85.26(13)	84.9(15)	84.03(7)	85.23(2)
X-C(1)-C(9)	125.3(2)	124.5(9)	126.7(3)	122.8(5)	127.2(6)	125.0(4)	121(2)	125.8(5)	127.8(3)
Y-C(8)-C(9)	125.4(2)	127.8(9)	126.7(3)	121.8(5)	127.3(6)	128.6(4)	126.4(10)	125.9(5)	127.7(3)
C(8)-C(9)-C(1)	125.4(3)	123.8(12)	126.2(4)	126.9(6)	125.8(8)	124.6(4)	124.5(12)	124.1(5)	124.2(4)
X-C(1)…C(8)-Y	−1.64(13)[b]	−0.7(6)	1.84(15)	20.7(3)	3.1(5)	2.9(3)	-15.8(16)	1.8(3)	−1.46(17)
X…Y	3.0159(10)[b]	3.013(5)	3.1939(6)	3.1374(9)	3.2101(12)	3.105(6)	3.07(5)	3.008(3)	3.1836(8)
Angle between Planes 1 and 2[e]	93.21(4)	92.4(2)	93.46(5)	68.91(9)	89.42(12)	93.51(6)	71.4(2)	89.00(8)	88.20(5)

[a] Data taken from reference [122]. CCDC 723538. [b] X,Y= chalcogen, [c] backbone (naph= naphthalene, phenan= phenanthrene), [d] R= *ortho*-substituent on the naphthalene ring, [e] Plane 1 is the least-squares plane through C(1)-C(10). Plane 2 is the least squares plane through Fe(1), Fe(2) and the two "in-line" carbonyl groups, (C(13), O(3), C(16), O6) in **89a**; C(11), O(1), C(16), O(6) in **91a** and **92a**; C(11), O(1), C(14), O(4) in **89d**, **91b** and **d**, **92b**, **93** and **94**.

Electron-donating groups (*t*Bu, OMe) on the naphthalene ring have little effect on the iron-chalcogen bond length. However the two bulky *t*Bu groups in the *ortho* positions on the ring decrease the non-bonding distance between the chalcogen atoms (as seen in the observed values of Se1…Se2 distances for **91a**, **b** and **d** (3.1939(6), 3.1374(9) and 3.2101(12) Å respectively, **Table 2.5**). The van der Waals repulsion of the *t*Bu groups also cause a displacement of the chalcogens either side of the naphthalene plane, as seen in the X-C(1)…C(8)-Y torsion angle (**Table 2.5**).[126,128] This effect is more pronounced for **91b** than **92b** due to the relative size of selenium and sulfur. A third pronounced effect of the *t*Bu groups is on the alignment of the Fe-Fe bond with the plane of the naphthalene ring. For all of the complexes, except **91b** and **92b**, the Fe-Fe bond is aligned perpendicularly to the plane of the aromatic ring system (**Table 2.5**, angles between plane 1 and 2). In comparison, the 2,7-di-*tert*-butyl naphthalene systems **91b** and **92b** are notably twisted by almost 20 °C (**Figure 2.8**), slightly more for **91b**, containing two selenium atoms, than **91b**, containing one selenium and one sulfur. The disruption of symmetry in **91b** could help explain its anomalous electrochemical behaviour (Section 2.3.3).

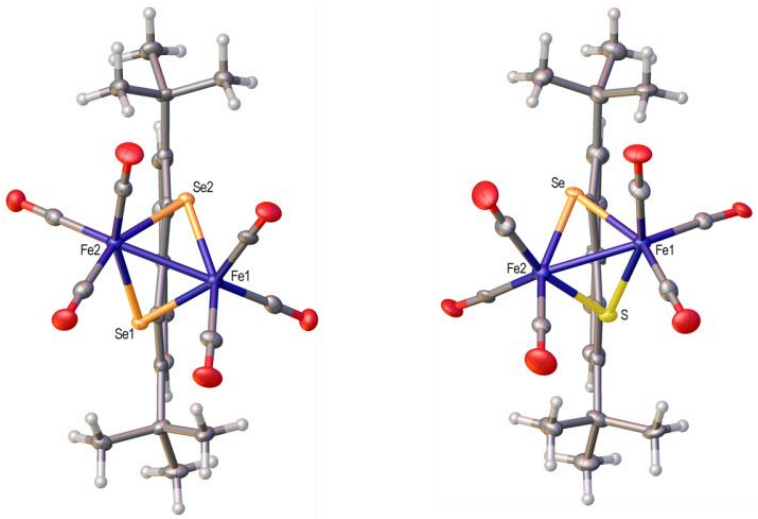

Figure 2.8 Projections of the alignment of the plane through C(1)-C(10) (plane 1) and plane through Fe(1), Fe(2) and the two "in-line" carbonyl groups, C(11), O(1), C(14), O(4) in [FeFe]-complexes **91b** (left) and **92b** (right).

2.3.3 Electrochemical Characterisation

The investigation of the electrochemical properties of [FeFe]-complexes **89d**, **91a**, **b** and **d**, **92a-b**, **93**, **94** and **96** (**Scheme 2.15**) was carried out by using cyclic voltammetry (CV). Measurements were recorded in acetonitrile (CH_3CN) at room temperature, using a three electrode-cell with glassy carbon as working electrode, silver/silver nitrate ($Ag/AgNO_3$) as reference electrode and platinum as counter electrode. Ferrocene was used as internal reference and all the potentials herein were quoted with respect to the Fc/Fc^+ couple (Section 6.1.3 in Chapter 6 for experimental details). The half-wave potentials ($E_{1/2}$) derived from the CVs are all reported in Table 2.6, along with the literature values of complexes **89a-b**.

Table 2.6 Electrochemical reduction potentials (vs. Fc/Fc^+) [FeFe]-complexes **89d**, **91a**, **b** and **d**, **92a-b**, **93**, **94** and **96** (1 mM) in 0.1 M NBu_4PF_6/CH_3CN at 0.01 V s^{-1} scan rate.

Complex	E'_{pc}	$E'_{1/2}$ $Fe^IFe^I \rightarrow Fe^IFe^0$	E''_{pc}	$E''_{1/2}$ $Fe^IFe^0 \rightarrow Fe^0Fe^0$	E_{pa}
89a[a]	–1.52 V	–1.48 V	–1.96 V	-	0.87 V
89b	–1.63 V	–1.54 V	1.99 V	–1.87 V	0.62 V 1.13 V
89d	–1.65 V	–1.52 V	–2.08 V	–1.92 V	0.99 V 1.20 V
91a	–1.54 V	–1.44 V	–1.86 V	–1.75 V	1.00 V
91b	–1.50 V	–1.40 V	–2.15 V	–2.01 V	0.55 V 0.90 V
91d	–1.64 V	–1.50 V	–2.01 V	–1.90 V	0.88 V 1.13 V
92a	–1.60 V	–1.47 V	–1.91 V	–1.82 V	0.68 V 1.12 V
92b	–1.61 V	–1.48 V	–1.90 V	–1.82 V	1.07 V
93	–1.64 V	–1.51 V	–2.02 V	–1.84 V	0.87 V 1.14 V
94	–1.52 V	–1.39 V	-	-	0.98 V 1.31 V
96	–1.32 V	–1.43 V	–1.80 V	–1.69 V	1.07 V

[a]Data taken from reference [122]

Each complex gives two reduction waves, which are assigned to Fe(I)Fe(I)→Fe(I)Fe(0) and Fe(I)Fe(0)→Fe(0)Fe(0), by analogy with data previously reported for complexes **89a-b**.[122] The peak separation of the first reduction wave are all greater than that observed for the Fc^+/Fc internal redox couple, indicating quasi-reversible behaviour (intermediate electron transfer kinetics) in each case. The second reduction wave (except for **96**) is closer to reversible. It has been suggested that the first reduction wave results in a small structural rearrangement, [113,114] which would both slow electron transfer kinetics and result in a reduced amplitude of the return wave. This rearrangement is unlikely to involve fragmentation of the backbone, [122,125] because an oxidation peak is observed on the return sweep. The oxidation peak currents are difficult to measure because of the difficulty in determining the baseline but it appears in some cases (i. e. compounds **91** and **92**) that such electrochemical (EC) reaction does take place. The product of the second reduction appears more stable, which is likely to result from a slower chemical decomposition of the reduction product.

To confirm the accuracy of the measurements, the electrochemical analysis of [FeFe]-complex **89b** was repeated (**Table 2.6**). The first and the second $E_{1/2}$ values are consistent with those reported previously; [122] however, **89b** exhibits a reversible second reduction process, in opposition to the irreversible described by Tilley and co-workers (**Figure 2.9**).[122]

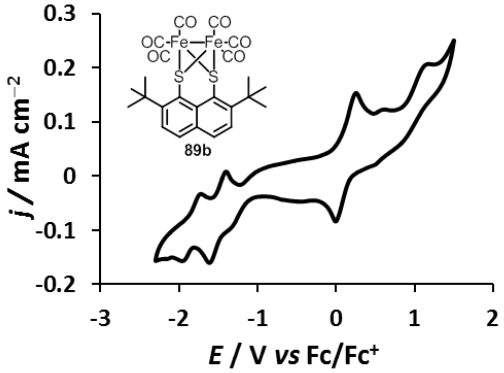

Figure 2.9 Cyclic voltammogram for [FeFe]-complex **89b** (1 mM) in 0.1 M NBu_4PF_6/CH_3CN at 0.01 V s^{-1} scan rate.

Comparison of complex **89d** with **89a-b** shows that reduction of **89b** occurs at the most negative potential for both processes. Complex **89d** has a more negative potential than **89a** for the first reduction process (**Table 2.6**). A more negative reduction potential indicates that the reduced form is thermodynamically less stable; the electron donating *t*Bu and OMe groups thus destabilise the reduced forms, as might be expected, and the *t*Bu groups have a stronger electron donating effect than the OMe groups, contrary to what is observed by IR spectroscopy (**Table 2.3**). In general, the reduction products appear stable, which has been observed for similar aromatic ligand-based [FeFe]-complexes to be a result of partial delocalization of the negative charges on the aromatic backbone and a degree of rigidity that prevents dimerization of the complex.[112,122,125] Compound **89d** also exhibits two irreversible oxidations (E_{pa} 0.99 V and 1.2 V), most likely oxidation of the iron centre, Fe(I)Fe(I)→Fe(I)Fe(II) and Fe(I)Fe(II)→Fe(II)Fe(II) respectively (**Figure 2.10**).

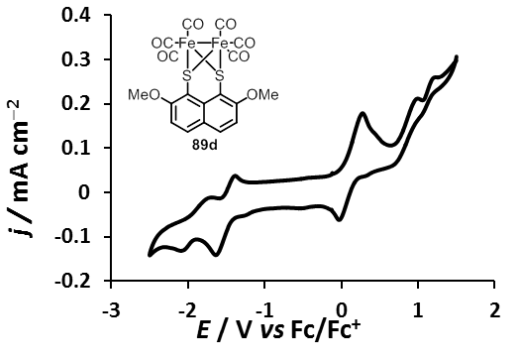

Figure 2.10 Cyclic voltammogram for [FeFe]-complex **89d** (1 mM) in 0.1 M NBu_4PF_6/CH_3CN at 0.01 V s^{-1} scan rate.

Surprisingly, the replacement of the sulfur atoms with selenium results in a positive shift in reduction potential of **91a**, **b** and **d** and reversible oxidation processes are also observed for each complex (**Table 2.6**). The effect of selenium on reduction potential is not expected by considering the increase of electron density on the iron centres, shown in the IR spectra (see

previous paragraph). Complex **91d** is reduced at more negative potentials than **91a**, similarly to the behaviour of complexes **89d** and **89a**. However, the first reduction of compound **91b** occurs at a more positive potential than that of **91a**, which might imply that the reduction promotes structural rearrangements to lessen the steric hindrance caused by the *t*Bu groups and the two seleniums. The three reduction processes, observed for complex **91b** might also suggest, in this case, fragmentation of the backbone (**Figure 2.11**). The reduction products of the diselenolate-based [FeFe]-complex **91a**, **b** and **d** appears less stable than those observed for the corresponding dithiolate-based complexes **89a**, **b** and **d**, since the oxidation peak current (particularly for **91d**) appears smaller than the reduction peak current. Assuming that the diffusivities of the oxidized and reduced forms of the complex are similar, a difference in peak height would suggest decomposition of the reduced product in an EC reaction. Thus, although the incorporation of selenium facilitates the reduction of the iron centres, it has an adverse effect on the complex stability under reducing conditions (**Figure 2.11**).

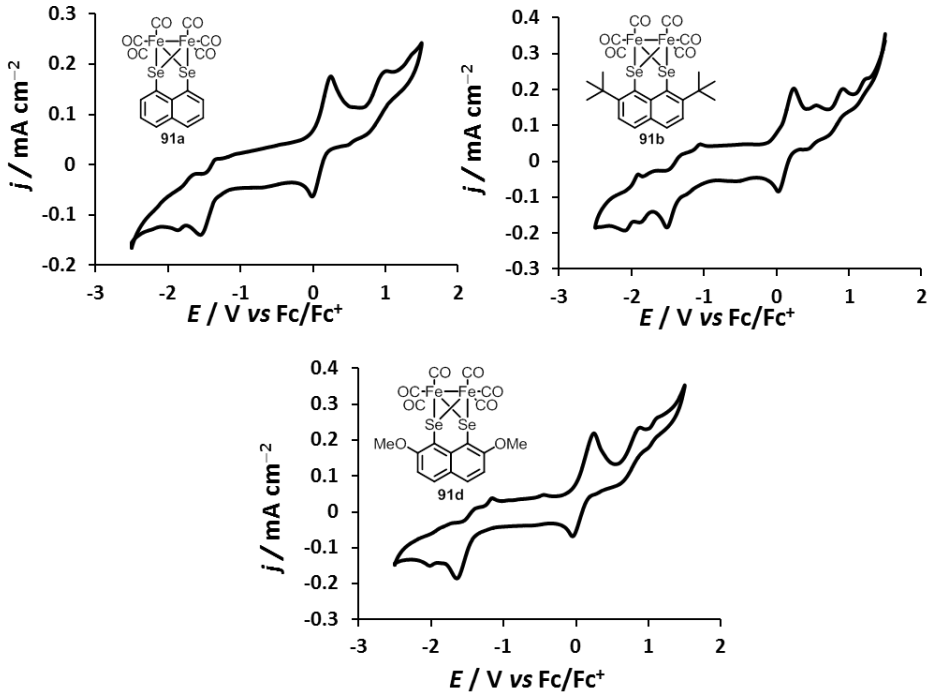

Figure 2.11 Cyclic voltammograms for [FeFe]-complexes **91a**, **b** and **d** (1 mM) in 0.1 M NBu_4PF_6/CH_3CN at 0.01 V s^{-1} scan rate.

The thiaselenolate-based [FeFe]-complexes **92a-b** exhibit reduction waves for the first process in between those of the corresponding dithiolate and diselenolate-based complexes, consistent with previous reports (**Table 2.6**).[90] Interestingly, the peak positions observed for **92a-b** are similar. However, the oxidation behaviour differs, with the oxidation peak position of **92a** being substantially more negative than that of **92b** (**Figure 2.12**).

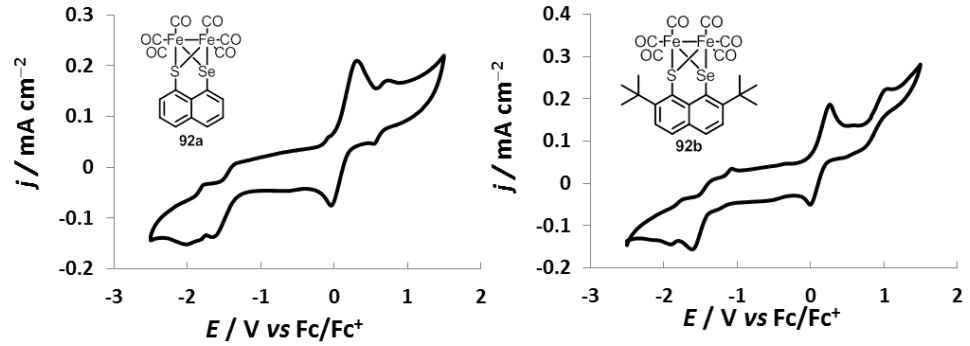

Figure 2.12 Cyclic voltammograms for [FeFe]-complexes **92a-b** (1 mM) in 0.1 M NBu_4PF_6/CH_3CN at 0.01 V s^{-1} scan rate.

The [FeFe]-complex **93**, based on phenanthrene-1,10-dithiolate, exhibits reduction waves at −1.51 V and –1.84 V, both more negative than the unsubstituted naphthalene **89a** (**Table 2.6**). In contrast, reduction of the phenanthrene-4,5-dithiinate-bridged [FeFe]-complex **90** [125] occurs at a less negative potential than that of **89a**. Comparison of the behaviour of **93** with **90** demonstrates that the addition of an aromatic ring does not necessarily increase stabilization of the reduced form of the complex. On the other hand, the reduction of the corresponding diselenolate-linked **94** occurs at –1.39 V, more positive than that of **93**, in line with the trend observed for the naphthalene-based complexes. However, the $E_{1/2}$, calculated for **94** is more positive than that of **89a**, indicating that, in this case, the additional ring does stabilise the reduced form of the complex. The second reduction process is less well-defined for complex **94**, which might suggest a lack of stability of the second reduction product and, as suggested

for **90**, [125] structural rearrangement of the reduced forms of these complexes might take place, resulting in a lack of reversibility of the second process (**Figure 2.13**).

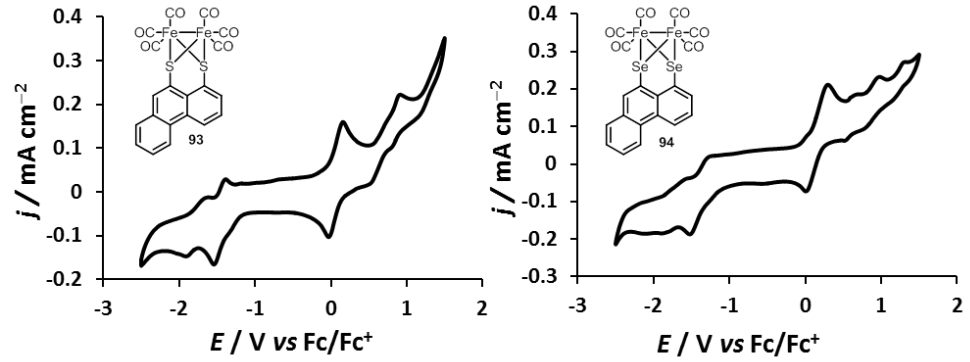

Figure 2.13 Cyclic voltammograms for [FeFe]-complexes **93** and **94** (1 mM) in 0.1 M NBu_4PF_6/CH_3CN at 0.01 V s^{-1} scan rate.

The fluorene-4,5-dithiine-based [FeFe]-complex **96** undergoes two reduction processes at −1.32 V and –1.80 V, more positive than those reported for the conjugated polyaromatic naphthalene and phenanthrene systems (**Table 2.6**). An irreversible reduction process also occurs at –2.3 V. It is not attributed to a further reduction of [FeFe]-cluster, but most likely to an irreversible chemical reaction, which might explain the difference in height between the reduction and the oxidation peaks for the previous processes (**Figure 2.14**).

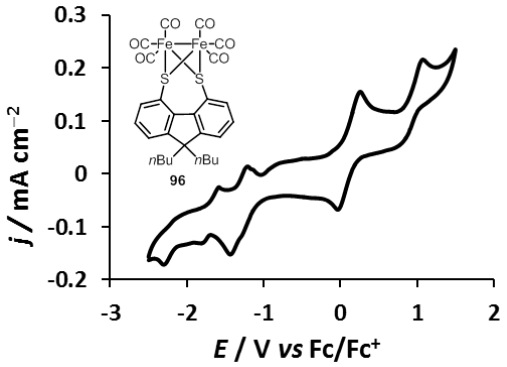

Figure 2.14 Cyclic voltammogram for [FeFe]-complex **96** (1 mM) in 0.1 M NBu_4PF_6/CH_3CN at 0.01 V s^{-1} scan rate.

2.3.4 Proton Reduction Catalysis

Complexes **89d**, **91a**, **b** and **d**, **92a-b**, **93**, **94** and **96** were tested as proton reduction electrocatalysts by monitoring their electrochemical properties on addition of *p*TsOH acid (concentration from 2.5 mM to 10 mM), which is mildly acidic in organic solvents (pK_a= 8 in CH_3CN).[145] Previous studies on [FeFe]-hydrogenase synthetic mimics reported that upon increasing the concentration of acid the catalytic reduction wave was shifted towards more positive potentials, becoming irreversible, and the peak current (I_{pc}) increased linearly as a function of the acid concentration.[146] This behaviour, typical of electrocatalytic processes, was also observed for proton reduction catalysts based on Fe-porphyrin complexes, and it was suggested that the reaction is fast and the current is controlled by the diffusion of the molecules at the electrode's surface.[147] Generally, it has been suggested that the mono-reduced species, formed during the first one-electron reduction, react rapidly with protons before subsequently being reduced by a second one-electron reduction. This anionic species then combines with a proton to afford molecular hydrogen (Process I, **Scheme 2.16**).[52,113,122,147a)] However, Pickett and Best described an alternative proton reduction mechanism: complex **9** (**Scheme 1.5**) undergoes the first reduction, which corresponds to the formation of the first mono-anion and its rapid reaction with the acid forming a protonated neutral species (*e.g.* **9H)**, which is then reduced to form $\mathbf{9H^-}$. This species is rapidly protonated a second time (at more negative potentials than the monoanion), leading to $\mathbf{9H_2}$, which can be further reduced to $\mathbf{9H_2^-}$ and liberates hydrogen and releases the mono-reduced form of the complex $\mathbf{9^-}$ (or **9A** in **Scheme 1.5**) (Process II, **Scheme 2.16**).[52]

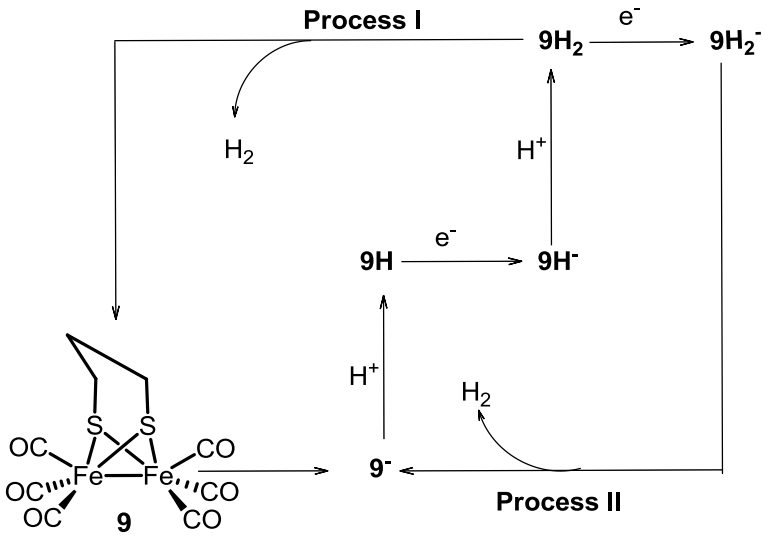

Scheme 2.16 Proposed proton reduction mechanisms of [FeFe]-complex **9**.[113]

Complexes **91b** and **d**, **92b** and **94** follow the catalytic process I shown in Scheme 2.16 (**Figure 2.15**).

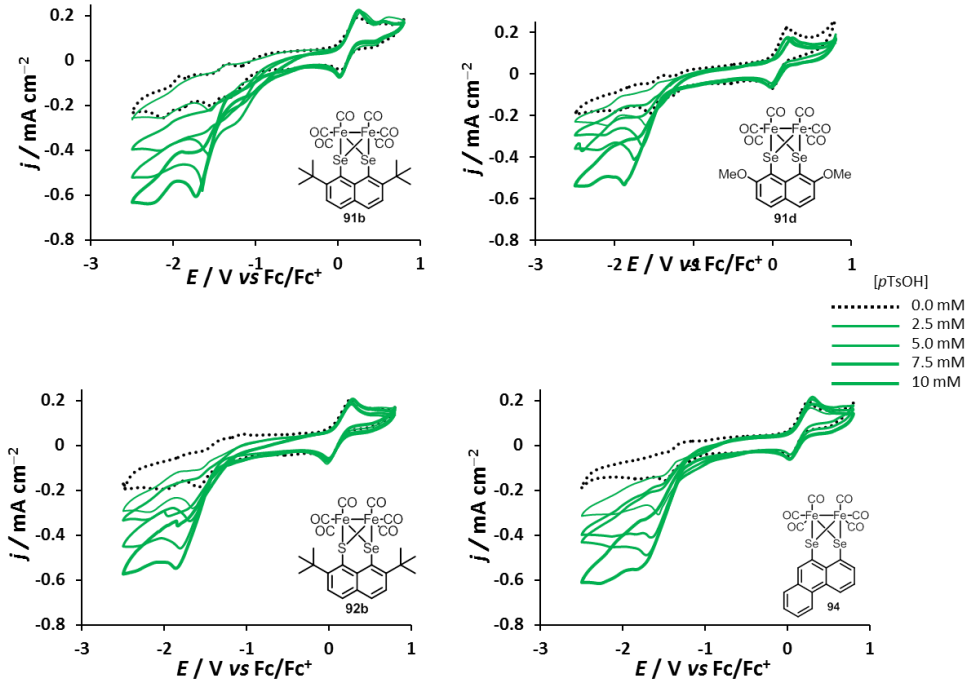

Figure 2.15 Cyclic voltammograms for [FeFe]-complexes **91b** and **d**, **92b** and **94** (1 mM) in 0.1 M NBu_4PF_6/CH_3CN at 0.01 V s^{-1} scan rate with increasing concentration of *p*TsOH (from 2.5 M to 10 mM).

Complexes **89d**, **91a**, **93** and **96** do not display the same catalytic behaviour but, instead, a new reduction wave appears upon addition of *p*TsOH, between the first and the second reduction peaks, and this wave does not have any anodic counterpart. Its intensity increases with the acid concentration. In order to exclude the contribution of the working electrode in proton reduction, [112] the same experiment was performed in the absence of catalysts (**Figure 2.16**). Proton reduction at the glassy carbon electrode in the absence of catalyst occurs at more negative potentials than the peaks observed in the presence of catalysts and the reduction peaks are broader.[52] Hence, the new peak does not correspond to proton reduction at carbon electrode but it is instead indicative of a different mechanism from that mentioned before.

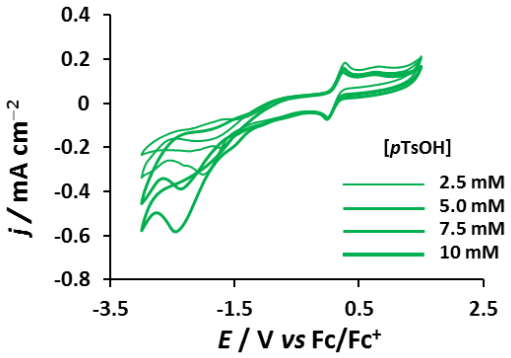

Figure 2.16 Cyclic voltammogram of the glassy carbon in 0.1 M NBu_4PF_6/CH_3CN at 0.01 V s^{-1} scan rate referenced to Fc/Fc^+ couple with increasing concentrations of *p*TsOH (from 2.5 M to 10 mM).

According to Pickett and Best's studies, three different reduction waves are possible: complexes **89d**, **91a**, **93** and **96** undergo a proton reduction cycle which involves two distinct reduced/protonated species (Process II, **Scheme 2.16**). The new reduction wave of **89d**, **91a** and **96** appears at concentrations of 2.5 mM of *p*TsOH and above but for complex **93** only above 7.5 mM of acid (**Figure 2.17**). Complexes **89a** and **89b** were reported by Tilley *et al.* to give similar results to complex **89d** under the same conditions and the second new reduction wave was assigned to an intermediate that was not identified experimentally.[122]

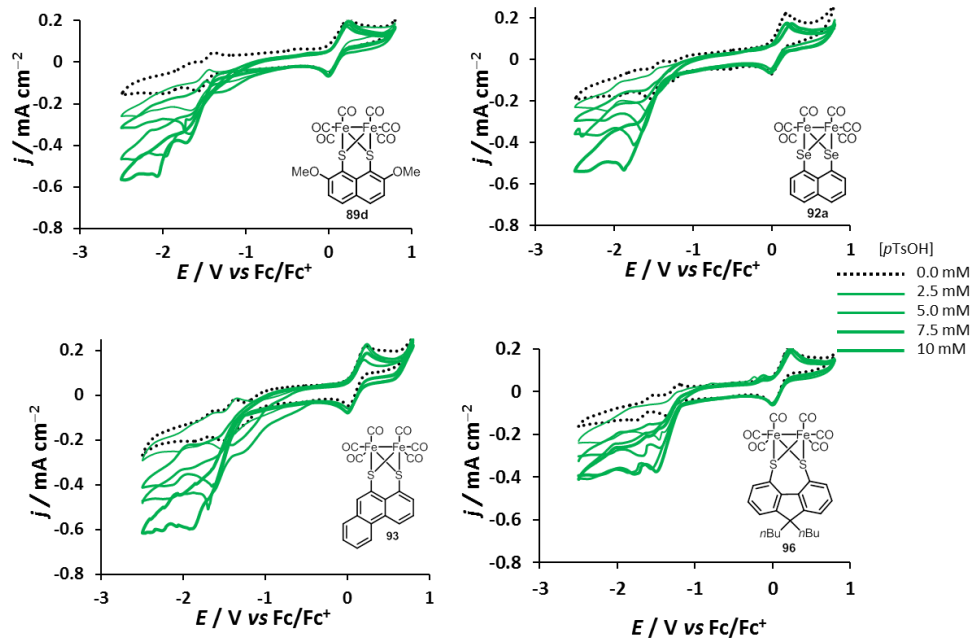

Figure 2.17 Cyclic voltammograms for [FeFe]-complexes **89d**, **91a**, **93** and **96** (1 mM) in 0.1 M NBu_4PF_6/CH_3CN at 0.01 V s^{-1} scan rate with increasing concentrations of *p*TsOH (from 2.5 M to 10 mM).

The dependence of this new wave on acid concentration is suggestive of a parallel mechanism, such as that proposed by Tilley and co-workers (Process II, **Scheme 2.16**), and that pathway is favoured by high acid concentration. It is also possible that protons are associated only with the di-anion produced in the second reduction process but this behaviour was shown to occur only with weaker acids than *p*TsOH.[112] In the presence of *p*TsOH, it is more likely that the protonation step of the monoanion is rapid.

Upon addition of 2.5 mM of *p*TsOH, complex **92a** displays a first reduction wave at –1.28 V, which could be assigned to both the first one-electron reduction and following protonation, while the second wave at –1.54 V leads to the proposed formation of molecular hydrogen (Process II, **Scheme 2.16**). Upon addition of higher concentration of acid, **92a** follows the general catalytic pattern described in Scheme 2.16 (Process I, **Figure 2.18**).

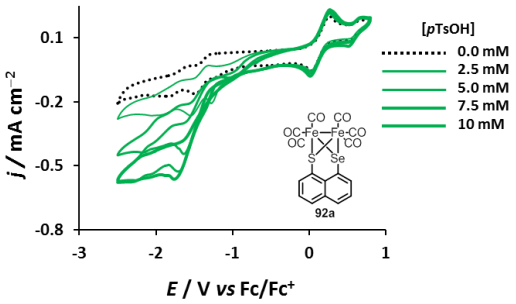

Figure 2.18 Cyclic voltammogram for [FeFe]-complex **92a** (1 mM) in 0.1 M NBu_4PF_6/CH_3CN at 0.01 V s^{-1} scan rate with increasing concentrationc of *p*TsOH (from 2.5 M to 10 mM).

The catalytic efficiency was evaluated considering the increase in the peak current on addition of acid [86,87] and also the potentials required in order to drive the reaction. Evans and co-workers calculated the standard potential ($E°_{HA}$) for many different acids, used to test the electrocatalytic activity of [FeFe]-hydrogenase synthetic mimics, which depends in each case on the pK_a and the solvent.[148] The standard potential for *p*TsOH reduction in CH_3CN is –0.65 V vs Fc/Fc^+. If proton reduction occurs at the same potential as the reduction of the catalyst, the difference between the catalyst's half-wave potential and the acid standard potential, $E_{1/2}$ - $E°_{HA}$ (hereafter overpotential, when experiments are performed at 0.01 V s^{-1}scan rate and in the range between -3 V and 0.8 V) provides a measure of the decrease in activation energy for the reaction in the presence of a catalyst. These values are reported in Table 2.7 for complexes **89d**, **91a**, **b** and **d**, **92a-b**, **93**, **94** and **96**.

Table 2.7 Overpotentials of complexes **89d**, **91a**, **b** and **d**, **92a-b**, **93**, **94** and **96**.

Complex	**89a**[a]	**89b**	**89d**	**91a**	**91b**	**91d**	**92a**	**92b**	**93**	**94**	**96**
$E_{1/2}$–$E°_{HA}$ / V	0.83	0.89	0.87	0.79	0.76	0.85	0.82	0.83	0.86	0.74	0.67

[a]Data taken from reference [122]

As previously reported (Section 1.3.2.3, Chapter 1), diselenolate-based [FeFe]-complexes show lower values of overpotential, indicating that they are more efficient proton reduction

catalysts than the corresponding dithiolates. The overpotential values of the thiaselenolate-based [FeFe]-complexes are intermediate between the corresponding diselenolates and dithiolates, while the fluorene-based displays the lowest value of overpotential for the *p*TsOH reduction catalysis among all the reported [FeFe]-complexes (**Table 2.7**).

In addition, the catalytic efficiency of the complexes was evaluated in terms of peak current increase (I_{pc}).[86,87] Figure 2.19 shows a comparison between **91d** and **89d** and between **93** and **94**. As expected by the measured overpotentials, a bigger increase in the peak current is produced by the latter two complexes than by their sulfur counterparts.

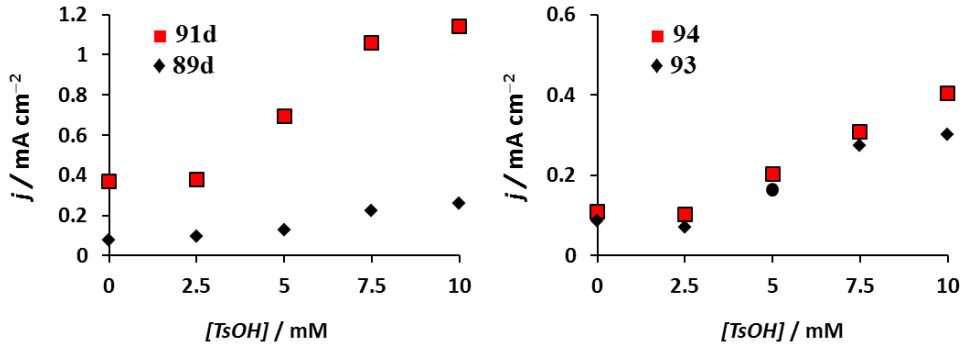

Figure 2.19 Peak current increase comparison between selected dithiolate and diselenolate-based [FeFe]-complexes.

2.3.5 Towards the synthesis of sulfur-oxygenated [FeFe]-complexes

In agreement with their biological role, [FeFe]-hydrogenase and [NiFe]-hydrogenase are highly air-sensitive.[149] In order to reduce O_2-damage, these enzymes maintain the active site protected in the protein core and usually operate in anaerobic conditions. In addition, [NiFe]-hydrogenase is known to repair the O_2-damages so that the air-inhibition becomes reversible. However, [FeFe]-hydrogenase can not be re-activated once inhibited.[28] In order to analyse the inhibited active site properties and the O_2 over H^+ reactivity for future applications in fuel cells, many biological and spectroscopic methods have been developed as well as advanced

electrochemical techniques, such as protein film voltammetry (PFV).[150,151] In particular, [FeFe]-hydrogenase active site synthetic analogues have been investigated in terms of reactivity towards O_2 and, consequently, physical, spectroscopic and electrochemical properties and possible deoxygenation processes of the corresponding sulfur-oxygenated derivatives have been analysed.[152,153]

A previous study in the Grainger group reported the thermal stability of thiosulfinate **125b** and *vic*-disulfoxide **126b**, which are accessible by direct oxidation of the disulfide **100b** (see below).[130] Hence, the oxidative insertion of Fe(0) into the S–S(O) and (O)S–S(O) bond was investigated and sulfur-oxygenated derivatives of **89b**, **127b** and **128b**, were thus targeted (**Figure 2.20**).

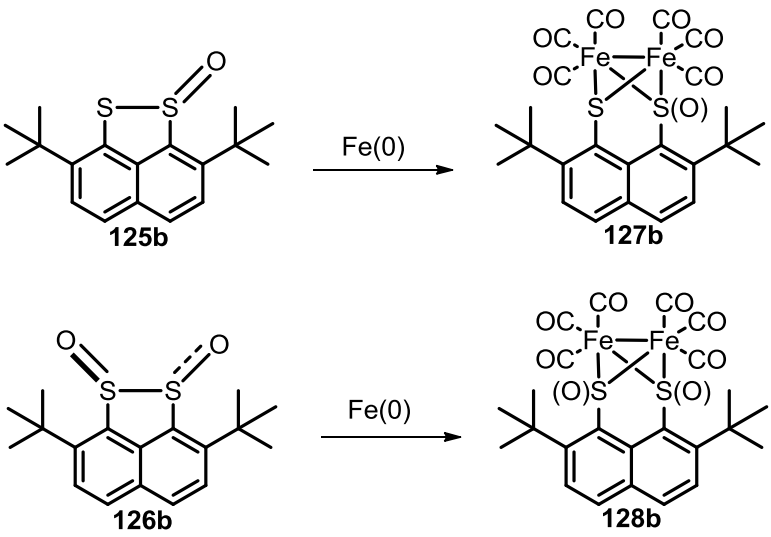

Figure 2.20 Attempted oxidative insertion of Fe(0) into the S–S(O) and (O)S–S(O) bond of **125b** and **126b**.

Following Grainger and co-workers procedure, [130] oxidation of 2,7-di-*tert*-butylnaphthalene-1,8-dithiole **100b** with *m*CPBA gave the corresponding thiosulfinate **125b** and the *trans vic*-disulfoxide **126b** in 65% and 76% yields respectively (**Scheme 2.17**).

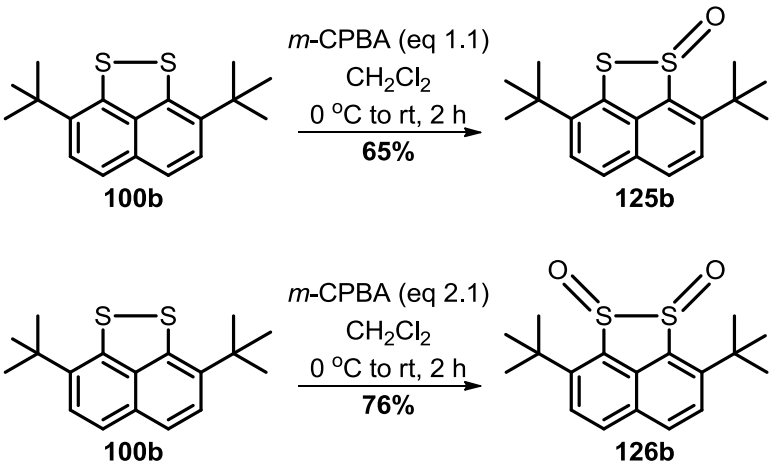

Scheme 2.17 Synthesis of 2,7-di-*tert*-butylnaphthalene-1,2-thiosulfinate **127b** and the corresponding *vic*-disulfoxide **128b**.

Attempts to obtain [FeFe]-complex **127b** by $Fe_3(CO)_{12}$ oxidative insertion into the S–S(O) bond of **125b**, applying the reaction conditions described previously in Scheme 2.15, resulted in the formation of the corresponding dithiole **100b** and the [FeFe]-complex **89b** (entry 1,**Table 2.8**). By switching solvent to THF and increasing equivalents of $Fe_3(CO)_{12}$ and time, [153c] both **100b** and **89b** were still isolated and the thiosulfinate **125b** was recovered (entry 2,**Table 2.8**).

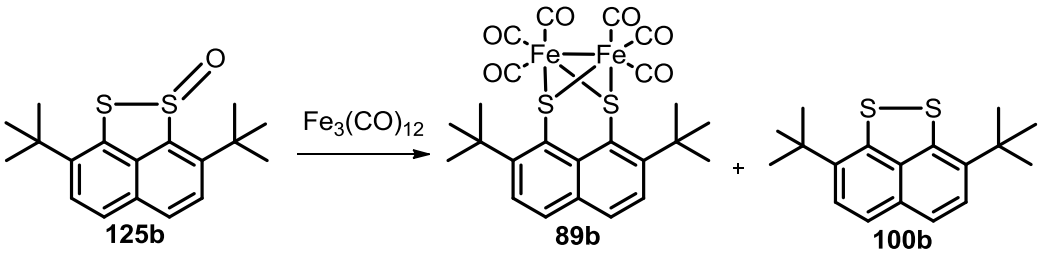

Table 2.8 Attempted oxidative insertion of $Fe_3(CO)_{12}$ into the S–S(O) of **125b**.

Entry	Reaction conditions	% Yield 89b	% Yield 100b	% Yield 125b	Reference
1	$Fe_2(CO)_{12}$ (1 eq) toluene, Δ, 5 h	3%	87%	-	122
2	$Fe_2(CO)_{12}$ (2 eq) THF, Δ, 6 h	7%	25%	33%	153c

Presumably, **125b** reacts with $Fe_3(CO)_{12}$ as a decarbonylation agent (such as trimethylamine oxide), performing a nucleophilic attack on the iron cluster, and oxidising one CO to CO_2. The reduced dithiole **100b** reacts then with the remaining cluster, giving the [FeFe]-complex **89b** in low yield (**Scheme 2.18**, **Table 2.8**). In THF, the thiosulfinate **125b** is less reactive with $Fe_3(CO)_{12}$ and it is the major compound isolated from the reaction mixture.

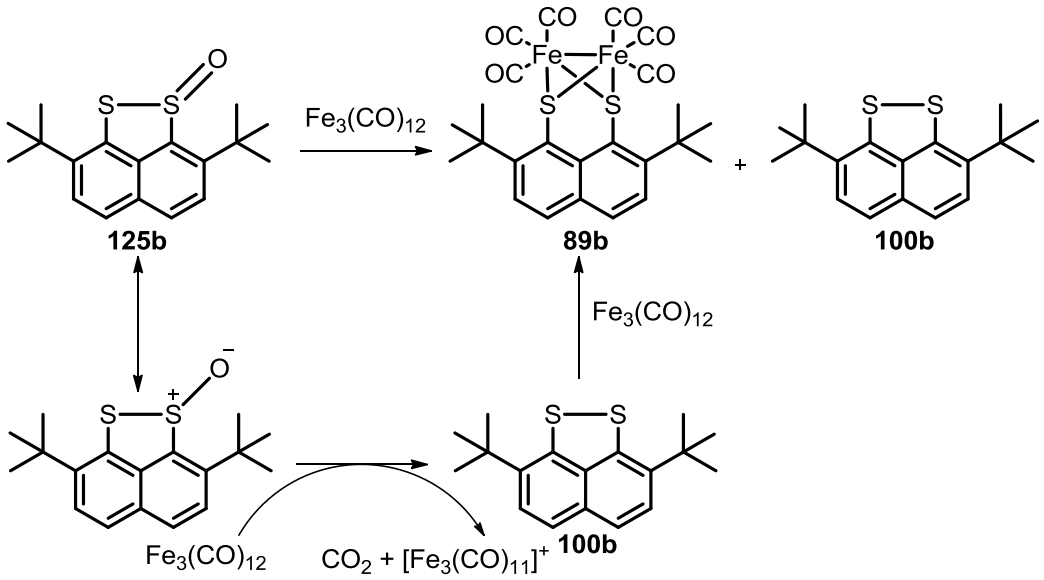

Scheme 2.18 Proposed mechanism for the oxidative decarbonylation in the reaction of **125b** with $Fe_3(CO)_{12}$.

Reacting the *vic*-disulfoxide **126b** with $Fe_3(CO)_{12}$ in either refluxing toluene (entry 1,**Table 2.9**) or THF (entry 2) gave the disulfide **100b**, the corresponding [FeFe]-complex **89b** and the thiosulfinate **125b**. The reactivity of the *vic*-disulfoxide **128b** is higher in both toluene and THF than that of **126b** and the reaction is consequently faster. In both cases, the starting material is not isolated from the reaction mixture.

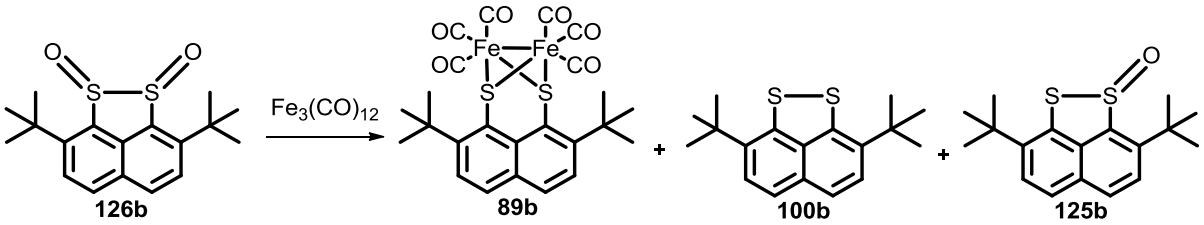

Table 2.9 Attempted oxidative insertion of $Fe_3(CO)_{12}$ into the (O)S–S(O) of **128b**.

Entry	Reaction conditions	% Yield 89b	% Yield 100b	% Yield 125b	% Yield 128	References
1	$Fe_2(CO)_{12}$ (1 eq) toluene, Δ, 2 h	8%	7%	36%	-	122
2	$Fe_2(CO)_{12}$ (1 eq) THF, Δ, 2 h	9%	13%	8%	-	153c

2.4 Summary

This chapter reported the successful synthesis and investigation of [FeFe]-hydrogenase model complexes **89d**, **91a**, **b** and **d**, **92a-b**, **93**, **94** and **96**.

Spectroscopic analysis of **89d**, **91a**, **b** and **d**, **92a-b**, **93**, **94** and **96** confirmed the influence of the chalcogen, the aromatic backbone and the ligand substituents on the [FeFe]-cluster's electronic properties. X-ray diffraction of **89d**, **91a**, **b** and **d**, **92a-b**, **93** and **94** showed a strong agreement with the reported crystal structure of **89a** and **c** and the [FeFe]-hydrogenase active site.

Electrochemical analysis showed that diselenolate-based [FeFe]-complexes are reduced at more positive reduction potential than the corresponding dithiolates; this effect was not expected from IR analysis, where the electron-density on the metal centres is clearly higher when the iron is bonded to selenium rather than sulfur. According to cyclic voltammetry measurements, dithiolate-based systems showed better stabilization of the [FeFe]-cluster reduced species in a redox cycle than the corresponding diselenoles, even though both

systems undergo a quasi-reversible process for the first reduction and a reversible one for the second. However, the diselenolate-based [FeFe]-complexes were found more effective proton reduction catalysts than their sulfur counterparts in terms of calculated overpotential and catalytic peak current increase.

The initial investigation on the oxidative insertion of $Fe_3(CO)_{12}$ into the S–S(O) and (O)S–S(O) bond of the thiosulfinate **125b** and *vic*-disulfoxide **126b** showed instead oxidative decarbonylation of $Fe_3(CO)_{12}$ and formation of the [FeFe]-complex **89b**, the reduced disulfide **100b** and, in the case of **126b**, the thiosulfinate **125b**.

Chapter 3: Incorporation of amine and imine functionality on naphthalene backbone

3.1 Light-driven hydrogen production

One of the main advantages of using hydrogen as an energy carrier is the variety of renewable primary sources exploited for its production (Section 1.1.3, Chapter 1).[4] Water photolysis, that is the direct conversion of solar energy to chemical energy by splitting water into hydrogen and oxygen, is the most fascinating and promising method for hydrogen production, since it is a clean and non-polluting process and the starting and final product is water.[154] This process needs systems which absorb visible light, convert photons to electrons and, finally, reduce water. Effectively, the water reduction involves two electrons (eq. 1, standard potentials, $E°$, are measured vs normal hydrogen electrode, NHE, at physiological conditions, pH = 7) and the oxidation requires four electrons (eq. 2).

$$2H_2O + 2e^- \rightarrow H_2 + 2OH^-, \qquad E° = -0.41 \text{ V versus NHE} \qquad \text{(eq. 1)}$$

$$2H_2O \rightarrow O_2 + 4H^+ + 4e^-, \qquad E° = -0.82 \text{ V versus NHE} \qquad \text{(eq. 2)}$$

Since water does not absorb visible light and a multi-electron transfer process is involved, light-driven hydrogen production does not occur under ambient conditions and requires large overpotentials.[155] In order to facilitate industrial water photolysis, catalysts, particularly noble metals, are used, and water is combined with both sacrificial reducing agents and methanol (Section 1.1.3, Chapter 1).[4]

3.1.1 Key features for photochemical hydrogen production

A photochemical system, aiming to produce hydrogen from water, must include a photosensitizer (PS), which harvests photons producing then the excited species PS^*, an electron acceptor (R), which oxidises PS^* to PS^+ converting photons to electrons, and a catalyst (Cat), which accumulates electrons from R^- and reduces water to H_2 and O_2. However, the charge recombination between R^- and PS^+, which regenerates the neutral PS

and R, is faster than electron transfer to the water by the catalyst. Consequently, in order to slow down this side process, a sacrificial electron donor (D) is usually added to the system. D reacts with PS^+ in an electron transfer process and gives PS and the oxidised D^+, which then decomposes irreversibly.[154]

In the presence of D, hydrogen is produced by either an oxidative quenching mechanism, because it involves the oxidation of PS^* to PS^+ by R (1, **Scheme 3.1**) or a reductive quenching mechanism, since PS^* is reductively quenched to PS^- by D (2, **Scheme 3.1**).[154]

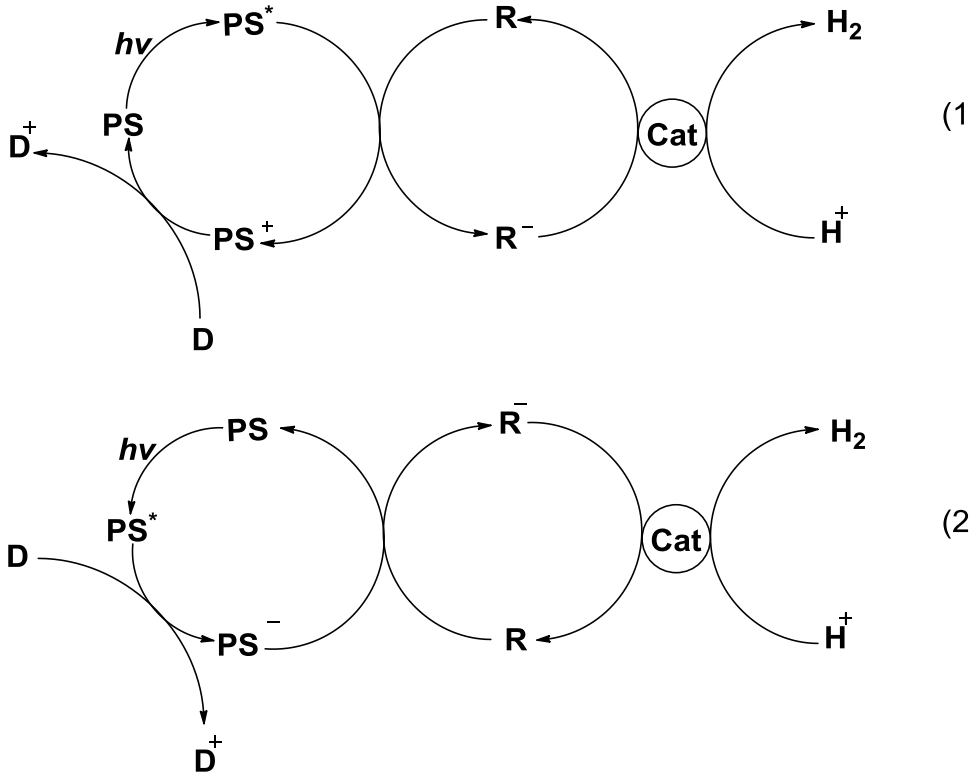

Scheme 3.1 Photochemical hydrogen production by oxidative quenching of PS^* by R (1) or reductive quenching of PS^* by D (2).[154]

Generally, transition and noble metal complexes (*i.e.* Cr, Ru, Ir, Os, Re, Pt), metalloporphyrins and metallophthalocyanines are employed as photosensitizers, while noble metal complexes and colloids (Pt and Pd), together with cobalt complexes, are used as catalysts.[154-157] Bipyridines, but also lanthanides ions and transition metal complexes, are

efficient electron acceptors in the light-driven hydrogen production. Amines and thiols are the most utilised electron donors.[154,155]

3.1.2 Principles for efficient photoactive [FeFe]-hydrogenase model systems

The remarkable conversion of protons into hydrogen catalysed by the [FeFe]-hydrogenase inspired many research groups to further investigate the application of analogues of the enzyme's active site in photochemical systems, where the [FeFe]-cluster functions as electron acceptor and hydrogen production catalyst (R and Cat, **Scheme 3.1**).[155-157]

In order to build efficient photochemical systems based on [FeFe]-hydrogenase analogues some features must be considered. Depending on the quenching mechanism (**Scheme 3.1**, Section 3.1.1) the reduction potential of [FeFe]-complexes should be less negative than the oxidation or the reduction potential of the PS^* in order to favour electron transfer from the photosensitizer to the electron acceptor and to avoid undesired side processes, such as charge recombination.[157,158] Since [FeFe]-hydrogenase synthetic mimics show an intense MLCT absorption band at wavelengths < 400 nm and a weak d-d transition band in the range 400-600 nm, [157] ultraviolet and visible light irradiation might promote complex degradation in form of CO loss and Fe–Fe bond elongation, respectively. Consequently, photoexcitation should be limited to the photosensitizer and above 550 nm, where the [FeFe]-complex absorption is marginal.[157] Finally, photochemical systems need to be water soluble in order to combine catalytic proton reduction with water splitting.[158] Based on these properties, efficient proton reduction photocatalysts are still rare compared to the variety of reported electrocatalysts, partly described in Chapters 1 and 2.

3.2 Aims and objectives

Zinc tetraphenylporphyrin (ZnTPP), covalently linked to naphthalene-1,8-dichalcogenides **99a** and **100a** (Chapter 2), were targeted as suitable photochemical systems for hydrogen evolution. Functional groups such as amines, imines and amides, in one *ortho* position on the naphthalene ring, were selected as linkers between the photosensitizer and the [FeFe]-complex. Particularly, amines and imines represent a basic site, which might favour proton reduction catalysis (**Figure 3.1**).[48]

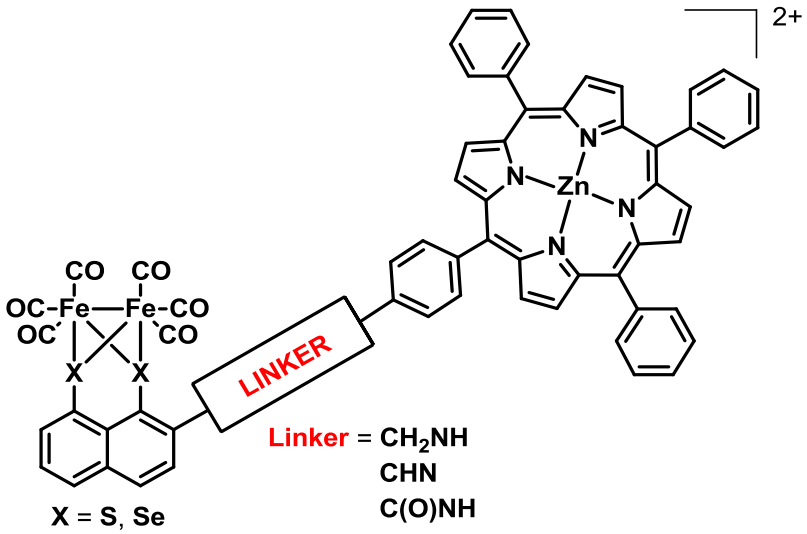

Figure 3.1 Photochemical system based on *peri*-substituted dichalcogenide-bridged [FeFe]-complexes and ZnTTP linked by an amine/imine/amide group.

This chapter describes the synthetic work on functionalising naphthalene-1,8-dichalcogenides and reports the spectroscopic and electrochemical characterisation of the corresponding [FeFe]-complexes. In order to develop an accessible and reproducible synthetic methodology, [FeFe]-complexes **129a** and **130a**, containing an *N*-isopropyl amino group in one *ortho* position on the naphthalene ring were first investigated (**Figure 3.2**).

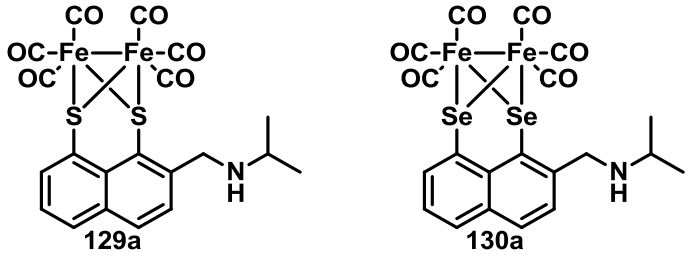

Figure 3.2 *N*-Isopropylamine-functionalised [FeFe]-complexes **129a** and **130a**.

Subsequently, [FeFe]-complexes **131a-c** and **132a-c** with *p*-methoxyaniline as nitrogen source and amine, imine and amide as linking functional group were targeted (**Figure 3.3**) as model systems en route to porphyrin-based photochemical dyads (**Figure 3.1**),

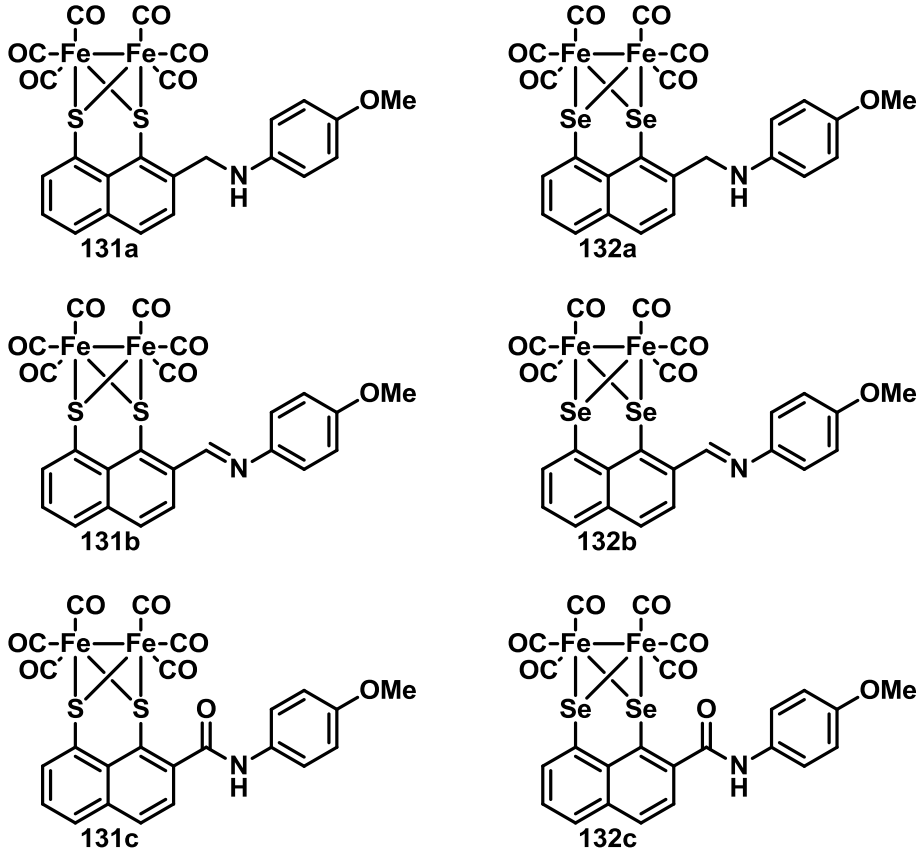

Figure 3.3 *N*-(*p*-Methoxyphenyl)amine-functionalised **131a** and **132a**, *N*-(*p*-methoxyphenyl)imine-functionalised **131b** and **132b**, and *N*-(*p*-methoxyphenyl)amide-functionalised **131c** and **132c** [FeFe]-complexes.

3.3 Results and discussion

3.3.1 Functionalization of *peri*-substituted naphthalene dichalcogenides

Vilsmeier-Haak formylation of *peri*-substituted dichalcogenides **99a** and **100a** with phosphoryl trichloride ($POCl_3$) in dimethylformamide (DMF) afforded the known *ortho* formylate derivatives **133** and **134** in good yields (**Scheme 3.2**).[159,160]

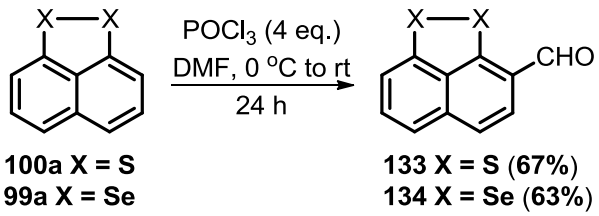

Scheme 3.2 Synthesis of aldehydes **133** and **134**.

Mugesh and co-workers reported the condensation of aldehyde **134** and isopropylamine (*i*$PrNH_2$) in refluxing dry CH_3CN gave the Schiff base **136b** in 90% yield.[160] The reaction was repeated, but **136b** was isolated in only 50% yield and starting material **134** was recovered (33%). The same synthetic procedure was also applied to aldehyde **133** to give the novel Shiff base **135b** in 60% yield together with **133** (25%). Variation of the solvent, CH_2Cl_2 instead of CH_3CN, and the use of $MgSO_4$ [161] as drying agent, did not favour the formation of **135b** and **136b**, which were isolated in 71% and 57% yields along with the corresponding aldehydes **133** or **134** in 38% and 20% yields respectively. However, following the literature procedure for the synthesis of aromatic ketimines, [162] condensation of **133** and **134** with stoichiometric amounts of *i*$PrNH_2$ using titanium tetrachloride ($TiCl_4$) as a catalyst and an excess of NEt_3 gave the expected products in significantly higher yields. As previously reported, [160] reduction of the imine double bond with a large excess of sodium borohydride ($NaBH_4$) generated amines **135a** and **136a** which, after an aqueous work-up and no further

purification, were reacted with $Fe_3(CO)_{12}$ to yield the novel [FeFe]-complexes **129a** and **130a** by oxidative insertion of Fe(0) into the dichalcogenide bond (**Scheme 3.3**).

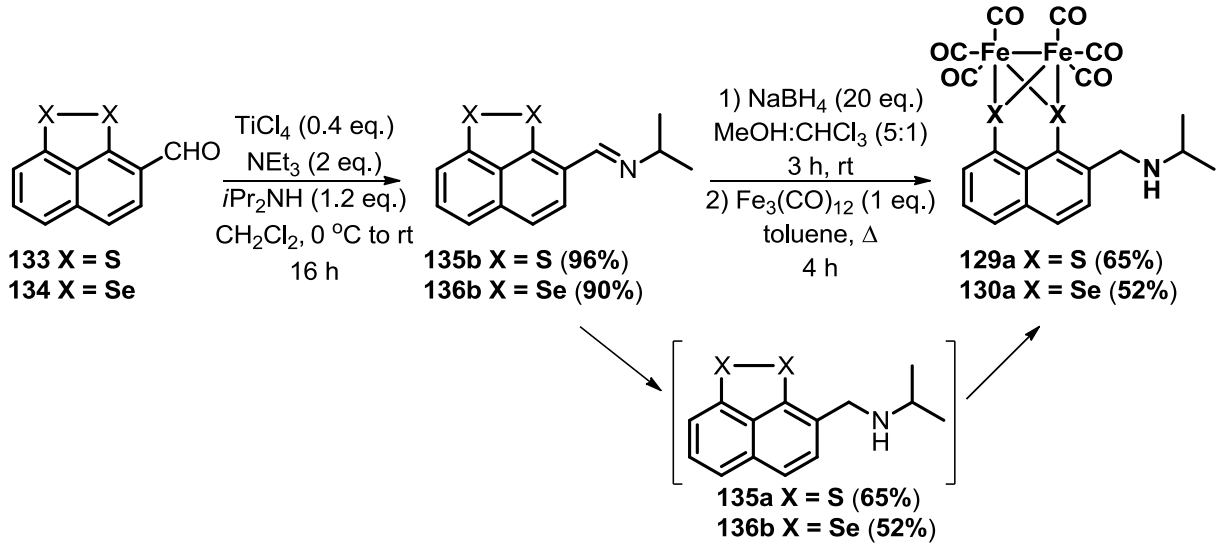

Scheme 3.3 Synthesis of [FeFe]-complexes **129a** and **130a**.

The novel Schiff base **138b** was obtained following the synthetic procedure described for compounds **135b** and **136b**.[162] Surprisingly, condensation between 2-formyl-naphthalene-1,8-dithiole **133** and *p*-methoxyaniline, using $TiCl_4$ and NEt_3, gave the imine **137b** in very low yield (24%) compared with the selenium counterpart (94%) and the reaction mixture was difficult to purify. However, upon refluxing **133** and a large excess of *p*-methoxyaniline in dry CH_3CN, [160] the Schiff base **137b** was instead obtained in high yield. As previously reported, [160] the novel amine-substituted dichalcogenides **137a** and **138a** were obtained by reduction of imines **137b** and **138b** with $NaBH_4$.[160] The oxidative insertion of $Fe_3(CO)_{12}$ into the S–S or Se–Se bond gave the expected [FeFe]-complexes **131a** and **132a** respectively. Similarly, [FeFe]-complexes **131b** and **132b** were successfully isolated in good yields by reacting the Shiff bases **137b** or **138b** with $Fe_3(CO)_{12}$ (**Scheme 3.4**).

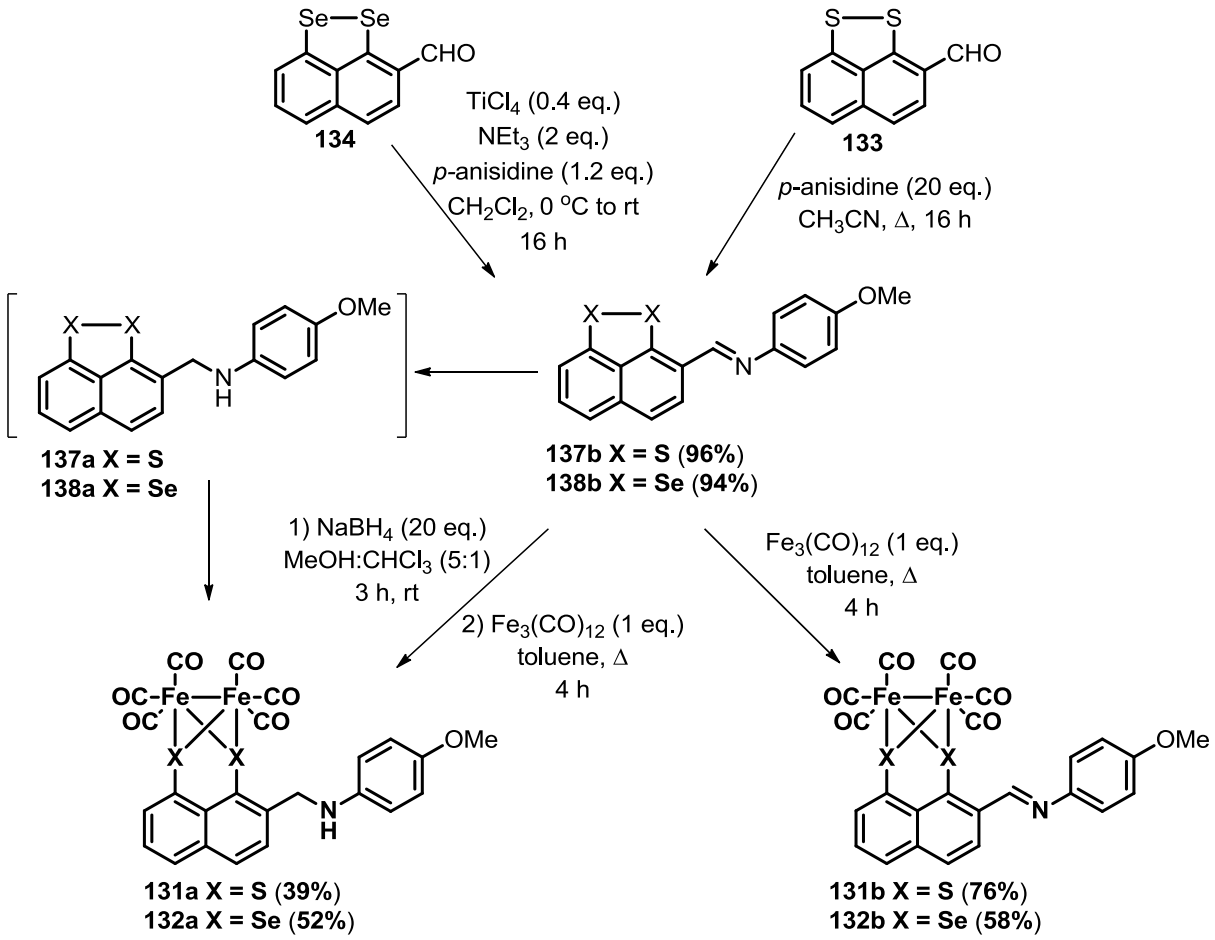

Scheme 3.4 Synthesis of [FeFe]-complexes **131a-b** and **132a-b**.

In order to obtain [FeFe]-complexes **131c** and **132c**, containing an amido-linker between the naphthalene backbone and *p*-methoxyphenyl group, oxidation of aldehydes **133** and **134** to the corresponding carboxylic acids **139** and **140** was investigated.

Liu and Kataoka showed the successful aldehyde oxidation of sulfur and selenium-containing substrates using silver oxide (Ag_2O) as a mild oxidising agent.[163,164] However, reaction of both aldehydes **133** and **134** with Ag_2O, prepared *in situ* from silver nitrate ($AgNO_3$) in an aqueous solution of sodium hydroxide (NaOH), [165] proceeded slowly, because the starting material was insoluble in the reaction solvents (EtOH and H_2O), even under refluxing conditions. One unidentified product was formed from the consumption of the aldehydes (entries 1 and 2, **Table 3.1**). Attempts to oxidise **133** to the carboxylic acid using Pinnick

oxidation [166] were unsuccessful and starting material was recovered (entries 3 and 4, **Table 3.1**).[167,168]

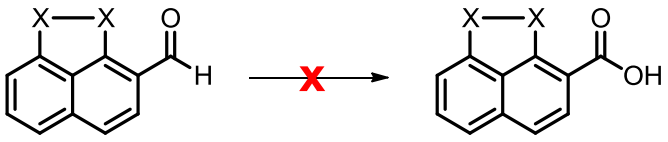

133 X = S
134 X = Se

139 X = S
140 X = Se

Table 3.1 Attempts to oxidise aldehydes **133** and **134** to carboxylic acids **139** and **140**.

Entry	Reaction condition	Isolated product	Reference
1	**134** (1 eq.), Ag_2O (2 eq.), EtOH/H_2O, Δ, 2 h	not identified	163
2	**133** (1 eq.), Ag_2O (2 eq.), H_2O, rt to Δ, 25 h	not identified	164
3	**133** (1 eq.), $NaClO_2$ (5 eq.), 2-methyl-2-butene (10 eq.), NaH_2PO_4 (3.3 M, 5 eq.), THF, rt to Δ, 22 h	81% **133**	167
4	**133** (1 eq.), AcOH (112 eq.), NaOAc (3.50 eq.), sulfamic acid (2 eq.), $NaClO_2$ (2 eq.), dioxane, 40 °C, 27 h	28% **133**	168

Oxidation of imines to amides is a well-known and versatile synthetic reaction, which is usually performed under mild oxidation conditions.[167] Tomioka and co-workers described a synthetic protocol, based on Pinnick oxidation, to oxidize imines to amides in high yields.[167] The reported procedure was applied to imine **137b**, which was treated with sodium chlorite ($NaClO_2$) under buffered conditions (NaH_2PO_4, 3.3 M aq. solution) and in the presence of 2-methyl-2-butene as a chlorine scavenger either at room temperature or under reflux; however, the reaction was unsuccessful and, in both cases, starting material was recovered (entries 1 and 2, **Table 3.2**). Treating a 1:1.5 mixture of aldehyde **133** and *p*-methoxyaniline with $NaClO_4$ [169] was also ineffective and the isolated major product was imine **137b** (entry 3, **Table 3.2**).

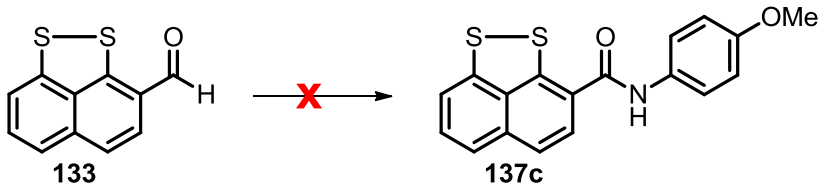

Table 3.2 Attempted oxidation of aldehyde **133** to amide **137c**.

Entry	Reaction condition	Isolated product	Reference
1	$NaClO_2$ (5 eq.), 2-methyl-2-butene (10 eq.), NaH_2PO_4 (3.3 M, 5 eq.), THF, rt, 4 h	99% **137b**	167
2	$NaClO_2$ (5 eq.), 2-methyl-2-butene (10 eq.), NaH_2PO_4 (3.3 M, 5 eq.), THF, rt to Δ, 21 h	88% **137b**	167
3	$NaClO_2$ (3.13 eq.), 2-methyl-2-butene (10 eq.), NaH_2PO_4 (3.3 M, 3.5 eq.), toluene, 40 °C 16 h	47% **137b** 37% **133**	169

Consequently, attention was directed to an alternative multi-step synthetic route in order to obtain carboxylic acids **139** and **140** from aldehydes **133** and **134**.

Aldehyde **133** was readily converted to the novel oxime **141** by reacting with hydroxylamine chloride ($NH_2OH{\cdot}HCl$) in refluxing EtOH, and it was used without any further purification.[170] Dehydration of **141** using NEt_3 in refluxing CH_3CN gave the corresponding nitrile **142** which was then hydrolysed to the carboxylic acid **139** by KOH in a 1:7 mixture of H_2O and ethyl glycol (**Scheme 3.5**).[171,172]

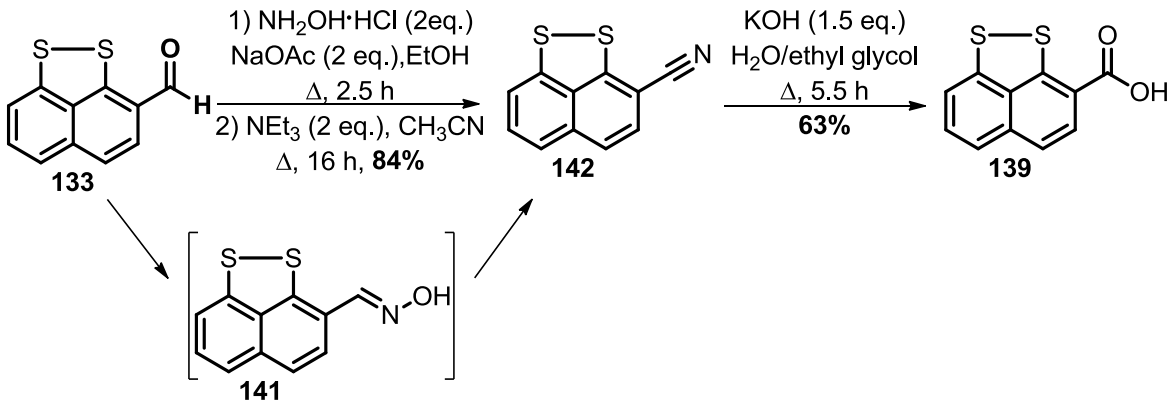

Scheme 3.5 Synthesis of carboxylic acid **139**.

Conversion of naphthalene-1,8-dithiole-3-carboxylic acid **139** to the corresponding amide **137c** upon reaction with freshly distilled thionyl chloride ($SOCl_2$), followed by addition of *p*-methoxyaniline, resulted in the isolation of an unidentified product (entry 1, **Table 3.3**).[173] Treatment of **139** with $SOCl_2$ in refluxing CH_2Cl_2 resulted, instead, in the degradation of the starting material, observed by thin layer chromatography (t.l.c.) analysis and, consequently, the following addition of the amine was not performed (entry 2, **Table 3.3**).[174] Reaction of **139** with known activating groups, such as *N*,*N*,*N*′,*N*′-tetramethyl-O-(benzotriazol)uranium hexafluorophosphate (HBTU) or 1-hydroxybenzotriazole (HOBt) coupled with dicyclohexylcarbodiimide (DCC), [175,176] followed by addition of *p*-methoxyaniline, resulted only in the recovery of carboxylic acid **139** (entries 3 and 4, **Table 3.3**) and amine (entry 3, **Table 3.3**).

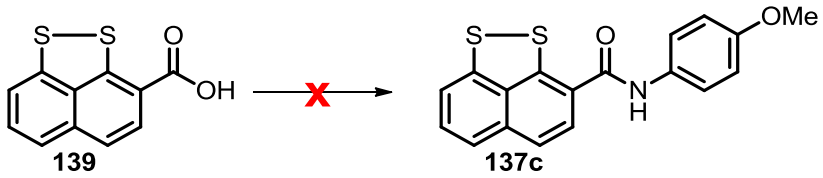

139 **137c**

Table 3.3 Attempted condensation of carboxylic acid **139** and *p*-methoxyaniline.

Entry	Reaction condition	Isolated product	Reference
1	1) $SOCl_2$ (2 eq.), Δ, 2 h, 2) KCO_3 (2.5 eq.), *p*-methoxyaniline (1.5 eq.), THF, 0 °C to rt, 30 h	unidentified product	173
2	1) $SOCl_2$ (2 eq.), CH_2Cl_2, Δ, 3 h, 2) *p*-methoxyaniline (2 eq.), NEt_3 (2 eq.), Et_2O, rt, 2 h	degradation	174
3	1) HBTU (1.4 eq.), dry DMF, rt, 30 min, 2) *p*-methoxyaniline (1.6 eq.), NEt_3 (2 eq.), DMF, 50 °C, 24 h	14% **139** 59% *p*-methoxyaniline	175
4	1) HOBT (1.5 eq.), DCC (1.5 eq.), dry DMF, rt, 30 min, 2) *p*-methoxyaniline (1.6 eq.), NEt_3 (2 eq.), rt, 24 h	90% **139**	176

Naphthalene-1,8-diselenole 2-oxime **143**, obtained by the same procedure described for **141**, [170] was not dehydrated to the corresponding nitrile **144** with NEt_3 in refluxing CH_3CN. Therefore, in order to facilitate the oxime dehydration, the hydroxyl group was converted into a better leaving group and the benzoyl and pivaloyl derivatives **145** and **146** were synthesised (**Scheme 3.6**).[177,178]

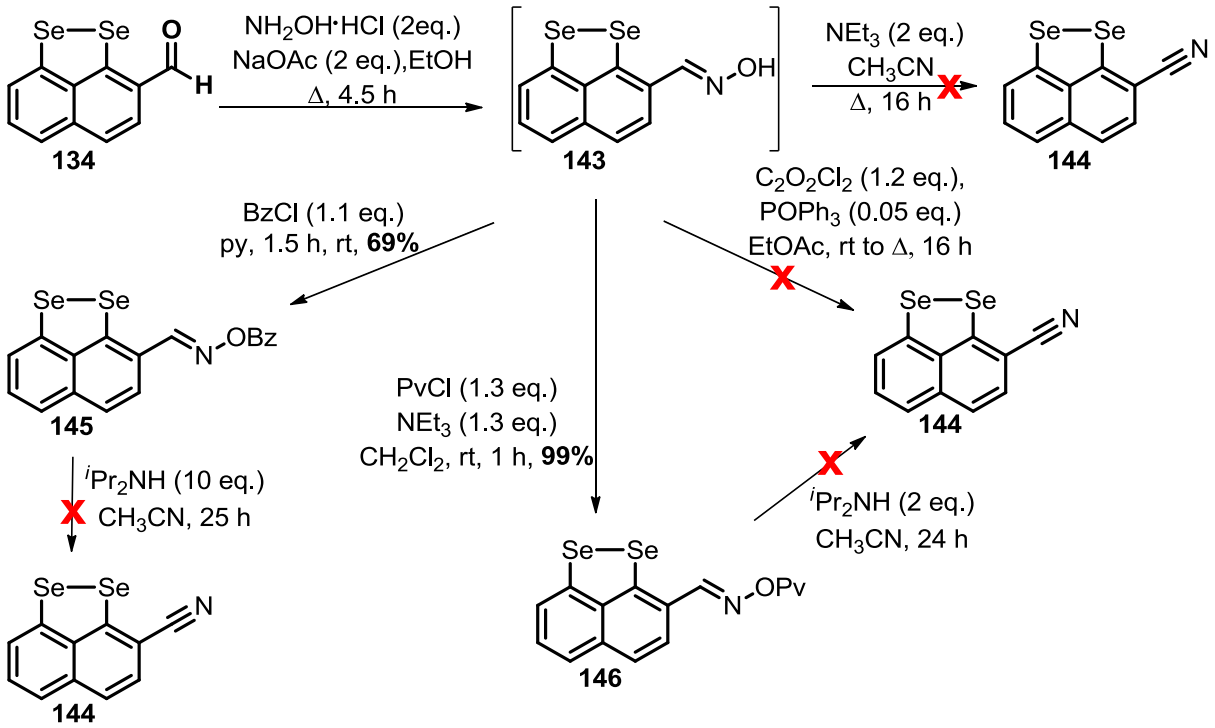

Scheme 3.6 Attempts to obtain nitrile **144** by dehydration of oxime **143** and benzoyl and pivaloyl activated oximes **145** and **146**.

However, attempted elimination of the esters in **145** and **146** by reaction with *i*PrNH$_2$ [179,180] was unsuccessful and both starting materials were completely recovered. Similarly, *in situ* activation of **143** by oxalyl chloride ($C_2O_2Cl_2$), followed by subsequent elimination using triphenylphosphine oxide ($POPh_3$), [181] did not give the excepted nitrile **144** and, again, the unreacted naphthalene-1,8-diselenole 2-oxime **143** was completely recovered (**Scheme 3.6**).

3.3.2 Spectroscopic and X-ray analysis of amine and imine-functionalised [FeFe]-complexes

[FeFe]-complexes **129a**, **130a**, **131a-b** and **132a-b** were characterised by ^{1}H, ^{13}C NMR, IR and UV/vis spectroscopy. Molecular structures of [FeFe]-complexes **131a-b** and **132b** were also confirmed by X-ray diffraction. In analogy to [FeFe]-complexes **89d**, **91a**, **b** and **d**, **91a-b**, **93**, **94** and **96** (Chapter 2), ^{1}H NMR spectra of **129a**, **130a**, **131a-b** and **132a-b** displayed the expected downfield shift of the aromatic protons compared with those of the corresponding ligands **135a-b**, **136a-b**, **137a-b** and **138a-b** (**Scheme 3.3** and **Scheme 3.4**), associated with the insertion of the [FeFe]-cluster into the dichalcogenide bond.[122] Despite the asymmetry of **129a**, **130a**, **131a-b** and **132a-b**, ^{13}C NMR spectra showed one single peak at 207 or 208 ppm, assigned to the carbonyl ligands binding the iron centre in the dithiolate and diselenolate-bridged complexes, respectively.

In Table 3.4 the IR stretching wavenumbers of the carbonyl ligands are listed. As previously observed (Chapter 2), the absorption bands are all in the range 2070-1950 cm^{-1}. [112,117,122] According to the IR analysis of diselenolate-based [FeFe]-complexes (Chapter 2), **130a** and **132a-b** display a bathochromic shift of the carbonyl stretching compared with that for the analogous dithiolates **129a** and **131a-b**, because of the different electronegativity of the chalcogens (**Table 3.4**). The electron-density on the iron centres is decreased by the presence of the selenium, which is less electronegative than the sulfur, and, consequently, the back bonding donation from the occupied metal d-orbitals to the CO π^{*} antibonding orbital is favoured and the C–O bond weakened. Substitution of the *ortho* position on the naphthalene ring of the dithiolate-based **129a** and **131a-b**, notably shifts the first two carbonyl absorption bands towards lower wavenumbers than those of the unsubstituted **89a** and the alkyl-substituted **89b** (**Table 3.4**). The carbonyl IR spectra of diselenolate-bridged [FeFe]-complexes **130a** and **132a** show a shift of the middle three absorption bands towards higher

wavenumbers than those recorded for the unsubstituted **91a** and the alkyl-substituted **91b** (**Table 3.4**), The imino substituent in [FeFe]-complex **132b** causes, instead, a more unpredictable effect on the carbonyl IR stretches relative to the unsubstituted **91a** the alkyl-substituted **91b** (**Table 3.4**). Amine-substituted [FeFe]-complexes **131a** and **132a** feature comparable wavenumbers values in the first two absorption bands to those of the imine-substituted **131b** and **132b**. The recorded wavenumbers of the last three stretches are, instead, shifted to lower values in the imine than in the amine-substituted [FeFe]-complexes (**Table 3.4**). No significant differences between aromatic and non-aromatic amino substituents on the naphthalene are observed.

Table 3.4 Carbonyl IR stretches of [FeFe]-complexes **129a**, **130a**, **131a-b** and **132a-b**.

	Complex	***ν*(CO)[cm^{-1}]**
X= Y= S[a], R= H[b]	**89a**[c]	2074, 2039, 2001
X= Y= S, R= *t*Bu	**89b**[c]	2071, 2036, 1997
X= Y= Se, R= H	**91a**[d]	2058, 2016, 1996, 1979, 1822
X= Y= Se, R= *t*Bu	**91b**[d]	2057, 2015, 1979, 1970, 1956
X= Y= S, R= *i*Pr-*NHCH$_2$*	**129a**	2064, 2028, 2002, 1986, 1962
X= Y= Se, R= *i*Pr-*NHCH$_2$*	**130a**	2056, 2020, 1994, 1980, 1956
X= Y= S, R= PMP-*NHCH$_2$*	**131a**	2064, 2026, 2005, 1988, 1963
X= Y= S, R= PMP-*N=CH*	**131b**	2066, 2024, 1977, 1959
X= Y= Se, R= PMP-*NHCH$_2$*	**132a**	2057, 2020, 1997, 1981, 1958
X= Y= Se, R= PMP-*N=CH*	**132b**	2061, 2024, 1978, 1953

[a] X,Y= chalcogen, [b] R= substituent in position 2 on the naphthalene ring, data taken from [c] reference [122] and [d] Chapter 2

Figure 3.4 shows the UV/vis spectra of [FeFe]-complexes **129a**, **130a**, **131a-b** and **132a-b** and the corresponding absorbance extinction coefficients are reported in Table 3.5.

Table 3.5 Absorption values of [FeFe]-complexes **129a**, **130a**, **131a-b** and **132a-b**.

Complex	λ / nm (ε / $M^{-1}cm^{-1}$)
129a	253 ($\varepsilon = 2.1 \times 10^4$), 352 ($\varepsilon = 1.8 \times 10^4$)
130a	253 ($\varepsilon = 1.6 \times 10^4$), 345 ($\varepsilon = 1.7 \times 10^4$)
131a	253 ($\varepsilon = 3.0 \times 10^4$), 307 ($\varepsilon = 1.4 \times 10^4$), 351 ($\varepsilon = 1.7 \times 10^4$)
131b	242 ($\varepsilon = 2.2 \times 10^4$), 288 ($\varepsilon = 2.4 \times 10^4$)
132a	250 ($\varepsilon = 3.4 \times 10^4$), 305 ($\varepsilon = 1.4 \times 10^4$), 346 ($\varepsilon = 1.6 \times 10^4$)
132b	242 ($\varepsilon = 2.7 \times 10^4$), 290 ($\varepsilon = 2.5 \times 10^4$)

Concentration used for the measurements is 1×10^{-5} M.

The UV/vis spectra of the amine-substituted [FeFe]-complexes **129a**, **130a**, **131a** and **132a**, each display an intense band in the range of 210-260 nm, which is assigned to the naphthalene π-π^* transition, and in the range of 310-410 nm, which is attributed to the iron-carbonyls MLTC or LMCTor to the naphthalene π-π^* transition, [123,125,144] consistent with what has previously been described in Chapter 2. Additionally, a weak absorption band is observed in the range 410-510 nm, which is assigned to the metal d-d transition (**Figure 3.4**).[125,144]

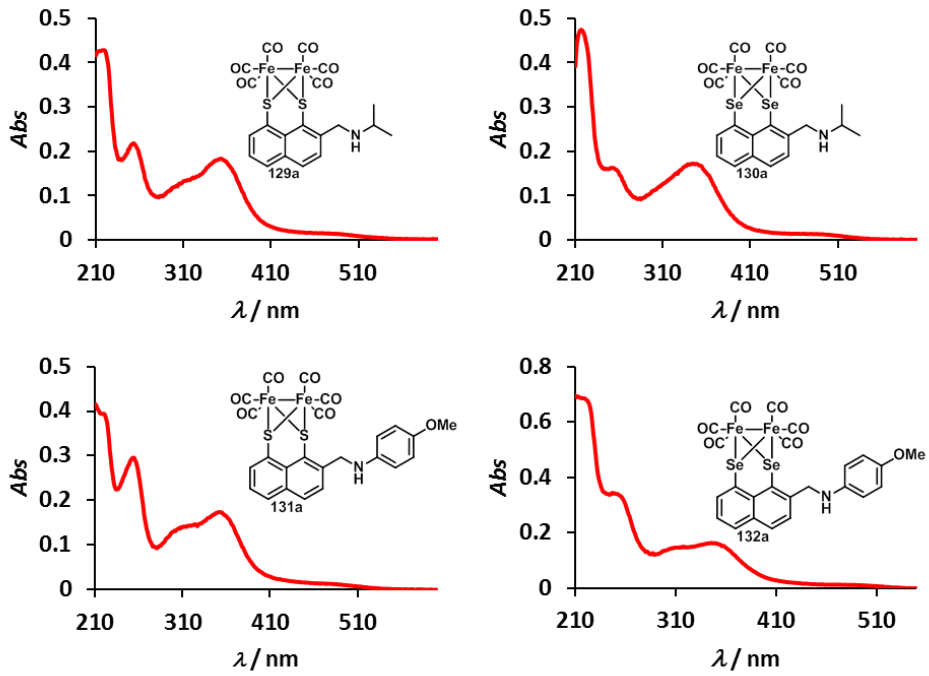

Figure 3.4 UV/vis absorption spectra of [FeFe]-complexes **129a**, **130a**, **131a** and **132a**.

Imine-substituted [FeFe]-complexes **131b** and **132b** display very different UV/vis spectra from the corresponding amines (**Figure 3.5**). A continuous absorption band is observed in the range of 250-400 nm, because the conjugated system extends from the naphthalene backbone to the *p*-methoxyaniline *via* imino group. The metal d-d transition band is stronger in the imine-derivatives than in the corresponding amines, especially for the diselenolate-bridged [FeFe]-complex **131b**.[125,144]

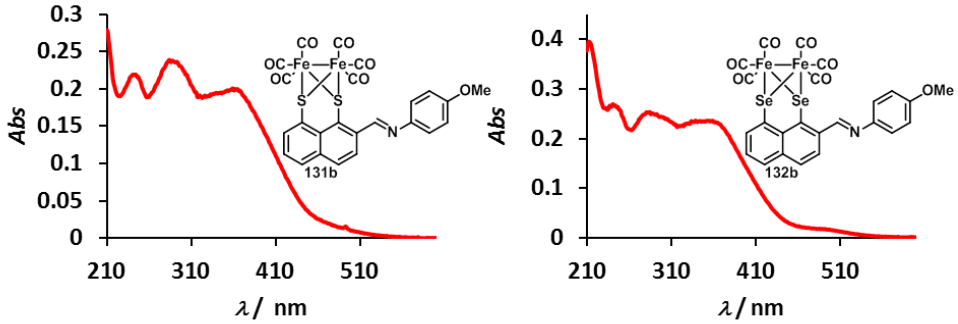

Figure 3.5 UV/vis absorption spectra of [FeFe]-complexes **131b** and **132b**.

Titration of a 1 μM solution of [FeFe]-complexes **129a**, **130a**, **131a-b** and **132a-b** in CH_3CN with increasing concentration of *p*TsOH (from 0.5 μM to 10 μM, see Chapter 6 for experimental details) was monitored by UV/vis spectroscopy.[55a)] Each addition of acid resulted in a remarkable change in the complex absorption profile, accompanied by an intense colour change from orange to red. Figure 3.6 shows the titration of [FeFe]-complex **129a**. A plot of the absorbance at 353 nm as a function of the acid concentration indicates two processes (inset at the right in **Figure 3.6**). The addition up to 1.0 μM of acid results in a stepwise increase of the absorbance at 353 nm, while further acid addition is associated with its decrease. The slope is less sharp than the first one and tends to zero after 2 μM of acid. Furthermore, the decrease of the absorbance at 353 nm is combined with the formation of a new peak at 299 nm, whose intensity decreases then at each subsequent addition of acid (left

inset in **Figure 3.6**). The slope of the plot of the absorbance at 299 nm as a function of the acid concentration also displays a change in the slope after 2 μM of acid, tending to zero.

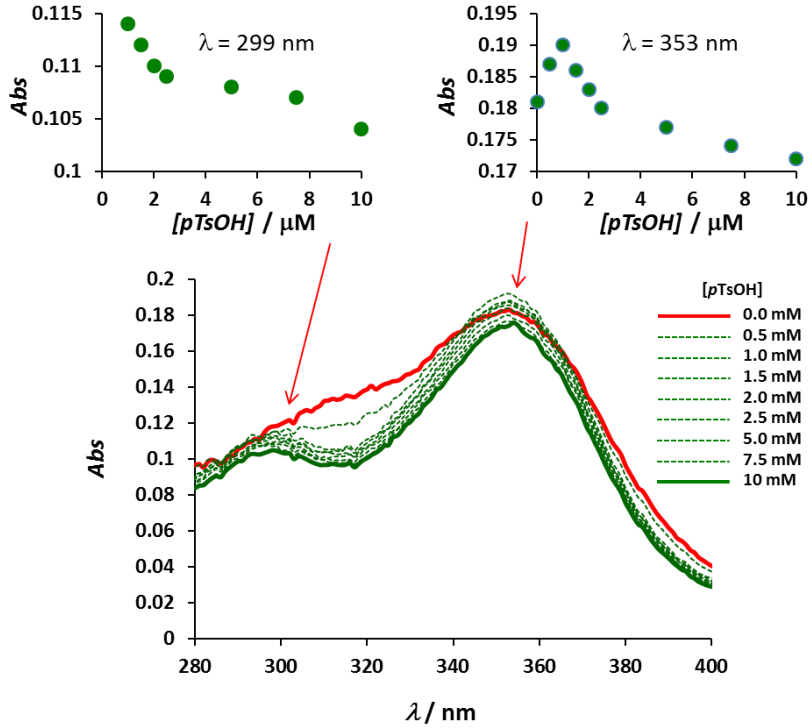

Figure 3.6 Titration of 1 μM solution of [FeFe]-complex **129a** with *p*TsOH (from 0.5 μM to 10 μM), monitored by UV/vis spectroscopy. The insets show the absorbance peak at 353 nm and 299 nm plotted vs the acid concentration.

Amine-substituted dithiolate and diselenolate-based [FeFe]-complexes **130a**, **131a** and **132b** show similar behaviour to **129a**. In addition, **130a** and **132a** exhibit a shift of the absorption band at 345 nm (**130a**) and 346 nm (**132a**) to 349 nm and 350 nm respectively (**Figure 3.7**).

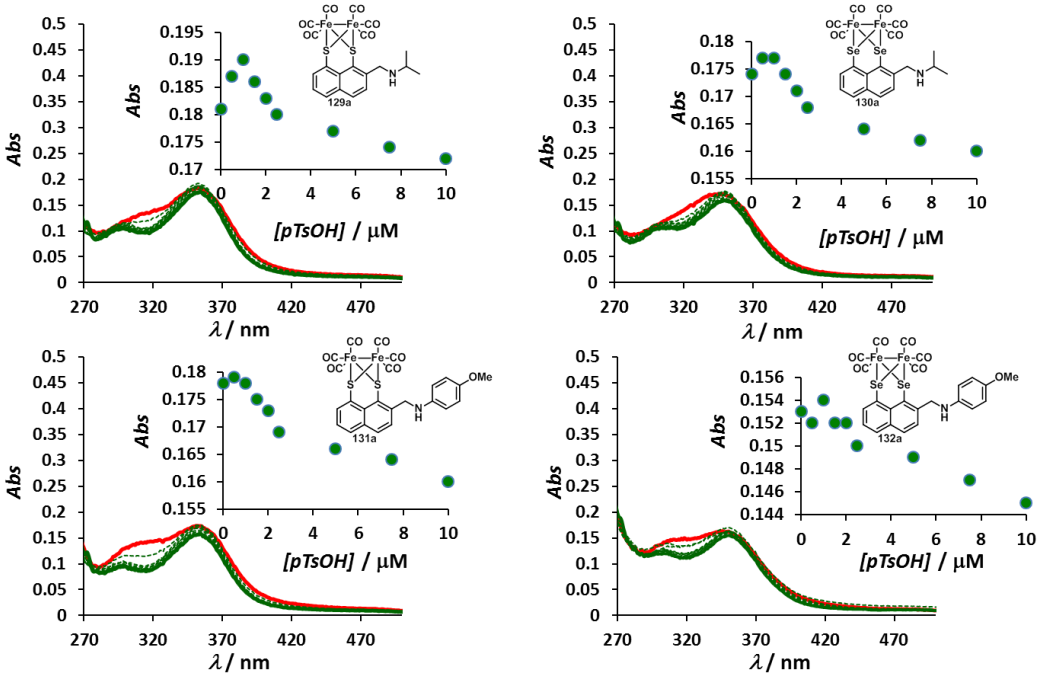

Figure 3.7 Titration of 1 μM solution of [FeFe]-complexes **129a, 130a, 131a** and **132a** with *p*TsOH (from 0.5 μM to 10 μM), monitored by UV/vis spectroscopy. The insets show the absorbance peaks at 353 nm (**129a**), 349 nm (**130a**), 353 nm (**131a**) and 351 nm (**132a**) plotted vs the acid concentration.

Upon addition of increasing concentration, imine-substituted [FeFe]-complexes **131b** and **132b** undergo only one process, which is associated with decrease of the absorption bands at 359 nm and 290 nm for **131b** and 359 nm and 285 nm for **132b**. The increase of the d-d transition absorption band in the range 410-500 nm is also observed (**Figure 3.8**). In analogy with the amine-substituted [FeFe]-complexes, the slope tends to zero after 2 μM of acid.

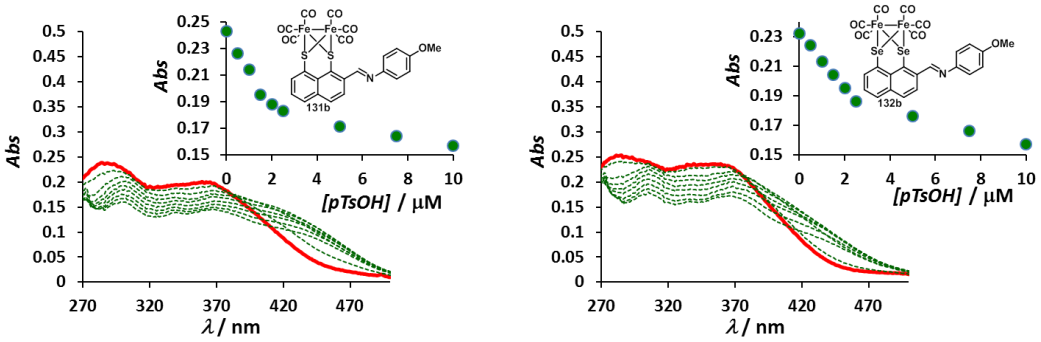

Figure 3.8 Titration of 1 μM solution of [FeFe]-complexes **131b** and **132b** with *p*TsOH (from 0.5 μM to 10 μM), monitored by UV/vis spectroscopy. The insets show the absorbance peak at 359 nm (**131b** and **132b**) plotted vs the acid concentration.

In order to exclude the protonation of the linking sulfurs/seleniums, titration of the unsubstituted [FeFe]-complexes **89a** and **91a** was carried out in the same experimental conditions and no significant changes were observed upon addition of acid (**Figure 3.9**).

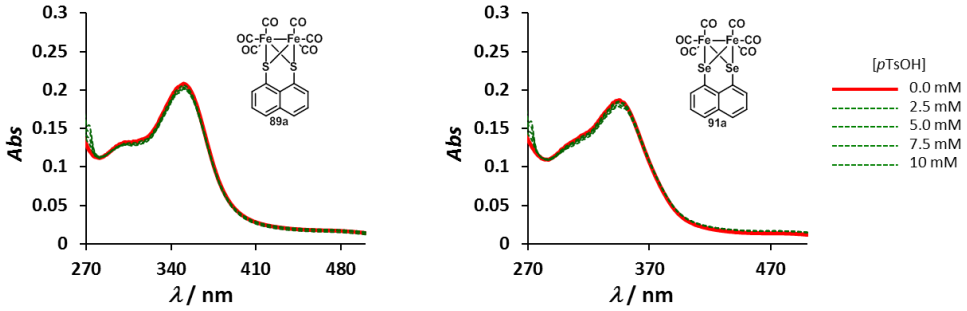

Figure 3.9 Titration of [FeFe]-complexes **89a** and **91a** with pTsOH (from 0.5 μM to 10 μM), monitored by UV/vis spectroscopy.

Furthermore, in order to check that decomposition of the [FeFe]-complexes, by loss of the $Fe_2(CO)_6$, did not occur, UV/vis spectra of **137b** and **138b** were recorded for comparison purposes. However, they show a different absorption profile from those recorded for the corresponding [FeFe]-complexes (**Figure 3.10**).

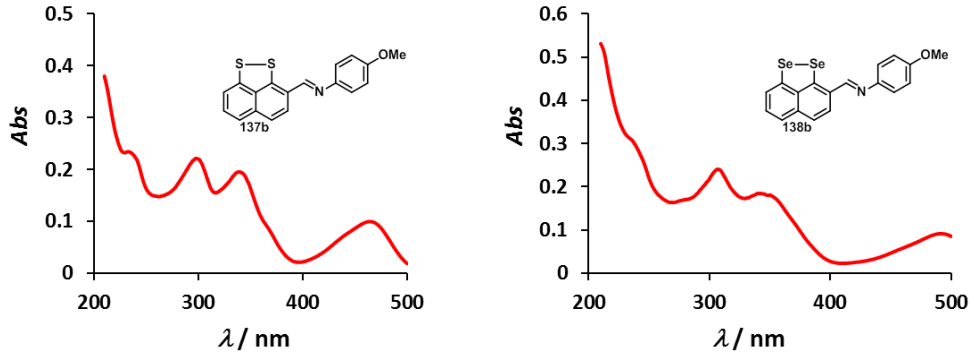

Figure 3.10 UV/vis absorption spectra of the imine-substituted ligands **137b** and **138b**.

Accordingly, the increase of the absorption around 350 nm in the UV/vis spectra of [FeFe]-complexes **129a**, **130a**, **131a** and **132a** may suggest that protonation of the nitrogen occurs upon addition of *p*TsOH up to 1 μM.[55a)] The decrease of the same peak and the formation of a new absorption band around 300 nm may indicate a second protonation event, presumably formation of H-bonds with either the proximal carbonyls or the metal. In the protonation of the imine-substituted **131b** and **132b**, this second event may occur after the first addition of *p*TsOH, since both peaks around 290 nm and 360 nm exhibit a remarkable decrease in intensity. The change of slope at 2 μM, observed for all the complexes (insets in **Figure 3.7** and **Figure 3.8**), may indicate that the second protonation event is associated with lower proton affinity than the first. Comparison with the UV/vis spectra of **89a** and **91a** suggests that the protonation does not involve the bridging sulfurs/seleniums (**Figure 3.9**).[55a)]

The molecular structures of [FeFe]-complexes **131a-b** and **132a** were confirmed by X-ray analysis. Crystal structures of **131a-b** and **132a** are shown in Figure 3.11; bond lengths and angles of **131a-b** are listed in Table 3.6. Due to problems with the crystal, and thus data quality, the crystal structure of **132a** is intended to be used only for the purpose of identity and the corresponding bond lengths and angles are neither reported nor discussed (see Chapter 6 for the experimental details).

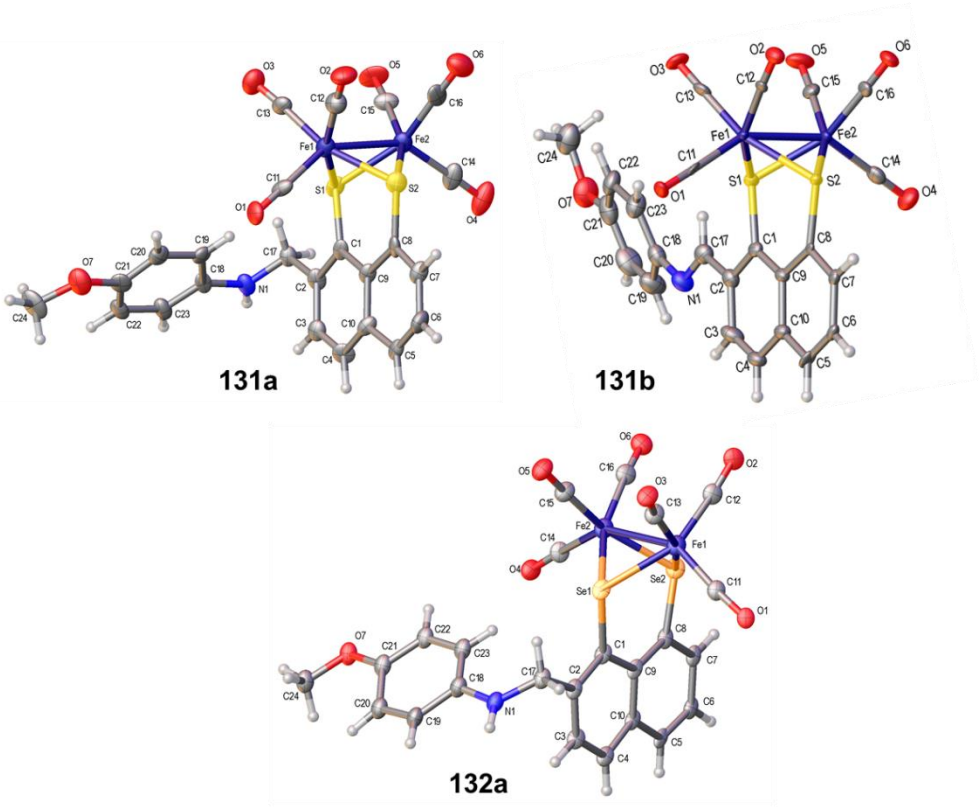

Figure 3.11 Crystal structure of [FeFe]-complexes **131a-b** and **132a**.

The crystal structures of **131a-b** possess a dichalcogenide-bridged [FeFe]-core which assumes the typical butterfly architecture with two iron centres linked to three carbonyl ligands in a distorted square-pyramidal geometry, consistent with the previously described **89d**, **91a**, **b** and **d**, **92a-b**, **93** and **94** (Chapter 2) and with the literature compounds **89a** and **c** (**Figure 3.11**).[122]

The Fe-Fe bond length for each complex is comparable with those reported for the active site of [FeFe]-hydrogenase (2.6 Å), as well as the bond length between each iron and sulfur (Fe1-S1 = Fe1-S2 = Fe2-S2 = Fe2-S2 = 2.3 Å in the enzyme).[39] The *p*-methoxyaniline in position 2 on the naphthalene ring of both [FeFe]-complexes **131a-b** does not change the general structure, which is comparable in bond lengths and angles with the data reported for the literature compound **89a** (**Table 3.6**).[122]

The crystal structure of **131b** displays a *trans* geometry of the imine double bond and, in addition, the phenyl substituent on the nitrogen is twisted outside of the plane of the conjugated system by rotation around the N(1)-C(18) bond (Torsion angles: C(23)-C(18)-N(1)-C(17) = −25.7(14)° and C(19)-C(18)-N(1)-C(17) = 155.4(9)°).

Table 3.6 Selected bond lengths (Å) and angles (°) for compounds **131a-b** and **132a**.

	89a[a]	**131a**	**131b**
Fe(1)-Fe(2)	2.506(1)	2.545(4)	2.5094(16)
Fe(1)-S(1)	2.254(1)	2.261(6)	2.249(2)
Fe(1)-S(2)	2.248(1)	2.236(6)	2.243(2)
Fe(2)-S(1)	2.255(1)	2.271(6)	2.245(2)
Fe(2)-S(2)	2.249(1)	2.241(5)	2.239(2)
Fe(1)-C(11)	1.788(3)	1.83(2)	1.798(9)
Fe(1)-C(12)	1,797(3)	1.79(2)	1.810(9)
Fe(1)-C(13)	1.805(3)	1.83(2)	1.806(9)
Fe(2)-C(14)	1.801(3)	1.81(2)	1.804(10)
Fe(2)-C(15)	1.801(3)	1.820(19)	1.796(9)
Fe(2)-C(16)	1.805(4)	1.81(2)	1.816(10)
S(1)-C(1)	1.777(3)	1.754(18)	1.769(8)
S(2)-C(8)	1.778(3)	1.77(2)	1.773(8)
S(1)-Fe(1)-S(2)	84.12(3)	84.3(2)	83.84(8)
S(1)-Fe(2)-S(2)	84.08(3)	84.0(2)	84.00(8)
S(1)-C(1)-C(9)	125.3(2)	124.3(15)	123.8(6)
S(2)-C(8)-C(9)	125.4(2)	128.1(14)	126.3(6)
C(8)-C(9)-C(1)	125.4(3)	122.8(16)	124.9(7)
C(1)-C(2)-C(17)-N(1)	-	−146.0(18)	179.0(8)
C(3)-C(2)-C(17)-N(1)	-	33(2)	0.8 (13)
C(19)-C(18)-N(1)-C(17)	-	−2(2)	155.4(9)
C(23)-C(18)-N(1)-C(17)	-	177.9(16)	−25.7(14)

[a]Data taken from reference [122].

3.3.3 Electrochemical characterisation

The electrochemical properties of amine and imine-substituted [FeFe]-complexes **129a**, **130a**, **131a-b** and **132a-b** (**Figure 3.2** and **Figure 3.3**) were investigated by cyclic voltammetry. Based on the previous analysis of [FeFe]-complexes **89d**, **91a**, **b** and **d**, **92a-b**, **93**, **94** and **96** (Chapter 2), all the measurements were recorded in CH_3CN at room temperature, using a three electrode-cell with glassy carbon as working electrode, $Ag/AgNO_3$ as reference electrode, and platinum as counter electrode. All the potentials were measured with respect to the ferrocene redox couple (Fc/Fc^+), which was used as internal reference (see Chapter 6 for experimental details). All the potentials and the corresponding half-wave potentials of [FeFe]-complexes **129a**, **130a**, **131a-b** and **132a-b** are listed in Table 3.7 and cyclic voltammograms are shown in Figure 3.12, Figure 3.13 and Figure 3.14.

Table 3.7 Electrochemical reduction potentials (vs Fc/Fc^+) of [FeFe]-complexes **129a**, **130a**, **131a-b** and **132a-b** (1 mM) in 0.1 M NBu_4PF_6/CH_3CN at 0.01 V s^{-1} scan rate.

Complex	E'_{pc}	$E'_{1/2}$ $Fe^IFe^I \rightarrow Fe^IFe^0$	E''_{pc}	$E''_{1/2}$ $Fe^IFe^0 \rightarrow Fe^0Fe^0$	E_{pa}
89a[a]	−1.52 V	−1.48 V	−1.96 V	−1.96 V	0.87
91a[b]	−1.54 V	−1.44 V	−1.86 V	−1.75 V	1.00 V
129a	−1.52 V	−1.42 V	−1.94 V	−1.79 V	0.82 V
130a	−1.51 V	−1.46 V	−2.03 V	−1.87 V	1.17 V
131a	−1.51 V	−1.62 V	−1.85 V	−1.78 V	0.46 V 0.76 V
131b	−1.51 V	−1.44 V	−1.74 V	-	1.00 V
132a	−1.51 V	−1.41 V	−1.90 V	-	0.52 V 0.68 V
132b	−1.45 V	−1.41 V	−1.86 V	−1.81 V	0.96

Data are taken from [a] reference [122] and [b] Chapter 2.

All complexes undergo two one-electron reductions, which are assigned to Fe(I)Fe(I)→Fe(0)Fe(I) and Fe(0)Fe(I)→Fe(0)Fe(0), by analogy with [FeFe]-complexes **89d**, **91a**, **b** and **d**, **92a-b**, **93**, **94** and **96** (Chapter 2) and with the literature compounds **89a-b**.[122] In

each case, the peak separations of the first and the second reduction waves are similar to that observed for the Fc/Fc^+ internal redox couple, indicating reversible behaviour (fast electron transfer kinetics), except for [FeFe]-complexes **131b** and **132a-b** (*vide infra*). As previously described in Chapter 2 and reported in the literature, [112,117,125] the first and the second reduction event is an electrochemical process (EC), which may involve rearrangement of the complex and, consequently, reduces the amplitude of the return wave. This rearrangement is unlikely to involve fragmentation of the backbone because an oxidation peak is observed on the return sweep.[122] In addition, each [FeFe]-complex shows one or two one-electron oxidations, which are assigned to Fe(I)Fe(I)→Fe(II)Fe(I) and Fe(II)Fe(I)→Fe(II)Fe(II) respectively (Chapter 2 and reference [122]). The absence of a reduction peak indicates decomposition of the corresponding oxidized species after oxidation of the iron centres (except for **131a** and **132a**) (**Table 3.7**).

N-Isopropyl amine-substituted [FeFe]-complex **129a** undergoes two one-electron reductions at −1.42 V and −1.79 V, respectively (**Table 3.7**). Comparison of **129a** with **89a** shows that the amine-substituted complex is reduced at less negative potentials than the unsubstituted **89a**.[122] Consequently, the reduction events are more thermodynamically favoured for [FeFe]-complex **129a** than for **89a** (**Figure 3.12**). On the other hand, the first and second reduction of the diselenolate analogue **130a** appears less thermodynamically favourable than the corresponding unsubstituted **91a** (−1.46 V vs −1.44 V and −1.87 V vs −1.75 V respectively, **Table 3.7**). Contrary to what was observed in Chapter 2, reduction of **130a** occurs at more negative potential than the corresponding sulfur-based [FeFe]-complex **129a**. However, this result was in line with the IR spectra analysis (**Table 3.4**), which clearly showed higher electron-density on the iron centres and, consequently, was consistent with the literature.[87,88]

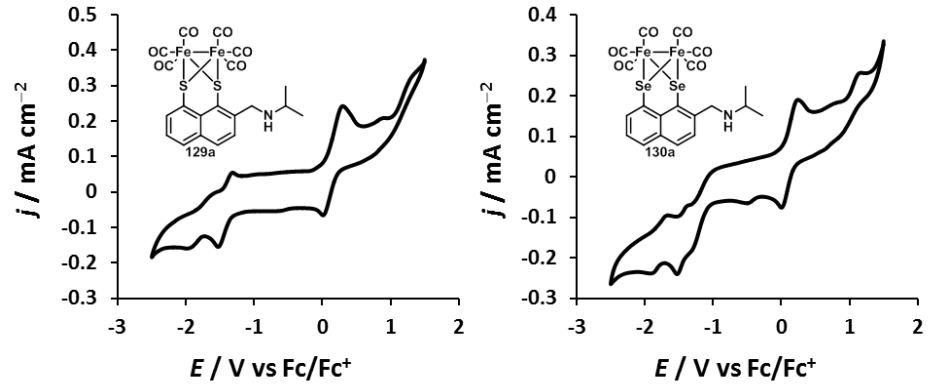

Figure 3.12 Cyclic voltammograms for [FeFe]-complexes **129a** and **130a** (1 mM) in 0.1 M NBu_4PF_6/CH_3CN at 0.01 V s^{-1} scan rate.

The cyclic voltammogram of the aromatic amine-substituted [FeFe]-complex **131a** shows the first reduction wave occurring at more negative potentials than those for **129a** and **89a** and it suggests that the process is less thermodynamically favoured (**Table 3.7**). However, a second reduction wave for **131a** occurs at less negative potential than for **89a**, close to that observed for **129a** (**Figure 3.13**).

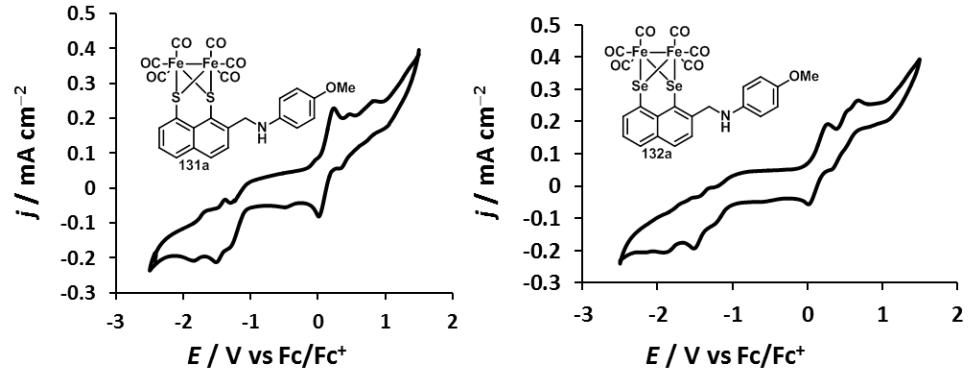

Figure 3.13 Cyclic voltammograms for [FeFe]-complexes **131a** and **132a** (1 mM) in 0.1 M NBu_4PF_6/CH_3CN at 0.01 V s^{-1} scan rate.

The reduction of the diselenolate-based [FeFe]-complex **132a** is shifted towards less negative potential than **130a** and **91a**. However, the second reduction process is irreversible, suggesting that decomposition of the doubly reduced species occurs. Comparison of **131a** and **132a** shows that the presence of the selenium promotes the first reduction at less negative

potential than the sulfur equivalent, despite the higher electron-density on the iron centres, as seen in the IR analysis and described in Chapter 2.

The imine-substituted [FeFe]-complex **131b** exhibits a first reduction wave at less negative potential than the unsubstituted **89a**, but more negative than the amine-substituted equivalent **131a** (**Table 3.7**). However, the process is reversible, indicating higher stability of the corresponding reduced species compared with those generated from **89a** and **131a**. The second reduction process is shifted towards less negative potential than for **89a** and **131a** but decomposition of the corresponding reduced species is observed.

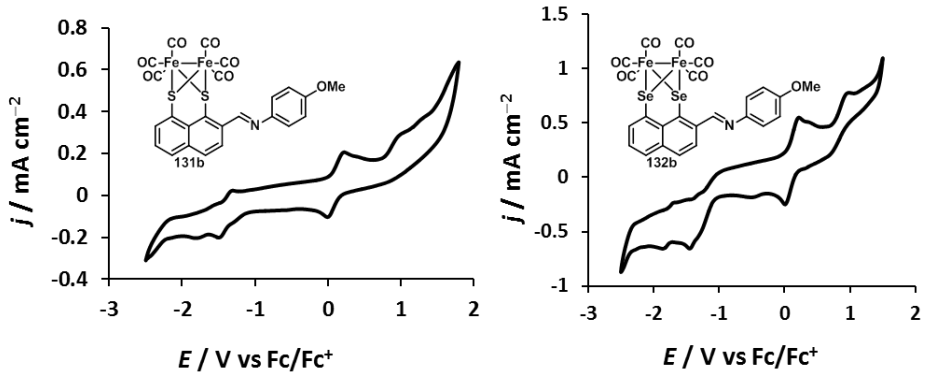

Figure 3.14 Cyclic voltammograms for [FeFe]-complexes **131b** and **132b** (1 mM) in 0.1 M NBu_4PF_6/CH_3CN at 0.01 V s^{-1} scan rate.

Cyclic voltammetry of the equivalent selenium-based [FeFe]-complex **132b** shows similar results to those discussed for **132a**, in terms of both electrochemical behaviour and potential values for the first reduction process. However, the second reduction is more thermodynamically favoured for **132b** than for **132a**. Additionally, the first reduction event of **132b** occurs at less negative potential than the corresponding sulfur counterpart **131b**, consistent to that observed for **131a** and **132a**.

3.3.4 Proton reduction catalysis

[FeFe]-complexes **129a**, **130a**, **131a-b** and **132a-b** were investigated as proton reduction catalysts by monitoring their electrochemical properties upon addition of *p*TsOH (concentration 0.5 mM to 10 mM).

Upon raising the concentration of *p*TsOH (0.5 mM to 1.5 mM for **129a** and 0.5 mM to 2 mM for **130a**) [FeFe]-complexes **129a** and **130a** exhibit an anodic shift of the first reduction peak in the range between −0.5 V and −0.7 V (**Figure 3.15**). A corresponding oxidation peak on the return sweep (in the range −0.5 V and −0.3 V) is also observed. The position of this reduction wave is independent of the addition of the acid. However, the peak current increases linearly as a function of the acid concentration as do those of the second and the third reduction waves (−1.42 V and −1.79 V for **129a**, −1.46 V and −1.87 V for **130a** in **Table 3.7**), which are slightly shifted towards more negative potentials. Upon increasing the concentration of *p*TsOH (2 mM to 10 mM for **129a** and 2.5 mM to 10 mM for **130a**) the catalytic behaviour of complexes **129a** and **130a** follows that described for **89d**, **91a**, **b** and **d**, **92a-b**, **93**, **94** and **96** (Chapter 2). The second reduction peak is notably shifted towards more negative potential and its height is significantly increased at each concentration of acid. The second reduction process becomes irreversible and the first reduction process, observed at low acid concentration, becomes negligible (**Figure 3.15**).

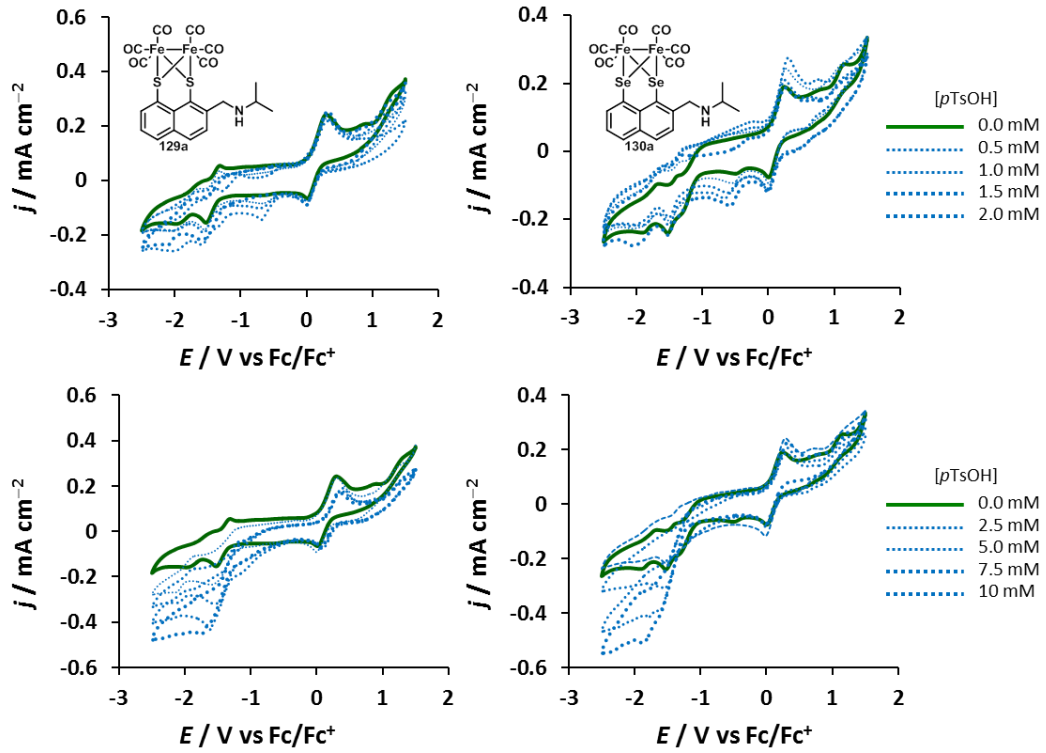

Figure 3.15 Cyclic voltammograms for [FeFe]-complexes **129a** and **130a** (1 mM) in 0.1 M NBu_4PF_6/CH_3CN at 0.01 V s^{-1} scan rate with increasing concentrations of *p*TsOH from 0.5 mM to 2 mM (top graphs) and from 2.5 mM to 10 mM (bottom graphs).

Following the UV/vis analysis and consistent with previous results in the literature, [55a),182,183] the first process may involve the reduction of the protonated [FeFe]-complexes **129a** and **130a** upon addition of *p*TsOH. The introduction of a positive charge explains the anodic shift towards more positive potential than that observed for the neutral complex. At low concentration of acid, the protonation of the amino substituent on the naphthalene ring might be involved in proton reduction.[55a),184,185] The catalytic peak current at −1.42 V (**129a**) and −1.46 V (**130a**) increases linearly with the addition of acid and it is shifted towards negative potential values but the reversibility of the process is not affected.[55a),183]

Dithiolate and diselenolate-based complexes **131a-b** and **132a-b** show similar electrochemical responses to the corresponding *N*-isopropylamine-substituted **129a** and **130a** (**Figure 3.16** and **Figure 3.17**).

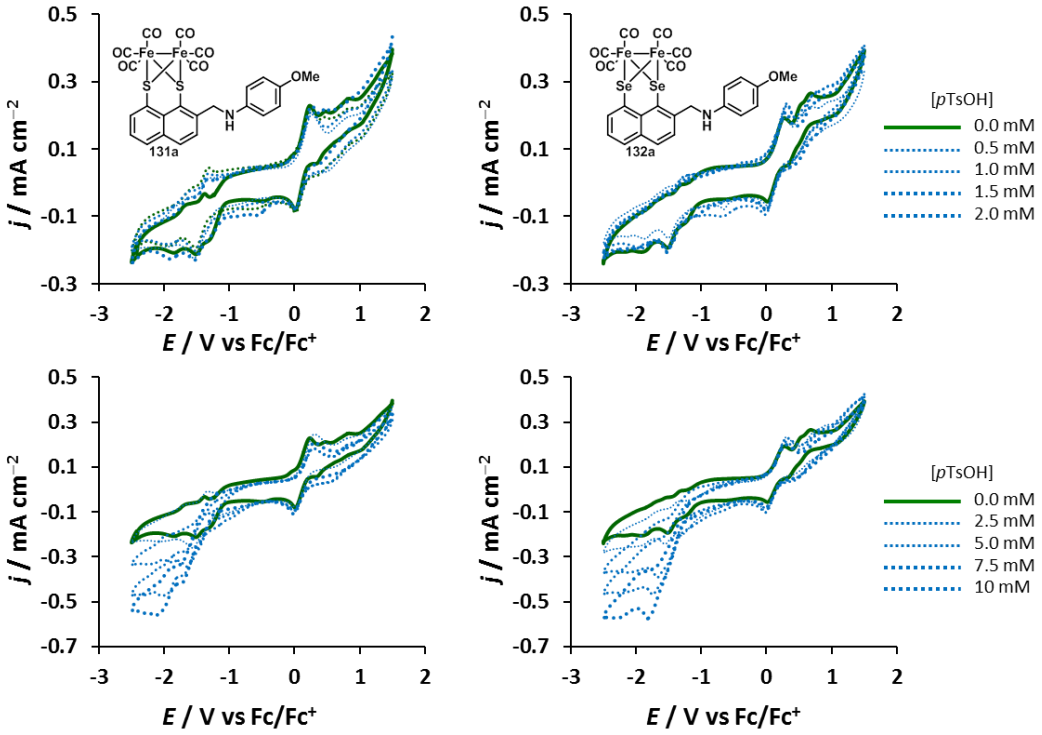

Figure 3.16 Cyclic voltammograms for [FeFe]-complexes **131a** and **132a** (1 mM) in 0.1 M NBu_4PF_6/CH_3CN at 0.01 V s^{-1} scan rate with increasing concentrations of *p*TsOH from 0.5 mM to 2 mM (top graphs) and from 2.5 mM to 10 mM (bottom graphs).

Upon addition of acid at low concentration (0.5 mM and 1 mM) complexes **131a** and **132a** exhibit the first reduction peak in the range between -0.5 V and -0.6 V; however, this process is less defined than for **129a** and **130a** and the corresponding return oxidation peak is not observed (**Figure 3.16**). As described for **129a** and **130a**, at low concentration of acid proton reduction catalysis for complexes **131a** and **132a** may be favoured by protonation of the amino group, event that becomes marginal at high concentration.

Imine-substituted **131b** and **132b** also show the first reduction process occurring at less negative potentials than that in the absence of acid. Furthermore, the first reduction wave moves cathodically, from −0.7 V to −1.1 V (**131b**) and from −0.5 V to −1.17 V (**132b**), upon increasing the acid concentration from 0.5 mM to 2.5 mM. As shown in Figure 3.17 (bottom graph), protonation of the imino group occurs both at low and high concentration of acid,

since the first reduction peak is still distinguishable at 10 mM of acid for both complexes, different from that observed for **129a**, **130a**, **131a** and **132a.**

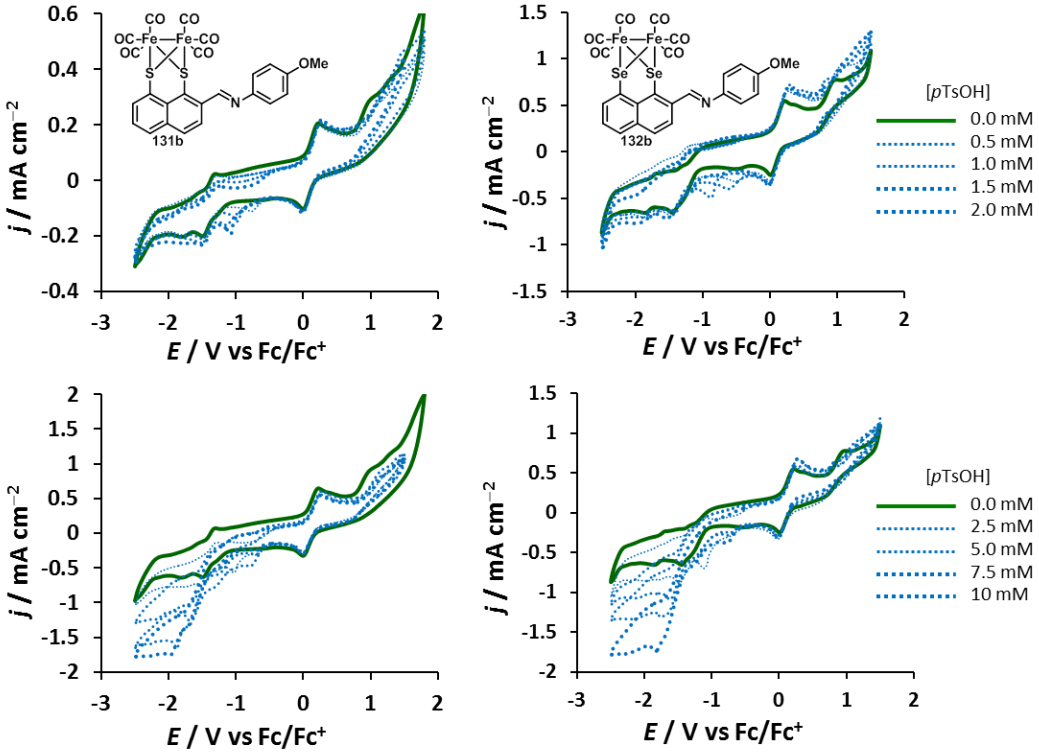

Figure 3.17 Cyclic voltammograms for [FeFe]-complexes **131a** and **132b** (1 mM) in 0.1 M NBu_4PF_6/CH_3CN at 0.01 V s^{-1} scan rate with increasing concentrations of *p*TsOH from 0.5 mM to 2 mM (top graphs) and from 2.5 mM to 10 mM (bottom graphs).

The proposed mechanism [55a),183] for the proton reduction catalysis of [FeFe]-complexes **129a**, **130a**, **131a-b** and **132a-b** is shown in Scheme 3.7. At low concentrations of *p*TsOH, $[Fe(I)Fe(I)NH_n]$ (n = 0 for the imine-substituted **131b** and **132b**, n = 1 for the amine-substituted **129a**, **130a**, **131a** and **132a**) is protonated to $[Fe(I)Fe(I)NH_{n+1}]^+$, which causes an anodic shift of the first reduction potential and gives $[Fe(0)Fe(I)NH_{n+1}]^+$. This species reacts again with acid to generate $[HFe(II)Fe(I)NH_{n+1}]^+$, which liberates hydrogen and regenerates the initial $[Fe(I)Fe(I)NH_n]$ after two more one-electron reductions.[183,55a)] At high concentration of acid, [FeFe]-complexes **129a**, **130a**, **131a** and **132a** follow the proton reduction mechanism described in Scheme 2.16 (Chapter 2).[52] Notably, complexes **129a**,

130a and **132a** follow Process I, while **131a** seems follow Process II in Scheme 2.16 (Chapter 2). The imine-substituted **131b** and **132b**, instead, appear to follow the mechanism described in Scheme 3.7, even at high concentration of acid.

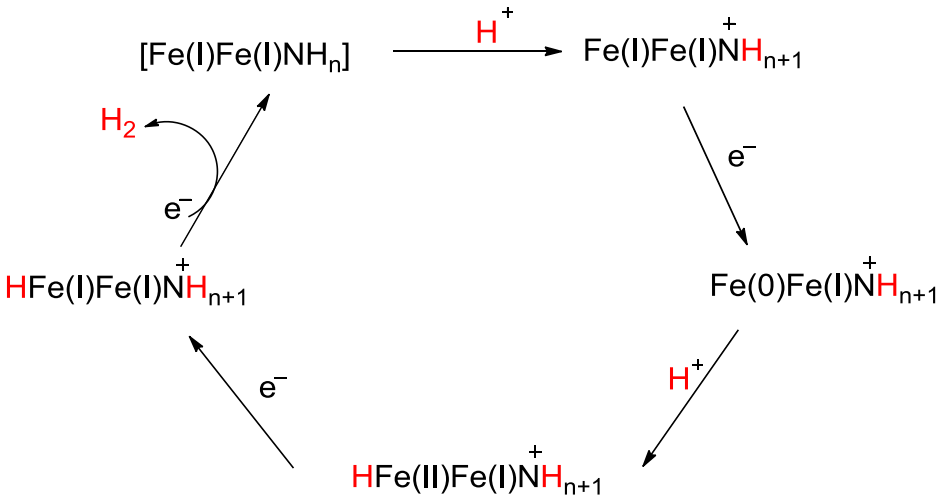

Scheme 3.7 Proposed mechanism for proton reduction catalysis by [FeFe]-complexes **129a**, **130a**, **131a-b** and **132a-b** in presence of *p*TsOH.

The efficiency in proton reduction catalysis of [FeFe]-complexes **129a**, **130a**, **131a-b** and **132a-b** was evaluated in terms of $E_{1/2}$-E°_{HA} (Chapter 2), [148] which gives a measure of the overpotential for the acid reduction to occur in the presence of the catalyst. Table 3.8 reports the values of **129a**, **130a**, **131a-b** and **132a-b** for *p*TsOH reduction. Diselenolate-bridged [FeFe]-complexes, except for **129a** and **130a**, show lower values than the sulfur counterpart, suggesting they are more efficient catalysts towards proton reduction. This is consistent with the literature [86-88] and with the results previously described in Chapter 2.

Table 3.8 Overpotentials of complexes **129a**, **130a**, **131a-b** and **132a-b**.

Complex	**129a**	**130a**	**131a**	**131b**	**132a**	**132b**
$\boldsymbol{E_{1/2}-E^{\circ}_{HA}}$ **/ V**	0.77 V	0.81 V	0.97 V	0.80 V	0.76 V	0.76 V

The catalytic efficiency was also estimated by comparing **129a** and **130a**, **131a** and **132a**, **131b** and **132b** in terms of peak current increase (**Figure 3.18**).[86,87] Only high concentrations

of acid were considered, since the peak height is more markedly affected than at low concentration. In general, diselenolate-based [FeFe]-complexes **130a** and **132a-b** give a bigger peak current increase than the equivalent dithiolates. However, this effect is less predictable than that observed for **89d**, **91a**, **b** and **d**, **92a-b**, **93**, **94** and **96** (Chapter 2). Complexes **129a** and **130a** cause the same increase in the peak height with 5 mM and 7.5 mM of acid; **131a** gives, instead, a more pronounced rise than **132a** with 2.5 mM of acid. Complexes **131b** and **132b** feature the same peak current increase at high concentration of *p*TsOH (7.5 mM and 10 mM).

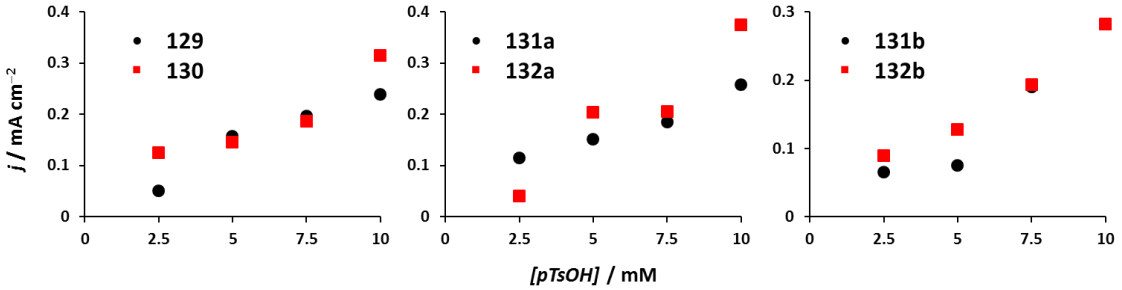

Figure 3.18 Comparison between **129a** and **130a**, **131a** and **132a**, **131b** and **132b** in terms of peak current increase upon increasing concentration of *p*TsOH (from 2.5 mM to 10 mM).

3.4 Summary

This chapter described the synthesis of amine and imine-functionalised *peri*-substituted dichalcogenide-based [FeFe]-hydrogenase synthetic mimics **129a**, **130a**, **131a-b** and **132a-b**. Spectroscopic analysis of **129a**, **130a**, **131a-b** and **132a-b** showed similar features to the [FeFe]-complexes previously described in Chapter 2 and, in addition, IR analysis confirmed the chalcogen effect on the electron-density at the iron centres. Cyclic voltammetry revealed that the electrochemical properties of **132a-b** reflect the trend described in Chapter 2 for diselenolate-based [FeFe]-complexes, which are reduced at less negative potentials than the equivalent dithiolates. Furthermore, analysis of the measured overpotentials and the peak

current increase confirmed the selenium-based **130a** and **132a-b** as more efficient catalysts for proton reduction compared to their sulfur analogues.

Protonation of the amino and imino group was analysed by titrating the [FeFe]-complexes **129a**, **130a**, **131a-b** and **132a-b** with *p*TsOH and was monitored by UV/vis spectroscopy and cyclic voltammetry. All the [FeFe]-complexes displayed a significant change in the absorption profile upon addition of acid. At low concentrations of *p*TsOH, the amine-substituted **129a**, **130a**, **131a** and **132a** exhibit an anodic shift of the first reduction peak, suggesting that reduction of the protonated complexes occurs; this event becomes, instead, negligible at high concentrations of acid. Protonation and subsequent reduction of the protonated species of the imine-substituted **131b** and **132b** seems to occur both at low and at high concentration.

Based on the reported analysis, [FeFe]-complexes **131a-b** and **132a-b** are considered to be suitable model systems for the development of photochemical dyads containing ZnTPP (**Figure 3.1**) in terms of reduction potential, which is less negative than that required to oxidise the excited species $ZnTTP^{*}$ (E° = −1.74 V).[157] Furthermore, protonation of the nitrogen may facilitate photochemical hydrogen production catalysis. However, the d-d transition, observed by UV/vis spectroscopy, may restrict the irradiation range for exciting the ZnTPP and, additionally, it may cause decomposition of the complexes.

Chapter 4: Studies towards photoactivated [FeFe]-hydrogenase synthetic mimics

4.1 Photocatalytic systems for the hydrogen production

Photochemical systems for hydrogen production, which are based on [FeFe]-hydrogenase bio-inspired catalysts, are categorised as molecular dyads/triads, self-assemblies and bimolecular systems.[155 -186] In molecular dyads, a photosensitizer and a catalyst are covalently linked, whereas an additional electron donor is included in molecular triads. Self-assemblies are defined by supramolecular interactions between a photosensitizer and a catalyst. In contrast, in bimolecular systems the photosensitizer and the catalyst are neither covalently linked nor self-assembled.

Catalytic efficiency is commonly expressed in terms of turnover number (TON), which refers to moles of produced hydrogen per moles of catalyst before the system becomes inactivated, and in terms of turnover frequency (TOF), which is equal to the turnover number per unit time.[187]

The initial work of Sun and Åkermark showed that molecular dyads, consisting of a Ru-based photosensitizer and a hexacarbonyl adt-bridged [FeFe]-complex, do not produce hydrogen upon light irradiation.[188] The electron transfer from the photosensitizer to the [FeFe]-cluster is thermodynamically unfeasible, since the catalyst reduction potential is more negative than the oxidation potential of the species PS^{-}, generated by the electron donor via reductive quenching of the excited species PS^{*} (**Scheme 3.1**, Chapter 3). Similarly, a photochemical system with a Ru-polypyridine complex, covalently linked to the iron centre via acetylene-functionalised triphenylphosphine ligand, does not show catalytic hydrogen evolution.[189] According to previous investigations on bimolecular systems, [190] the same group reported the first photocatalytic system, **147** (**Figure 4.1**).[191] It is composed of an *N*-benzyl adt-bridged [FeFe]-complex, substituted on the irons by one or two tris(*N*-pyrrolyl)phosphine ligands, $P(Pyr)_3$ and tris(bipyridine)ruthenium(II), $Ru(bpy)_3^{2+}$. The weak electron-donating $P(Pyr)_3$

causes a small cathodic shift of the catalyst reduction potential, which is close to the oxidation potential of the species $Ru(bpy)_3^{+}$, generated by the excited species $[Ru(bpy)_3^{*}]^{2+}$ via reductive quenching. Consequently, the electron transfer from the photosensitizer to the catalyst is thermodynamically favoured. The photochemical system **147** catalyses 4.3 turnovers of hydrogen production.[191]

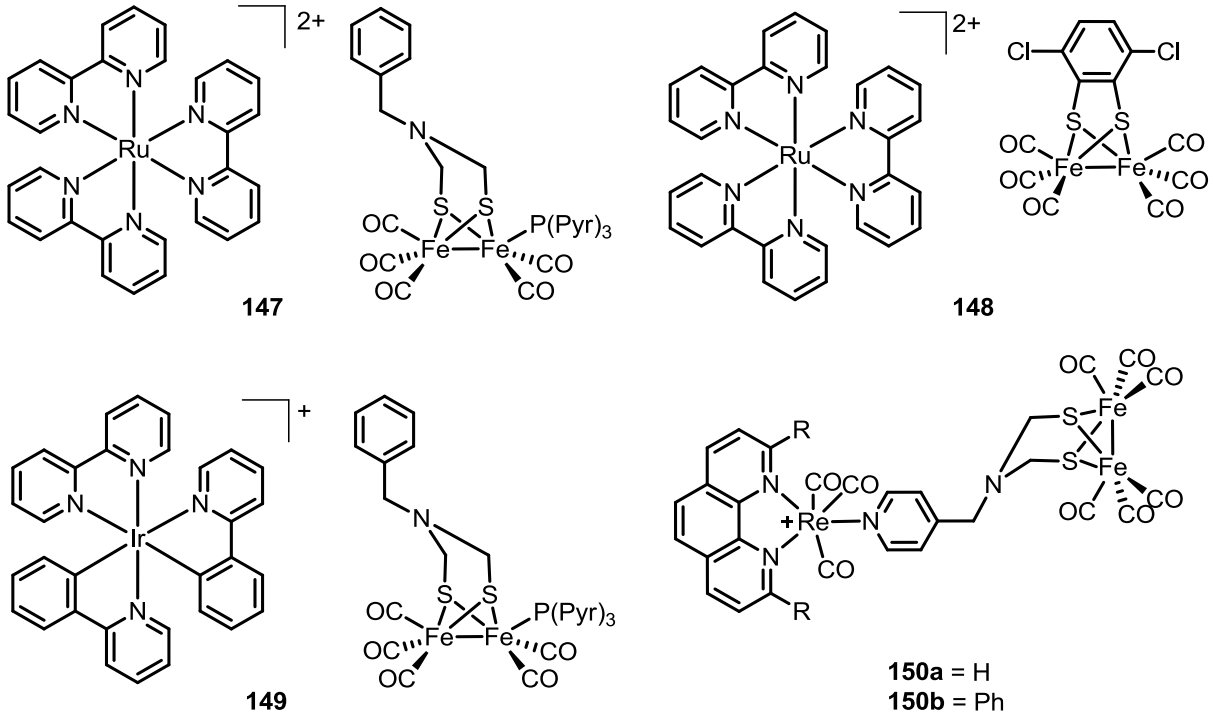

Figure 4.1 Photocatalytic Ru and Ir-based bimolecular systems **147**-**149** and self-assembling Re-based system **150a-b**.[191,192,193,197b)]

The addition of chloro substituents to benzenedithiolates results in a shift of the hexacarbonyl [FeFe]-cluster reduction potential towards more positive values than the unsubstituted **88** (Section 2.1, Chapter 2). Consequently, Ott and co-workers investigated the bimolecular system **148** using 3,6-dichlorobenzene-1,2-dithiolate-bridged [FeFe]-complex as catalyst, and $Ru(bpy)_3^{2+}$ as photosensitizer (**Figure 4.1**).[192] This system displayed remarkable catalytic efficiency compared with **147**: [191] the reported TON of **148** is up to 200 and the TOF is 2.4 min^{-1}.[192]

Replacing $Ru(bpy)_3^{2+}$ in **147** with the bis(2-phenylpyridinato-)(2,2′-bypyridine)iridium(III) complex, $[Ir(ppr)_2bpy]^+$, the catalytic efficiency of the bimolecular system improved: **149** generates a TON of 132 (**Figure 4.1**).[193] As described for Ru-containing systems, [190,191] molecular dyads with Ir-based photosensitizers show lower catalytic efficiency than the corresponding bimolecular systems.[194]

The combination of [FeFe]-hydrogenase synthetic mimics and Re-based photosensitizers has been investigated in both dyads and bimolecular systems, since the reduction potentials of rhenium complexes are more negative and the excited state has longer lifetime than the Ru and Ir-complexes.[157,195] Following initial studies, [195,196,197a)] the photochemical systems **150a-b**, which are composed of a Re-phenanthroline complex coordinated by an *N*-functionalised pyridine adt-bridged [FeFe]-complex, are currently the most efficient among the Re-based photocatalysts (**Figure 4.1**). The supramolecular system performs 9-12 turnovers of hydrogen evolution and the corresponding bimolecular system 4-5.[197b)]

According to these reports, it has been suggested that bimolecular systems of Ru/Ir-photosensitizers and [FeFe]-complexes are preferred over dyads, if a reductive quenching mechanism is required for the electron transfer to occur. On the contrary, Re-based molecular dyads are more efficient than bimolecular systems in performing the electron transfer from the rhenium excited species to the catalyst, which requires an oxidative quenching mechanism (**Scheme 3.1**, Chapter 3).[158]

Besides the use of expensive and rare complexes containing noble metals, tetraphenylporphyrin (TPP) and zinc tetraphenylporphyrin (ZnTPP) have been investigated as photosensitizers in both molecular dyads and self-assembling systems.[198-202] However, the catalytic efficiency of the photoactive systems is relatively low: the reported TONs are in the range of 0.16-2.[199-202]

Wu and Wasielewski reported the first examples of catalytic triads for photoinduced hydrogen production, **151** and **152a-b** (**Figure 4.2**).[203,204]

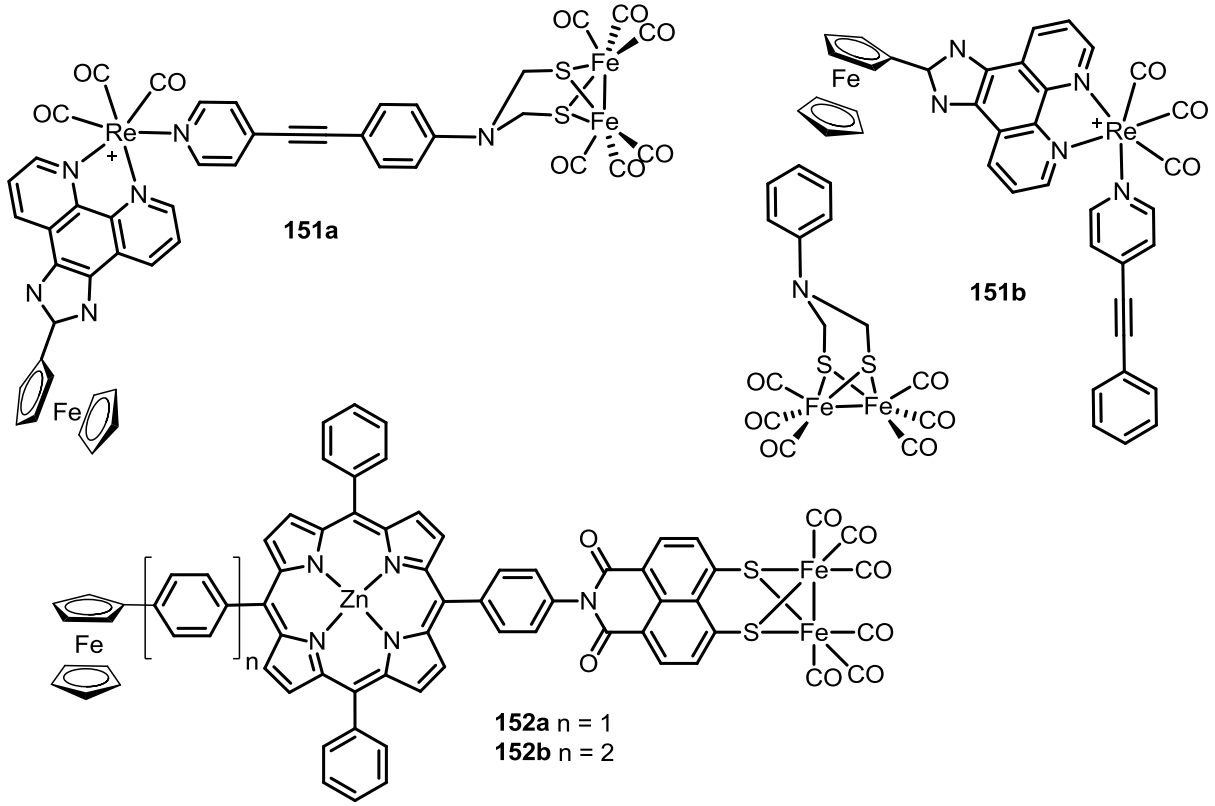

Figure 4.2 Photoactivated molecular triads **151a-b** and **152a-b**.[203,204]

The molecular system **151a** contains a Re-based photosensitizer, which is covalently attached to the electron donor ferrocene (Fc) and to the *N*-phenyl adt-bridged [FeFe]-complex, via an acetylenic linker. This system produces 0.35 turnovers of hydrogen and, as expected, is more efficient than the corresponding bimolecular system **151b**, which, instead, catalyses 0.04 turnovers of hydrogen.[203] Wasielewski and co-workers built the photoactive triads **152a-b** by functionalizing the ZnTPP with Fc on one side of the porphyrin core, and with the naphthalene monoimide (NMI) dithiolate-bridged [FeFe]-complex on the other.[202] Initial studies on these systems show that only **152b** catalyses 0.56 turnovers of hydrogen, since two

phenyl spacers between the Fc and the porphyrin core allow a longer charge separation than in **152a** and hence the stability of the system in catalytic conditions increases (**Figure 4.2**).[204]

4.1.1 Water-soluble phoactivated systems

In order to generate photoactive systems able to catalyse water splitting (Section 3.1, Chapter 3), many strategies have been developed aiming to improve catalysts solubility in water.[16,156]

Li and co-workers reported the photoactivated system **153**, in which the hydrophobic [μ-$S_2(Fe)_2(CO)_6$] is encapsulated in a dendritic scaffold that stabilises the cluster and is suitable for photo-induced hydrogen production (**Figure 4.3**).[205]

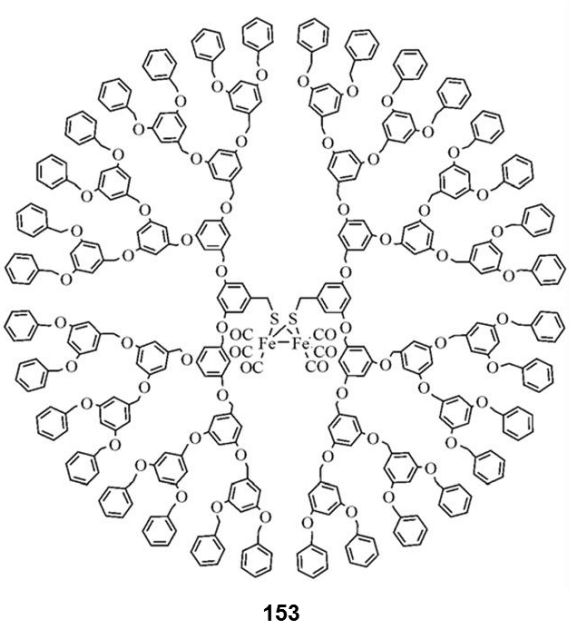

153

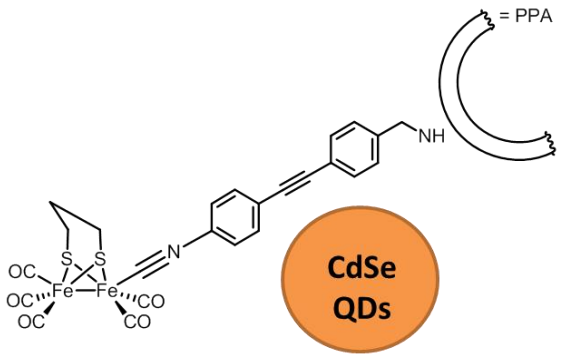

154

Figure 4.3 Water soluble photoactivated systems **153** and **154**.[205,207b)] This figure was adapted with permission from reference 16, copyright 2014 Elsevier.

In a mixture of acetone and water (9:1), **153** produces 22,200 turnovers of hydrogen (TOF = 7240 h^{-1}), using an Ir-containing photosensitizer (**Figure 4.3**).[205]

Quantum dots (QDs) are nanomaterials whose sizes are highly tunable as well as their emission and conductive properties.[206] Accordingly CdTe, CdSe and CdS-based QDs were

employed as photosensitizers, in combination with [FeFe]-hydrogenase analogues.[207] Currently, the highest photocatalytic efficiency (TON = 27,135) is obtained from CdSe-based QDs **154** in pure water (**Figure 4.3**).[207b)] ZnS-based QDs also show efficient photocatalytic activity for hydrogen production and, additionally, are cadmium-free.[208] Photoactive hybrids of *N*-phenyl adt-bridged [FeFe]-complex and ZnS perform 4950 turnovers of hydrogen in a mixture of DMF and water (9:1).[209]

In order to increase water solubility, one strategy consists of linking [FeFe]-hydrogenase synthetic mimics to artificial protein-like scaffolds (Section 1.3.2.5, Chapter 1). The system containing [μ-$S_2(Fe)_2(CO)_6$] anchored to the natural amino acids sequence Cys-X-X-Cys and combined in a bimolecular system with a Ru-based photosensitizer performs 82 turnovers of hydrogen from water.[210] The same cluster is also linked to an artificial amino acid and incorporated into a peptide. On irradiating the final adduct in the presence of a Ru-based photosensitizer, 84 turnovers of hydrogen are generated.[211]

4.2 Aims and objectives

Following the studies on amine/imine-substituted model systems **131a-b** and **132a-b** (Chapter 3), this chapter describes the synthesis of molecular dyads **155a-b** and **156a-b**, consisting of the photosensitizer ZnTPP covalently linked to *peri*-substituted dichalcogenide-bridged [FeFe]-complexes, via amino and imino linkers. In addition, the potential photocatalytic activity of **155a-b** and **156a-b** towards hydrogen production is meant to be investigated (**Figure 4.4**).

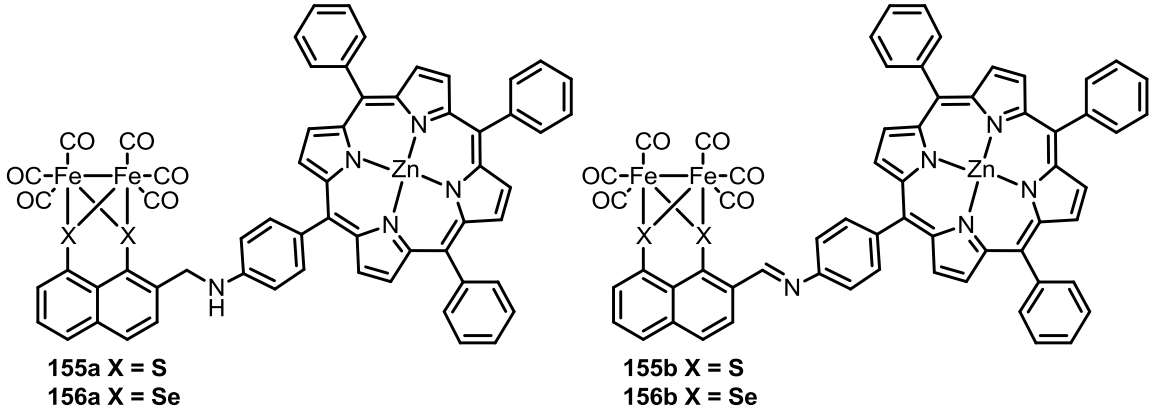

Figure 4.4 Molecular dyads **155a-b** and **156a-b**, based on *peri*-substituted dichalcogenides, targeted in this study.

4.3 Results and discussion

4.3.1 Synthesis of zinc porphyrin-functionalised [FeFe]-complexes

According to Adler and co-workers procedure, [212] condensation of freshly distilled pyrrole **157** and benzaldehyde **158** in refluxing propionic acid gave 5,10,15,20-tetraphenylporphyrin (TPP) **159** in relatively low yield. TPP was reacted with sodium nitrite ($NaNO_2$) in acidic conditions to afford the nitro-substituted 5,10,15-triphenyl-20-(4-nitro)phenyl porphyrin ($TPPNO_2$) **160** in 57% yield, as previously reported in the literature.[213] The known 5,10,15-triphenyl-20-(4-amino)phenyl porphyrin ($TPPNH_2$) **161** was synthesised by reduction of the nitro group in **160** with tin chloride ($SnCl_2$) in concentrated hydrochloric acid (**Scheme 4.1**).[214]

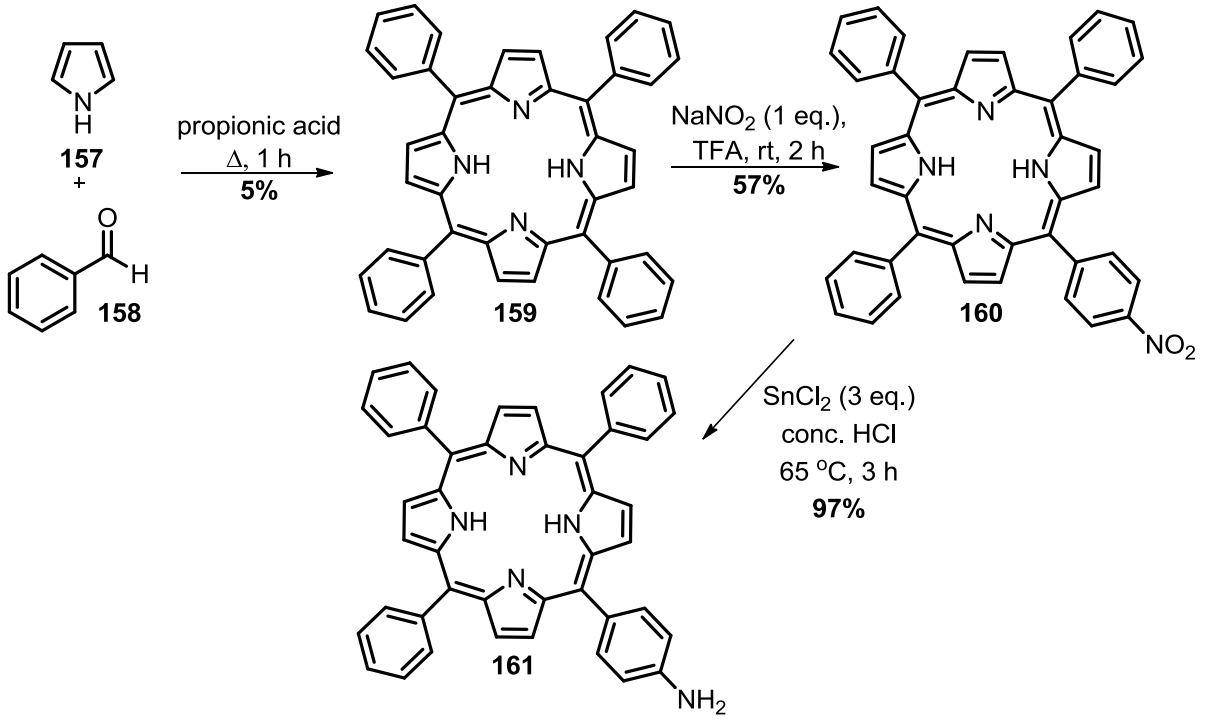

Scheme 4.1 Synthesis of 5,10,15-triphenyl-20-(4-amino)phenyl porphyrin **161**.

Based on the synthesis described for imines **135b**, **136b**, **137b** and **138b** (**Scheme 3.3** and **Scheme 3.4**, Chapter 3), [162] aldehydes **133** or **134** (**Scheme 3.2**, Chapter 3) were reacted with amine **161** in the presence of $TiCl_4$ and NEt_3 in order to synthesise the corresponding imines **162b** and **163b** (entries 1 and 2, **Table 4.1**). However, after work-up, the reaction mixture resulted in a dark green solid, which was difficult to solubilise in common organic solvents and, consequently, to purify by column chromatography. Nevertheless, after CH_2Cl_2:MeOH (95:5) washes of the column, a product was isolated, which was not the expected imine and was not identified. The unreacted $TPPNH_2$ was not recovered. In refluxing dry CH_3CN, aldehyde **134** did not react with the amine **161** and the starting material was recovered (entry 3, **Table 4.1**).[160] Novel imines **162b** and **163b** were isolated in very low yield by refluxing aldehydes **133** or **134** with **161** in dry CH_2Cl_2 with a catalytic amount of formic acid (entries 4 and 5, **Table 4.1**).[215] Lanthanum triflate ($La(OTf)_3$) was previously reported as catalyst of the reaction between amine **161** and an aromatic aldehyde.[216] Refluxing **161** with aldehydes **133**

or **134** in toluene in the presence of catalytic amounts of $La(OTf)_3$ afforded imines **162b** and **163b** in higher yields, 87% and 75%, respectively (entries 6 and 7, **Table 4.1**).

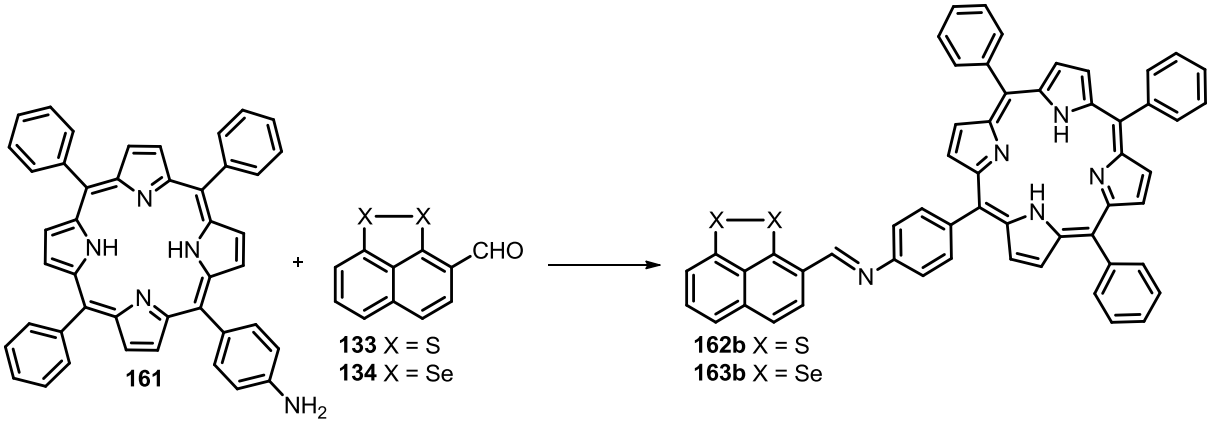

Table 4.1 Attempted synthesis of *N*-TPP imines **162b** and **163b**.

Entry	Reaction conditions	Isolated product	Reference
1	**133** (1 eq.), $TiCl_4$ (0.4 eq.), NEt_3 (2 eq.), **161** (1.2 eq.) dry CH_2Cl_2, 0 °C to rt, 16 h	unidentified	162
2	**134** (1 eq.), $TiCl_4$ (0.4 eq.), NEt_3 (2 eq.), **161** (1.2 eq.) dry CH_2Cl_2, 0 °C to rt, 16 h	unidentified	162
3	**134** (1 eq.),**161** (1.2 eq.), dry CH_3CN, Δ, 20 h	63% **134**	160
4	**133** (1 eq.), **161** (1 eq.), formic acid (3 drops), Na_2SO_4 (3 eq.), dry CH_2Cl_2, Δ, 16 h	12% **162b**	215
5	**134** (1 eq.), **161** (1 eq.), formic acid (3 drops), Na_2SO_4 (3 eq.), dry CH_2Cl_2, Δ, 16 h	9% **163b**	215
6	**133** (1.4 eq.), **161** (1 eq.), $La(OTf)_3$ (0.4 eq.), dry toluene, Δ, 16 h	87% **162b**	216
7	**134** (1 eq.), **161** (1 eq.), $La(OTf)_3$ (0.4 eq.), dry toluene, Δ, 16 h	75% **163b**	216

Zinc 5,10,15-triphenyl-20-(4-amino)phenyl porphyrin ($ZnTPPNH_2$) **164** was synthesised by refluxing TPP-NH_2 **161** with zinc acetate ($Zn(OAc)_2$) in a 1:5 mixture of MeOH:$CHCl_3$.[217] Using the best conditions from Table 4.1 (entries 4 and 5), **164** was refluxed with the aldehydes **133** or **134** in dry CH_2Cl_2 and in the presence of catalytic amount of acetic acid and the corresponding *N*-ZnTPP imines **165b** and **166b** were isolated in very low yields 14% and 8%, respectively (**Scheme 4.2**).[218]

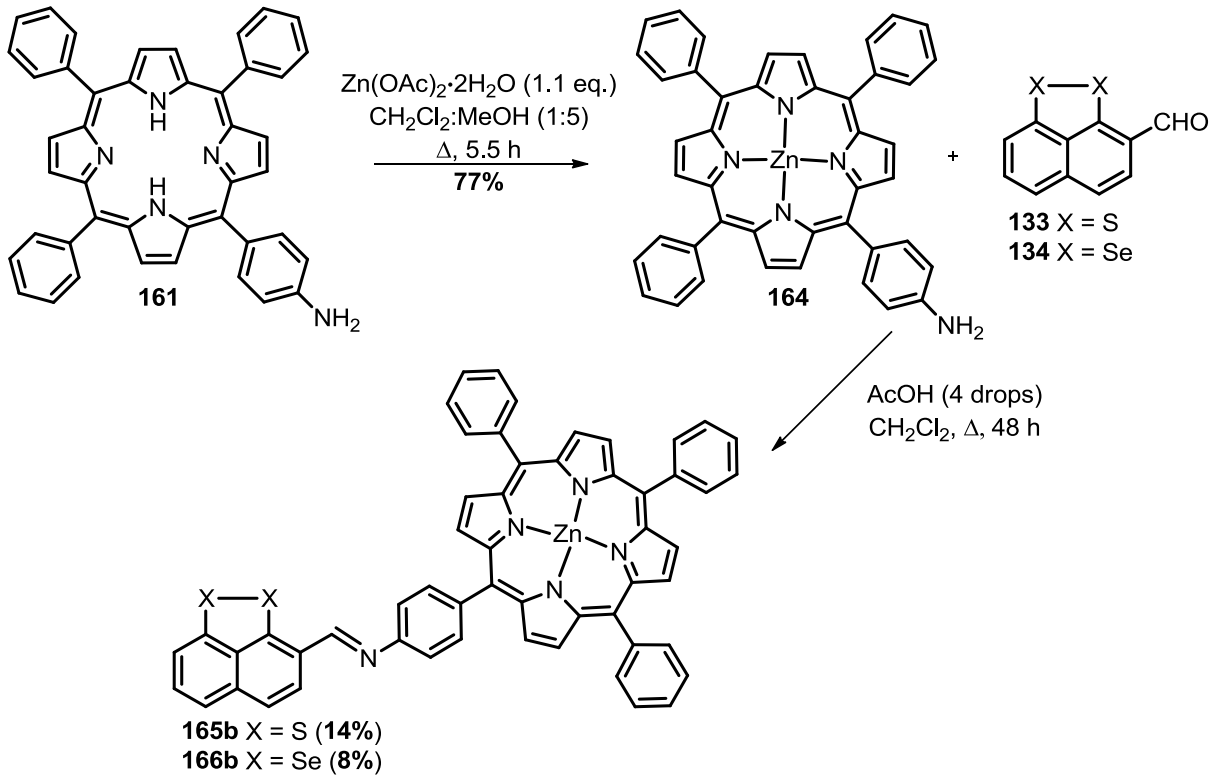

Scheme 4.2 Synthesis of *N*-ZnTPP imines **165b** and **166b**.

Wasielewski and co-workers synthesised the naphthalene monoimide dithiole **168** by refluxing the naphthalene-1,8-dicarboxyanhydride-4,5-disulfide **167** with *p*-toluidine and $Zn(OAc)_2$ in pyridine (Py) (**Scheme 4.3**).[202]

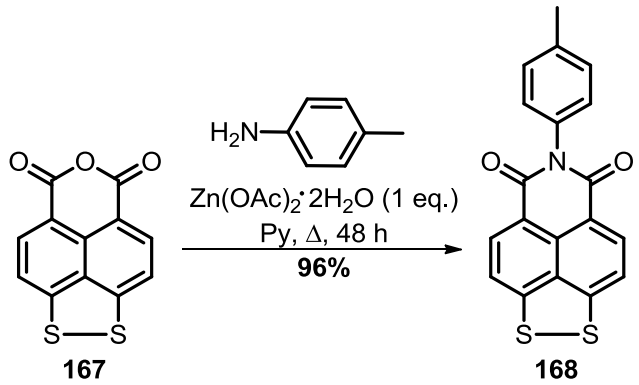

Scheme 4.3 Synthesis of naphthalene monoimide dithiole **168**.[202]

Accordingly, aldehydes **133** or **134** were refluxed with **164** and a large excess of $Zn(OAc)_2$ in pyridine for two days and the Schiff bases **165b** and **166b** were successfully isolated in 96% and 61% yields, respectively. Following the synthetic sequence described for [FeFe]-complexes **131b** and **132b** (**Scheme 3.4**, Chapter 3), **165b** and **166b** were then reacted with $Fe_3(CO)_{12}$ in refluxing toluene and afforded the expected [FeFe]-complexes **155b** and **156b**, which were poorly stable during purification by column chromatography. ^{1}H NMR and mass spectrometry analyses showed both the formation of the expected products **155b** or **156b** and the presence of the starting aldehyde and imine. This could be explained by the hydrolysis of the unstable imino group on silica (**Scheme 4.4**, yields of **155b** and **156b** are not reported because of the significant degradation of the products following purification).

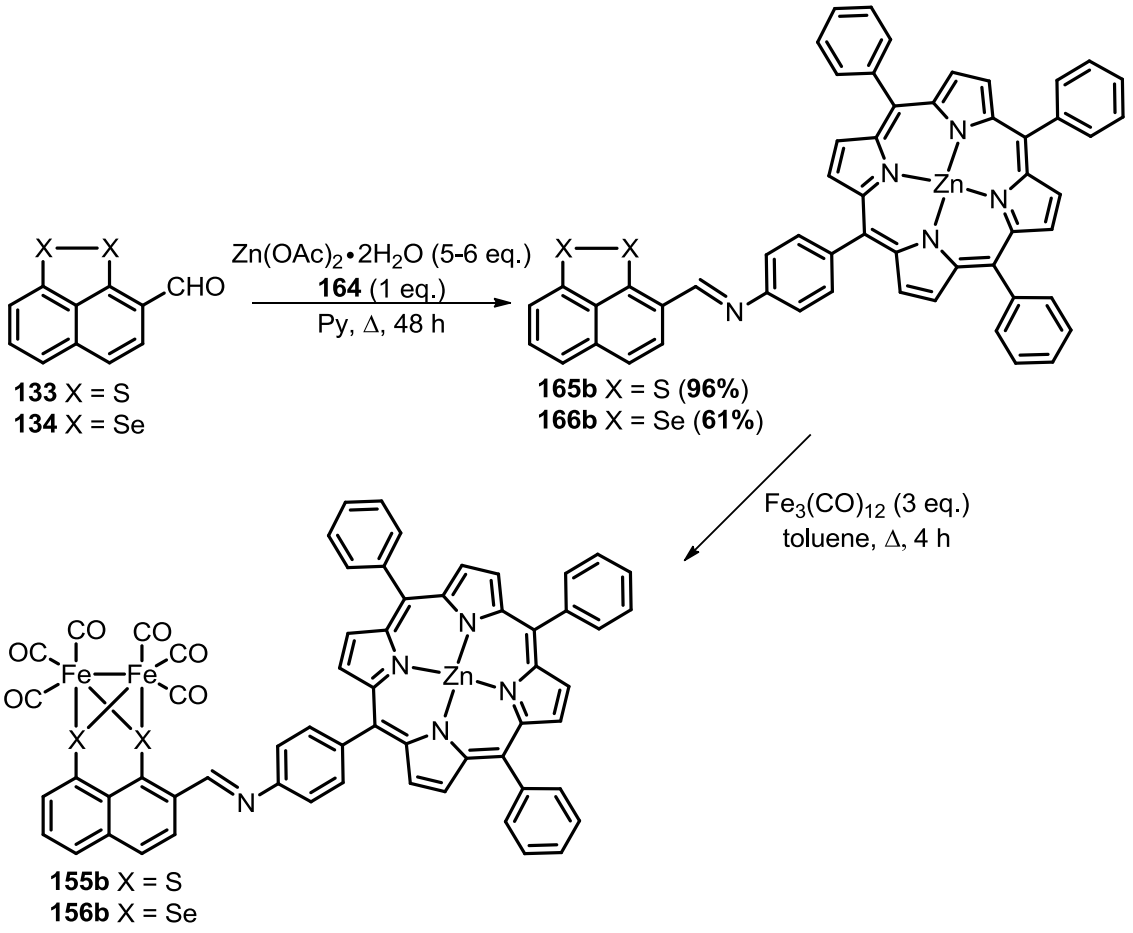

Scheme 4.4 Synthesis of [FeFe]-complexes **155b** and **156b**.

In order to synthesise molecular dyads **155a** and **156a** (**Figure 4.4**, Section 4.2) reduction of the imino group in **165b** and **166b** was investigated. However, reaction of **165b** with $NaBH_4$ was unsuccessful, [160] probably due to the high stability of the extended conjugated system. Surprisingly, reduction of imine **162b** to amine **162a** was successfully achieved using sodium cyanoborohydride ($NaBH_3CN$) and catalytic amounts of AcOH.[215] Metallation of the porphyrin core in **162a** with $Zn(OAc)_2$ followed by oxidative insertion of $Fe_3(CO)_{12}$ into the S–S bond of the naphthalene-1,8-dithiole gave [FeFe]-complex **155a** (**Scheme 4.5**).

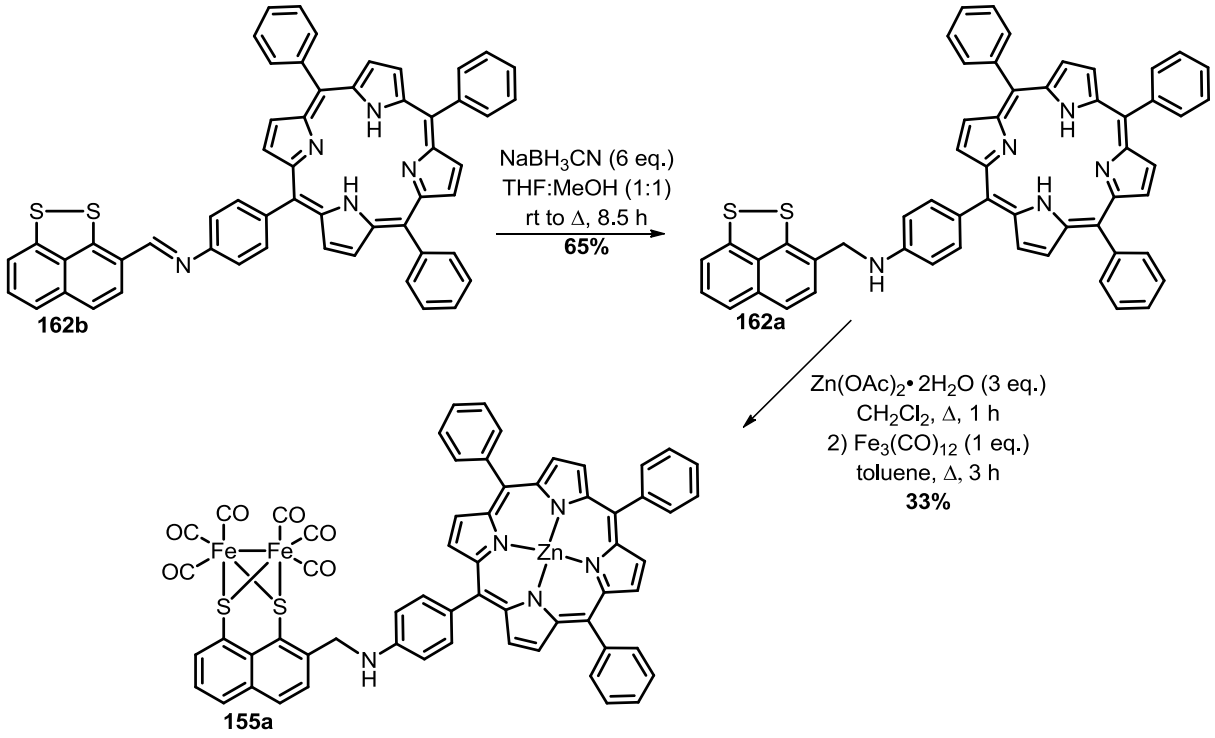

Scheme 4.5 Synthesis of molecular dyad **155a**.

In contrast, attempts to reduce imine **163b** to amine **163a** were unsuccessful (**Table 4.2**). The reducing agent $NaBH_4$ caused degradation of **163b** (entry 1, **Table 4.2**), while $NaBH_3CN$, sodium triacetoxyborohydride ($NaBH(OAc)_3$) as well as the hydrogenation only resulted in recovered starting material (entries 2-4, **Table 4.2**).

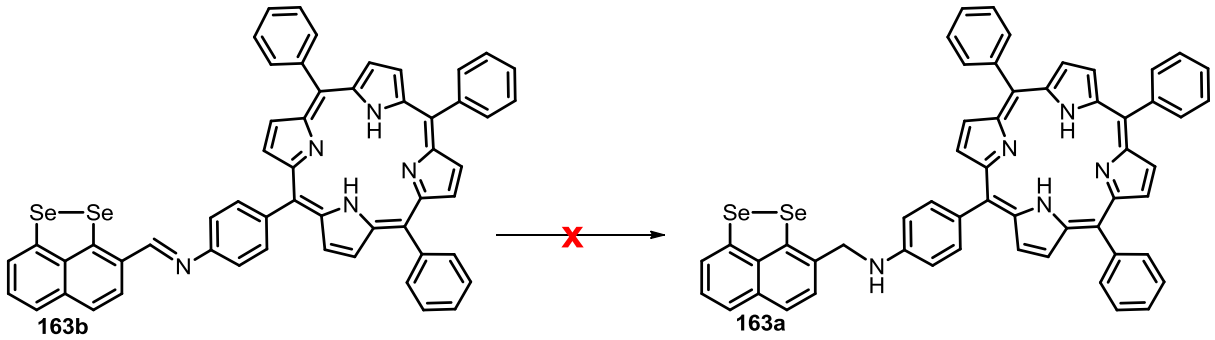

Table 4.2 Attempted reduction of imine **163b** to amine **163a**.

Entry	Reaction conditions	Isolated product	Reference
1	$NaBH_4$ (12 eq.), MeOH:$CHCl_3$ (1:10), rt, 3.5 h	degradation	216
2	$NaBH_3CN$ (12 eq.), MeOH:THF (1:1), AcOH (2 drops), Δ, 7.5 h	90% **163b**	215
3	$NaBH(OAc)_3$ (13.5 eq.), AcOH (1 eq.), rt to Δ, 24 h	95% **163b**	219
4	H_2, Pd/C, MeOH, rt, 24 h	95% **163b**	220

4.3.2 Spectroscopic and electrochemical analysis of zinc porphyrin-functionilised [FeFe]-complex

[FeFe]-complex **155a** is analysed by NMR, IR, UV/vis and emission spectroscopy. As expected from the results, previously discussed in Chapters 2 and 3, the ^{1}H NMR spectra displayed a significant downfield shift of naphthalene and amino-linker peaks of **155a** compared with those of the precursor **162a**, associated with the insertion of the [FeFe]-cluster.[122] Similarly, the metallation of the porphyrin produces a downfield shift of the pyrrole protons in **155a** compared to **162a**. In contrast, the presence of the metal shifts the *N*-phenyl protons and the remaining phenyl protons upfield compared with **162a**.[198b)] Molecular dyad **155a** and the model system **131a** (Chapter 3) showed similar proton resonances for both the naphthalene core and the amine, suggesting that *p*-methoxyaniline and $ZnTPPNH_2$ induces

similar electronic effects. ^{13}C NMR showed the characteristic peak for the carbonyls of the [FeFe]-cluster at 207 ppm.

IR spectroscopy displayed three stretching bands at 2072, 2032 and 1982 cm^{-1}, which are assigned to the iron-bound carbonyl ligands.[112,117,122,202,204] [FeFe]-complexes **155a** and **131a** (**Table 3.4**, Chapter 3) showed comparable wavenumbers for the carbonyl stretching, suggesting that ZnTPP in the ground state does not significantly affect the [FeFe]-cluster.[202]

As for previously reported ZnTPP-containing molecular dyads, [198-204] the UV/vis absorption spectrum of **155a** shows one intense Soret band at 422 nm and two weak Q bands at 550 nm and 593 nm, respectively (**Figure 4.5**). By analogy with the model system **131a** (Chapter 3), the absorption band at 254 nm is assigned to the naphthalene π-π^* transition and those at 308 nm and 355 nm are assigned to either the iron-carbonyls MLTC or LMCT or to the naphthalene π-π^* transition.

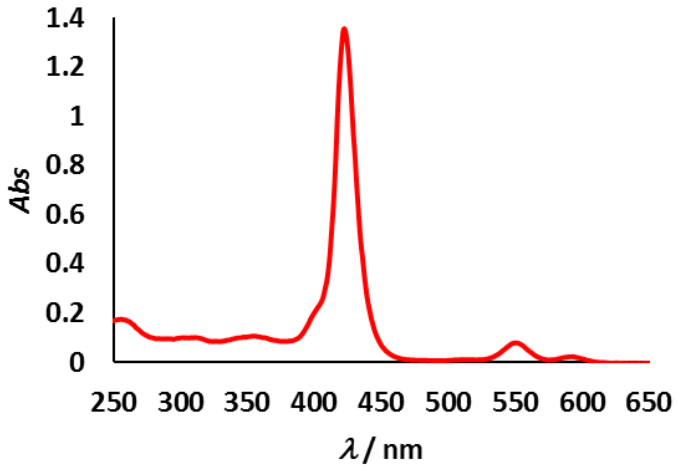

Figure 4.5 UV/vis spectra of [FeFe]-complex **155a**.

Metalloporphyrins exhibit an intense fluorescent emission, the quenching of which indicates the electron transfer ability of the photoactivated system.[198,199,200] Indeed, comparison of the emission spectra of **155a** and **164** (λ_{552} and λ_{558}, respectively) displays a decrease of the

fluorescence yield of the excited species of ZnTPP, potentially associated with the electron transfer to the [FeFe]-cluster.[198,199,200]

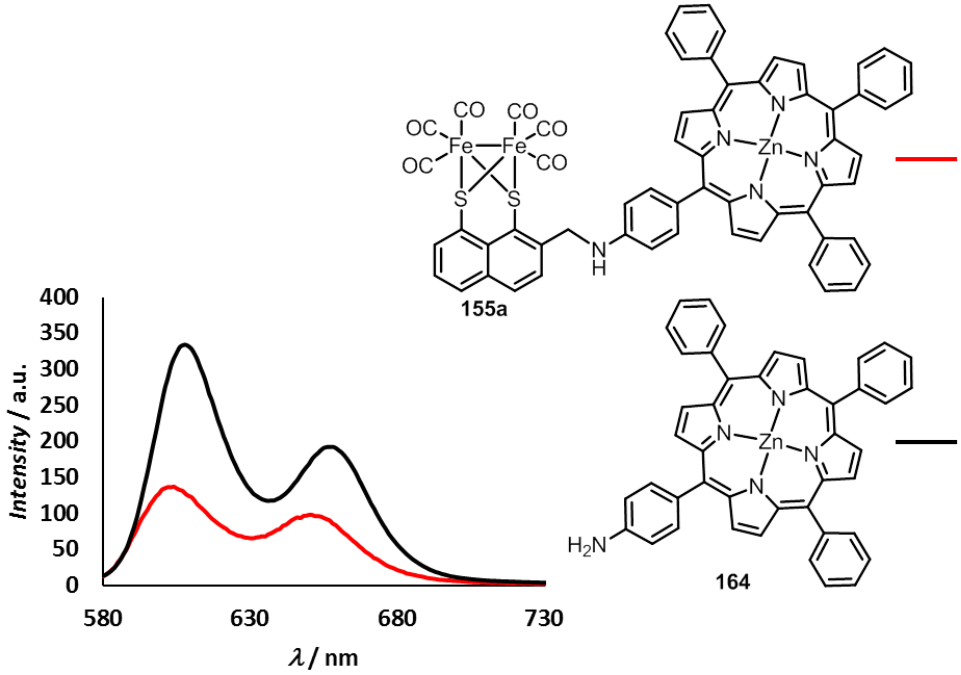

Figure 4.6 Emission spectra of [FeFe]-complex **155a** and $ZnTPPNH_2$ **164**.

In addition, by selecting the emission wavelength at 602 nm and 650 nm (**Figure 4.6**), absorption in the dithiolate-based [FeFe]-complex region is observed, suggesting that the electron transfer between the two moieties of the molecular dyads could occur (**Figure 4.7**).

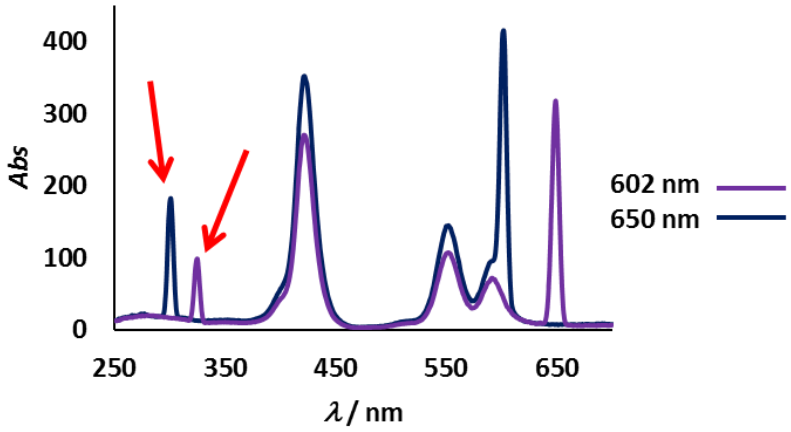

Figure 4.7 Excitation spectrum of [FeFe]-complex **155a** after emission recorded at 602 nm and 650 nm.

Based on the spectroscopic analysis, the electrochemical behaviour of molecular dyad **155a** was investigated in order to verify whether the electron transfer from the ZnTPP moiety to the [FeFe]-cluster is thermodynamically feasible. Cyclic voltammetry was recorded in CH_2Cl_2 at room temperature, using a three electrode-cell with glassy carbon as working electrode, $Ag/AgNO_3$ as reference electrode, and platinum as counter electrode. All the potentials were calculated with respect to the ferrocene redox couple (Fc/Fc^+), which is used as internal reference (see Chapter 6 for experimental details).

Cyclic voltammogram of **155a** in Figure 4.8 displays two reduction processes at –1.72 V and –2.05 V ($E'_{1/2}$ = –1.65 V and $E''_{1/2}$ = –1.94 V), which are assigned to Fe(I)Fe(I)→Fe(0)Fe(I) and Fe(0)Fe(I)→Fe(0)Fe(0), respectively, in analogy with [FeFe]-complex **131a** (**Table 3.6**, Chapter 3). Two oxidation waves are also shown at 0.4 V and 0.7 V, which are attributed to Fe(I)Fe(I)→Fe(II)Fe(I) and Fe(II)Fe(I)→Fe(II)Fe(II) respectively.[122] The electrochemical response of the ZnTPP moiety of the molecular dyad is excluded, since the recorded voltammogram of **155a** differs from those reported in the literature.[221]

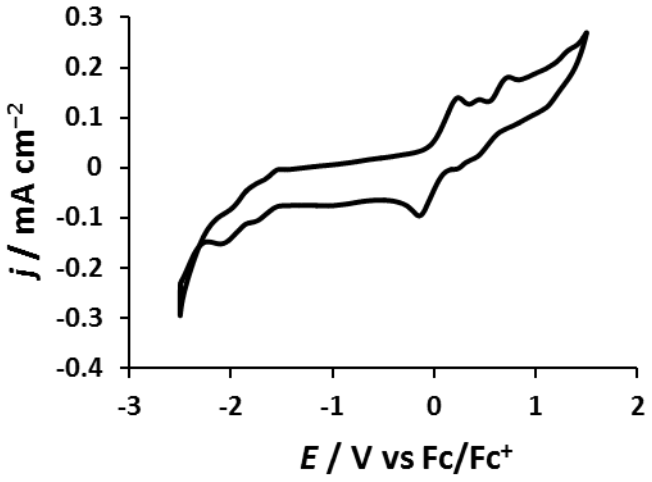

Figure 4.8 Cyclic voltammogram of **155a** (1 mM) in 0.1 M NBu_4PF_6/CH_2Cl_2:CH_3CN (7:3) at 0.01 V s^{-1} scan rate.

The first and the second reduction potentials of **155a** are shifted towards more negative potentials than those of model system **131a** (Chapter 3); however, the first reduction wave, which is the catalytic peak by analogy with **131a**, is still less negative than the oxidation potential reported for the excited species $ZnTPP^*$ (= –1.74 V).[157] Consequently, the oxidative quenching of excited species $ZnTPP^*$ by the [FeFe]-cluster is thermodynamically favoured, since the oxidation potential of $ZnTPP^*$ is close to the reduction potential of the [FeFe]-cluster moiety of the molecular dyad (Section 4.3.3). Furthermore, the previous analysis on electrocatalytic proton reduction (Chapter 3) and the spectroscopic and electrochemical similarities between **131a** and **155a** suggest that the reduced [FeFe]-cluster in **155a** will catalyse proton reduction, thus generating hydrogen.

4.3.3 Initial studies on photocatalytic hydrogen production

Photocatalytic activity of molecular dyad **155a** was investigated by irradiating a 5 mL sealed vial containing 2 mL of 1 mM solution of the complex in CH_2Cl_2 with a 125 W mercury pressure lamp in the presence of *p*TsOH or trifluoroacetic acid (TFA), from 100 mM to 1 M. In order to avoid degradation of the [FeFe]-cluster, the light was filtered to exclude radiation < 450 nm, allowing the excitation of the zinc porphyrin core (Q bands) but not the iron centres (d-d transition). After one hour of irradiation hydrogen in the vial headspace was measured by gas chromatography (GC) and quantified using a calibration curve (**Figure 4.9**), obtained with known concentrations of pure hydrogen in argon, which was used as carrier gas (see Chapter 5 for experimental details). The calibration curve in Figure 4.9 is divided in low hydrogen concentrations (from 0.01% to 0.625%, left in **Figure 4.9**) and in high hydrogen concentrations (from 1.25% to 100%, right in **Figure 4.9**). Since hydrogen produced by **155a** exhibited a peak with associated area in the low range of the calibration curve, the first

equation ($y = 0.22071 \times 10^5 x$) is used in order to determine the concentration of hydrogen after one hour irradiation.

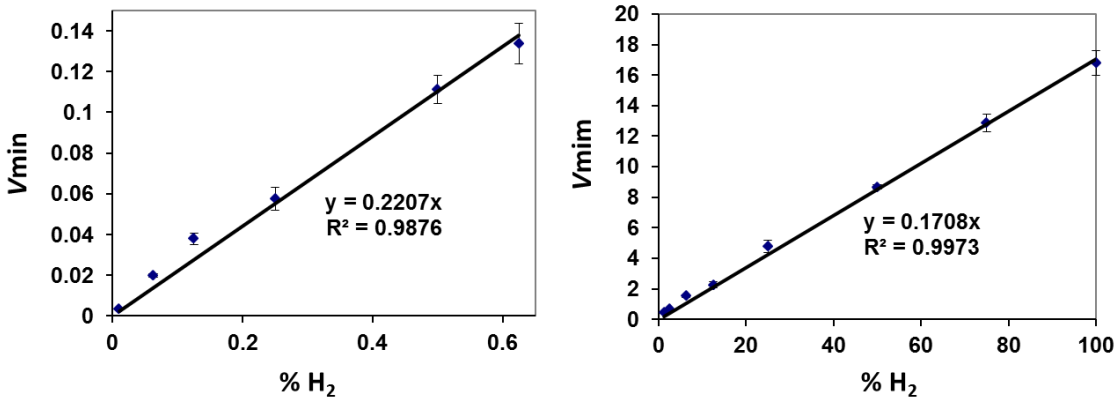

Figure 4.9 Calibration curve obtained with known concentrations of pure hydrogen in 2 mL of argon.

Photocatalytic activity of [FeFe]-complex **155a** was investigated first using *p*TsOH as proton source. Photochemical hydrogen evolution was observed with 100 mM and 250 mM of *p*TsOH. However, since the acid was insoluble in CH_2Cl_2 at high concentrations (from 500 mM to 1 M), TFA is then used instead.[199,201,202,204] Table 4.3 reports the turnovers of hydrogen evolution in the presence of TFA and the corresponding TOF after one hour of irradiation.

Table 4.3 Photocatalytic hydrogen production by a 1 mM solution of **155a** in 2 mL of CH_2Cl_2 after addition of TFA at increasing concentrations.

Entry	[TFA] / mM	TOF / h^{-1}	TOF / s^{-1}
1	100	0.008 (±0.001)	5.2×10^{-6} ($\pm 1.8 \times 10^{-7}$)
2	250	0.019 (±0.001)	2.2×10^{-6} ($\pm 2.5 \times 10^{-7}$)
3	500	0.037 (±0.002)	1.0×10^{-5} ($\pm 5.1 \times 10^{-7}$)
4	750	0.009 (±0.001)	2.4×10^{-6} ($\pm 3.5 \times 10^{-7}$)
5	1000	0.013 (±0.002)	3.5×10^{-6} ($\pm 5.8 \times 10^{-7}$)

Under the above-mentioned experimental conditions and in the absence of an electron donor, hydrogen production was observed and it increased linearly as function of the acid

concentration, from 100 mM to 500 mM (**Figure 4.10**). The maximum TOF after one hour of irradiation is 0.037 obtained with 500 mM of TFA (**Table 4.3**).

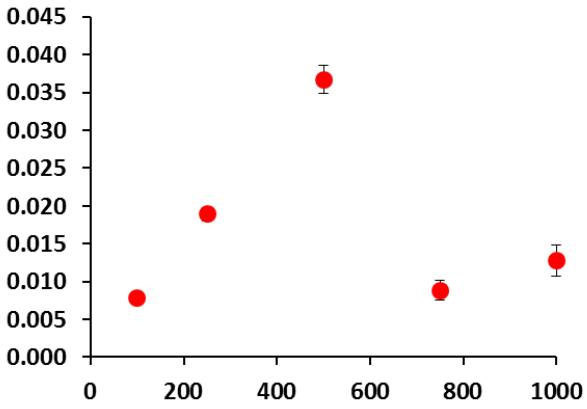

Figure 4.10 TOF/ acid concentration trend after one hour of irradiation.

On the contrary, the amount of hydrogen decreased dramatically upon addition of 750 mM, becoming unpredictable with 1 M of TFA (entries 4 and 5, **Table 4.3**). Furthermore, partial decomposition of the [FeFe]-complex **155a** was observed after one hour of irradiation. The acidic solution of **155a** in CH_2Cl_2 was washed first with a concentrated solution of ammonium hydroxide (NH_4OH) and then purified by column chromatography. The isolated compound (53%) was analysed by mass spectrometry (ES^+) and a peak corresponding to the mass of **155a** – 3 CO is detected.

Control experiments in the absence of the molecular dyad **155a** and the light showed no hydrogen detected by GC.

These initial results suggested that molecular dyad **155a** does catalyse light-driven hydrogen production. It is suggested that, after light-induced excitation, ZnTPP* transfers the electron to the [FeFe]-cluster through an oxidative quenching mechanism (**Scheme 3.1**) to generate the species $ZnTPP^+$, a process which is shown to be thermodynamically feasible through the ground and excited state electrode potentials of $E_{1/2}$= −1.65 V (**155a**) and −1.74 V

(ZnTPP*[157]) respectively. Then the acceptor and catalyst, [FeFe]-cluster of **155a**, catalyses the reduction of protons, provided by TFA, to molecular hydrogen (**Scheme 4.6**).

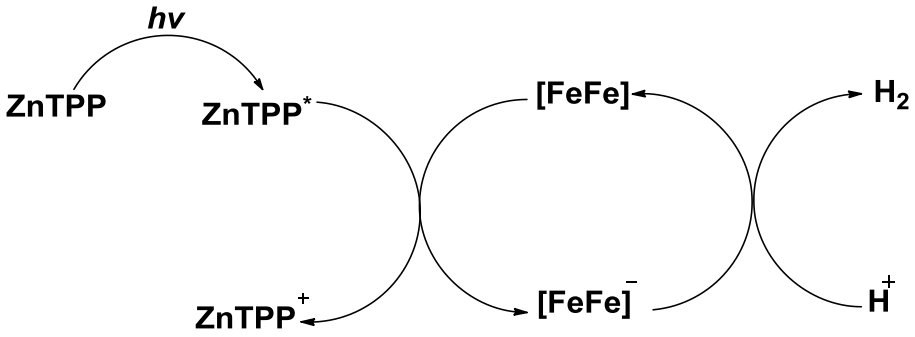

Scheme 4.6 Proposed mechanism for light-induced hydrogen production by molecular dyad **155a**.

However, the relatively low turnovers of hydrogen, compared with previously described porphyrin-based photochemical systems,[199-202,204] could be due to decomposition of the [FeFe]-cluster, caused by light-promoted iron d-d transitions, which occurred despite the light filter. Furthermore, ZnTPP is not regenerated after oxidative quenching of ZnTPP* and formation of the species ZnTPP$^+$ and this could further lower the catalytic activity of the system. Moreover, cyclic voltammetry on **155a** gave evidence for the poor stability of the reduced species of the [FeFe]-cluster, since two irreversible EC processes were observed.

4.3.4 Initial studies on synthesis of persubstituted polyaromatic ligands

Polychloroarenes have been commonly used for the synthesis of a wide range of dendrimeric nanomolecules, which exhibit remarkable spectroscopic and electrochemical properties. Therefore, they have been applied in various chemistry fields, particularly in supramolecular and synthetic chemistry.[222-224]

Following the aim of developing new photoactive [FeFe]-hydrogenase synthetic mimics based on polyaromatic ligands (Chapter 2), [FeFe]-complex **169** was targeted because of the potential photochemical properties of the coronene as backbone (**Scheme 4.7**).

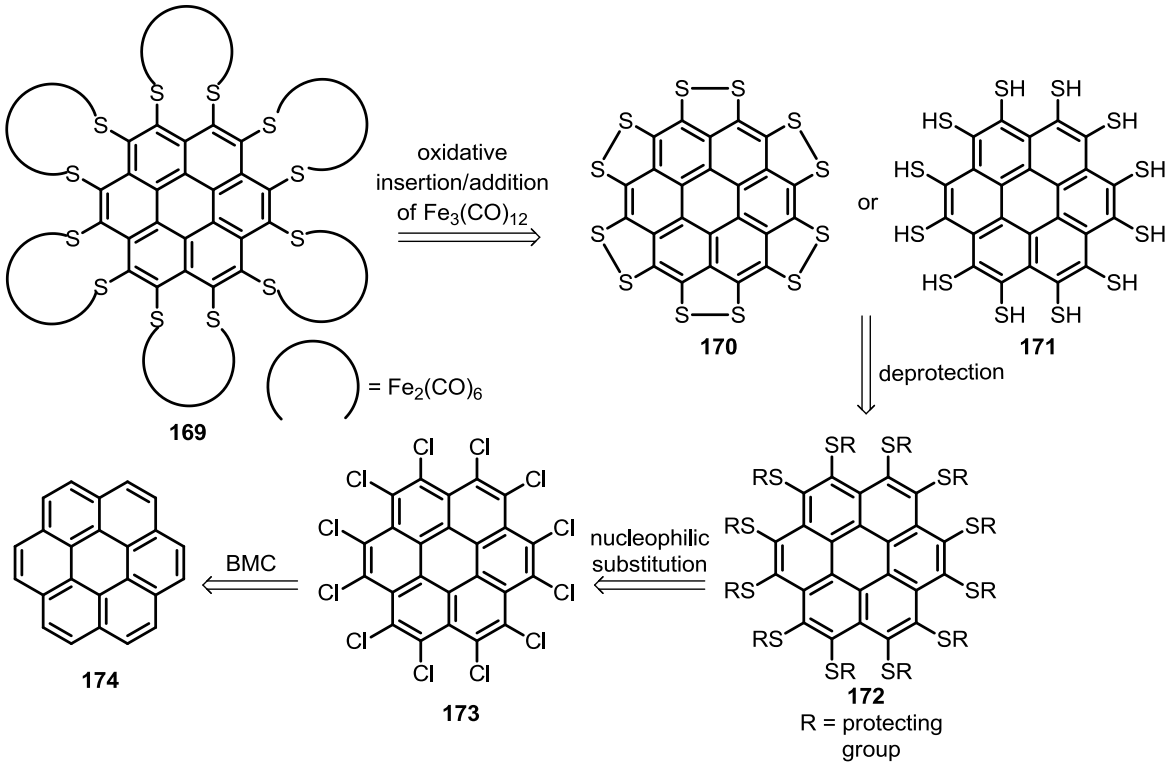

Scheme 4.7 Retrosynthetic analysis of hexakis(dithiolate)-persubstituted coronene-based [FeFe]-complex **173**.

In a retrosynthetic analysis, **169** can be obtained by either oxidative insertion of $Fe_3(CO)_{12}$ into the S-S bonds of dodecadithiole **170** or oxidative addition to dodecathiol coronene **171** (Chapter 2). Depending on the reaction conditions, **170** and **171** were proposed to be synthesised by removal of the R groups in **172**, in turn produced from the perchlorocoronene **173**, which is known to undergo multiple nucleophilic substitution with thiolates (**Scheme 4.7**).[222,224g)] Interestingly, compounds **170** and **171** could be applied either to the development of electronic devices [224f),h)] or to the formation of polynuclear gold complex-based nanoparticles.[224e),l)] Perchlorocoronene **173** is synthesised from the commercially available coronene **174** through the Ballester, Molinet and Castaner (BMC) synthetic procedure.[225]

In order to develop a reproducible and accessible synthetic methodology, the known octachloronaphthalene **175** was synthesised and utilised as a model system towards persubstituted derivative **172** (**Scheme 4.7**). Following a modification of the BMC procedure,[224c)] decachloronaphthalene **176** was successfully synthesised from the reaction of naphthalene **98** with sulfur monochloride (S_2Cl_2) and aluminium chloride ($AlCl_3$) in sulfuryl chloride (SO_2Cl_2). Compound **176** was then refluxed in diisopropyl ether in order to give the octachloronaphthalene **175** in good yield (**Scheme 4.8**).

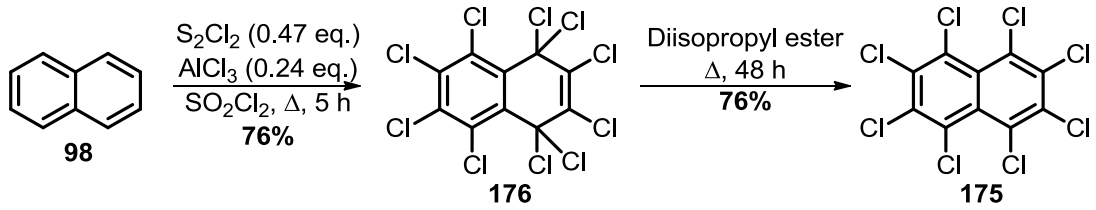

Scheme 4.8 Synthesis of octachloronaphthalene **175**.

The octyldithiocarbamate **177** and the commercially available sodium 2-propanethiolate **178** were chosen as nucleophiles in the substitution reaction with compound **175**.[226] The literature compound **177** was synthesised in 49% yield from the octyl amine **179** with carbon disulfide (CS_2) (**Scheme 4.9**).[227]

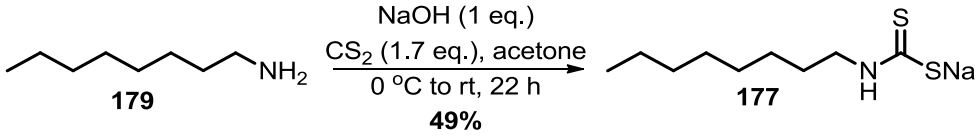

Scheme 4.9 Synthesis of octyldithiocarbamate **177**.

Following a literature procedure for chlorine displacement, [226] the expected product **180** was not obtained but, instead, an unidentified compound was isolated after consumption of the starting material. However, reaction of **175** with sodium 2-propanedithiolate **178** gave a thioether-substituted product, which was identified by mass spectrometry as compound **181**

with one remaining chlorine on the naphthalene ring (**Scheme 4.10**).[226] The position of the chloro substituent on the naphthalene ring could not be identified.

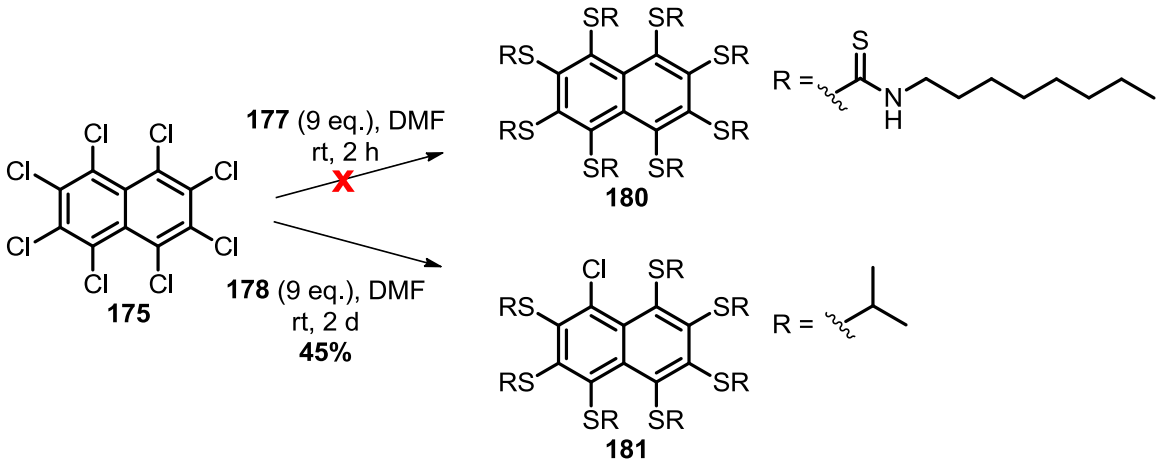

Scheme 4.10 Attempts to obtain persubstituted **180** and synthesis of **181**.

Perchlorocoronene **173** was successfully obtained from coronene **174** by modifying the synthetic procedure described for compound **175** (**Scheme 4.11**).[224c),228]

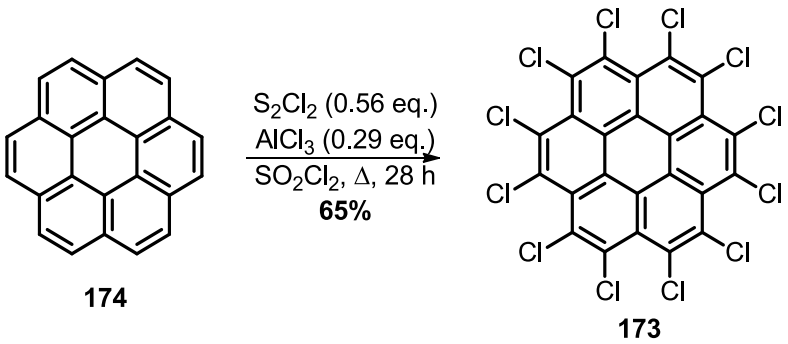

Scheme 4.11 Synthesis of perchlorocoronene **173**.

Following the experimental conditions in Scheme 4.10,[226] substitution of **173** with sodium 2-propanethiolate **178** was then attempted, unsuccessfully. Lehn and co-workers achieved the chloride displacement by adding **173** to a solution of the *p*-toluene thiolate, prepared *in situ* from the corresponding thiol with sodium hydride (NaH) in 1,3-dimethyl-2-imidazolidinone (DMI).[224f)] The reaction was repeated and the corresponding thioether-persubstituted **182** was successfully obtained in comparable yield to that reported in the literature (**Scheme 4.12**).

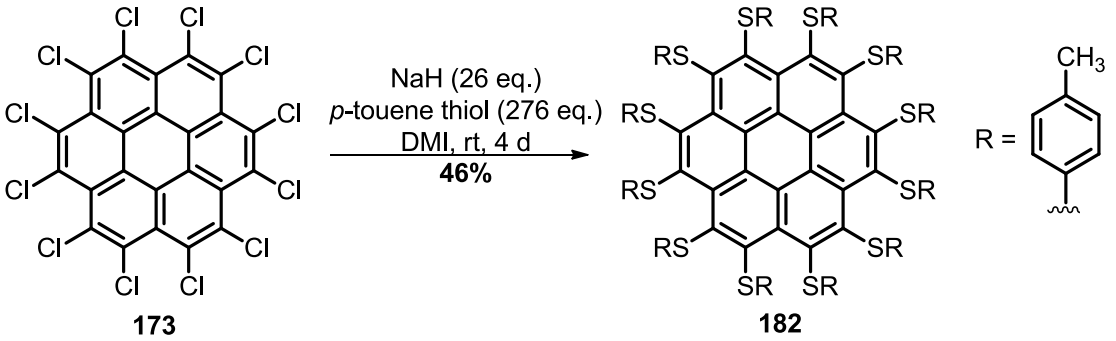

Scheme 4.12 Synthesis of the dodecakis(*p*-methylphenylthio)coronene **182**.[224f)]

The conditions described above were then applied to nucleophiles which are compatible with a subsequent thiol deprotection step (**Scheme 4.7**).[229] However, in no case the expected product was formed and the isolated compounds were difficult to analyse by NMR spectroscopy or by mass spectrometry. The starting material **173** was not recovered, since it was presumably consumed or degraded during the reaction (entries 1-7, **Table 4.4**).

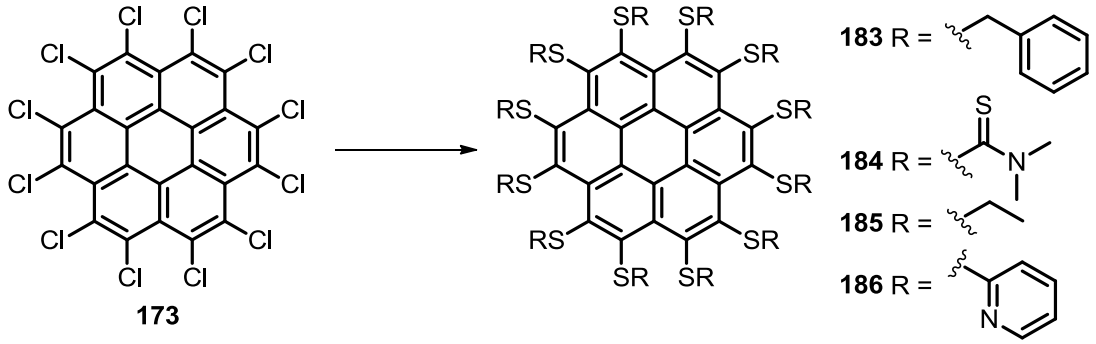

Table 4.4 Attempted chlorine displacement from **173**.

Entry	Reaction conditions	Isolated product	Reference
1	**187** (276 eq.), NaH (26 eq.), DMI, rt, 4 d	unidentified	224f)
2	dimethyldithiocarbamate (276 eq.), DMI, rt, 4 d	unidentified	224f)
3	**177** (276 eq.), DMI, rt, 4 d	unidentified	224f)
4	NaSEt (72 eq.), DMI, rt, 4 d	unidentified	224f)
5	NaSEt (72 eq.), DMF, rt, 4 d	unidentified	226
6	NaSEt (72 eq.), DMF, Δ, 24 h	unidentified	131
7	**188** (276 eq.), NaH (26), DMI, rt, 4 d	**189** and **190**	224f)

Benzyl thiolate **191**, both prepared *in situ* and synthesised from the corresponding mercaptan **187** (**Scheme 4.13**),[230] was used unsuccessfully in the substitution reaction with perchlorocoronene **173** (entry 1, **Table 4.4**).[224f)]

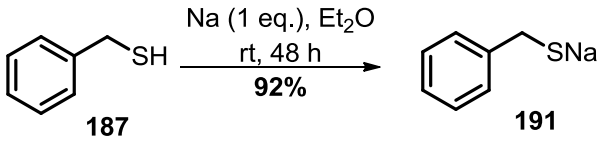

Scheme 4.13 Synthesis of the nucleophile **191**.

After reaction of **173** with 2-mercaptopyridine **188** (entry 7, **Table 4.4**), two compounds were isolated and identified by ^{1}H and ^{13}C NMR and mass spectrometry as the known the bis(2-pyridinyl)disulfide **189** [231] and bis-(2-mercaptopyridyl)methane **190**.[232] Presumably NaH deprotonates the thiol group of **188**, which is then oxidised to disulfide **189** during the work-up of the reaction. Compound **190** might be formed by reaction of deprotonated **188** and DMI in strong basic conditions. Disulfide **189** was also obtained by reacting **188** with NaH in either distilled or non-distilled DMI in the absence of perchlorocoronene **173**; however, the formation of **190** was not observed (**Scheme 4.14**).

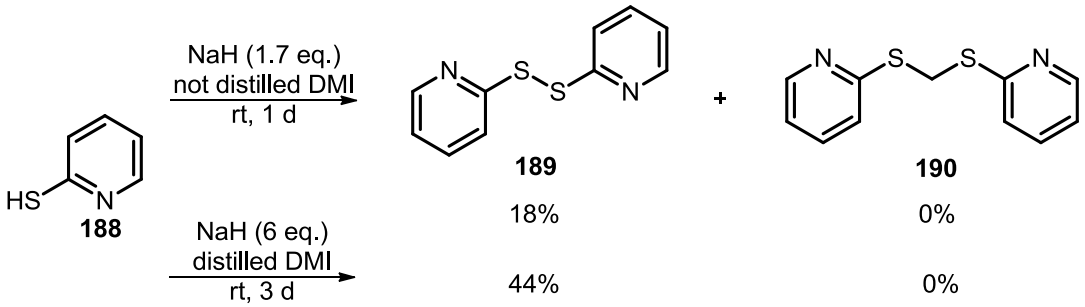

Scheme 4.14 Synthesis of **189** and **190** from the reaction of **188** and in absence of **173**.

4.4 Summary

This chapter described the investigation into the synthesis of molecular dyads consisting of the photosensitizer $ZnTPPNH_2$ covalently linked to *peri*-substituted dichalcogenide-based

[FeFe]-complexes via imino/amino group and the successful preparation of photochemical systems **155a-b** and **156a-b**.

NMR, IR and UV/vis spectroscopy showed that the porphyrin core in **155a** and the *p*-methoxyphenyl group in **131a** similarly affect the [FeFe]-cluster, suggesting that **155a** and **131a** exhibit similar electronic properties. The electrochemical behaviour of **155a** is consistent with that of **131a**, although both reduction processes of the [FeFe]-cluster in **155a** are shifted to more negative potentials than those recorded for **131a**. Preliminary spectroscopic results are consistent with a potential oxidative quenching of the excited $ZnTPP^*$ by the naphthalene moiety (**Scheme 4.6**). Moreover, electrochemical studies indicate that electron transfer from the light-excited porphyrin core to the [FeFe]-cluster is feasible, considering the reduction potential measured for **155a**. Indeed, initial investigations on **155a** as a photocatalyst for hydrogen production showed that hydrogen is produced in the presence of acid after one hour of irradiation. The maximum turnover after one hour of irradiation is 0.037, obtained with 500 mM of TFA. However, mass spectrometry showed decomposition of **155a** after one hour of irradiation.

Chloride displacement from perchlorocoronene **173** was investigated. Successful reaction conditions were found for the model system **175** and persubstituted naphthalene **181** was obtained. However, nucleophilic substitutions with alkyl/aromatic thiolate nucleophiles were unsuccessful and synthesis of compounds**183-186** could not be achieved.

Chapter 5: Conclusion and future work

Electrochemical studies on [FeFe]-complexes **89d**, **91a**, **b** and **d**, **92a-b**, **93** and **94** (Chapter 2) showed that diselenolate-based [FeFe]-complexes are more efficient proton reduction catalysts than the sulfur counterparts in terms of both calculated overpotential and catalytic peak current increase. However, the dithiolate-based systems produced more stable reduced species of [FeFe]-cluster than the corresponding selenium systems. In order to complete the studies on bio-inspired synthetic models **89d**, **91a**, **b** and **d**, **92a-b**, **93**, **94** and **96**, the reactivity of the [FeFe]-cluster could be investigated (**Scheme 5.1**).[16,17] Displacement of the terminal carbonyls with stronger electron-donating ligands, such as phosphines, carbenes and isocyanides (L, **Scheme 5.1**) should be first targeted. In particular, it has been reported that the reduced species of phosphine-substituted iron centres are more stable in a redox cycle than the corresponding hexacarbonyl [FeFe]-cluster (Section 1.3.2.2, Chapter 1).

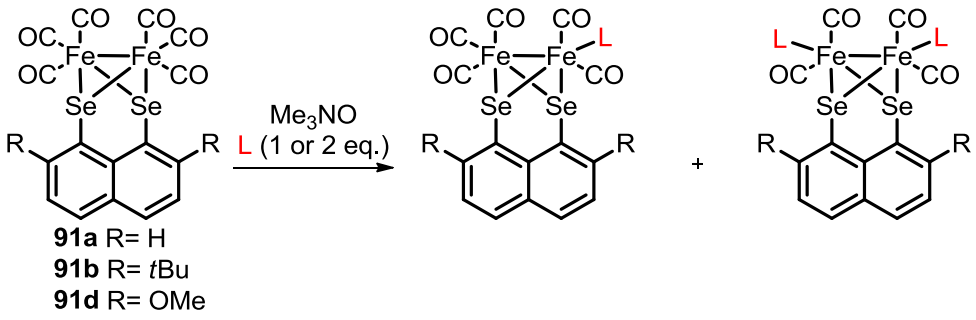

Scheme 5.1 Example of carbonyl displacement with phosphine, carbene and isocyanide ligands (L) on [FeFe]-complexes **91a**, **b** and **d**.

Reaction of electron-rich [FeFe]-clusters with both weak (AcOH) and strong (TFA) acid is expected to protonate the iron centres, since the electron-density and, hence, the basicity of the iron centres will be greater in the ligand (L)-substituted than in the corresponding hexacarbonyl [FeFe]-cluster. Investigation on whether the proton binds the iron, either to a terminal or to a bridging position (example in **Scheme 5.2**) will be required and could be analysed by IR and NMR spectroscopy. It is expected that, although the reduction of the metal centres will be shifted towards more negative potentials than that recorded for the

hexacarbonyl [FeFe]-cluster, proton reduction catalysis will be facilitated. The electron-rich iron centres will be protonated first and then reduced at anodically shifted potentials, therefore the complex overpotential will be decreased (**Scheme 5.2**).[17]

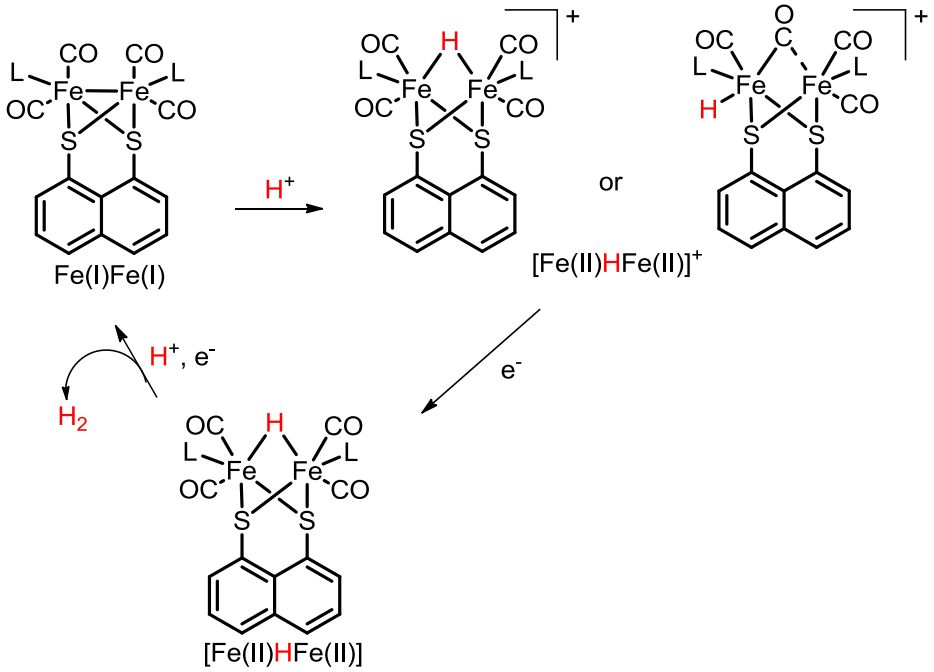

Scheme 5.2 Proton reduction catalysis by electron-donating ligand-substituted [FeFe]-hydrogenase synthetic mimics

Regarding the amine and imine-substituted [FeFe]-complexes, **129a**, **130a**, **131a-b**, **132a** and **b** (Chapter 3), the possible protonation of the amino/imino group was analysed by titrating the [FeFe]-complexes with *p*TsOH and it was monitored by UV/vis spectroscopy and cyclic voltammetry. All the [FeFe]-complexes displayed a significant change in the absorption profile upon addition of acid. At low concentration of *p*TsOH, the amino-substituted **129a**, **130a**, **131a** and **132a** exhibit an anodic shift of the first reduction peak, suggesting reduction of the protonated complexes, which becomes, instead, negligible at high concentration. On the contrary, protonation of the imine-substituted **131b** and **132b** seems to occur, facilitating the proton reduction catalysis, even at high concentration. Further investigations on the

protonation of the nitrogen by titration with suitable acids, such as TFA, monitored by NMR spectroscopy could be carried on.

The reported initial results suggest that molecular dyad **155a** does catalyse the light-driven hydrogen production through oxidative quenching mechanism (**Scheme 4.6**, Chapter 4). However, the relatively low turnovers of hydrogen (0.037 after one hour of irradiation) may be due to the decomposition of the [FeFe]-cluster, caused by the light-promoted irons d-d transitions. In addition, the negligible difference between the observed reduction potential of **155a** and the oxidation potential of the excited species $ZnTPP^*$ ($E^\circ = -1.74$), [157] may affect the efficiency of the electron transfer between the two moieties of the molecular dyad. Moreover, cyclic voltammetry analysis on **155a** provides evidences of the poor stability of the reduced species of the [FeFe]-cluster, since two quasi-reversible reduction waves are observed. Consequently, optimization of the photochemical system **155b** is required. The introduction of an electron donor, such as ascorbic acid or NEt_3, which will consequently regenerate the neutral ZnTPP from the oxidized $ZnTPP^+$ should delay the charge recombination between the photosensitizer and the catalyst, and, hence, may improve the photocatalytic efficiency of the system. However, the observed decomposition of [FeFe]-cluster by CO loss could be prevented by studying how long the [FeFe]-cluster can be irradiated before the decomposition process occurs. Accordingly, the hydrogen production requires to be followed over time, limited to one hour, and with the most effective acid concentration.

The employment of bimolecular systems (Section 4.1, Chapter 4) might avoid unwanted energy transfer or reverse electron transfer reactions affecting the stability and catalytic efficiency of the molecular dyads.[156,157,158,191] Consequently, a comparative analysis of the bimolecular systems, consisting of the ZnTPP as photosensitizer and the model system **131a** as catalyst, may be also required in order to complete the study on molecular dyad **155a**.

In order to promote photocatalytic water splitting, the combination of various bimolecular systems, including simple *peri*-substituted dichalcogenide-based [FeFe]-complexes and different photosensitizers (porphyrins, zinc porphyrins, Ru, Ir and Re-containing complexes) could be studied in micelles, which are known to promote the water-solubility of organic molecules (**Figure 5.1**).[233]

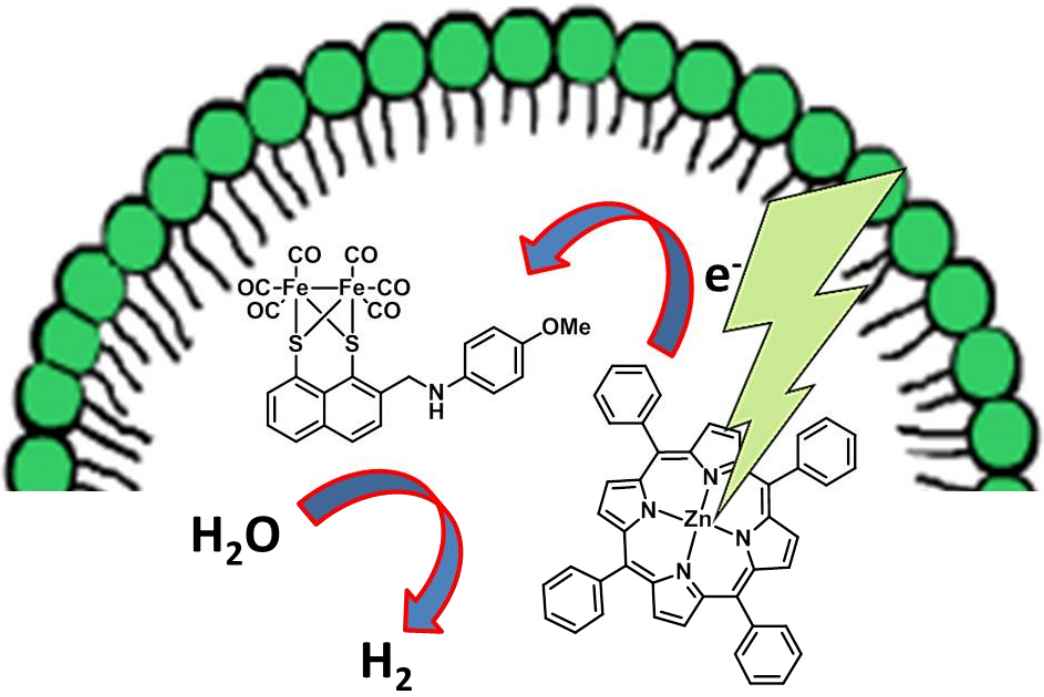

Figure 5.1 Example of photocatalytic water splitting in micellar solution.

Chapter 6: Experimental section

6.1 General experimental

Solvents and reagents were purified as follows:

*n*BuLi was purchased as either 2.5 M or 1.6 M solutions in hexane and the solutions titrated with menthol in the presence of 1-(biphenyl-4-yl)-3-phenyl-2-azapropene ("BLUE"). TMEDA was distilled from CaH_2.[234] Sulfur was recrystallized from toluene.[234] *m*CPBA was purified by washing with a pH 7 phosphate buffer which was prepared from 0.1 M NaOH (154 mL) and 0.2 M KH_2PO_4 (94 mL), distilled water was added up to 376 mL. A solution of *m*CPBA (77% w/w, 10 g) in Et_2O (100 mL) was washed with the buffer solution (× 3); the combined organic layers were then dried over $MgSO_4$, evaporated under reduced pressure to yield pure *m*CPBA (7.3 g, 73%).[235] Pyrrole was distilled from CaH_2.[234] SO_2Cl_2 was purified by fractional distillation; pure SO_2Cl_2 was collected at 69-70 °C.[234] *p*-Toluenesulfonic acid monohydrate (*p*TsOH·H_2O) was dehydrated by heating at 100 °C for 4 hours under vacuum and then recrystallized from $CHCl_3$.[234] All other reagents and solvents were purchased from Sigma Aldrich, Alfa Aesar, Fisher Scientific and were used as received. Dry solvents were obtained and purified using a Pure Solv-MD solvent purification system (SPS) and were transferred under argon. Solvents were degassed by bubbling argon through a needle immersed in the solvent for 15-30 minutes. The following cooling baths were used: 0 °C (ice/water), –30 and –78 °C (dry ice/acetone). All reactions in non-aqueous solvents were carried out under argon in oven dried glassware. Analytical t.l.c. was carried out on Merck 60 F245 aluminium-backed silica gel plates. Short wave UV (245 nm) and $KMnO_4$ were used to visualize components. Compounds were purified by flash column chromatography using Merck silica gel 60 or alumina basic 60-325. Melting points were determined using open glass capillaries on a Gallenkamp melting point apparatus and are uncorrected. Elemental

analysis was performed on a Carlo Erba EA1110 Flash Combustion Instrument for CHN analysis.

6.1.1 Spectroscopy

^{1}H and ^{13}C NMR data were recorded on a Bruker AVIII300 (300 MHz ^{1}H, T = 293 K), Bruker AVIII400 (400 MHz ^{1}H, 101 MHz ^{13}C, T = 293 K) or on a Bruker AV400 (400 MHz ^{1}H, 101 MHz ^{13}C, T = 293 K) spectrometer. Spectra were recorded in CD_2Cl_2 referenced to residual CH_2Cl_2 (^{1}H, 5.33 ppm; ^{13}C, 53.84 ppm), C_6D_6 referenced to residual C_6H_6 (^{1}H, 7.15 ppm; ^{13}C, 128.06 ppm), DMSO-d_6 referenced to residual DMSO (^{1}H, 2.50 ppm; ^{13}C, 39.52 ppm) and $CDCl_3$ referenced to residual $CHCl_3$ (^{1}H, 7.26 ppm; ^{13}C, 77.16 ppm).[236] Chemical shifts (δ) are reported in ppm and coupling constants (J) are reported in Hz. The following abbreviations are used to describe multiplicity: s-singlet, d-doublet, t-triplet, q-quartet, m-multiplet, br-broad. All the reported coupling constants are averaged, when the coupling constants are close in values. Data were processed using Mestrenova 6.0. Mass spectra (MS) were recorded on a Microwaters LCT TOF with a mixture (2:1) of MeOH and $CHCl_3$ as mobile phase, Microwaters SynaptG26 with mixture (2:1) of $CHCl_3$ and MeOH as mobile phase or on a Microwaters GCT Premier Probe, utilising electrospray ionisation (recorded in the positive mode), or electron impact ionisation, and both are reported as *m/z* (%) and they are given as $[M+H]^+$ and M^+. Mass spectra were also recorded on a Microwaters MALDI MicroMX spectrometer utilising laser desorption (recorded in positive mode) with 1 μL of gentisic acid as matrice and they are reported as *m/z* (%). High resolution mass spectra (HRMS) were recorded on a Microwaters LCT TOF, Microwaters SynaptG26 or on Microwaters GCT Premier Probe using a leucine enkephalin-lock mass incorporated into the mobile phase. IR spectra were recorded neat on a Perkin–Elmer 100 FT-IR spectrometer.

6.1.2 UV-visible and emission spectroscopy

UV-visible spectra were recorded in a 1 mL quartz cuvette of 1 cm pathlength at 298 K on a CARY50 spectrometer. Wavelengths are given in nm, and extinction coefficients in $M^{-1}cm^{-1}$. Emission spectra were recorded on a Shimadzu RF-5301PC spectrophotometer with excitation and emission slit width both set at 10 nm and using 1 mL quartz cuvette of 1 cm pathlength; wavelengths are given in nm.

Prior to recording each measurement, UV-visible of blank solutions, containing only solvent (CH_3CN or CH_2Cl_2), were acquired in the range 210-500 nm. Aliquots (10 μL or 30 μL) of complexes **89d**, **91a**, **b** and **d**, **92a-b**, **93**, **94** and **96** and dichalcogens **99a**, **b** and **d**, **100a-b**, **103d**, **113**, **114** and **120** (Chapter 2) from stock solutions (2.5 mM) were then added to the cuvette and diluted with 990 or 970 μL of solvent (CH_3CN) such that their final concentration was equal to 2.5 and 7.5 × 10^{-5} M (respectively), and new spectra were recorded. Each measurement was repeated three times and the reported absorbance values were averaged and then used to obtain the extinction coefficient (M^{-1} cm^{-1}).

Aliquots (10 μL) of complexes **129a**, **130a**, **131a-b**, **132a-b**, dichalcogens **137b** and **138b** (Chapter 3) and complexes **89a** and **91a** (Chapter 2) from stock solutions (1 mM) was added to the cuvette and diluted with 990 μL of solvent (CH_3CN) such that their final concentration was equal to 1 × 10^{-5} M, and new spectra were recorded. Titration with *p*TsOH was performed by adding sequentially aliquots (10 μL) of acid from a stock solution (0.5 mM and 2.5 mM) to the same cuvette containing the complex, and the new spectra were recorded. After titration with acid, the absorbance, obtained from each measurement, was corrected for the dilution relative to acid addition. Each measurement was repeated three times and the absorbance then averaged.

Aliquots (3 or 10 μL) of complex **155a** and amine **164** (Chapter 4) from a stock solution (1 mM) was added to the cuvette and diluted with 997 or 990 μL of solvent (CH_2Cl_2) such that their final concentration was equal to 1×10^{-5} and 1×10^{-6} M (respectively), and new spectra were recorded. Each measurement was repeated three times and the absorbance then averaged.

Aliquots (5 or 3 μL) of complex **155a** and amine **164** (Chapter 4) from stock solutions (1 mM) were added to the cuvette and diluted with 995 or 997 μL of solvent (CH_2Cl_2) such that their final concentration was equal to 5 and 3×10^{-6} M (respectively), and emission spectra were acquired in the range 560-800 nm, using $\lambda_{exc.}$ = 552 nm and 558 nm and slits width excitation and emission = 10 nm. Each measurement was repeated three times.

6.1.3 Electrochemistry

Electrochemical studies were performed with a CHI601B Electrochemical Analyzer. All measurements were carried out under argon at room temperature in dry CH_3CN. Tetrabutylammomiun hexafluorophosphate (NBu_4PF_6, 0.1 M in CH_3CN) was used as supporting electrolyte, without any further purification and without being dried. A conventional 3-electrode system was employed. The working electrode was a glassy carbon electrode (diameter: 1.0 mm). Silver/silver nitrate ($Ag/AgNO_3$, 10 mM solution in CH_3CN) was used as an external reference electrode and a platinum wire was used as auxiliary electrode. Ferrocene was used as an internal reference. All potentials reported in this work are with reference to the Fc/Fc^+ couple (0.450 vs. SHE) and they are expressed in volt (V). All cyclic voltammograms were carried out at a scan rate of 0.01 V s^{-1}. The peak current (mA) is expressed in current density (j = mA cm^{-2}), which was obtained by dividing the peak current by the glassy carbon area (= 0.0314 cm^2). All glassware was cleaned using a 1:1 mixture of

ammonia and hydrogen peroxide (30%) followed by rinsing with pure water. Glassware was soaked in pure water for 12 hours and then rinsed and overnight oven-dried. Water used throughout (including solution preparation and rinsing) was purified by a Millipore™ system (resistivity 18.2 MΩ cm, TOC ≤ 5 ppb). The working electrode was prepared by polishing with aqueous slurries of successively finer grades of alumina powder (1 μm, 0.3 μm and 0.05 μm, Buehler), followed by rinsing and placing in pure water in an ultrasonic bath for several minutes, then dried in a stream of argon.

Solutions of complexes (1 mM), ferrocene (1 mM) and NBu_4PF_6, (0.1 M) in CH_3CN or CH_2Cl_2 were prepared and cyclic voltammograms were recorded in the range between 1.5 and –2.5 V (× 3). Potential and peak current values were averaged. Titration with *p*TsOH was performed by adding from 2.5 to 10 equivalents (0.5 to 10 eq. in Chapter 3) of acid to a solution of the [FeFe]-complex, freshly prepared for each acid addition, and cyclic voltammograms were then recorded (× 3). Potentials and peak current (I_{pa} and I_{pc}) values were averaged.

6.1.4 Photochemical hydrogen production

Gas analysis was performed on a Shimadzu GC-2010 using a Programmed Temperature Vaporization (PVT) injector set up at 200 °C, a Thermal Conductivity Detector (TCD) at 350 °C, a 5 Å molecular sieves column (Quadret, 30 mL × 0.53 mm ID × 25 μm df) and argon as carrier gas (gas flow was set to 35.5 kPa). The GC oven temperature was kept at 27 °C. Data were processed with Chromeleon 6.8 SR8 build 2623. Fixed needle-syringes (Hamilton) of 1 mL, 500 μL and 250 μL were used for the gas injection.

A solution of **155a** (1 mM, 2 μmol) in dry CH_2CH_2 (2 mL) was added with TFA (100 mM to 1M, 200 μmol to 2 mmol) in a 5 mL quartz glass vial, equipped with silica septum and

aluminium cap, at room temperature. After bubbling argon and stirring in the dark for 10 minutes, the solution was irradiated by a 125 W mercury pressure lamp (Photochemical Reactor) in a water-cooling jacket and wavelengths < 450 nm were cut off by a dichroic longpass filter (diameter = 12.5 mm). The reaction temperature was considered at 20 °C. After 1 hour of irradiation the amount of produced hydrogen was identified by gas chromatography, using aliquots (100 μL) from the vial headspace (3 mL); hydrogen in solution was neglected for calculation of the volume of produced hydrogen. A new solution of **155a** was prepared for each acid addition, each analysis was repeated at least twice and the obtained areas were then averaged.

Fourteen-point calibration curve for hydrogen was created by using known percentages of pure hydrogen in 2 mL of argon, used as carrier gas. The percentage of produced hydrogen was obtained by the integrated peak areas (Vmin) and, consequently, the corresponding volume of hydrogen in 3 mL vial headspace. Micromoles (n) of hydrogen were calculated using the ideal gas law:

$$PV = n\mathrm{R}T$$

- P = 101,325 N m^{-2}, is the absolute pressure of the gas
- V is the volume of the gas and it is expressed in m^3
- T = 293.15 K, is the room temperature of the gas
- R = 8.31432 × 10^3 N m kmol·K^{-1}, is the gas constant

6.2 Experimental section: Chapter 2

Naphtho[1,8-*cd*][1,2]diselenole (**99a**)

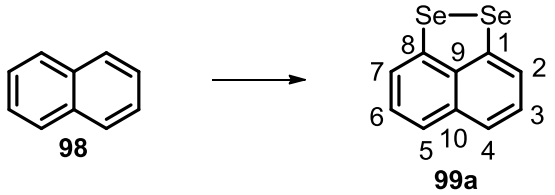

98 **99a**

Naphtho[1,8-*cd*][1,2]diselenole **99a** [237] was prepared according to a literature procedure.[126] *n*BuLi (41.0 mL of a 1.88 M solution in hexane, 78.0 mmol) and TMEDA (12.0 mL, 78.0 mmol) were added dropwise over a period of 30 minutes to naphthalene **98** (4.00 g, 31.2 mmol) under argon atmosphere in a flame dried round-bottomed flask. The mixture was stirred at 70 °C for 2 hours and then allowed to cool down to room temperature. The reaction was slowly diluted with THF (98 mL), cooled to – 78 °C and Se (7.50 g, 95.0 mmol) was added in one portion. The mixture was slowly warmed at room temperature and stirred for 16 hours under argon atmosphere. The reaction mixture was poured into a conical flask containing H_2O (50 mL) and hexane (50 mL) and the two layers were separated. The aqueous layer was extracted with Et_2O (3 × 30 mL). The combined organic layers were washed with brine (30 mL), dried over $MgSO_4$, filtered, concentrated under reduced pressure. The residue was purified by column chromatography (hexane) to give dichalcogen **99a** as a purple solid (2.90 g, 33%). λ_{nm} (CH_3CN) 259 ($\varepsilon = 1.7 \times 10^4$ $M^{-1}cm^{-1}$), 373 ($\varepsilon = 1.6 \times 10^4$ $M^{-1}cm^{-1}$); δ_H(400 MHz, $CDCl_3$): 7.24 (2 H, t, J = 7.8 Hz, H-3 and H-6), 7.35 (2 H, d, J = 7.8 Hz, H-2 and H-7), 7.47 (2 H, d, J = 7.8 Hz, H-4 and H-5); δ_C (101 MHz, $CDCl_3$): 121.2 (2 × CH, C-2 and C-7), 123.9 (2 × CH, C-4 and C-5), 127.7 (2 × CH, C-3 and C-6), 137.6 (C, C-9), 138.0 (C, C-10), 140.9 (2 × C, C-1 and C-8); m/z (EI^+) 287.8950 ($[M+2H]^+$, $C_{10}H_8{}^{80}Se_2$ requires 287.8956), 286 (100%), 126 (25), 206 (25), 280 (19), 282 (40), 284 (98), 288 (30).

Literature data: [237] Anal. calcd. for $C_{10}H_6Se_2$: C, 42.28; H, 2.12; Se, 55.59. Found: C, 42.26; H, 2.12; Se, 55.46. IR (KBr): 3060, 1901(w), 1748(w), 1595, 1534, 1481, 1413, 1345, 1188, 1142, 1043, 959, 891, 859, and 751 cm^{-1}. UV λ_{max} (cyclohexane) 212 (ε 3.9 × 10^{-4}), 255 (shoulder)(ε 1.1 × 10^{-4}), 262 (ε 1.5 × 10^{-4}), 367 (shoulder) (ε 1.2 × 10^{-4}), and 380 nm (ε 1.6 × 10^{-4}) δ_H (220 MHz, $CDCl_3$) 2 H, dd; 2 H, dd; 2 H, t; extending from 7.20 to 7.51; δ_C 121.12, 123.75, 127.62, 137.50, 137.89, 140.91 ppm relative to Me_4Si.

$[Fe_2(CO)_6(1,8\text{-}Se_2\text{-}C_{10}H_6)]$ (91a)

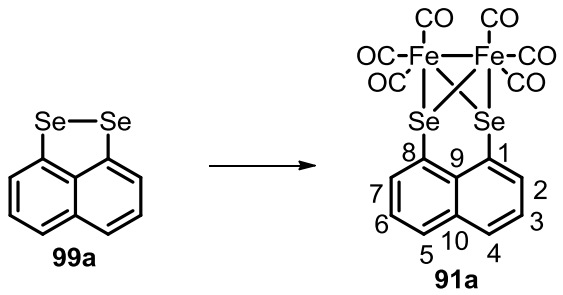

$[Fe_2(CO)_6(1,8\text{-}Se_2\text{-}C_{10}H_6)]$ **91a** is a novel compound, prepared according to a modified literature procedure.[122]

A solution of dichalcogen **99a** (0.08 g, 0.28 mmol) and $Fe_3(CO)_{12}$ (0.14 g, 0.28 mmol) in toluene (7.5 mL) was refluxed for 2.5 hours under argon atmosphere. The mixture was cooled down to room temperature, filtered and concentrated under reduced pressure. The residue was purified by column chromatography (hexane) to afford complex **91a** as a dark red solid (0.15 g, 96%). R_f: 0.47 (hexane); mp: decomp. above 130 °C; λ_{nm} (CH_3CN) 253 (ε = 6.2 × 10^3 $M^{-1}cm^{-1}$), 345 (ε = 5.4 × 10^3 $M^{-1}cm^{-1}$); ν_{max} (solid neat, ATR)/cm^{-1} 2058 (CO), 2016 (CO), 1996 (CO), 1979 (CO), 1822 (CO); δ_H (400 MHz, $CDCl_3$): 7.40 (2 H, t, *J* = 9.0 Hz, H-3 and H-6), 7.99 (2 H, d, *J* = 9.0 Hz, H-2 and H-7), 8.29 (2 H, d, *J* = 9.0 Hz, H-4 and H-5); δ_C (101 MHz, $CDCl_3$): 119.2 (2 × C, C-1 and C-8), 125.4 (2 × CH, C-3 and C-6), 128.9 (C, C-9), 132.9 (2 ×

CH, C-2 and C-7), 134.2 (C, C-10), 134.9 (2 × CH, C-4 and C-5), 208.6 (6 × C, CO); *m*/*z* (EI^+) 565.7173 (M^+, $C_{16}H_6O_6{}^{56}Fe_2{}^{80}Se_2$ requires 565.7193), 564 (100%), 557 (8), 560 (43), 561 (19), 562 (82), 563 (9), 565 (9). Anal. calcd. for $C_{16}H_6O_6Fe_2Se_2$: C, 34.08; H, 1.07; found: C, 34.14; H, 1.01.

2,7-Di-*tert*-butyl-naphtho[1,8-*cd*][1,2]diselenole (**99b**)

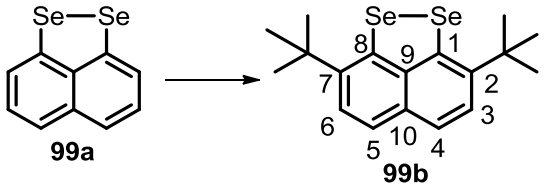

99a **99b**

2,7-Di-*tert*-butyl-naphtho[1,8-*cd*][1,2]diselenole **99b** [126] was prepared according to a literature procedure.[130]

$FeCl_3$ (0.02 g, 0.14 mmol) was added to a solution of *t*BuBr (0.16 mL, 1.40 mmol) and dichalcogen **99a** (0.20 g, 0.70 mmol) in CH_2Cl_2 (5 mL). The mixture was refluxed for 24 hours, then allowed to cool to room temperature, concentrated under reduced pressure and purified by column chromatography (hexane) to give disubstituted dichalcogen **99b** as dark red crystalline solid (0.15 g, 56%). λ_{nm} (CH_3CN) 264 ($\varepsilon = 3.1 \times 10^4$ $M^{-1}cm^{-1}$), 380 ($\varepsilon = 1.5 \times 10^4$ $M^{-1}cm^{-1}$); δ_H (400 MHz, C_6D_6): 1.43 (18 H, s, *t*Bu), 7.29 (2 H, d, J = 8.6 Hz, H-3 and H-6), 7.37 (2 H, d, J = 8.6 Hz, H-4 and H-5); δ_C (101 MHz, C_6D_6): 29.1 (6 × CH_3, *t*Bu), 36.6 (2 × C, *t*Bu), 124.6 (2 × CH, C-3 and C-6), 126.0 (2 × CH, C-4 and C-5), 135.6 (C, C-9), 138.0 (C, C-10), 141.1 (2 × C, C-1 and C-8), 143.7 (2 × C, C-2 and C-7); *m*/*z* (ES^+) 396.0063 (M^+, $C_{18}H_{22}{}^{78}Se^{80}Se$ requires 396.0060), 454 (100%), 394 (26), 396 (63), 398 (68), 450 (34), 452 (91).

Literature data: [126] δ_H (300 MHz, $CDCl_3$) 1.56 (18 H, s), 7.17-7.44 (4 H, m, J = 8.2 Hz); ^{77}Se NMR ($CDCl_3$) δ = 353 (s) ppm; δ_C (75 MHz, $CDCl_3$) 29.2, 36.7, 124.4, 125.8, 134.9, 137.0, 140.4, 144.1; *m/z* (TOF MS CI) 396 [^{78}Se ^{80}Se], 398 [^{80}Se].

[$Fe_2(CO)_6$(1,8-Se_2-2,7-di-*tert*-butyl-$C_{10}H_4$)] (**91b**)

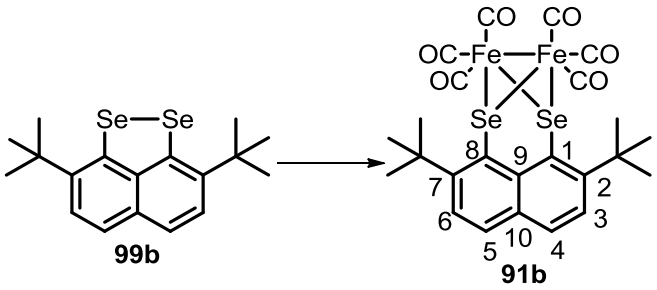

[$Fe_2(CO)_6$(1,8-Se_2-2,7-di-*tert*-butyl-$C_{10}H_4$)] **91b** is a novel compound, prepared according to a modified literature procedure.[122]

A solution of **91b** (0.15 g, 0.39 mmol) and $Fe_3(CO)_{12}$ (0.18 g, 0.39 mmol) in toluene (14 mL) was refluxed for 4 hours under argon atmosphere. The mixture was cooled down to room temperature, filtered and concentrated under reduced pressure. The residue was purified by column chromatography (hexane) to afford complex **91b** as a dark orange solid (0.12 g, 44%). R_f: 0.50 (hexane); mp: decomp. above 150 °C; λ_{nm} (CH_3CN) 265 (ε = 1.7 × 10^4 $M^{-1}cm^{-1}$), 346 (ε = 1.3 × 10^4 $M^{-1}cm^{-1}$); ν_{max} (solid neat, ATR)/cm^{-1} 2057 (CO), 2015 (CO), 1979 (CO), 1970 (CO), 1956 (CO); δ_H (400 MHz, $CDCl_3$): 1.83 (18 H, s, *t*Bu), 7.66 (2 H, d, J = 8.5 Hz, H-3 and H-6), 7.75 (2 H, d, J = 8.5 Hz, H-4 and H-5); δ_C (101 MHz, $CDCl_3$): 33.5 (6 × CH_3, *t*Bu), 39.7 (2 × C, *t*Bu), 118.8 (2 × C, C-1 and C-8), 125.1 (2 × CH, C-3 and C-6), 131.0 (2 × CH, C-4 and C-5), 131.1 (C, C-9), 133.0 (C, C-10), 154.0 (2 × C, C-2 and C-7), 208.8 (6 × C, CO); *m/z* (ES^+) 698.8378 ($[M+Na]^+$, $C_{24}H_{22}O_6Na^{56}Fe_2{}^{78}Se^{80}Se$ requires 698.8351), 702

(100%), 698 (61), 699 (42), 700 (99), 701 (35), 703 (30), 704 (35). Anal. calcd. for $C_{24}H_{22}Fe_2O_8Se_2$: C, 42.64: H, 3.28; found: C, 42.85; H, 3.21.

Naphthalene-1-thiol (**102**)

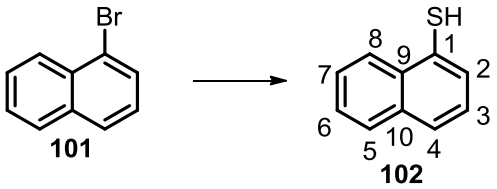

Naphthalene-1-thiol **102** was prepared according to a literature procedure.[131]

A solution of 1-bromonaphthalene **101** (1.00 g, 4.81 mmol) and NaSEt (2.45 g, 29.0 mmol) in dry DMF (24 mL) was refluxed for 22 hours under argon atmosphere. The mixture was cooled down to room temperature and the solvent was removed under reduced pressure. The residue was poured onto HCl (10 mL of a 1.0 M aq. solution) and extracted with Et_2O (3 × 10 mL). The organic layer was washed with H_2O (1 × 10 mL) and brine (1 × 10 mL), dried over $MgSO_4$, evaporated under reduced pressure and the residue purified by column chromatography (9:1, hexane:EtOAc) to give thiol **102** as a colorless crystalline solid (0.70 g, 90%). δ_H (400 MHz, $CDCl_3$): 3.61 (1 H, s), 7.31-7.37 (1 H, m, H-2), 7.48-7.61 (3 H, m, H-3, H-6 and H-7), 7.72 (1 H, d, *J* = 8.2 Hz, H-4), 7.85 (1 H, dd, *J* = 9.0, 3.0 Hz, H-8), 8.17 (1 H, d, *J* = 8.3, H-5); δ_C (100 MHz, $CDCl_3$): 125.3 (CH, C-4), 125.8 (CH, C-6), 126.5 (CH, C-7), 126.6 (CH, C-3), 127.2 (CH, C-5), 128.2 (C, C-1), 128.7 (CH, C-8), 128.9 (CH, C-2), 132.4 (C, C-9), 134.1 (C, C-10); *m/z* (EI^+) 160.0344 (M^+, $C_{10}H_8S$ requires 160.0347) 160 (100%), 115 (33), 128 (36), 159 (10), 161 (11), 162 (5).

Literature data: [131] m.p. 79-80 °C; δ_H = 3.50 (s, 1 H); 7.00-7.70 (m, 7 H).

Naphtho[1,8-*cd*][1,2]thiaselenole (**103a**)

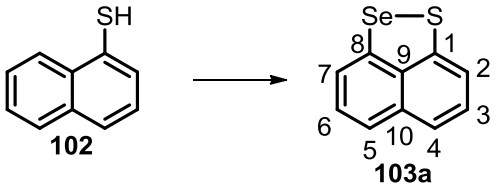

Naphtho[1,8-*cd*][1,2]thiaselenole **103a** was prepared according to a literature procedure.[132] *n*BuLi (17.0 ml of a 1.90 M solution in hexane, 33.0 mmol) was added dropwise over 20 minutes to a solution of thiol **102** (1.74 g, 11.0 mmol) and TMEDA (110 mL) in hexane (100 mL) at 0 °C. The reaction mixture was stirred for 8 hours at room temperature under argon atmosphere and Se (0.87 g, 11.0 mmol) was then added in one portion. The mixture was stirred for additional 16 hours at room temperature and under argon atmosphere. HCl (100 mL of a 1.0 M aq. solution) in ice H_2O was added and the two layers were separated. The aqueous layer was extracted with CH_2Cl_2 (3 × 50 ml). The combined organic layers were washed with water (50 mL) and brine (50 mL), dried over $MgSO_4$, filtered and the solvent was removed under reduced pressure. Purification by column chromatography (hexane) yielded dichalcogen **103a** as a dark red solid (1.01 g, 39%). λ_{nm} (CH_3CN) 255 ($\varepsilon = 1.9 \times 10^4$ $M^{-1}cm^{-1}$), 370 ($\varepsilon = 1.2 \times 10^4$ $M^{-1}cm^{-1}$); δ_H (400 MHz, $CDCl_3$): 7.15 (1 H, dd, J = 7.6, 1.1 Hz, H-2), 7.20 (1 H, t, J = 7.6 Hz, H-3), 7.24 (2 H, m, H-6 and H-7), 7.32 (1 H, dd, J = 7.6, 1.1 Hz, H-4), 7.42 (1 H, m, H-5); δ_C (101 MHz, $CDCl_3$): 118.4 (CH, C-2), 119.6 (CH, C-7), 122.4 (CH, C-4), 123.5 (CH, C-5), 127.7 (CH, C-3), 127.9 (CH, C-6), 134.2 (C, C-9), 136.3 (C-10), 136.9 (C, C-8), 140.7 (C, C-1); *m/z* (EI^+) 231.9413 (M^+, $C_{10}H_6S^{78}Se$ requires 231.9415) 237.9 (100%), 158 (23), 233.9 (13), 235.9 (35), 239.9 (21).

Literature data: [132] Anal. calcd. for $C_{10}H_6SSe$: C, 50.64; H. 2.55; S. 13.52; Se. 33.30; found: C, 50.58; H, 2.53; S, 13.55; Se, 33.64; IR (KBr cm^{-1}): 3007, 1900, 1739, 1594, 1533, 1478,

1407, 1342, 1188, 1135, 1033, 955, 945, 863, 778, 736; 'H NMR spectrum ($CDCl_3$): m, extending from δ 7.1 to 7.6. Mass spectrum m/e (rel. intensity): 238 (100 %, M^+), 158 (11), 126 (4), 114 (4), 113 (3).

$[Fe_2(CO)_6(1,8\text{-}SeS\text{-}C_{10}H_6)]$ (92a)

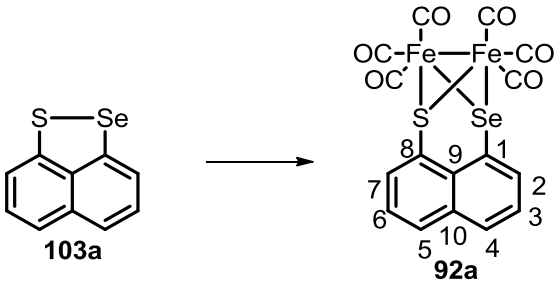

$[Fe_2(CO)_6(1,8\text{-}SeS\text{-}C_{10}H_6)]$ **92a** is a novel compound, prepared according to a modified literature procedure.[122]

A solution of dichalcogen **103a** (0.20 g, 0.84 mmol) and $Fe_3(CO)_{12}$ (0.43 g, 0.84 mmol) in toluene (22 mL) was refluxed for 4 hours under argon atmosphere. The mixture was cooled down to room temperature, filtered and concentrated under reduced pressure. The residue was purified by column chromatography (hexane) to afford complex **92a** as a red crystalline solid (0.14 g, 32%). R_f: 0.56 (hexane); mp: decomp. above 120 °C; λ_{nm} (CH_3CN) 253 ($\varepsilon = 1.1 \times 10^4$ $M^{-1}cm^{-1}$), 348 ($\varepsilon = 8.5 \times 10^3$ $M^{-1}cm^{-1}$); ν_{max} (solid neat, ATR)/cm^{-1} 2061 (CO), 2020 (CO), 1999 (CO), 1982 (CO), 1958 (CO), 1822 (CO); δ_H (400 MHz, $CDCl_3$): 7.37-7.44 (2 H, m, H-3 and H-2), 7.98-8.02 (2 H, m, H-6 and H-7), 8.23 (1 H, d, J = 6.9 Hz, H-4), 8.32 (1 H, d, J = 6.9 Hz, H-5); δ_C (101 MHz, $CDCl_3$): 117.0 (C, C-8), 125.3 (CH, C-6), 125.4 (CH, C-3), 126.7 (C, C-1), 132.4 (CH, C-4 and C-5), 133.6 (CH, C-2), 134.1 (CH, C-7), 134.2 (C, C-9 and C-10), 208.2 (6 × C, CO); *m/z* (EI^+) 517.7740 (M^+, $C_{16}H_6O_6S^{56}Fe_2{}^{80}Se$ requires 517.7749) 349 (100%, $[M - 6\ CO]^+$), 377 (14, $[M - 5\ CO]^+$), 405 (12, $[M - 4\ CO]^+$), 433 (7, $[M - 3\ CO]^+$),

461 (14, [M – 2 CO]$^+$), 517 (11, M$^+$). Anal. calcd. for $C_{16}H_6O_6SSeFe_2$: C, 37.18; H, 1.17; found: C, 37.45; H, 1.30.

2,7-Di-*tert*-butylnaphtho[1,8-cd][1,2]thiaselenole (**103b**)

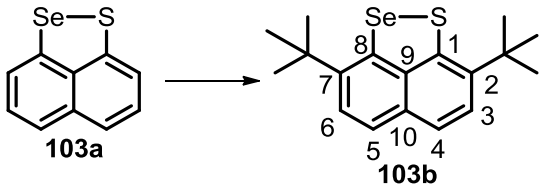

2,7-Di-*tert*-butylnaphtho[1,8-cd][1,2]thiaselenole **103b** is a novel compound, prepared according to the literature procedure.[130]

$FeCl_3$ (0.04 g, 0.25 mmol) was added in one portion to a solution of *t*BuBr (0.29 mL, 2.53 mmol) and dichalcogen **103a** (0.30 g, 1.27 mmol) in CH_2Cl_2 (3.0 mL). The mixture was refluxed for 16 hours, then allowed to cool down to room temperature, concentrated under reduced pressure and the residue purified by column chromatography (hexane) to give disubstituted dichalcogen **103b** as a dark orange crystalline solid (0.25 g, 56%). R_f: 0.59 (hexane); mp: 118-119 °C; λ_{nm} (CH_3CN) 259 ($\varepsilon = 9.8 \times 10^3$ $M^{-1}cm^{-1}$), 376 ($\varepsilon = 4 \times 10^3$ $M^{-1}cm^{-1}$); ν_{max} (solid neat, ATR)/cm^{-1}: 2292, 2253, 2056, 2016, 1979, 1443, 1375, 1038, 918, 833, 754; δ_H (400 MHz, $CDCl_3$): 1.37 (6 H, s, *t*Bu), 1.39 (3 H, s, *t*Bu), 1.44 (6 H, s, *t*Bu), 1.46 (3 H, s, *t*Bu), 7.24-7.36 (4 H, m, Ar*H*); δ_C (101 MHz, $CDCl_3$): 28.9 (3 × CH_3, *t*Bu), 31.4 (3 × CH_3, *t*Bu), 36.1 (C, *t*Bu), 36.3 (C, *t*Bu), 122.7 (CH, C-3), 124.0 (CH, C-6), 125.7 (CH, C-4), 125.8 (CH, C-5), 134.1 (2 × C, C-9 and C-10), 138.8 (C, C-8), 140.1 (C, C-1), 141.8 (C, C-2), 142.4 (C, C-7); *m/z* (EI$^+$) 350.0607 (M$^+$, $C_{18}H_{22}S^{80}Se$ requires 350.0607), 335 (100%), 331 (17), 333 (53), 350 (76), 352 (17), 353 (16).

[$Fe_2(CO)_6$(1,8-SeS-2,7-di-*tert*-butyl-$C_{10}H_4$)] (**92b**)

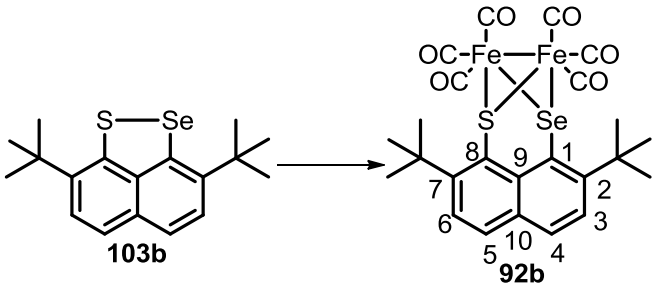

[$Fe_2(CO)_6$(1,8-SeS-2,7-di-*tert*-butyl-$C_{10}H_4$)] **92b** is a novel compound, prepared according to a modified literature procedure.[122]

A solution of **103b** (0.36 g, 1.02 mmol) and $Fe_3(CO)_{12}$ (0.51 g, 1.02 mmol) in toluene (27 mL) was refluxed for 4 hours under argon atmosphere. The mixture was cooled down to room temperature, filtered and concentrated under reduced pressure. The residue was purified by column chromatography (hexane) to afford complex **92b** as a red crystalline solid (0.31 g, 47%). R_f: 0.69 (hexane); mp: 122-124 °C; λ_{nm} (CH_3CN) 351 ($\varepsilon = 4.3 \times 10^3$ $M^{-1}cm^{-1}$), 309 ($\varepsilon = 3.7 \times 10^3$ $M^{-1}cm^{-1}$), 263 ($\varepsilon = 6.1 \times 10^3$ $M^{-1}cm^{-1}$); ν_{max} (solid neat, ATR)/cm^{-1} 2061 (CO), 2017 (CO), 1980 (CO), 1972 (CO), 1961 (CO), 1940 (CO); δ_H (400 MHz, $CDCl_3$): 1.78 (9 H, s, *t*Bu), 1.81 (9 H, s, *t*Bu), 7.66 (2H, d, J = 8.0 Hz, H-3 and H-6), 7.80 (2 H, d, J = 8.0 Hz, H-4 and H-5); δ_C (101 MHz, $CDCl_3$): 32.7 (3 × CH_3, *t*Bu), 33.4 (3 × CH_3, *t*Bu), 39.1 (C, *t*Bu), 39.6 (C, *t*Bu), 116.6 (C, C-8), 125.0 (CH, C-6), 125.2 (CH, C-3), 125.4 (C, C-1), 131.0 (CH, C-5), 131.2 (C, C-4), 131.4 (C, C-9), 131.5 (C, C-10), 153.7 (C, C-7), 154.9 (C, C-2), 208.5 (6 × C, CO); *m/z* (EI^+) 629.9018 (M^+, $C_{24}H_{22}O_6S^{56}Fe_2{}^{80}Se$ requires 629.9001), 490 (100%, [M – 5 CO]$^+$), 518 (38, [M – 4 CO]$^+$), 546 (33, [M – 3 CO]$^+$), 574 (29, [M – 2 CO]$^+$), 630 (31, M^+). Anal. calcd. for $C_{24}H_{22}O_6SSeFe_2$: C, 45.82; H, 3.52; found: C, 45.51; H, 3.42.

2,4,5,7-Tetrachloronaphtho[1,8-cd][1,2]diselenole (**99c**)

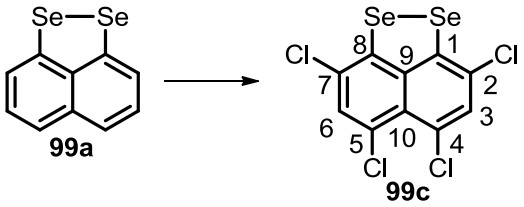

2,4,5,7-Tetrachloronaphtho[1,8-cd][1,2]diselenole **99c** is a novel compound, prepared according to a literature procedure.[122]

N-Chlorosuccinimide (0.56 g, 4.22 mmol) was added to a solution of dichalcogen **99a** (0.20 g, 0.70 mmol) in CH_2Cl_2 (9.5 mL) at room temperature. The reaction mixture was stirred for 16 hours under argon atmosphere, then was dry loaded onto silica (2.00 g) and purified by a flash column chromatography (hexane) to afford chloro-substituted **99c** (0.06 g, 21%) as a golden yellow solid. R_f: 0.79 (hexane); mp: 224-225 °C; ν_{max} (solid neat, ATR)/cm^{-1}: 3066, 2923, 2852, 1735, 1549, 1532, 1468, 1382, 1336, 1273, 1255, 1134, 1017, 982, 896, 869, 862, 740685, 661; δ_H (400 MHz, DMSO-d_6, 50 °C): 7.75 (2 H, s); δ_C (101 MHz, DMSO-d_6, 50 °C): 122.1 (2 × C, C-2 and C-7), 125.6 (2 × C, C-4 and C-5), 127.0 (C, C-9), 128.7 (C, C-10), 130.7 (2 × CH, C-3 and C-6), 141.6 (2 × C, C-1 and C-8); *m*/*z* (EI^+) 421.7231 (M^+, $C_{10}H_2{}^{35}Cl_3{}^{37}Cl^{80}Se_2$ requires 421.7241), 389 (100%), 321 (42), 353 (43), 393 (36), 423 (95), 427 (39).

2,7-Dimethoxynaphthalene (**105**)

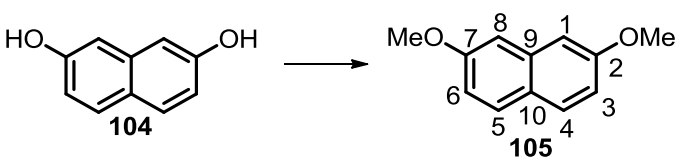

2,7-Dimethoxynaphthalene **105** [238] was prepared according to a modified literature procedure.[133a)]

Me_2SO_4 (7.50 mL, 78.8 mmol) was added dropwise over 5 minutes to a well stirred solution of 2,7-dihydroxynaphthalene **104** (5.00 g, 37.5 mmol) in NaOH (34 mL of a 10% aq. solution) at 0 °C. After stirring the mixture for 2 hours, H_2O (72 mL) was added and a grey precipitate was formed. The precipitate was filtered and washed with H_2O (3 × 60 mL) to give **105** (4.20 g, 60%) as bright grey solid. δ_H (400 MHz, $CDCl_3$): 3.91 (6 H, s, OCH_3), 6.98 (2 H, dd, *J* = 9.0, 3.0 Hz, H-3 and H-6), 7.07 (2 H, d, *J* = 3.0 Hz, H-1 and H-8), 7.66 (2 H, d, *J* = 9.0 Hz, H-4 and H-5); δ_C (101 MHz, $CDCl_3$): 55.4 (2 × CH_3, OCH_3), 105.4 (2 × CH, C-3 and C-6), 116.2 (2 × CH, C-1 and C-8), 124.4 (C, C-9), 129.3 (2 × CH, C-4 and C-5), 136.0 (C, C-10), 158.3 (2 × C, C-2 and C-7); *m/z* (EI^+) 188.0833 (M^+, $C_{12}H_{12}O_2$ requires 188.0837), 188 (100%), 189 (12), 145 (50).

Literature data: [133b)] mp 139 °C; IR ν_{max} (Nujol)/cm^{-1} 1627, 1228; ^{1}H-NMR (500 MHz, $CDCl_3$) δ_H 7.65 (2H, d, J 9, $H_{4,5}$), 7.06 (2H, s, $H_{1,8}$), 6.99 (2H, d, J 8.8, $H_{3,6}$), 3.91 (6H, s, –OCH_3); ^{13}C-NMR (67.8 MHz, $CDCl_3$) δ_C 158.4 (C_2, C_7), 135.6 (C_9), 129.3 (C_4, C_5), 124.5 (C_{10}), 116.2 (C_3, C_6), 105.4 (C_1, C_8), 55.4 (–OCH_3); MS (CI) m/z 189 ($[M + H]^+$, 100%).

1,8-Dibromo-2,7-dimethoxynaphthalene (**106**)

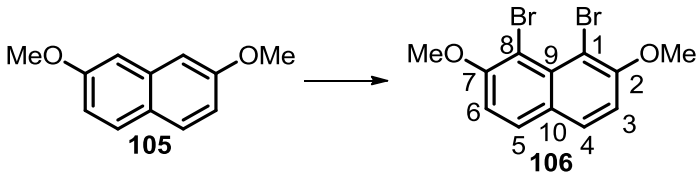

1,8-Dibromo-2,7-dimethoxynaphthalene **106** was prepared according to a literature procedure.[134]

A solution of *N*-bromosuccinimide (7.10 g, 40.0 mmol) in $CHCl_3$ (98 mL) was treated with pyridine (3.20 mL, 40.0 mmol) and refluxed for 1 hour affording an orange mixture. A

solution of **105** (1.90 g, 10.0 mmol) in $CHCl_3$ (52 mL) was added dropwise over 10 minutes and the mixture was then refluxed for additional 9 hours. It was then cooled down to room temperature, the solvent evaporated under reduced pressure and the residue purified by column chromatography (8:2, hexane:EtOAc) to give dibromo-substituted **106** (3.20 g, 92%) as a pale yellow solid. δ_H (400 MHz, $CDCl_3$): 4.02 (6 H, s, OCH_3), 7.16 (2 H, d, J = 9.0 Hz, H-3 and H-6), 7.74 (2 H, d, J = 9.0 Hz, H-4 and H-5); δ_C (101 MHz, $CDCl_3$): 57.4 (2 × CH_3, OCH_3), 106.2 (2 × C, C-1 and C-8), 111.9 (2 × CH, C-3 and C-6), 127.6 (C, C-9), 130.2 (2 × CH, C-4 and C-5), 131.8 (C, C-10), 156.6 (2 × C, C-2 and C-7); *m/z* (EI^+) 343.9059 (M^+, $C_{12}H_{10}O_2{}^{79}Br_2$ requires 343.9048) 346 (100%) 344 (59) 348 (52), 303 (49), 259 (22), 237 (29), 113 (36), 86 (42), 49 (56).

Literature data: [134] R_f 0.14 (9:1 hexane:EtOAc); mp 129-130 °C; ν_{max} (KBr)/cm^{-1} 3008, 2937, 2936, 2838, 1611, 1503, 1459, 1328, 1263, 1163 and 1056; δ_H (300 MHz; $CDCl_3$) 4.02 (6 H, s), 7.16 (2 H, d, J = 9.0 Hz) and 7.75 (2 H, d, J = 9.0 Hz); δ_C (75 MHz, $CDCl_3$) 57.1, 105.8, 111.5, 127.3, 130.0, 131.5, 156.3; *m/z* (EI^+) 343.9039 (M^+, $C_{12}H_{10}Br_2O_2$ requires 343.9048), 348 (M^+, 51%), 346 (100%), 344 (36), 288 (8), 250 (8), 235 (15), 222 (5), 179 (7), 158 (15), 113 (11), 100 (7), 74 (6).

2,7-Dimethoxynaphtho[1,8-*cd*][1,2]dithiole (**100d**)

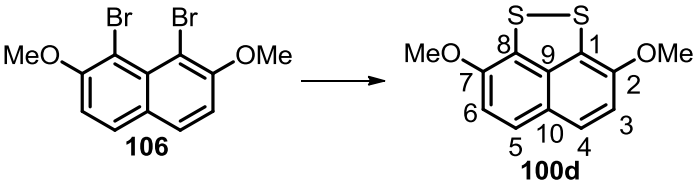

2,7-Dimethoxynaphtho[1,8-*cd*][1,2]dithiole **100d** was prepared according to the literature procedure.[134]

*n*BuLi (1.95 mL of a 2.13 M solution in hexane, 4.16 mmol) was added dropwise over a period of 5 minutes to a solution of **106** (0.72 g, 2.08 mmol) in Et_2O (5.0 mL) at room temperature under argon atmosphere. The mixture was stirred for 45 minutes, recrystallized S_8 (0.13 g, 4.16 mmol) was added in one portion and the stirring was kept for additional 2 hours. HCl (3 mL of a 1.0 M aq. solution) and H_2O (2 mL) were added and the two layers were separated. The aqueous layer was extracted with Et_2O (3 × 10 mL), the combined organic layers were washed with brine (2 × 10 mL), dried over $MgSO_4$ and concentrated under pressure. The residue was purified by column chromatography (9:1, hexane:EtOAc) to give dichalcogen **100d** as a red crystalline solid (0.321 g, 62 %). λ_{nm} (CH_3CN) 259 ($\varepsilon = 5.6 \times 10^4$ $M^{-1}cm^{-1}$), 364 ($\varepsilon = 1.1 \times 10^4$ $M^{-1}cm^{-1}$), 380 ($\varepsilon = 1.0 \times 10^4$ $M^{-1}cm^{-1}$); δ_H (400 MHz, $CDCl_3$): 3.94 (6 H, s, OCH_3), 6.98 (2 H, d, J = 8.8 Hz, H-3 and H-6), 7.37 (2 H, d, J = 8.8 Hz, H-4 and H-5); δ_C (101 MHz, $CDCl_3$): 56.5 (2 × CH_3, OCH_3), 112.6 (2 × CH, C-3 and C-6), 123.6 (2 × CH, C-4 and C-5), 126.2 (3 × C, C-1, C-8 and C-9), 137.6 (C, C-10), 150.0 (2 × C, C-2 and C-7); *m/z* (EI^+) 250.0120 (M^+, $C_{12}H_{10}O_2S_2$ requires 250.0122), 235 (100%), 220 (52), 250 (75).

Literature data: [134] R_f 0.29 (9:1 hexane: EtOAc); mp 119-120 °C (ethanol); ν_{max} (KBr)/cm^{-1} 2937, 2834 (OCH_3), 1615, 1505, 1427, 1265 and 1061; δ_H (300 MHz; $CDCl_3$) 3.95 (6 H, s), 7.00 (2 H, d, J = 8.8 Hz) and 7.39 (2 H, d, J = 8.8 Hz); δ_C (75 MHz; $CDCl_3$) 56.4, 112.6, 123.4, 126.1, 126.2, 137.5, 150.0; *m/z* (EI^+) 250.0127 (M^+, $C_{12}H_{10}O_2S_2$ requires 250.0122), 235 (100%), 220 (40), 192 (9), 164 (10), 137 (4), 125 (6), 95 (3), 81 (12), 69 (25), 57 (7), 43 (7).

$[Fe_2(CO)_6(1,8\text{-}S_2\text{-}2,7\text{-}OMe\text{-}C_{10}H_4)]$ (89d)

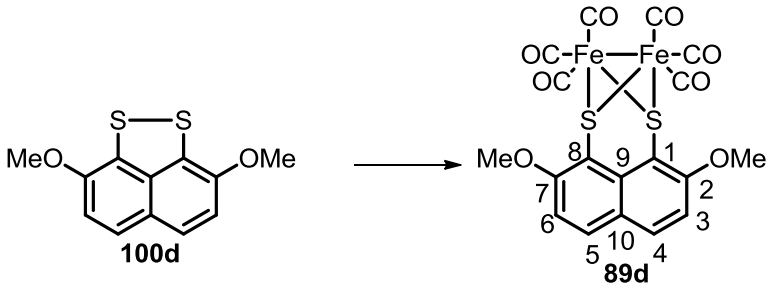

$[Fe_2(CO)_6(1,8\text{-}S_2\text{-}2,7\text{-}OMe\text{-}C_{10}H_4)]$ **89d** is a novel compound, prepared according to a modified literature procedure.[122]

A solution of dichalcogen **100d** (0.20 g, 0.80 mmol) and $Fe_3(CO)_{12}$ (0.40 g, 0.80 mmol) in toluene (17 mL) was refluxed for 4 hours . The mixture was cooled downto room temperature, filtered and concentrated under reduced pressure. The residue was purified by column chromatography (9:1, hexane:EtOAc) to give complex **89d** as a bright red crystalline solid (0.37 g, 69%). R_f: 0.13 (9:1, hexane:EtOAc); mp: decomp. above 160 °C; λ_{nm} (CH_3CN) 361 ($\varepsilon = 5.7 \times 10^3$ $M^{-1}cm^{-1}$), 327 ($\varepsilon = 6.1 \times 10^3$ $M^{-1}cm^{-1}$), 240 ($\varepsilon = 8.8 \times 10^3$ $M^{-1}cm^{-1}$); ν_{max} (solid neat, ATR)/cm^{-1} 2061 (CO), 2021 (CO), 1976 (CO), 1955 (CO), 1878 (CO); δ_H (400 MHz, $CDCl_3$): 4.10 (6 H, s, OCH_3), 7.15 (2 H, d, J = 9.0 Hz, H-3 and H-6), 7.90 (2 H, d, J = 9.0 Hz, H-4 and H-5); δ_C (101 MHz, $CDCl_3$): 57.2 (2 × CH_3, OCH_3), 108.7 (2 × C, C-1 and C-8), 110.3 (2 × CH, C-3 and C-6), 124.5 (C, C-9), 129.9 (C, C-10), 132.9 (2 × CH, C-4 and C-5), 160.0 (2 × C, C-2 and C-7), 208.2 (6 × C, CO); *m/z* (EI^+) 525.8586 ($[M + Na]^+$, $C_{18}H_{10}O_8S_2{}^{56}Fe_2Na$ requires 525.8609) 390 (100%, $[M - 4\ CO]^+$), 418 (52, $[M - 3\ CO]^+$), 446 (41, $[M - 2\ CO]^+$), 474 (34, $[M - CO]^+$), 502 (50, M^+), 530 (20). Anal. calcd. for $C_{18}H_{10}O_8S_2Fe_2$: C, 40.78; H, 1.90; found: C, 40.56; H, 1.88.

2,7-Dimethoxynaphtho[1,8-*cd*][1,2]diselenole (**99d**)

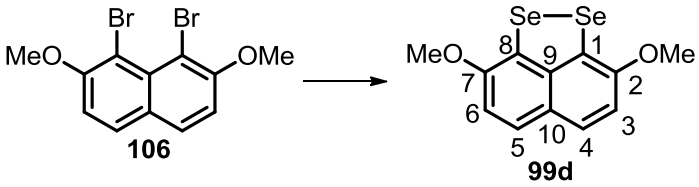

2,7-Dimethoxynaphtho[1,8-*cd*][1,2]diselenole **99d** was prepared according to a literature procedure.[135]

*n*BuLi (2.70 mL of a 2.13 M solution in hexane, 5.80 mmol) was added dropwise over 10 minutes to a solution of **106** (0.72 g, 2.08 mmol) in THF (10 mL) at−78 °C under argon atmosphere. The mixture was warmed to room temperature and stirred for an additional 1.5 hour. The mixture was cooled to 0 °C, Se (0.46 g, 5.80 mmol) was added in one portion and the mixture was stirred for additional 3 hours. NH_4Cl (5 mL of a saturated aq. solution) was added and air was rapidly bubbled through the mixture for 30 minutes. The two layers were separated and the aqueous layer was extracted with Et_2O (3 × 10 mL). The combined organic layers were washed with brine (2 × 10 mL), dried over $MgSO_4$, concentrated under reduced pressure and purified by column chromatography (8:2, hexane:EtOAc) to give dichalcogen **99d** as a purple solid (0.35 g, 49%). λ_{nm} (CH_3CN) 259 ($\varepsilon = 5.7 \times 10^4$ $M^{-1}cm^{-1}$), 364 ($\varepsilon = 1.1 \times 10^4$ $M^{-1}cm^{-1}$), 379 ($\varepsilon = 1.1 \times 10^4$ $M^{-1}cm^{-1}$); δ_H (400 MHz, $CDCl_3$): 3.97 (6 H, s, OCH_3), 6.98 (2 H, d, J = 9.0 Hz, H-3 and H-6), 7.56 (2 H, d, J = 9.0 Hz, H-4 and H-5); δ_C (101 MHz, $CDCl_3$) 56.6 (2 × CH_3, OCH_3), 111.9 (2 × CH, C-3 and C-6), 122.9 (C, C-9), 125.8 (2 × CH, C-4 and C-5), 128.0 (C, C-10), 140.1 (2 × C, C-1 and C-8), 153.3 (2 × C, C-2 and C-7); *m/z* (ES^+) 345.9011 (M^+, $C_{12}H_{10}O_2{}^{80}Se_2$ requires 345.9011) 346 (100%), 344 (94), 342 (36), 348 (10).

Literature data: [135] mp 155-156 ºC (from ethyl acetate); IR (KBr) 1490, 1262, 1057, 810 cm^{-1}; δ_H (300 MHz; $CDCl_3$) 3.97 (6 H, s), 6.97 (2 H, d, J = 8.8 Hz), 7.55 (2 H, d, J = 8.8 Hz); δ_C (75 MHz, $CDCl_3$) 56.6, 111.9, 123.0, 125.8, 128.1, 140.1, 153.3; *m/z* (EI) 346 (100, M^+), 331 (90), 316 (35); exact mass calcd. for $C_{12}H_{10}O_2{}^{80}Se_2$: 345.9011, found 345.9000.

$[Fe_2(CO)_6(1,8\text{-}Se_2\text{-}2,7\text{-}OMe\text{-}C_{10}H_4)]$ (91d)

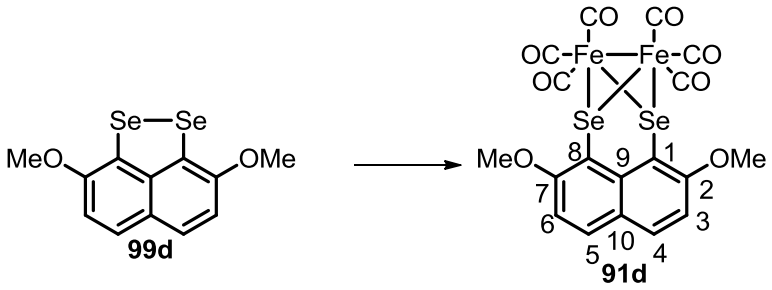

$[Fe_2(CO)_6(1,8\text{-}Se_2\text{-}2,7\text{-}OMe\text{-}C_{10}H_4)]$ **91d** is a novel compound, prepared according to a modified literature procedure.[122]

A solution of dichalcogen **99d** (0.35 g, 1.01 mmol) and $Fe_3(CO)_{12}$ (0.51 g, 1.01 mmol) in toluene (28 mL) was refluxed for 4 hours under argon atmosphere. The mixture was cooled down to room temperature, filtered and concentrated under reduced pressure. The residue was purified by column chromatography (8:2, hexane:EtOAc) to afford complex **91d** as a red crystalline solid (0.30 g, 47%). R_f: 0.13 (8:2, hexane:EtOAc); mp: decomp. above 140 °C; λ_{nm} (CH_3CN) 358 ($\varepsilon = 3.1 \times 10^3\ M^{-1}cm^{-1}$), 336 ($\varepsilon = 3.7 \times 10^3\ M^{-1}cm^{-1}$) 240 ($\varepsilon = 8.8 \times 10^3\ M^{-1}cm^{-1}$); ν_{max} (solid neat, ATR)/cm^{-1} 2054 (CO), 2014 (CO), 1970 (CO), 1950 (CO), 1875 (CO); δ_H (400 MHz, $CDCl_3$): 4.08 (6 H, s, OCH_3), 7.13 (2 H, d, J = 6.0 Hz, H-3 and H-6), 7.85 (2 H, d, J = 6.0 Hz, H-4 and H-5); δ_C (101 MHz, $CDCl_3$): 57.3 (2 × CH_3, OCH_3), 103.6 (2 × C, C-1 and C-8), 110.1 (2 × CH, C-3 and C-6), 124.7 (C, C-9), 131.8 (C, C-10), 133.4 (2 × CH, C-4 and C-5), 160.0 (2 × C, C-2 and C-7), 209.0 (6 × C, CO). Anal. calcd. for $C_{18}H_{10}O_8Fe_2Se_2$: C, 34.65; H, 1.62; found: C, 35.15; H, 1.73.

1-Bromo-2,7-dimethoxynaphthalene (**107**)

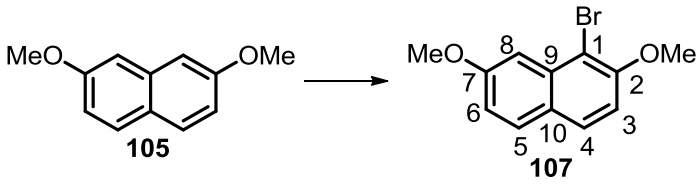

1-Bromo-2,7-dimethoxynaphthalene **107** is a novel compound, prepared according to a modified literature procedure.[134]

A solution of *N*-bromosuccinimide (2.10 g, 11.7 mmol) in $CHCl_3$ (25 mL) was treated with pyridine (0.96 mL, 11.7 mmol) and refluxed for 1 hour. The orange mixture was added dropwise over 20 minutes to a refluxing solution of **105** (2.00 g, 10.6 mmol) in $CHCl_3$ (75 mL). The reaction was then refluxed for additional 9 hours under argon atmosphere. The mixture was cooled down to room temperature, concentrated under reduced pressure and purified by column chromatography (8:2, hexane:EtOAc) to give **107** (2.6 g, 92%) as a pale pink solid. R_f: 0.62 (8:2, hexane:EtOAc); mp: 61-62 °C; ν_{max} (solid neat, ATR)/cm^{-1}: 3011, 2966, 2937, 2839, 1625, 1606, 1509, 1455, 1414, 1383, 1356, 1152, 1137, 1070, 1025, 864, 833, 774; δ_H (400 MHz, $CDCl_3$): 3.97 (3 H, s, OCH_3), 4.02 (3 H, s, OCH_3), 7.04 (1 H, dd, *J* = 8.9, 2.5 Hz, H-6), 7.12 (1 H, d, *J* = 8.9 Hz, H-3), 7.50 (1 H, d, *J* = 2.5 Hz, H-8), 7.67 (1 H, d, *J* = 8.9 Hz, H-5), 7.73 (1 H, d, *J* = 8.9 Hz, H-4); δ_C (101 MHz, $CDCl_3$): 55.4 (CH_3, OCH_3), 57.2 (CH_3, OCH_3), 104.5 (CH, C-8), 106.3 (C, C-1), 111.1 (CH, C-3), 112.1 (CH, C-6), 120.3 (C, C-9), 128.1 (CH, C-5), 130.2 (CH, C-4), 133.8 (C, C-10), 155.3 (C, C-7) 157.0 (C, C-2); *m/z* (EI^+) 265.9944 (M^+, $C_{12}H_{11}O_2{}^{79}Br$ requires 265.9942) 266 (100%) 223 (50) 225 (48), 226 (5), 268 (97), 269 (12).

2,7-Dimethoxynaphthalen-1-yl dimethylcarbamodithioate (**109**)

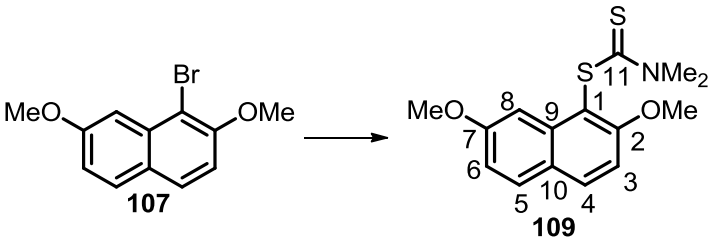

2,7-Dimethoxynaphthalen-1-yl dimethylcarbamodithioate **109** is a novel compound, prepared according to a modified literature procedure.[137]

*n*BuLi (2.70 mL of a 1.70 M solution in hexane, 4.50 mmol) was added dropwise over a period of 10 minutes to a solution of **107** (0.60 g, 2.25 mmol) in THF (11 mL) at −78 °C under argon atmosphere. The reaction mixture was then allowed to warm at room temperature and the stirring was kept for an additional 1 hour. The mixture was cooled down to −78 °C and bis(*N*,*N*-dimethylthiocarbamoyl)-disulfide (0.81 g, 3.37 mmol) was added, the temperature was then raised to 25 °C and the stirring kept for additional 3 hours. NH_4Cl (5 mL of a saturated aq. solution) was added, the two layers were separated and the aqueous layer was extracted with Et_2O (3 × 10 mL). The combined organic layers were washed with brine (2 × 10 mL), dried over $MgSO_4$, concentrated under reduced pressure and purified by column chromatography (8:2 to 6:4, hexane:EtOAc) to give dithiocarbamate **109** as pale yellow solid (0.58 g, 83%). R_f: 0.42 (8:2, hexane:EtOAc); mp: 108-109 °C; ν_{max} (solid neat, ATR)/cm^{-1}: 2066, 2031, 1991, 1627, 1510, 1464, 1378, 1265, 1222, 1156, 1072, 976, 896, 831, 743, 706; δ_H (400 MHz, $CDCl_3$): 3.57 (3 H, s, OCH_3), 3.64 (3 H, s, OCH_3), 3.92 (3 H, s, NCH_3), 3.99 (3 H, s, NCH_3), 7.03 (1 H, dd, *J* = 8.9, 2.4 Hz, H-6), 7.21 (1 H, d, *J* = 9.0 Hz, H-3), 7.54 (1 H, d, *J* = 2.4 Hz, H-8), 7.71 (1 H, d, *J* = 8.9 Hz, H-5), 7.93 (1 H, d, *J* = 9.0 Hz, H-4); δ_C (101 MHz, $CDCl_3$) 42.3 (CH_3, NCH_3), 45.8 (CH_3, NCH_3), 55.4 (CH_3, OCH_3), 57.1 (CH_3, OCH_3), 103.6 (CH, C-8), 110.9 (CH, C-3), 112.2 (C, C-1), 116.5 (CH, C-7), 124.9 (C,

C-9), 130.2 (CH, C-5), 132.9 (CH, C-4), 138.2 (C, C-10), 159.4 (C, C-7) 160.2 (C, C-2), 196.0 (C, C-11); *m/z* (ES^+) 330.0598 ($[M+Na]^+$, $C_{15}H_{17}NO_2S_2Na$ requires 330.0593) 330 (100%) 301 (13) 331 (17), 332 (9).

2,7-Dimethoxynaphthalene-1-thiol (**108**)

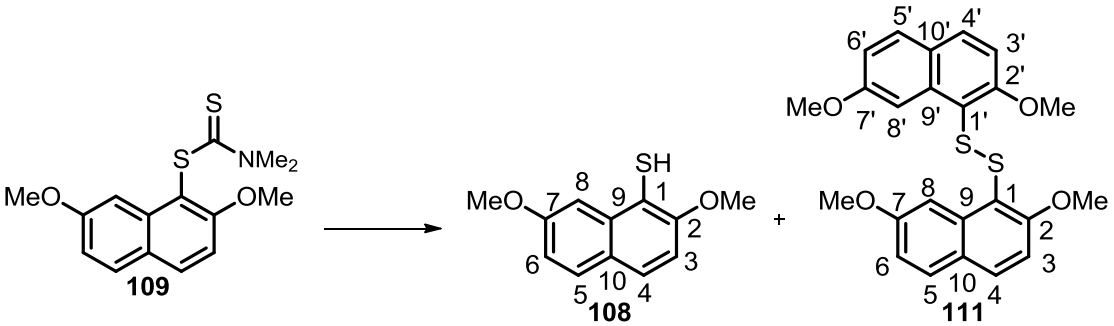

2,7-Dimethoxynaphthalene-1-thiol **108** is a novel compound, prepared according to a modified literature procedure.[141]

A solution of dithiocarbamate **109** (0.15 g, 0.49 mmol) and $NH_2NH_2{\cdot}H_2O$ (0.47 mL) in EtOH (2.0 mL) was refluxed for 4 hours under argon atmosphere. The reaction mixture was diluted with EtOAc (2 mL) and acidified with HCl (1 mL of a 1.0 M aq. solution). The two layers were separated and the aqueous layer was extracted with EtOAc (3 × 2 mL). The combined organic layers were washed with brine (2 × 5 mL), dried over $MgSO_4$, concentrated under reduced pressure and purified by column chromatography (8:2, hexane:EtOAc) to give thiol **108** as bright yellow oil (0.034 g, 32%) and disulfide **111** oil (0.013 g, 6%). R_f: 0.69 (8:2, hexane:EtOAc); ν_{max} (solid neat, ATR)/cm^{-1}: 3401, 1616, 1597, 1571, 1511, 1462, 1424, 1375, 1362, 1277, 1220, 1031, 1005, 984, 828, 800, 761, 731, 694; δ_H (400 MHz, $CDCl_3$): 3.46 (3 H, s, OCH_3), 3.57 (3 H, s, OCH_3), 6.91 (1 H, dd, *J* = 8.9, 2.4 Hz, H-6), 6.95 (1 H, d, *J* = 8.9 Hz, H-3), 7.51 (1 H, d, *J* = 2.4 Hz, H-8), 7.60 (1 H, d, *J* = 8.9 Hz, H-5), 7.73 (1 H, d, *J* = 8.9 Hz, H-4); δ_C (101 MHz, $CDCl_3$): 54.9 (CH_3, OCH_3), 56.3 (CH_3, OCH_3), 103.8 (CH, C-8),

110.2 (CH, C-6), 117.0 (CH, C-3), 117.8 (C, C-1), 124.7 (C, C-9), 129.6 (CH, C-5), 131.8 (CH, C-4), 137.9 (C, C-10), 158.9 (C, C-7), 159.9 (C, C-2); *m/z* (EI^+) 220.0558 (M^+, $C_{12}H_{12}O_2S$ requires 220.0562) 220 (100%) 205 (25) 213 (8), 219 (17).

1,2-bis(2,7-dimethoxynaphthalen-1-yl)disulfane (**111**): R_f: 0.96 (8:2, hexane:EtOAc); ν_{max} (solid neat, ATR)/cm^{-1}: 3001, 2934, 2837, 1625, 1595, 1509, 1461, 1414, 1384, 1355, 1315, 1264, 1247, 1222, 1079, 1033, 961, 827, 772; δ_H (400 MHz; $CDCl_3$) 3.96 (6 H, s, OCH_3), 4.02 (6 H, s, OCH_3), 7.04 (2 H, dd, *J* = 8.9, 1.5 Hz, H-6 and H-6′), 7.11 (2 H, d, *J* = 9.0 Hz, H-3 and H-3′), 7.24 (2 H, bs, H-8 and H-8′), 7.60 (2 H, d, *J* = 8.9 Hz, H-5 and H-5′), 7.67 (2 H, d, *J* = 9.0 Hz, H-4 and H-4′); δ_C (101 MHz, $CDCl_3$) 55.5 (CH_3, OCH_3), 56.8 (CH_3, OCH_3), 102.5 (2 × CH, C-8 and C-8′), 110.1 (2 × CH, C-3 and C-3′), 113.0 (2 × C, C-1 C-1′), 117.0 (2 × CH, C-6 and C-6′), 124.7 (2 × C, C-9 and C-9′), 126.2 (2 × CH, C-5 and C-5′), 130.1 (2 × CH, C-4 and C-4′), 133.5 (2 × C, C-10 and C-10′), 152.4 (2 × C, C-7 and C-7′) 158.6 (2 × C, C-2 and C-2′); *m/z* (ES^+) 461.0868 ($[M+Na]^+$, $C_{24}H_{22}O_4S_2Na$ requires 461.0857) 461 (100%) 339 (27) 361 (30), 477 (28), 765 (33).

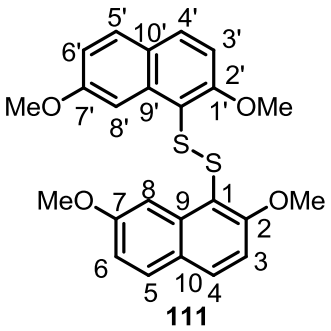

111

Attempted synthesis of 2,7-dimethoxynaphtho[1,8-*cd*][1,2]thiaselenole (**103d**)

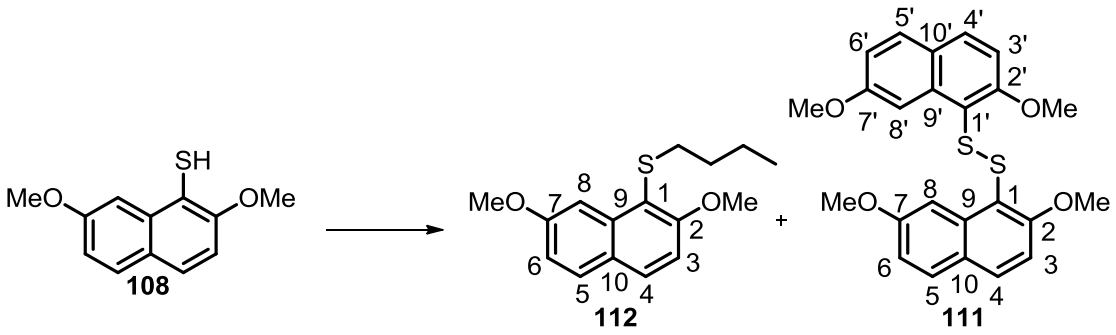

Thiol **108** (0.33 g, 1.05 mmol) was dissolved in hexane (9.5 mL), TMEDA (10.5 mL) and *n*BuLi (1.7 mL of a 1.90 M solution in hexane, 3.15 mmol) were added dropwise over 10 minutes to the reaction mixture at 0 °C under argon atmosphere. The lithiated mixture was stirred for 8 hours at room temperature. Se (0.08 g, 1.05 mmol) was added in one portion. The mixture was stirred for further 12 hours at room temperature under argon atmosphere. HCl (10 mL of a 1.0 M aq. solution) in ice H_2O was added and the two layers were separated. The aqueous layer was extracted with Et_2O (3 × 10 ml). The combined organic layers were washed with water (1 × 50 mL) and brine (1 × 50 mL), dried over $MgSO_4$, filtered and concentrated under reduced pressure. Purification by column chromatography (8:2, hexane:EtOAc) yielded sulfide **112** as brown crystalline solid (0.036 g, 12%) and disulfide **111** (0.016 g, 3%). 0.094 g (41%) of thiol **108** was recovered.

1-butyl-2,7-dimethoxynaphthalen-sulfide (**112**): R_f: 0.78 (8:2, hexane:EtOAc); mp: 45-46

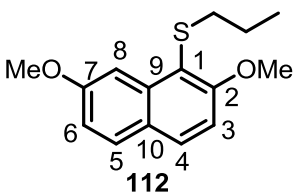

°C; ν_{max} (solid neat, ATR)/cm^{-1}: 2922, 2839, 1625, 1593, 1508, 1459, 1450, 1414, 1381, 1350, 1313, 1260, 1243, 1215, 1182, 1067, 1029, 850, 827, 771, 723; δ_H (400 MHz, $CDCl_3$): 0.85 (3 H, t, J = 7.1, CH_3), 1.40-1.51 (4 H, m, CH_2), 2.84 (2 H, t, J = 7.1, CH_2), 3.97 (3 H, s, OCH_3), 4.02 (3 H, s, OCH_3), 7.03 (1 H, dd, J = 8.9, 2.5 Hz, H-6), 7.13 (1 H, d, J = 9.0 Hz, H-3), 7.67 (1 H,

d, J = 8.9 Hz, H-5), 7.76 (1 H, d, J = 9.0 Hz, H-4), 8.00 (1 H, d, J = 2.5 Hz, H-8); δ_C (101 MHz, $CDCl_3$): 13.8 (CH_3, butyl), 22.1 (CH_2, butyl), 32.0 (CH_2, butyl), 34.8 (CH_2, butyl), 55.4 (CH_3, OCH_3), 56.7 (CH_3, OCH_3), 104.1 (CH, C-8), 110.4 (CH, C-3), 115.3 (C, C-1), 116.8 (CH, C-6), 124.9 (C, C-9), 129.9 (CH, C-5), 130.2 (CH, C-4), 138.3 (C, C-10), 159.0 (C, C-7) 159.3 (C, C-2); *m/z* (ES^+) 277.1272 ($[M+H]^+$, $[C_{16}H_{21}O_2S]$ requires 277.1262) 235 (100%), 277 (20).

Phenanthro[1,8-*cd*][1,2]dithiole (**113**)

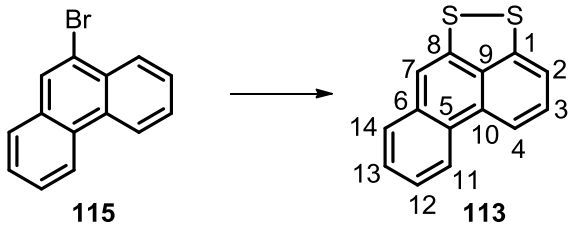

115 **113**

Phenanthro[1,8-*cd*][1,2]dithiole **113** was prepared according to a literature procedure.[142] *n*BuLi (1.10 mL of a 1.83 M solution in hexane, 1.94 mmol) and TMEDA (0.29 mL, 1.94 mmol) were added dropwise over 30 minutes to a suspension of 9-bromophenanthrene **115** (0.50 g, 1.94 mmol) in hexane (10 mL) at −30 °C under argon atmosphere. The yellow mixture was stirred for 1 hour at −30 °C and then allowed to warm to room temperature for 20 minutes. *n*BuLi (3.10 mL of a 1.83 M solution in hexane, 5.83 mmol) and TMEDA (0.87 mL, 5.83 mmol) were added dropwise over a period of 30 minutes to the mixture and the resulting dark red solution was heated at 60 °C for 3 hours. The mixture was cooled down to −78 °C and diluted with THF (10 mL). S_8 (0.50 g, 15.5 mmol) was added in one portion and the mixture was stirred for 16 hours at room temperature under argon atmosphere. The mixture was added to an excess of water (20 mL) and the two layers were separated. The organic layer was washed with brine (20 mL), dried over $MgSO_4$, filtered, concentrated under reduced pressure and purified by column chromatography (hexane) to give dichalcogen **113** as bright

orange solid (0.08 g, 17%). λ_{nm} (CH_3CN) 276 ($\varepsilon = 2.4 \times 10^4$ $M^{-1}cm^{-1}$) 356 ($\varepsilon = 1.5 \times 10^4$ $M^{-1}cm^{-1}$); δ_H (400 MHz, $CDCl_3$): 7.39 (1 H, d, *J* = 7.0 Hz, H-2), 7.44 (1 H, s, H-7), 7.50-7.59 (3 H, m, H-3, H-12 and H-13), 7.67 (1 H, d, *J* = 9.4 Hz, H-14), 8.21 (1 H, d, *J* = 8.0 Hz, H-4), 8.47 (1 H, d, *J* = 9.4 Hz, H-11); δ_C (101 MHz, $CDCl_3$): 115.1 (CH, C-7), 118.1 (CH, C-4), 118.3 (CH, C-2), 122.9 (CH, C-11), 125.4 (CH, C-12), 126.9 (C, C-5), 127.1 (CH, C-14), 127.8 (CH, C-13), 128.4 (CH, C-3), 132.8 (C, C-10), 133.0 (C, C-9), 133.5 (C, C-6), 141.7 (C, C-8), 143.5 (C, C-1); *m/z* (EI^+) 240.0061 (M^+, $C_{14}H_8S_2$ requires 240.0067), 240 (100%), 241 (17), 241 (9).

Literature data: [142] δ_H (360 MHz, $CDCl_3$) 7.37 (1 H, d, *J* = 7.7 Hz), 7.42 (1 H, s), 7.49-7.54 (3 H, m), 7.65 (1 H, d, *J* = 9.4 Hz), 8.19 (1 H, d, *J* = 8 Hz), 8.44 (1 H, d, *J* = 9.4 Hz); δ_C (90.6 MHz; $CDCl_3$) 115.1 (CH), 118 (CH), 118.2 (CH), 122.8 (CH), 125.3 (CH), 127 (C), 127.1 (CH), 127.7 (CH), 128.3 (CH), 132.6 (C), 132.7 (C), 133.5 (C), 141.7 (C), 143.6 (C); *m/z* (EI) 240.0055.

$[Fe_2(CO)_6(1,8\text{-}S_2\text{-}C_{14}H_8)]$ (**93**)

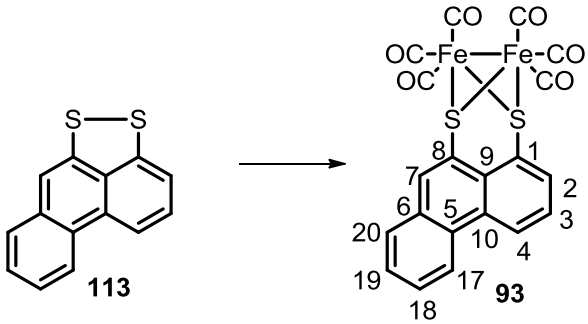

$[Fe_2(CO)_6(1,8\text{-}S_2\text{-}C_{10}H_8)]$ **93** is a novel compound, prepared according to a modified literature procedure.[122]

A solution of dichalcogen **113** (0.11 g, 0.47 mmol) and $Fe_3(CO)_{12}$ (0.24 g, 0.47 mmol) in toluene (13 mL) was refluxed for 4.5 hours under argon atmosphere. The mixture was cooled

down to room temperature, filtered and concentrated under reduced pressure. The residue was purified by column chromatography (hexane) to afford complex **93** as a red solid (0.125 g, 51%). R_f: 0.63 (hexane); mp: > 360 °C with decomp.; λ_{nm} (CH_3CN) 346 ($\varepsilon = 6.3 \times 10^3$ $M^{-1}cm^{-1}$), 248 ($\varepsilon = 3.4 \times 10^4$ $M^{-1}cm^{-1}$); ν_{max} (solid neat, ATR)/cm^{-1} 2065 (CO), 2028 (CO), 1978 (CO), 1957 (CO), 1946 (CO), 1936 (CO); δ_H (400 MHz, $CDCl_3$): 7.56 (1 H, t, *J* = 7.7 Hz, H-2), 7.70 (2 H, m, H-3 and H-18), 7.92 (1 H, d, *J* = 7.3 Hz, H-19), 8.29 (1 H, d, *J* = 7.3 Hz, H-20), 8.63 (1 H, s, H-7), 8.66 (1 H, s, H-4), 8.86 (1 H, d, *J* = 8.1 Hz, H-17); δ_C (101 MHz, $CDCl_3$): 122.1 (C, C-1), 123.4 (CH, C-7), 125.8 (CH, C-4), 126.0 (CH, C-2), 126.5 (C, C-8), 128.2 (CH, C-17), 128.3 (CH, C-18), 128.7 (CH, C-20), 130.4 (2 × C, C-5 and C-6), 131.7 (C, C-10), 132.0 (C, C-9), 133.2 (CH, C-19), 134.5 (CH, C-3), 207.8 (6 × C, CO); *m*/*z* (EI^+) 519.8473 (M^+, $C_{20}H_8O_6S_2{}^{56}Fe_2$ requires 519.8461), 352 (100%, $[M - 6\ CO]^+$), 380 (11, $[M - 5\ CO]^+$), 408 (11, $[M - 4\ CO]^+$), 464 (5, $[M - 2\ CO]^+$), 492 (4, $[M - CO]^+$), 520 (5, M^+). Anal. calcd. for $C_{20}H_8O_6S_2Fe_2$ requires C, 46.19: H, 1.45; found: C, 46.18; H, 1.48.

Phenanthro[1,8-*cd*][1,2]diselenole (**114**)

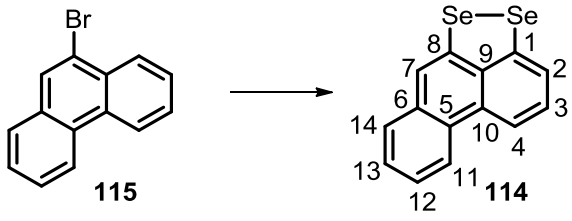

115 **114**

Phenanthro[1,8-*cd*][1,2]diselenole **114** is a novel compound, prepared according to a literature procedure.[142]

*n*BuLi (1.20 mL of a 1.68 M solution in hexane, 1.94 mmol) and TMEDA (0.29 mL, 1.94 mmol) were added dropwise over a period of 30 minutes to a suspension of 9-bromophenanthrene (0.50 g, 1.94 mmol) in hexane (10 mL) at −30 °C under argon atmosphere. The yellow mixture was stirred for 1 hour at −30 °C and then allowed to warm to

room temperature. *n*BuLi (3.50 mL of a 1.68 M solution in hexane, 5.83 mmol) and TMEDA (0.87 mL, 5.83 mmol) were added dropwise over 30 minutes to the mixture and the resulting dark red solution was heated at 60 °C for 3 hours. The mixture was cooled down to −78 °C and diluted with THF (10 mL). Se (1.20 g, 15.6 mmol) was added in one portion and the mixture was stirred overnight at room temperature under argon atmosphere. The mixture was added to an excess of H_2O (20 mL) and the two layers were separated. The organic layer was washed with brine (20 ml), dried over $MgSO_4$, filtered, concentrated under reduced pressure and purified by column chromatography (hexane) to give the *title product* as dark purple solid (0.09 g, 14%). R_f: 0.68 (hexane); mp: 121-122 °C; λ_{nm} (CH_3CN) 274 ($\varepsilon = 2.4 \times 10^4$ $M^{-1}cm^{-1}$), 360 ($\varepsilon = 1.5 \times 10^4$ $M^{-1}cm^{-1}$); ν_{max}(solid neat, ATR)/cm^{-1} 1575, 1557, 1473, 1440, 1397, 1360, 1285, 1196, 1197, 1110, 1066, 863, 835, 799, 748; δ_H (400 MHz, $CDCl_3$): 7.42-7.50 (2 H, m, Ar*H*), 7.51-7.55 (2 H, m, Ar*H*), 7.60 (1 H, s, Ar*H*), 7.61-7.65 (1 H, m, Ar*H*), 8.28 (1 H, d, *J* = 7.7 Hz, Ar*H*), 8.46-8.51 (1 H, m, Ar*H*); δ_C (101 MHz, $CDCl_3$): 119.5 (CH), 120.9 (CH), 123.0 (CH), 125.8 (CH), 127.2 (CH), 127.9 (C), 128.0 (C), 128.2 (C), 133.4 (C), 134.7 (C), 135.7 (C), 138.8 (C), 140.3 (C); *m/z* (ES^+) 333.8961 (M^+, $C_{14}H_8{}^{78}Se^{80}Se$ requires 333.8964), 336 (100%), 332 (53), 333 (40), 334 (96), 335 (22), 337 (23), 338 (34).

[$Fe_2(CO)_6$(1,8-Se_2-$C_{10}H_8$)] (**94**)

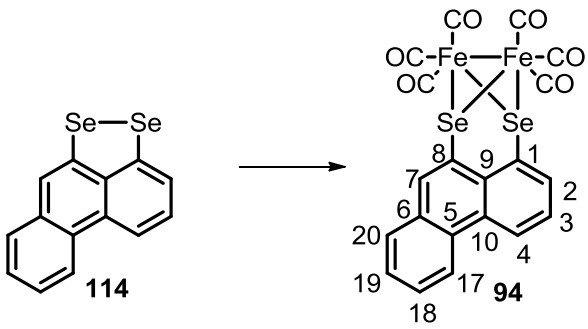

[$Fe_2(CO)_6$(1,8-Se_2-$C_{10}H_8$)] **94** is a novel compound, prepared according to a modified literature procedure.[122]

A solution of dichalcogen **114** (0.09 g, 0.28 mmol) and $Fe_3(CO)_{12}$ (0.28 g, 0.28 mmol) in toluene (7.0 mL) was refluxed for 4 hours under argon atmosphere. The mixture was cooled down to room temperature, filtered and concentrated under reduced pressure. The residue was purified by column chromatography (hexane) to afford complex **94** as a red solid (0.05 g, 26%). R_f: 0.65 (hexane); mp: decomp. above 140 °C; λ_{nm} (CH_3CN) 341 ($\varepsilon = 1.6 \times 10^4$ $M^{-1}cm^{-1}$), 251 ($\varepsilon = 3.1 \times 10^4$ $M^{-1}cm^{-1}$); ν_{max} (solid neat, ATR)/cm^{-1} 2055 (CO), 2021 (CO), 1996 (CO), 1976 (CO), 1962 (CO), 1942 (CO); δ_H (400 MHz, $CDCl_3$): 7.53 (1 H, t, *J* = 7.3 Hz, Ar*H*), 7.69 (2 H, m, Ar*H*), 7.90 (1 H, d, *J* = 7.0 Hz, Ar*H*), 8.33 (1 H, d, *J* = 6.8 Hz, Ar*H*), 8.64 (1 H, s, Ar*H*), 8.67 (1 H, s, Ar*H*), 8.86 (1 H, d, *J* = 5.8 Hz, Ar*H*); δ_C (101 MHz, $CDCl_3$): 116.1 (C), 120.6 (C), 123.3 (C), 125.8 (CH), 126.4 (CH), 127.6 (C), 128.2 (CH), 128.6 (CH), 130.1 (C), 131.5 (C), 132.1 (C), 134.6 (CH), 136.1 (CH), 208.6 (6 × C, CO); *m*/*z* (EI^+) 613.7343 (M^+, $C_{20}H_8O_6{}^{56}Fe_2{}^{78}Se^{80}Se$ requires 613.7358), 530 (100%, $[M - 3\ CO]^+$), 474 (74, $[M - 4\ CO]^+$), 476 (81), 532 (72), 558 (57, $[M - 2\ CO]^+$), 560 (42), 614 (10, M^+). Anal. calcd. for $C_{20}H_8O_6Fe_2Se_2$ requires C, 39.13: H, 1.31; found: C, 39.44; H, 1.23.

Anthra[11,14-*cd*][1,2]dithiole (**116**)

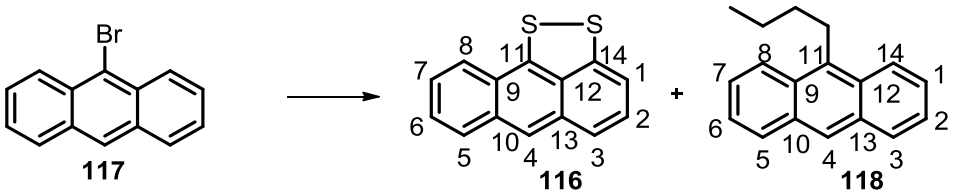

Anthra[11,14-*cd*][1,2]dithiole **116** is a novel compound, prepared according to a literature procedure.[130]

*n*BuLi (7.70 mL of a 1.83 M solution in hexane, 14.0 mmol) was diluted with Et_2O (8.0 mL). The mixture was cooled to −10 °C and 9-bromoanthracene **117** (0.30 g, 11.7 mmol) was added in one portion to the reaction mixture under argon atmosphere. The temperature was allowed to rise to 10 °C and stirring was continued for additional 15 minutes. The suspension was cooled to −10 °C and stirring was stopped. After standing for 10 minutes, the supernatant solution was removed *via* cannula. Hexane (24 mL) was added and the stirring was continued for 10 minutes at −20 °C. The stirring was stopped and the mixture was left to stand for 10 minutes and the supernatant was removed using a cannula (x 2). A solution of *n*BuLi (8.30 mL of a 1.83 M solution in hexane, 15.2 mmol) and TMEDA (2.50 mL, 16.4 mmol) was added dropwise over 15 minutes to the suspension. The mixture was refluxed for 3 hours and then cooled to −78 °C, THF (8.0 mL) was added and the reaction mixture was stirred for 20 minutes at −78 °C. Recrystallised S_8 (0.75 g, 23.4 mmol) was added in one portion and the reaction mixture was stirred for 16 hours at room temperature under argon atmosphere. HCl (1 mL of a 1.0 M aq. solution) was added to the mixture, which was then filtered through celite and the organic phase separated. The aqueous layer was acidified (pH < 1) with HCl (3 mL of a 1.0 M aq. solution) and extracted with Et_2O (3 × 3 mL). The combined organic layers were washed with brine (3 ml), dried over $MgSO_4$, purified on neutral alumina using hexane as eluent to give dichalcogen **116** (0.17 g, 6%) as yellow crystalline solid and 9-

butylanthracene **118** as a bright orange solid (0.20 g, 7%). R_f: 0.54 (hexane); mp: 98-99 °C; ν_{max}(solid neat, ATR)/cm^{-1} 3050, 2955, 2924, 1621, 1600, 1544, 1535, 1512, 1447, 1400, 1311, 1272, 1147, 1118, 997, 956, 906, 882, 759, 722; δ_H (400 MHz, $CDCl_3$): 7.11 (1 H, dd, *J* = 7.2, 0.5 Hz, H-1), 7.24 (1 H, dd, *J* = 8.3, 7.2 Hz, H-2), 7.40-7.52 (2 H, m, H-6 and H-7), 7.67 (1 H, m, H-5), 7.70 (1 H, m, Hz H-8), 7.91-7.95 (2 H, m, H-3 and H-4); δ_C (101 MHz, $CDCl_3$): 113.9 (CH), 120.5 (CH), 121.6 (CH), 125.0 (CH), 125.2 (CH), 126.7 (CH), 127.0 (CH), 129.1 (CH), 131.7 (C), 131.7 (C) 133.4 (C), 133.6 (C), 141.7 (C), 145.1 (C); *m*/*z* (EI$^+$) 240.0061 (M^+, $C_{14}H_8S_2$ requires 240.0067), 240 (100%), 241 (16), 242 (10).

9-Butylanthracene (**118**): δ_H (400 MHz, $CDCl_3$): 1.04 (3 H, t, *J* = 7.5 Hz, CH_3), 1.61 (2 H, m, CH_2), 1.81 (2 H, m, CH_2), 3.56-3.66 (2 H, m, CH_2), 7.45-7.49 (4 H, m, H-1, H-2, H-6 and H-7), 7.99-8.04 (2 H, m, H-8 and H-14), 8.28 (2 H, d, *J* = 8.6 Hz, H-3 and H-5), 8.33 (1 H, s, H-4); δ_C (101 MHz, $CDCl_3$): 14.2 (CH_3), 23.6 (CH_2), 27.9 (CH_2), 33.7 (CH_2), 124.7 (2 × CH), 125.5 (2 × CH), 126.4 (2 × CH), 128.3 (2 × CH), 129.3 (C), 129.7 (CH), 131.8 (C), 135.7 (C); *m*/*z* (EI$^+$) 234.1406 (M^+, $C_{18}H_{18}$ requires 234.1409), 191 (100%), 234 (34), 235 (7).

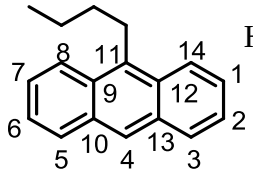

118

Literature data for 9-butylanthracene: [239] mp: 45-47 °C; δ_H 8.32 (s, 1H), 8.27 (d, 2H, *J* = 8.1 Hz), 8.00 (d, 2H, *J* = 7.7 Hz), 7.47 (m, 4H), 3.60 (t, 2H, *J* = 7.8 Hz), 1.81 (m, 2H), 1.61 (m, 2H), 1.03 (t, 3H, *J* = 7.2 Hz); δ_C 14.0735, 23.4014, 27.7665, 33.5163, 124.7396, 125.2788, 128.1355, 128.5727, 129.1703, 129.5201, 131.6261, 135.4301; HRMS (EI): calc. for $C_{18}H_{18}$ 234.1409, found 234.1410.

Anthracene-9-thiol (**119**)

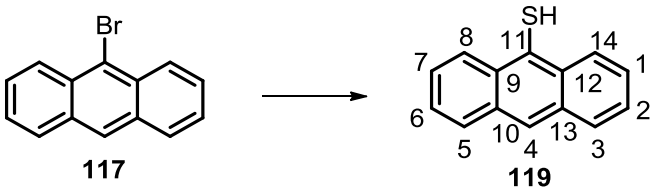

117 **119**

Anthracene-9-thiol **119** [240] was prepared according to a modified literature procedure.[131] 9-Bromoanthracene **117** (0.25 g, 1.00 mmol) and sodium ethanethiolate (0.70 g, 8.30 mmol) in dry DMF (5.0 mL) were refluxed for 16 hours under argon atmosphere. The reaction mixture was allowed to cool down to room temperature, concentrated under reduced pressure and HCl (20 mL of a 1.0 M aq. solution) was added under vigorous stirring. CH_2Cl_2 (5 mL) was then added to the aqueous solution, the two layers were separated and the aqueous layer was extracted with CH_2Cl_2 (3 × 10 mL). The combined organic layers were washed with brine (2 × 10 mL), dried over $MgSO_4$, concentrated under reduced pressure and purified by column chromatography (hexane) to give thiol **119** as bright orange crystalline solid (0.16 g, 75%). δ_H (400 MHz, $CDCl_3$): 7.05 (2 H, ddd, *J* = 8.9, 6.6, 1.2 Hz, H-1 and H-7), 7.28 (2 H, ddd, *J* = 8.9, 6.6, 1.2 Hz, H-2 and H-6), 7.82 (2 H, d, *J* = 8.9 Hz, H-8 and H-14), 8.14 (2 H, dd, *J* = 8.9, 1.2 Hz, H-3 and H-5), 8.40 (1 H, s, H-4); δ_C (101 MHz, $CDCl_3$): 125.3 (2 × CH), 126.2 (2 × CH), 126.5 (2 × CH), 128.5 (2 × CH), 129.9 (C), 130.3 (CH), 131.5 (2 × C), 135.0 (2 × C); *m*/*z* (EI^+) 210.0504 (M^+, $C_{14}H_{10}S$ requires 210.0504), 210 (100%), 165 (36), 178 (59), 211 (16), 212 (5).

Literature data: [240a)] mp: 65-66 °C; anal. calcd. for $C_{l5}H_{12}S$: C, 80.33; H, 5.39, found: C, 80.69; H, 5.52.

9,9-Dibutyl-9*H*-fluorene (**123**)

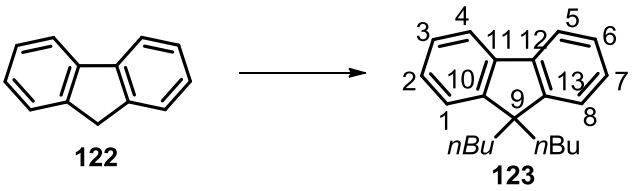

9,9-Dibutyl-9*H*-fluorene **123** is a novel compound, prepared according to a literature procedure.[143]

*t*BuOK (2.70 g, 24.0 mmol) was added in one portion to a solution of fluorene **122** (1.00 g, 6.11 mmol) in THF (40 mL) at room temperature under argon atmosphere. 1-Butylbromide (2.00 mL, 18.0 mmol) was added dropwise over a period of 10 minutes and the dark red suspension was stirred for 16 hours. NH_4Cl (15 mL of a saturated aq. solution) was added to the pale green mixture and the two layers were separated. The aqueous layer was extracted with CH_2Cl_2 (3 × 10 mL). The combined organic layers were washed with brine (15 mL), dried over $MgSO_4$, concentrated under reduced pressure and purified by column chromatography (hexane) to give dialkylated **123** as a colourless oil (1.35 g, 81%). R_f: 0.06 (hexane); mp: 49-50 °C; ν_{max}(solid neat, ATR)/cm^{-1} 2958, 2927, 2856, 1465, 1447, 1376, 1332, 1299, 1221, 1128, 1028, 1005, 932, 872, 771, 733; δ_H (400 MHz, $CDCl_3$): 0.54-0.64 (4 H, m, CH_2), 0.67 (6 H, t, J = 7.3 Hz, CH_3), 1.08 (4 H, m, CH_2), 1.91-2.02 (4 H, m, CH_2), 7.29-7.37 (6 H, m, H-1, H-2, H-3, H-6, H-7 and H-8), 7.70 (1 H, m, H-4), 7.72 (1 H, m, H-5); δ_C (101 MHz, $CDCl_3$): 14.0 (CH_3), 23.2 (CH_2), 26.1 (CH_2), 40.3 (CH_2), 55.1 (C, C-9), 119.8 (2 × CH), 123.0 (2 × CH), 126.8 (2 × CH), 127.1 (2 × CH), 141.4 (2 × C), 150.8 (2 × C); *m/z* (EI$^+$) 278.2023 (M^+, $C_{21}H_{26}$ requires 278.2035), 179 (100%), 165 (63), 221 (67), 278 (32).

9,9-Dibutyl-9*H*-fluoreno[4,5-*cde*][1,2]dithiine (**120**)

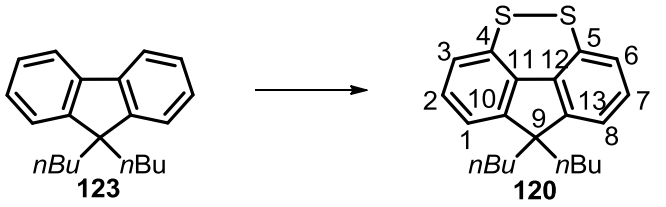

9,9-Dibutyl-9*H*-fluoreno[4,5-*cde*][1,2]dithiine **120** is a novel compound, prepared according to a literature procedure.[143]

Dialkylated **123** (1.07 g, 3.84 mmol) was stirred with *n*BuLi (11.0 mL of a 1.37 M solution in hexane, 15.4 mmol) and TMEDA (2.30 mL, 15.4 mmol) at 60 °C for 3 hours under argon atmosphere. The resulting dark red solution was cooled to −78 °C and diluted with THF (14 mL). Recrystallised S_8 (0.99 g, 30.7 mmol) was added in one portion and the mixture was stirred for 16 hours at room temperature. NaOH (5 mL of a 1.0 M aq. solution) and H_2O (5 mL) were added. The aqueous layer was extracted with Et_2O (3 × 30 mL). The combined organic layers were washed with brine (30 ml), dried over $MgSO_4$, concentrated under reduced pressure and purified by column chromatography (hexane) to give dichalcogen **120** as a bright yellow solid (0.67 g, 51%). R_f: 0.42 (hexane); mp: 77-78 °C; λ_{nm} (CH_3CN) 272 ($\varepsilon = 2.4 \times 10^4$ $M^{-1}cm^{-1}$); ν_{max}(solid neat, ATR)/cm^{-1} 3047, 2955, 2927, 2855, 1568, 1464, 1454, 1431, 1406, 1377, 1187, 1164, 1145, 1120, 787, 733; δ_H (400 MHz, $CDCl_3$): 0.63-0.68 (4 H, m, CH_2), 0.71 (6 H, t, J = 7.3 Hz, CH_3), 1.04-1.17 (4 H, m, CH_2), 1.87-1.96 (4 H, m, CH_2), 7.05 (2 H, dd, J = 7.6, 0.8 Hz, H-3 and H-6), 7.12 (2 H, dd, J = 7.5, 0.8 Hz, H-1 and H-8), 7.21 (2 H, t, J = 7.5 Hz, H-2 and H-7); δ_C (101 MHz, $CDCl_3$): 13.9 (CH_3), 23.2 (CH_2), 26.3 (CH_2), 39.2 (CH_2), 56.7 (C, C-9), 121.9 (2 × CH, C-1 and C-8), 123.8 (2 × CH, C-3 and C-6), 125.3 (2 × CH, C-2 and C-7), 129.2 (2 × C, C-4 and C-5), 137.3 (2 × C, C-11 and C-12), 150.7 (2 × C, C-10 and C-13); m/z (EI^+) 340.1329 (M^+, $C_{21}H_{24}S_2$ requires 340.1319), 340 (100%), 179 (41), 221 (49), 240 (39), 278 (19).

[$Fe_2(CO)_6$(4,5-S_2-$C_{27}H_{24}$)] (**96**)

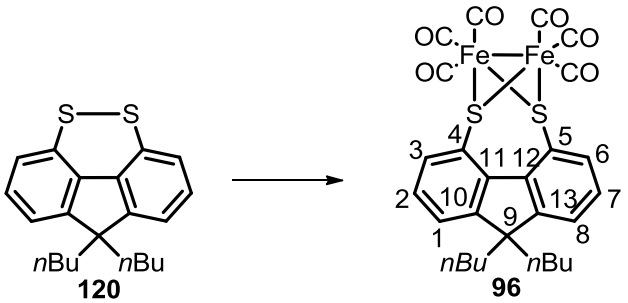

[$Fe_2(CO)_6$(4,5-S_2-$C_{27}H_{24}$)] **96** is a novel compound, prepared according to a modified literature procedure.[122]

A solution of dichalcogen **120** (0.20 g, 0.60 mmol) and $Fe_3(CO)_{12}$ (0.30 g, 0.60 mmol) in toluene (17 mL) was refluxed for 4 hours under argon atmosphere. The mixture was cooled down to room temperature, filtered and concentrated under reduced pressure. The residue was purified by column chromatography (hexane) to afford complex **96** as a purple solid (0.13 g, 35%). R_f: 0.86 (hexane); mp: > 102-103 °C; λ_{nm} (CH_3CN) 330 ($\varepsilon = 3.1 \times 10^3$ $M^{-1}cm^{-1}$), 259 ($\varepsilon = 7.6 \times 10^3$ $M^{-1}cm^{-1}$); ν_{max} (solid neat, ATR)/cm^{-1} 2072 (CO), 2030 (CO), 1990 (CO), 1986 (CO), 1974 (CO), 1952 (CO); δ_H (400 MHz, $CDCl_3$): 0.26 (4 H, br s, CH_2), 0.54 (6 H, t, J = 6.8 Hz, CH_2), 0.85-1.01 (4 H, m, CH_2), 1.87-2.04 (4 H, m, CH_2), 7.31 (2 H, br d, J = 7.7 Hz, H-2 and H-7), 7.44 (2 H, d, J = 7.1 Hz, H-1 and H-8), 8.11 (2 H, d, J = 7.3 Hz, H-3 and H-6); δ_C (101 MHz, $CDCl_3$): 13.8 (CH_3), 22.9 (CH_2), 25.4 (CH_2), 41.0 (CH_2), 55.3 (C, C-9), 123.3 (2 × CH, C-1 and C-8), 125.8 (2 × CH, C-2 and C-7), 137.0 (2 × CH, C-3 and C-6), 137.8 (2 × C, C-4 and C-5), 139.6 (2 × C, C-11 and C-12), 154.1 (2 × C, C-10 and C-13), 207.3 (6 × C, CO); m/z (EI^+) 619.9759 (M^+, $C_{27}H_{24}O_6S_2{}^{56}Fe_2$ requires 619.9713), 452 (100%), 480 (20), 508 (9), 536 (17), 620 (5).

9,9-Dibutyl-9*H*-fluoreno[4,5-*cde*][1,2]diselenine (121)

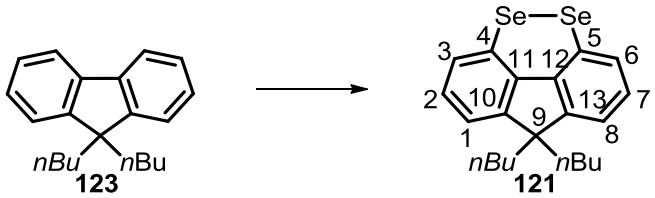

9,9-Dibutyl-9*H*-fluoreno[4,5-*cde*][1,2]diselenine **121** is a novel compound, prepared according to a literature procedure.[143]

Dialkylated **123** (1.00 g, 3.60 mmol) was stirred with *n*BuLi (8.00 mL of a 1.77 M solution in hexane, 14.4 mmol) and TMEDA (2.20 mL, 14.4 mmol) at 60 °C for 3 hours under argon atmosphere. The resulting dark red solution was cooled to −78 °C and diluted with THF (12.8 mL). Se (2.80 g, 36.0 mmol) was added in one portion and the mixture was stirred for 16 hours at room temperature. NaOH (5 mL of a 1.0 M aq. solution) and H_2O (5 mL) were added. The organic layer was separated and the aqueous layer was extracted with Et_2O (3 × 30 mL). The combined organic layers were washed with brine (30 mL), dried over $MgSO_4$, concentrated under reduced pressure and purified by column chromatography (hexane) to give dichalcogen **121** as a dark orange solid (1.10 g, 68%). R_f: 0.54 (hexane); mp: 110-111 °C; ν_{max}(solid neat, ATR)/cm^{-1} 2954, 2924, 2850, 1562, 1453, 1425, 1405, 1376, 1339, 1288, 1183, 1142, 1114, 1066, 895, 787, 734; δ_H (400 MHz, $CDCl_3$): 0.63-0.69 (4 H, m, CH_2), 0.72 (6 H, t, J = 7.4 Hz, CH_3), 1.06-1.16 (4 H, m, CH_2), 1.91-1.99 (4 H, m, CH_2), 7.14 (2 H, dd, J = 7.1, 1.7 Hz, H-3 and H-6), 7.22 (2 H, t, J = 7.1 Hz, H-2 and H-7), 7.23 (2 H, d, J = 7.1, 1.7 Hz, H-1 and H-8); δ_C (101 MHz, $CDCl_3$): 13.9 (CH_3), 23.1 (CH_2), 26.0 (CH_2), 39.6 (CH_2), 55.4 (C, C-9), 117.8 (2 × CH, C-3 and C-6), 121.9 (2 × CH, C-2 and C-7), 126.2 (2 × CH, C-1 and C-8), 129.2 (2 × C, C-4 and C-5), 139.5 (2 × C, C-11 and C-12), 151.1 (2 × C, C-10 and C-13); *m*/*z* (ES$^+$) 435.0296 (M$^+$, $C_{21}H_{24}{}^{78}Se^{80}Se$ requires 435.0296), 436 (100%), 432 (37), 221 (59), 434 (83), 437 (61), 473 (60), 475 (75).

Naphtho[1,8-*cd*][1,2]dithiole

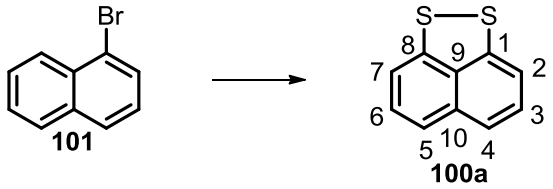

Naphtho[1,8-*cd*][1,2]dithiole **100a** [241] was prepared according to a literature procedure.[130] *n*BuLi (64.2 mL of a 1.87 M solution in hexane, 120 mmol) was diluted with dry Et_2O (80.0 mL). The mixture was cooled down to −10 °C and 1-bromonaphthalene **101** (13.9 mL, 100 mmol) was added dropwise over a period of 5 minutes. The temperature was allowed to rise to 10 °C and stirring was continued for additional 15 minutes. The suspension was cooled to −10 °C and the stirring was stopped. After standing for 10 minutes, the supernatant solution was removed *via* cannula under strictly anaerobic conditions. Hexane (250 mL) was added and the stirring was continued for 10 minutes at −20 °C. The stirring was stopped and the mixture was left to stand for 10 minutes and the supernatant was removed using a cannula (x 2). A solution of *n*BuLi (65.3 mL of a 1.99 M solution in hexane, 130 mmol) and TMEDA (21.2 mL, 140 mmol) was added to the suspension. The mixture was refluxed for 3 hours and then cooled to –78 °C, THF (80 mL) was added and the reaction mixture was stirred for 20 minutes at –78 °C. Recrystallised S_8 (6.54 g, 202 mmol) was added in one portion and the reaction mixture was stirred for 16 hours warming to room temperature. HCl (30 mL of a 1.0 M aq. solution) was added to the mixture, which was then filtered through celite and the organic phase separated. The aqueous layer was acidified (pH < 1) with HCl (20 mL of a 1.0 M aq. solution) and extracted with Et_2O (3 × 30 mL). The combined organic layers were dried over $MgSO_4$, purified by column chromatography (hexane) and recrystallised from EtOH (5.0 mL) to give dichalcogen **100a** as a red crystalline solid (6.97 g, 37%). δ_H (400 MHz, $CDCl_3$): 7.16 (2 H, d, *J* = 7.3 Hz, H-2 and H-7), 7.27 (2 H, t, *J* = 7.7 Hz, H-3 and H-6), 7.36 (2 H, d, *J*

= 7.6 Hz, H-4 and H-5); δ_C (101 MHz, $CDCl_3$): 116.0 (2 × CH, C-2 and C-7), 121.7 (2 × CH, C-4 and C-5), 128.0 (2 × CH, C-3 and C-6), 134.8 (C, C-9), 135.8 (C, C-10), 144.2 (2 × C, C-1 and C-8); *m*/*z* (ES^+) 189.9915 (M^+, $C_{10}H_6S_2$ requires 189.9911), 190 (100%), 191 (3).

Literature data: [130] R_f 0.48 (60-80 pet ether); mp 110-112 °C (EtOH); found: C, 63.35; H, 3.0. $C_{10}H_6S_2$ requires C, 63.1; H, 3.2%; λ_{max} (CH_3CN)/nm 366 (ε/dm^3 mol^{-1} cm^{-1} 13,300) and 250 (22,900); v_{max} (KBr)/cm-1 1544 (aromatic), 1485, 1349 and 1206; δ_H (300 MHz, $CDCl_3$) 7.16 (2 H, d, *J* = 7.3 Hz), 7.27 (2 H, t, *J* = 7.7 Hz), 7.36 (2 H, d, *J* = 7.6 Hz); δ_C (75 MHz, $CDCl_3$) 115.9, 121.6, 127.8, 134.7, 135.7, 144.0; m/z (EI) 189.9907 ($C_{10}H_6S_2$ requires 189.9911), 158 (5%), 145 (18), 126 (5), 114 (21), 102 (7), 95 (22), 74 (5), 69 (8), 63 (5).

$[Fe_2(CO)_6(1,8\text{-}S_2\text{-}C_{10}H_6)]$ (89a)

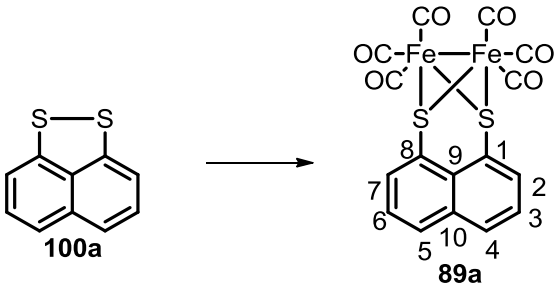

$[Fe_2(CO)_6(1,8\text{-}S_2\text{-}C_{10}H_6)]$ **89a** was prepared according to a modified literature procedure.[122]

A solution of dichalcogen **100a** (0.20 g, 1.05 mmol) and $Fe_3(CO)_{12}$ (0.53 g, 1.05 mmol) in toluene (27 mL) was refluxed for 45 minutes. The mixture was cooled down to room temperature, filtered and concentrated under reduced pressure. Hexane was added and the residue was recrystallised to give complex **89a** as thin red crystals (0.35 g, 70%). mp: 199-200 °C; λ_{nm} (CH_3CN) 349 (ε = 2.7 × 10^3 $M^{-1}cm^{-1}$), 249 (ε = 3.5 × 10^3 $M^{-1}cm^{-1}$); ν_{max} (solid neat, ATR)/cm^{-1} 2065 (CO), 2031 (CO), 1986 (CO), 1964 (CO); δ_H (400 MHz, $CDCl_3$): 7.42 (2 H, bs, H-2 and H-7), 8.01 (2 H, app d, *J* = 7.3 Hz, H-3 and H-6), 8.26 (2 H, app d, *J* = 6.2

Hz, H-4 and H-5); δ_C (101 MHz, $CDCl_3$): 125.2 (2 × C, C-1 and C-8), 125.6 (2 × CH, C-2 and C-7), 126.8 (C, C-9), 132.2 (2 × CH, C-3 and C-6), 133.0 (2 × CH, C-4 and C-5), 134.5 (C, C-10), 207.8 (6 × C, CO); *m*/*z* (EI^+) 469.8288 (M^+, $C_{16}H_6O_6S_2{}^{56}Fe_2$ requires 469.8305), 302 (100%), 144 (14), 190 (12), 252 (18), 284 (12), 330 (18, $[M - 5\ CO]^+$), 358 (20, $[M - 4\ CO]^+$), 414 (8, $[M - 2\ CO]^+$), 470 (12, M^+).

Literature data: [122] mp: 200-201 °C; IR (Nujol) 2074, 2039, 2001 (CO) ; δ_H (300 MHz, $CDCl_3$) 7.41 (2 H, t, *J* = 7.5 Hz), 8.01 (2 H, d, *J* = 7.8 Hz), 8.26 (2 H, d, *J* = 6.9 Hz); δ_C (75 MHz; $CDCl_3$) 125.1, 125.5, 126.7, 132.2, 132.9, 134.5, 207.8; anal. calcd. (%) for $C_{16}H_6O_6S_2Fe_2$: C 40.88, H 1.29: found C 40.78, H 1.20.

2,7-Di-*tert*-butyl-naphtho[1,8-*cd*][1,2]dithiole (**100b**)

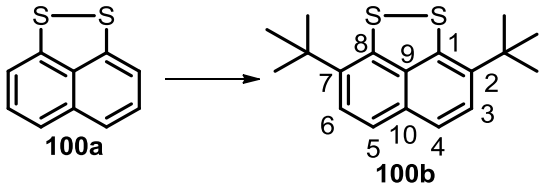

2,7-Di-*tert*-butyl-naphtho[1,8-*cd*][1,2]dithiole **100b** [242] was prepared according to a literature procedure.[130]

$FeCl_3$ (0.085, 0.53 mmol) was added in one portion to a solution of *t*BuBr (0.49 mL, 5.26 mmol) and dichalcogen **100a** (0.50 g, 2.63 mmol) in CH_2Cl_2 (1.0 mL). The mixture was refluxed for 16 hours under argon atmosphere, then allowed to cool down to room temperature, filtered through a plug of silica (petroleum ether), concentrated under reduced pressure and recrystallised from acetone (3.0 mL) to give disubstituted **100b** as bright orange crystals (0.25 g, 44%). δ_H (400 MHz, $CDCl_3$): 1.50 (18 H, s, *t*Bu), 7.35 (2 H, d, *J* = 8.6 Hz, H-3 and H-6), 7.41 (2 H, d, *J* = 8.6 Hz, H-4 and H-5); δ_C (101 MHz, $CDCl_3$): 28.5 (6 × CH_3,

*t*Bu), 35.7 (2 × C, *t*Bu), 122.0 (2 × CH, C-3 and C-6), 125.7 (2 × CH, C-4 and C-5), 132.9 (2 × C, C-1 and C-8), 137.1 (C, C-9), 138.9 (C, C-10), 139.5 (2 × C, C-2 and C-7); *m/z* (ES^+) 302.1155 (M^+, $C_{18}H_{22}S_2$ requires 302.1163), 302 (100%), 303 (32), 304 (9), 358 (10).

Literature data: [130] R_t 7.98 min; R_f 0.73 (95:5 hexane:Et_2O); mp 127-130 °C (acetone); ν_{max} (KBr)/cm^{-1} 2949 (CH), 1501, 1477, 1458, 1432, 1363, 1305 (t-Bu C-H), 1257, 1198, 1123 and 1007; δ_H (300 MHz; $CDCl_3$) 1.53 (18 H, s), 7.38 (2 H, d, J = 8.6 Hz), 7.43 (2 H, d, J = 8.5 Hz); δ_C (75 MHz; $CDCl_3$) 28.4, 35.6 , 121.9, 125.7, 132.9, 137.0, 138.9, 139.4; *m/z* (ESI) 303.1238 ($C_{18}H_{23}S_2$ requires 303.1241), 303 (100%).

[$Fe_2(CO)_6$(1,8-S_2-2,7-di-*tert*-butyl-$C_{10}H_4$)] (**89b**)

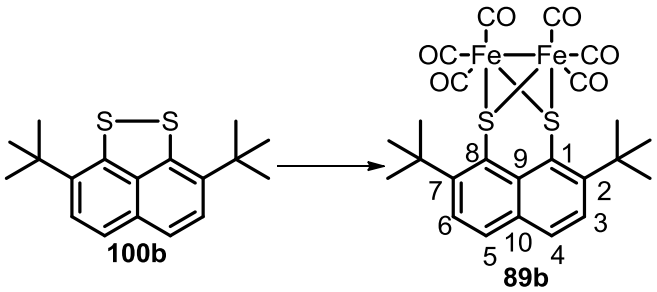

[$Fe_2(CO)_6$(1,8-S_2-2,7-di-*tert*-butyl-$C_{10}H_4$)] **89b** was prepared according to a modified literature procedure.[122]

A solution of **100b** (0.20 g, 0.66 mmol) and $Fe_3(CO)_{12}$ (0.33 g, 0.66 mmol) in toluene (17 mL) was refluxed for 4 hours under argon atmosphere. The mixture was cooled down to room temperature, filtered and concentrated under reduced pressure. The residue was purified by column chromatography (9:1, hexane:EtOAc) to afford complex **89b** as a red crystalline solid (0.18 g, 47%). R_f: 0.88 (9:1, hexane:EtOAc); mp: 159-160 °C; λ_{nm} (CH_3CN) 352 ($\varepsilon = 2.1 \times 10^4$ $M^{-1}cm^{-1}$), 310 ($\varepsilon = 1.9 \times 10^4$ $M^{-1}cm^{-1}$), 261 ($\varepsilon = 3.5 \times 10^4$ $M^{-1}cm^{-1}$); ν_{max} (solid neat, ATR)/cm^{-1} 2063 (CO), 2016 (CO), 1979 (CO), 1961 (CO), 1954 (CO); δ_H (400 MHz,

$CDCl_3$): 1.78 (18 H, s, *t*Bu), 7.66 (2 H, d, *J* = 8.8 Hz, H-3 and H-6), 7.84 (2 H, d, *J* = 8.8 Hz, H-4 and H-5); δ_C (101 MHz, $CDCl_3$): 32.4 (6 × CH_3, *t*Bu), 38.8 (2 × C, *t*Bu), 123.5 (2 × C, C-1 and C-8), 124.9 (2 × CH, C-3 and C-6), 130.1 (C, C-9), 130.9 (2 × CH, C-4 and C-5), 131.4 (C, C-10), 153.9 (2 × C, C-2 and C-7), 207.9 (6 × C, CO); *m*/*z* (EI^+) 581.9585 (M^+, $C_{24}H_{22}O_6S_2{}^{56}Fe_2$ requires 581.9557), 414 (100%, $[M - 6\ CO]^+$), 442 (44, $[M - 5\ CO]^+$), 470 (7, $[M - 4\ CO]^+$), 498 (7, $[M - 3\ CO]^+$), 582 (22, M^+).

Literature data: [122] mp: 160-162 °C; IR (Nujol) 2071, 2036, 1997 (CO); δ_H (300 MHz, CD_2Cl_2) 1.80 (18 H, s), 7.71 (2 H, d, *J* = 8.7 Hz), 7.90 (2 H, d, *J* = 8.7 Hz); δ_C (75 MHz; CD_2Cl_2) 32.7, 39.2, 123.9, 125.6, 130.5, 131.5, 131.9, 154.6, 208.6; anal. calcd. (%) for $C_{24}H_{22}O_6S_2Fe_2$: C 49.51, H 3.81: found C 49.32, H 3.65.

2,7-Di-*tert*-butyl-naphtho[1,8-*cd*][1,2]dithiole 1-oxide (**125b**)

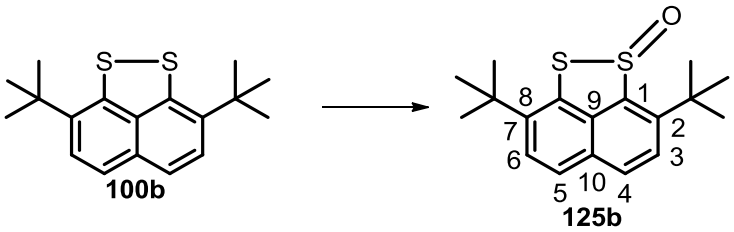

2,7-Di-*tert*-butyl-naphtho[1,8-*cd*][1,2]dithiole 1-oxide **125b** was prepared according to a literature procedure.[130]

To a solution of **100b** (0.21 g, 0.68 mmol) in CH_2Cl_2 (5.4 mL) was added a solution of *m*CPBA (0.13 g, 0.75 mmol) in CH_2Cl_2 (2.0 mL) over a period of 20 minutes and at 0 °C. The solution was stirred for additional 2 hours and slowly warmed to room temperature. The reaction mixture was washed with $NaHCO_3$ (3 × 5 mL of a saturated aq. solution) and extracted with CH_2Cl_2 (3 × 5 mL). The combined organic layers were washed with brine (5 mL), dried over $MgSO_4$, concentrated under reduced pressure and purified by column

chromatography (CH_2Cl_2) to give thiosulfinate **125b** (0.14 g, 65%) as a white solid. δ_H (400 MHz, $CDCl_3$): 1.58 (9 H, s, *t*Bu), 1.73 (9 H, s, *t*Bu), 7.72 (1 H, d, *J* = 8.6 Hz, H-6), 7.76 (1 H, d, *J* = 8.6 Hz, H-5), 7.81 (1 H, d, *J* = 8.6 Hz, H-3), 8.01 (1 H, d, *J* = 8.6 Hz, H-4); δ_C (101 MHz, $CDCl_3$): 30.7 (3 × CH_3, *t*Bu), 33.4 (3 × CH_3, *t*Bu), 36.6 (C, *t*Bu), 38.3 (C, *t*Bu), 125.5 (CH, C-5), 127.0 (CH, C-6), 127.2 (CH, C-3), 131.1 (C, C-8), 131.4 (C, C-9), 131.6 (C, C-10), 131.9 (CH, C-4), 145.8 (C, C-1), 146.3 (C, C-7), 151.8 (C, C-2); m/z (ES^+) 319.1200 ($[M+H]^+$, $C_{18}H_{23}OS_2$ requires 319.1190), 319 (100%), 302 (53), 320 (21), 341 (16).

Literature data: [130] R_f 0.50 (CH_2Cl_2); mp 146-148 °C (EtOAc); v_{max} (KBr)/cm^{-1} 2963, 1365 and 1071 (SO); δ_H (300 MHz; $CDCl_3$) 1.58 (9 H, s, $C(CH_3)_3$), 1.73 (9 H, s, $C(CH_3)_3$), 7.72 (1 H, d, *J* 8.6, Ar*H*), 7.76 (1 H, d, *J* 8.7, Ar*H*), 7.81 (1 H, d, *J* 8.6, Ar*H*) and 8.01 (1 H, d, *J* 8.6, Ar*H*); δ_C (75 MHz; $CDCl_3$) 30.4 (CH_3), 33.2 (CH_3), 36.3 (C), 38.1 (C), 125.3 (CH), 126.7(CH), 127.0 (CH), 130.9 (C), 131.2 (C), 131.4 (C), 131.7 (CH), 145.4 (C), 146.1 (C) and 151.6 (C); *m/z* (EI) 318.1098 (M^+, $C_{18}H_{22}OS_2$ requires 318.1112), 303 (19), 286 (21), 271 (10), 262 (45), 249 (41), 238 (18), 229 (34), 212 (17), 198 (17), 184 (11), 83 (47), 69 (20), 57 (32) and 49 (63).

2,7-Di-*tert*-butyl-naphtho[1,8-*cd*][1,2]dithiole 1,2-dioxide (**126b**)

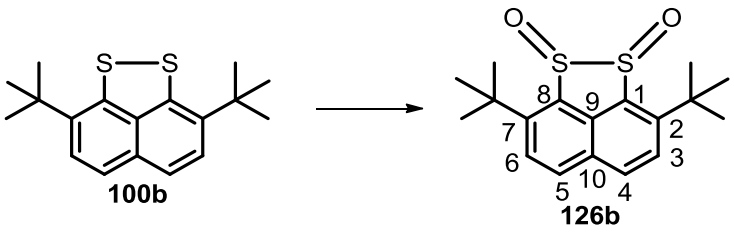

2,7-Di-*tert*-butyl-naphtho[1,8-*cd*][1,2]dithiole 1,2-dioxide **126b** was prepared according to a literature procedure.[130]

To a solution of **100b** (0.18 g, 0.60 mmol) in CH_2Cl_2 (4.7 mL) was added a solution of *m*CPBA (0.22 g, 1.25 mmol) in CH_2Cl_2 (3.4 mL) over a period of 20 minutes at 0 °C. The solution was stirred for additional 2 hours and slowly warmed to room temperature. The reaction mixture was washed with $NaHCO_3$ (3 × 5 mL of a saturated aq. solution) and extracted with CH_2Cl_2 (3 × 5 mL). The combined organic layers were washed with brine (5 mL), dried over $MgSO_4$, concentrated under reduced pressure and purified by column chromatography (8:2, hexane:EtOAc) to give *vic*-disulfoxide **126b** (0.15 g, 76%) as a white solid. δ_H (400 MHz, $CDCl_3$): 1.70 (18 H, s, *t*Bu), 7.82 (2 H, d, *J* = 8.7 Hz, H-3 and H-6), 8.06 (2 H, d, *J* = 8.7 Hz, H-4 and H-5); δ_C (101 MHz, $CDCl_3$): 33.4 (6 × CH_3, *t*Bu), 38.2 (2 × C, *t*Bu), 127.7 (2 × CH, C-3 and C-6), 132.5 (2 × CH, C-4 and C-5), 133.0 (2 × C, C-1 and C-8), 139.0 (C, C-9), 139.8 (C, C-10), 155.5 (2 × C, C-2 and C-7); m/z (ES^+) 335.1142 ($[M+H]^+$, $C_{18}H_{23}O_2S_2$ requires 335.1139), 335 (100%), 302 (35), 357 (35).

Literature data: [130] R_f 0.31 (8:2 hexane:EtOAc); mp 178-180 °C (EtOAc); ν_{max} (KBr)/cm^{-1} 2959, 1367, 1117, 1067 and 1040 (SO); δ_H (300 MHz; $CDCl_3$) 1.70 (18 H, s, $C(CH_3)_3$), 7.81 (2 H, d, *J* 8.6, Ar*H*) and 8.05 (2 H, d, *J* 8.6, Ar*H*); δ_C (75 MHz; $CDCl_3$) 33.2 (CH_3), 38.0 (C), 127.4 (CH), 132.2 (CH), 132.7 (C), 138.7 (C), 139.5 (C) and 155.1 (C); m/z (EI) 334.1045 (M^+, $C_{18}H_{22}O_2S_2$ requires 334.1061), 319 (10%), 286 (100), 271 (89), 255 (47), 239 (21), 229 (9), 215 (24), 198 (19), 184 (18), 165 (17), 152 (10), 139 (6), 57 (24) and 43 (9).

6.3 Experimental section: Chapter 3

Naphtho[1,8-*cd*][1,2]dithiole-3-carbaldehyde (**133**)

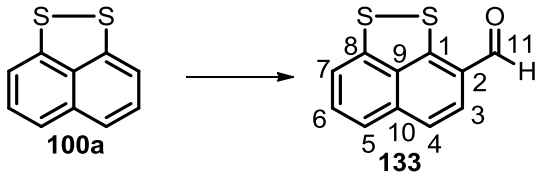

Naphtho[1,8-*cd*][1,2]dithiole-3-carbaldehyde **133** was prepared according to a literature procedure.[159]

$POCl_3$ (0.86 mL, 9.35 mmol) was added dropwise over 5 minutes to a vigorously stirred solution of dichalcogen **133** (0.45 g, 2.34 mmol) in dry DMF (7.5 mL) at 0 °C and under argon atmosphere. The reaction mixture was allowed to warm to room temperature and the stirring was kept for additional 24 hours. H_2O (30 mL) was added and a yellow precipitate was formed and solubilised upon addition of EtOAc (155 mL). The two layers were then separated and the aqueous layer was extracted with EtOAc (3 × 15 mL). The combined organic layers were washed with H_2O (3 × 30 mL) and brine (30 mL), dried over Na_2SO_4, concentrated under reduced pressure and purified by column chromatography (toluene) to give aldehyde **133** (0.28 g, 67%) as a bright yellow solid. δ_H (400 MHz, $CDCl_3$): 7.38-7.55 (4 H, m, Ar*H*), 7.64 (1 H, d, *J* = 8.6 Hz, Ar*H*), 10.04 (1 H, s, H-11); δ_C (101 MHz, $CDCl_3$): 117.1 (CH), 120.8 (CH), 122.2 (CH), 126.4 (C), 129.1 (CH), 130.7 (CH), 136.1 (C), 137.5 (C), 147.0 (C), 152.6 (C), 187.9 (CH, C-11); *m/z* (EI^+) 217.9857 (M^+, $C_{11}H_6OS_2$ requires 217.9860), 218 (100%), 145 (15), 149 (23), 189 (25), 217 (23), 219 (11).

Literature data: [159] ^{1}H NMR ($CDCl_3$, 300 MHz): δ 10.08 (1 H, s), 7.70 (1 H, d, J = 8.4 Hz), 7.49 (4 H, m); FAB-MS: calculated for [M^+] 218, found 218.

(*E*)-*N*-Isopropyl-1-(naphtho[1,8-*cd*][1,2]dithiol-3-yl)mathanimine (**135b**)

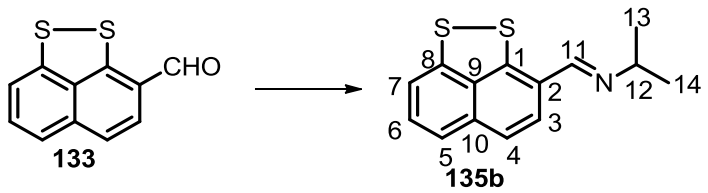

(*E*)-*N*-Isopropyl-1-(naphtho[1,8-*cd*][1,2]dithiol-3-yl)mathanimine **135b** is a novel compound, prepared according to a modified literature procedure.[162]

A solution of $TiCl_4$ (0.020 mL, 0.18 mmol) in dry CH_2Cl_2 (0.4 mL) was added dropwise over 10 minutes to a solution of aldehyde **133** (0.10 g, 0.46 mmol), *i*$PrNH_2$ (0.47 mL, 0.55 mmol) and NEt_3 (0.13 mL, 0.92) in dry CH_2Cl_2 (3.8 mL) at 0 °C and under argon atmosphere. After 30 minutes the reaction mixture was allowed to warm to room temperature and stirred for an additional 16 hours under argon atmosphere. The solvent was removed under reduced pressure and the crude product was then purified by column chromatography (8:2, hexane:EtOAc) to give imine **135b** (0.11 g, 96%) as an orange crystalline solid. R_f: 0.77 (8:2, hexane:EtOAc); mp: 94-95 °C; ν_{max} (solid neat, ATR)/cm^{-1} 3050, 2972, 2925, 1572, 1516, 1497, 1449, 1429, 1382, 1322, 1306, 1194, 1134, 1123, 973, 906, 809, 746, 776, 746, 650; δ_H (400 MHz, $CDCl_3$): 1.47 (6 H, d, J = 6.4 Hz, H-13 and H-14), 4.02 (1 H, dt, J = 6.4, 0.7 Hz, H-12), 7.39-749 (4 H, m, Ar*H*), 8.62 (1 H, d, J = 0.7 Hz, H-11); δ_C (101 MHz, $CDCl_3$): 23.3 (2 × CH_3, C-13 and C-14), 58.3 (CH, C-12), 117.9 (CH), 120.0 (CH), 122.5 (CH), 125.7 (C), 127.0 (CH), 128.3 (CH), 135.3 (C), 135.3 (C), 147.2 (C), 148.3 (C), 152.8 (CH, C-11); *m/z* (ES^+) 260.0560 ($[M+H]^+$, $C_{14}H_{14}NS_2$ requires 260.0568), 323 (100%), 260 (30), 324 (30), 338 (35), 382 (21). Anal. calcd. for $C_{14}H_{13}NS_2$: C, 64.83; H, 5.05; N, 5.40; found: C, 64.58; H, 5.03; N, 5.63.

***N*-(Naphtho[1,8-*cd*][1,2]dithiol-3-ylmethyl)propan-2-amine (135a)**

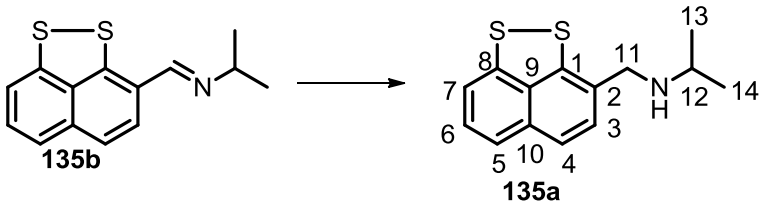

N-(Naphtho[1,8-*cd*][1,2]dithiol-3-ylmethyl)propan-2-amine **135a** is a novel compound, prepared according to a literature procedure.[160]

$NaBH_4$ (0.73 g, 19.2 mmol) was added in one portion to a solution of imine **135b** (0.25 g, 0.96 mmol) in a mixture of MeOH:$CHCl_3$ (5:1, 46 mL) and the reaction was then stirred for 3 hours at room temperature and under argon atmosphere. The resulting bright yellow solution was poured into H_2O (156 mL) and the two layers were then separated. The aqueous layer was extracted with CH_2Cl_2 (3 × 20 mL). The combined organic layers were washed with brine (20 mL), dried over $MgSO_4$ and concentrated under reduced pressure to give amine **135a** (0.25 g, 100%) as a bright yellow solid, which was used without further purification. R_f: 0.40 (8:2, hexane:EtOAc); mp: 51-52 °C; ν_{max} (solid neat, ATR)/cm^{-1} 3313, 3051, 2960, 2923, 2875, 2834, 1541, 1494, 1461, 1427, 1358, 1324, 1248, 1224, 1213, 1167, 1144, 1053, 985, 903, 811, 754; δ_H (400 MHz, $CDCl_3$) 1.17 (6 H, d, *J* = 6.3 Hz, H-13 and H-14), 2.90 (1 H, heptd, *J* = 6.3 Hz, H-12), 3.92 (2 H, s, H-11), 7.13 (1 H, d, *J* = 8.2 Hz, H-3), 7.16 (1 H, dd, *J* = 7.7, 0.8 Hz, H-7), 7.22 (1 H, t, *J* = 7.7 Hz, H-6), 7.30 (1 H, dd, *J* = 7.7, 0.8 Hz, H-5), 7.31 (1 H, d, *J* = 8.2 Hz, H-4); δ_C (101 MHz, $CDCl_3$): 22.6 (2 × CH_3, C-13 and C-14), 48.7 (CH, C-12), 49.7 (CH_2, C-11), 116.4 (CH, C-7), 120.9 (CH, C-5), 122.0 (CH, C-4), 127.4 (2 × CH, C-3 and C-6), 134.9 (C, C-10), 136.2 (C, C-9), 142.9 (2 × C, C-1 and C-2), 144.3 (C, C-8); *m/z* (EI^+) 261.0647 (M^+, $C_{14}H_{15}NS_2$ requires 261.0646), 203 (100%), 218 (20), 219 (28), 261 (45).

[$Fe_2(CO)_6$(1,8-S_2-2-CH_2-*Ni*Pr-$C_{10}H_5$)] (**129a**)

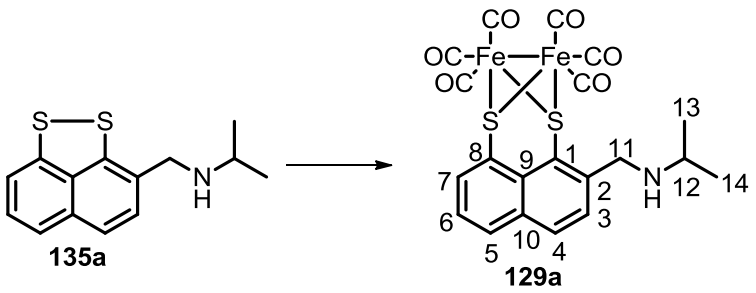

[$Fe_2(CO)_6$(1,8-S_2-2-CH_2-*Ni*Pr-$C_{10}H_5$)] **129a** is a novel compound, prepared according to a modified literature procedure.[122]

A solution of amine **135a** (0.25 g, 0.96 mmol) and $Fe_3(CO)_{12}$ (0.48 g, 0.96 mmol) in toluene (26 mL) was refluxed for 4 hours under argon atmosphere. The mixture was cooled down to room temperature, filtered and concentrated under reduced pressure. The residue was purified by column chromatography (7:2.5:0.5, hexane:EtOAc:Et_3N) to afford complex **129a** as a red solid (0.34 g, 65%). R_f: 0.72 (7:2.5:0.5, hexane:EtOAc:Et_3N); mp: 121-122 °C; λ_{nm} (CH_3CN) 352 ($\varepsilon = 1.8 \times 10^4$ $M^{-1}cm^{-1}$), 253 ($\varepsilon = 2.1 \times 10^4$ $M^{-1}cm^{-1}$); ν_{max} (solid neat, ATR)/cm^{-1} 2064 (CO), 2028 (CO), 2002 (CO), 1986 (CO), 1961 (CO); δ_H (400 MHz, $CDCl_3$): 1.15 (6 H, d, J = 6.2 Hz, H-13 and H-14), 2.85 (1 H, heptd, J = 6.2 Hz, H-12), 4.39 (2 H, s, H-11), 7.37 (1 H, t, J = 7.5 Hz, H-6), 7.58 (1 H, d, J = 8.3 Hz, H-3), 7.93 (1 H, d, J = 8.3 Hz, H-4), 7.96 (1 H, br d, J = 7.5 Hz, H-7), 8.25 (1 H, dd, J = 7.5, 0.9 Hz, H-5); δ_C (101 MHz, $CDCl_3$): 23.2 (2 × CH_3, C-13 and C-14), 48.0 (CH, C-12), 51.3 (CH_2, C-11), 123.3 (C, C-1), 124.8 (C, C-8), 125.0 (CH, C-6), 127.4 (C, C-9), 128.5 (CH, C-3), 131.2 (CH, C-4), 132.3 (CH, C-7), 133.2 (CH, C-5), 137.7 (C, C-10), 144.6 (C, C-2), 207.7 (6 × C, CO); *m/z* (ES^+) 541.9122 ($[M+H]^+$, $C_{20}H_{16}NO_6S_2{}^{56}Fe_2$ requires 541.9118), 542 (100%), 540 (7), 543 (19), 544 (9). Anal. calcd. for $C_{20}H_{15}NO_6S_2Fe_2$: C, 44.39; H, 2.79; N, 2.59; found: C, 44.24; H, 2.82; N, 2.76.

Naphtho[1,8-*cd*][1,2]diselenole-3-carbaldehyde (**134**)

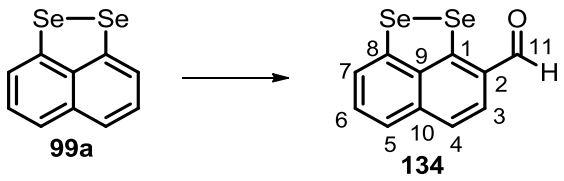

Naphtho[1,8-*cd*][1,2]diselenole-3-carbaldehyde **134** was prepared according to a literature procedure.[160]

$POCl_3$ (0.64 mL, 7.04 mmol) was added dropwise to a vigorously stirred solution of dichalcogen **99a** (0.50 g, 1.76 mmol) in dry DMF (5.4 mL) at 0 °C and under argon atmosphere. The reaction mixture was allowed to warm to room temperature and the stirring was kept for additional 24 hours. H_2O (20 mL) was added and a red precipitate was formed and solubilised upon addition of EtOAc (104 mL). The two layers were then separated and the aqueous layer was extracted with EtOAc (3 × 10 mL). The combined organic layers were washed with H_2O (3 × 30 mL) and brine (30 mL), dried over Na_2SO_4, concentrated under reduced pressure and purified by column chromatography (toluene) to give aldehyde **134** (0.34 g, 63%) as a bright red solid. δ_H (400 MHz, $CDCl_3$): 7.46 (1 H, t, J = 7.7 Hz, H-6), 7.55 (1 H, dd, J = 7.7, 0.7 Hz, H-7), 7.63 (1 H, d, J = 8.4 Hz, H-3), 7.68 (1 H, d, J = 8.4 Hz, H-4), 7.73 (1 H, dd, J = 7.7, 0.7 Hz, H-5), 10.2 (1 H, s, H-11); δ_C (101 MHz, $CDCl_3$): 122.5 (CH, C-7), 123.1 (CH, C-5), 124.2 (CH, C-3), 129.2 (CH, C-4), 130.1 (CH, C-6), 130.5 (C, C-1), 139.2 (C, C-9 or C-10), 139.5 (C, C-9 or C-10), 146.4 (C, C-8), 154.9 (C, C-2) 188.2 (CH, C-11); *m/z* (EI^+) 313.8735 (M^+, $C_{11}H_6O^{80}Se_2$ requires 313.8749), 314 (100%), 308 (9), 310 (36), 312 (79), 316 (14).

Literature data: [160] ^1H NMR ($CDCl_3$) δ (ppm): 7.47 (t, J = 7.6 Hz, 1H), 7.54 (d, J = 8 Hz, 1H), 7.61-7.69 (m, 2H), 7.72 (d, J = 7.2 Hz, 1H), 10.18 (s, 1H); ^{13}C NMR ($CDCl_3$) δ (ppm):

122.8, 123.4, 125.1, 129.5, 130.4, 130.8, 139.5, 146.8, 155.2, 188.6; ^{77}Se NMR ($CDCl_3$) δ (ppm): 408, 673; ESI-MS (m/z) calcd for $C_{11}H_6OSe_2$ $[M]^+$: 313.87, found 313.91.

(*E*)-*N*-Isopropyl-1-(naphtho[1,8-*cd*][1,2]diselenol-3-yl)mathanimine (**136b**)

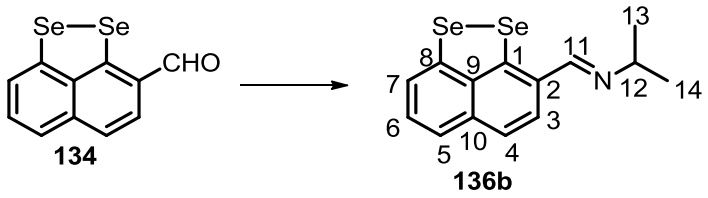

(*E*)-*N*-Isopropyl-1-(naphtho[1,8-*cd*][1,2]diselenol-3-yl)mathanimine **136b** [160] was prepared according to a modified literature procedure.[162]

A solution of $TiCl_4$ (0.008 mL, 0.07 mmol) in dry CH_2Cl_2 (0.2 mL) was added dropwise to a solution of aldehyde **134** (0.058 g, 0.19 mmol), *i*$PrNH_2$ (0.02 mL, 0.22 mmol) and NEt_3 (0.05 mL, 0.37) in dry CH_2Cl_2 (1.5 mL) at 0 °C and under argon atmosphere. After 30 minutes the reaction mixture was allowed to warm to room temperature and stirred for additional 16 hours under argon atmosphere. The solvent was removed under reduced pressure and the crude product was then purified by column chromatography (8:2, hexane:EtOAc) to give imine **136b** (0.06 g, 90%) as an orange crystalline solid. δ_H (400 MHz, $CDCl_3$): 1.54 (6 H, d, J = 6.5 Hz, H-13 and H-14), 4.09 (1 H, dt, J = 6.5, 0.8 Hz, H-12), 7.36 (1 H, t, J = 7.7 Hz, H-6), 7.49 (1 H, d, J = 8.4, 0.8 Hz, H-3), 7.55 (1 H, d, J = 7.7 Hz, H-7), 7.68 (1 H, d, J = 8.4 Hz, H-4), 7.84 (1 H, d, J = 7.7 Hz, H-5), 8.74 (1 H, d, J = 0.8 Hz, H-11); δ_C (101 MHz, $CDCl_3$): 25.6 (2 × CH_3, C-13 and C-14), 57.6 (CH, C-12), 121.6 (CH, C-7), 124.9 (2 × CH, C-4 and C-5), 126.7 (CH, C-3), 127.7 (CH, C-6), 128.9 (C, C-1), 136.5 (C, C-10), 138.0 (C, C-9), 145.6 (C, C-8), 150.5 (C, C-2), 153.8 (CH, C-11); *m/z* (EI^+) 354.9381 (M^+, $C_{14}H_{13}N^{80}Se_2$ requires 354.9378), 355 (100%), 336 (4), 338 (15), 340 (19), 351 (20), 353 (77). Anal. calcd. for $C_{14}H_{13}NSe_2$: C, 47.61; H, 3.71; N, 3.97; found: C, 46.89; H, 3.57; N, 4.19.

Literature data: [160] ^{1}H NMR ($CDCl_3$) δ (ppm): 1.53 (d, J = 6.4 Hz, 6H), 4.05-4.10 (m, 1H), 7.37 (t, J = 7.6 Hz, 1H), 7.48 (d, J = 8.4 Hz, 1H), 7.54 (d, J = 7.6 Hz, 1H), 7.67 (d, J = 8 Hz, 1H), 7.84 (d, J = 7.6 Hz, 1H), 8.73 (s, 1H); ^{13}C NMR ($CDCl_3$) δ (ppm): 26.1, 58.0, 122.1, 125.3, 125.4, 127.2, 128.2, 129.4, 136.9, 138.4, 146.0, 150.9, 154.2; ^{77}Se NMR ($CDCl_3$) δ (ppm): 341, 678; ESI-MS (m/z) calcd for $C_{14}H_{13}NSe_2$ $[M + H]^+$: 355.94, found 355.76.

***N*-(Naphtho[1,8-*cd*][1,2]diselenol-3-ylmethyl)propan-2-amine** (**136a**)

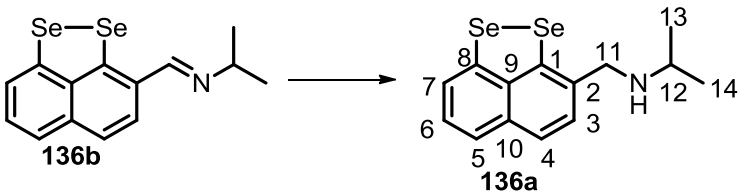

N-(Naphtho[1,8-*cd*][1,2]diselenol-3-ylmethyl)propan-2-amine **136a** was prepared according to a literature procedure.[160]

$NaBH_4$ (0.13 g, 3.34 mmol) was added in one portion to a solution of imine **136b** (0.06 g, 0.17 mmol) in a mixture of MeOH:$CHCl_3$ (5:1, 11 mL) and the reaction was then stirred for 3 hours at room temperature and under argon atmosphere. The resulting bright yellow solution was poured into H_2O (37 mL) and the two layers were then separated. The aqueous layer was extracted with CH_2Cl_2 (3 × 10 mL). The combined organic layers were washed with brine (20 mL), dried over $MgSO_4$ and concentrated under reduced pressure to give amine **136a** (0.06 g, 94%) as a bright orange solid, which was used without further purification. δ_H (400 MHz, $CDCl_3$): 1.17 (6 H, d, *J* = 6.3 Hz, H-13 and H-14), 2.92 (1 H, heptd, *J* = 6.3 Hz, H-12), 3.88 (2 H, s, H-11), 6.97 (1 H, d, *J* = 8.1 Hz, H-3), 7.16 (1 H, t, *J* = 7.7 Hz, H-6), 7.38 (1 H, d, *J* = 8.1 Hz, H-4), 7.44 (2 H, m, H-5 and H-7); δ_C (101 MHz, $CDCl_3$): 22.3 (2 × CH_3, C-13 and C-14), 49.4 (CH, C-12), 50.7 (CH_2, C-11), 122.5 (CH, C-4), 123.1 (CH, C-5 or C-7), 124.3 (CH, C-5 or C-7), 126.2 (CH, C-3), 127.1 (CH, C-6), 134.3 (C, C-10), 136.3 (C, C-9), 139.1 (C, C-

2), 140.6 (C, C-1), 141.3 (C, C-8); *m/z* (ES^+) 354.9529 (M^+, $C_{14}H_{15}N^{78}Se^{80}Se$ requires 354.9543), 355 (100%), 349 (16), 350 (11), 351 (48), 352 (31), 353 (96), 354 (17), 356 (14), 357 (25).

Literature data: [160] ^1H NMR ($CDCl_3$) δ (ppm): 1.22 (s, 6H), 2.95-3.01 (m, 1H), 3.97 (s, 2H), 7.04 (d, J = 8 Hz, 1H), 7.17 (t, J = 8 Hz, 1H), 7.39 (d, J = 8 Hz, 1H), 7.44−7.47 (m, 2H); ^{13}C NMR ($CDCl_3$) δ (ppm): 22.8, 49.7, 51.2, 123, 123.5, 124.8, 126.7, 127.6, 134.6, 136.8, 139.6, 141.1, 141.7; ^{77}Se NMR ($CDCl_3$) δ (ppm): 350, 445; ESI-MS (m/z) calcd for $C_{14}H_{15}NSe_2$ $[M]^+$: 356.95, found 356.98.

[$Fe_2(CO)_6$(1,8-Se_2-2-CH_2-*Ni*Pr-$C_{10}H_5$)] (**130a**)

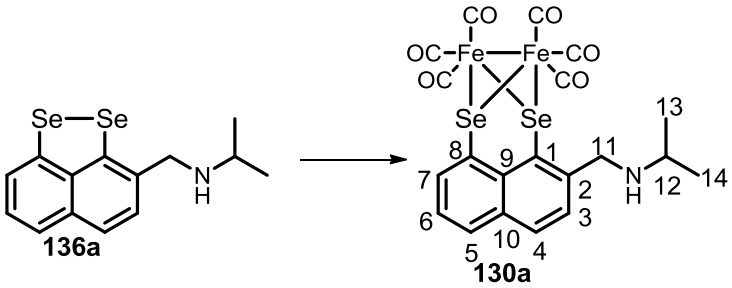

[$Fe_2(CO)_6$(1,8-Se_2-2-CH_2-*Ni*Pr-$C_{10}H_5$)] **130a** is a novel compound, prepared according to a modified literature procedure.[122]

A solution of amine **136a** (0.07 g, 0.20 mmol) and $Fe_3(CO)_{12}$ (0.10 g, 0.20 mmol) in toluene (5.4 mL) was refluxed for 4 hours under argon atmosphere. The mixture was cooled down to room temperature, filtered and concentrated under reduced pressure. The residue was purified by column chromatography (8:2, hexane:EtOAc) to afford complex **130a** as a red solid (0.07 g, 52%). R_f: 0.34 (8:2, hexane:EtOAc); mp: 127-128 °C; λ_{nm} (CH_3CN) 345 ($\varepsilon = 1.7 \times 10^4$ $M^{-1}cm^{-1}$), 253 ($\varepsilon = 1.6 \times 10^4$ $M^{-1}cm^{-1}$); ν_{max} (solid neat, ATR)/cm^{-1} 2056 (CO), 2020 (CO), 1994 (CO), 1980 (CO), 1956 (CO); δ_H (400 MHz, $CDCl_3$): 1.17 (6 H, d, *J* = 6.2 Hz, H-13 and H-

14), 2.92 (1 H, heptd, *J* = 6.2 Hz, H-12), 4.42 (2 H, s, H-11), 7.34 (1 H, t, *J* = 7.6 Hz, H-6), 7.60 (1 H, d, *J* = 8.3 Hz, H-3), 7.88 (1 H, d, *J* = 8.3 Hz, H-4), 7.94 (1 H, br d, *J* = 7.6 Hz, H-7), 8.28 (1 H, dd, *J* = 7.6, 0.7 Hz, H-5); δ_C (101 MHz, $CDCl_3$): 23.2 (2 × CH_3, C-13 and C-14), 48.5 (CH, C-12), 53.2 (CH_2, C-11), 118.7 (C, C-1), 124.8 (C, C-8), 124.8 (CH, C-6), 128.3 (CH, C-3), 129.7 (C, C-9), 131.7 (CH, C-4), 132.9 (CH, C-7), 133.4 (C, C-10), 134.7 (CH, C-5), 145.2 (C, C-2), 208.6 (6 × C, CO); *m/z* (ES^+) 635.8029 ($[M+H]^+$, $C_{20}H_{16}NO_6{}^{56}Fe_2{}^{78}Se^{80}Se$ requires 635.8015), 636 (100%), 632 (20), 633 (14), 634 (54), 635 (31), 637 (24), 638 (88), 639 (20), 640 (27). Anal. calcd. for $C_{20}H_{15}NO_6Fe_2Se_2$: C, 37.83; H, 2.38; N, 2.21; found: C, 37.99; H, 2.24; N, 2.44.

(*E*)-*N*-(4-Methoxyphenyl)-1-(naphtho[1,8-*cd*][1,2]-dithiol-3-yl)methanimine (**137b**)

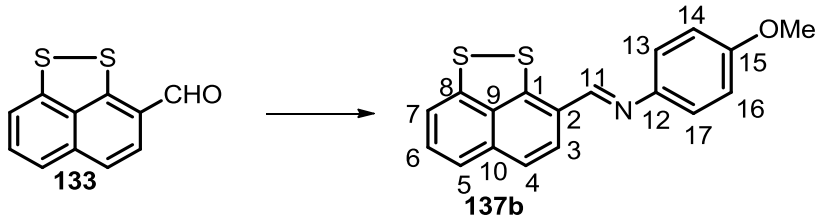

(*E*)-*N*-(4-Methoxyphenyl)-1-(naphtho[1,8-*cd*][1,2]-dithiol-3-yl)methanimine **137b** is a novel compound, prepared according to a literature procedure.[160]

A solution of aldehyde **133** (0.10 g, 0.46 mmol) and 4-methoxyaniline (1.10 g, 9.20 mmol) in dry CH_3CN (10 mL) was refluxed for 22 hours under argon atmosphere. The reaction mixture was allowed to cool down to room temperature and the solvent was removed under reduced pressure. Purification by column chromatography (toluene) gave imine **137b** (0.15 g, 96%) as a bright orange crystalline solid. R_f: 0.52 (toluene); mp: 125-126 °C; λ_{nm} (CH_3CN) 298 (ε = 2.2 × 10^4 $M^{-1}cm^{-1}$), 339 (ε = 2.0 × 10^4 $M^{-1}cm^{-1}$), 464 (ε = 1.0 × 10^4 $M^{-1}cm^{-1}$); ν_{max} (solid neat, ATR)/cm^{-1} 3050, 2996, 2951, 2832, 1600, 1572, 1520, 1503, 1494, 1430, 1316, 1289,

1243, 1205, 1183, 1144, 1105, 1058, 1031, 966, 908, 823, 811, 777, 754, 733; δ_H (400 MHz, $CDCl_3$): 3.85 (3 H, s, OCH_3), 6.97 (2 H, d, J = 8.5 Hz, H-14 and H-16), 7.38 (2 H, d, J = 8.5 Hz, H-13 and H-17), 7.41-7.47 (3 H, m, H-5, H-6 and H-7), 7.49 (1 H, d, J = 8.3 Hz, H-3), 7.57 (1 H, d, J = 8.3 Hz, H-4), 8.78 (1 H, s, H-11); δ_C (101 MHz, $CDCl_3$): 55.7 (CH_3, OCH_3), 114.8 (2 × CH, C-14 and C-16), 117.3 (CH, C-5, C-6 or C-7), 120.4 (CH, C-5, C-6 or C-7), 122.3 (2 × CH, C-13 and C-17), 126.4 (C, C-1), 128.1 (CH, C-4), 128.6 (CH, C-5, C-6 or C-7), 135.7 (C, C-9 or C-10), 135.8 (C, C-9 or C-10), 141.5 (C, C-12), 146.7 (C, C-8), 148.6 (C, C-2), 151.8 (CH, C-11), 158.7 (C, C-15); *m/z* (ES^+) 323.0441 (M^+, $C_{18}H_{13}NOS_2$ requires 323.0439), 323 (100%), 324 (34), 325 (7). Anal. calcd. for $C_{18}H_{13}NOS_2$: C, 66.84; H, 4.05; N, 4.33; found: C, 67.07; H, 3.86; N, 4.49.

[$Fe_2(CO)_6$(1,8-S_2-2-CH=*N*-(4-methoxyphenyl)-$C_{10}H_5$)] (**131b**)

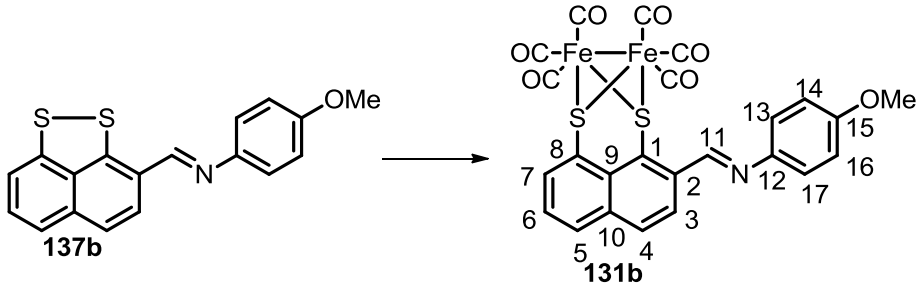

[$Fe_2(CO)_6$(1,8-S_2-2-CH=*N*-(-4-methoxyphenyl)-$C_{10}H_5$)] **131b** is a novel compound, prepared according to a literature procedure.[122]

A solution of imine **137b** (0.10 g, 0.31 mmol) and $Fe_3(CO)_{12}$ (0.16 g, 0.31 mmol) in toluene (8.0 mL) was refluxed for 2 hours under argon atmosphere. The mixture was cooled down to room temperature, filtered and concentrated under reduced pressure. The residue was purified by column chromatography (8:2, hexane:EtOAc) to afford complex **131b** as a bright orange solid (0.14 g, 76%). R_f: 0.75 (8:2, hexane:EtOAc); mp: decomp. above 140 °C; λ_{nm} (CH_3CN) 288 ($\varepsilon = 2.4 \times 10^4$ $M^{-1}cm^{-1}$), 242 ($\varepsilon = 2.2 \times 10^4$ $M^{-1}cm^{-1}$); ν_{max} (solid neat, ATR)/cm^{-1} 2066

(CO), 2024 (CO), 1977 (CO), 1959 (CO); δ_H (400 MHz, $CDCl_3$): 3.88 (3 H, s, OCH_3), 7.02 (2 H, d, *J* = 8.7 Hz, H-14 and H-16), 7.41-7.46 (3 H, m, H-13, H-17 and H-3), 8.00 (2 H, app d, *J* = 8.5 Hz, H-6 and H-7), 8.27 (1 H, d, *J* = 7.3 Hz, H-4), 8.41 (1 H, d, *J* = 8.5 Hz, H-5), 9.79 (1 H, s, H-11); δ_C (101 MHz, $CDCl_3$): 55.7 (CH_3, OCH_3), 114.7 (2 × CH, C-14 and C-16), 123.0 (2 × CH, C-13 and C-17), 125.2 (CH, C-5), 125.8 (C, C-1), 126.3 (CH, C-3), 126.6 (C, C-8), 127.5 (C, C-9), 131.3 (CH, C-6 or C-7), 132.3 (CH, C-6 or C-7), 133.6 (CH, C-4), 135.5 (C, C-10), 139.1 (C, C-2), 144.7 (C, C-12), 156.4 (CH, C-11), 159.2 (C, C-15), 207.5 (6 × C, CO); *m/z* (EI^+) 602.8836 (M^+, $C_{24}H_{13}NO_7S_2{}^{56}Fe_2$ requires 602.8832), 323 (100%), 308 (36), 435 (93, M^+ - 6 CO), 519 (72, M^+ - 3 CO), 603 (24, M^+). Anal. calcd. for $C_{24}H_{13}NO_7S_2Fe_2$: C, 47.79; H, 2.17; N, 2.32; found: C, 47.92; H, 2.13; N, 2.49.

4-Methoxy-*N*-(naphtho[1,8-*cd*][1,2]dithiol-3-ylmethyl)aniline (**137a**)

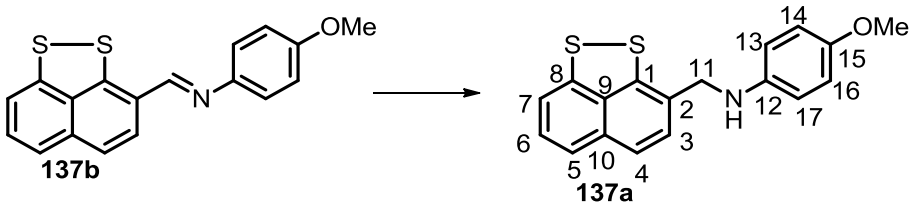

4-Methoxy-*N*-(naphtho[1,8-*cd*][1,2]dithiol-3-ylmethyl)aniline **137a** is a novel compound, prepared according to a literature procedure.[160]

$NaBH_4$ (0.23 g, 6.20 mmol) was added in one portion to a solution of imine **137b** (0.10 g, 0.31 mmol) in a mixture of MeOH:$CHCl_3$ (5:1, 15 mL) and the reaction was then stirred for 3 hours at room temperature and under argon atmosphere. The resulting bright yellow solution was poured into H_2O (51 mL) and the two layers were then separated. The aqueous layer was extracted with CH_2Cl_2 (3 × 20 mL). The combined organic layers were washed with brine (20 ml), dried over $MgSO_4$ and concentrated under reduced pressure to give amine **137a** (0.10 g, 99%) as a pale yellow solid, which was used without further purification. R_f: 0.47 (8:2,

hexane:EtOAc); mp: 95-96 °C; ν_{max} (solid neat, ATR)/cm^{-1} 3356, 2955, 2923, 2832, 1603, 1574, 1543, 1507, 1447, 1367, 1337, 1298, 1254, 1228, 1211, 1180, 1028, 899, 868, 810, 771, 746; δ_H (400 MHz, $CDCl_3$): 3.72 (3 H, s, OCH_3), 4.35 (2 H, s, H-11), 6.62-6.68 (2 H, m, H-14 and H-16), 6.73-6.79 (2 H, m, H-13 and H-17), 7.16 (1 H, dd, *J* = 7.5, 0.6 Hz, H-7), 7.23 (1 H, t, *J* = 7.5 Hz, H-6), 7.28 (1 H, d, *J* = 8.3 Hz, H-3), 7.34 (1 H, br d, *J* = 7.5 Hz, H-5), 7.38 (1 H, d, *J* = 8.3 Hz, H-4); δ_C (101 MHz, $CDCl_3$): 49.3 (CH_2, C-11), 56.0 (CH_3, OCH_3), 115.0 (2 × CH, C-14 and C-16), 115.1 (2 × CH, C-13 and C-17), 116.2 (CH, C-7), 121.2 (CH, C-5), 122.5 (CH, C-4), 127.4 (CH, C-6), 127.6 (CH, C-3), 128.9 (C, C-1), 135.1 (C, C-9), 136.1 (C, C-10), 141.1 (C, C-12), 141.9 (C, C-8), 143.9 (C, C-2), 153.4 (C, C-15); *m/z* (ES$^+$) 326.0527 ([M+H]$^+$, $C_{18}H_{16}NOS_2$ requires 326.0673), 323 (100%), 324 (94), 325 (51), 326 (14).

[$Fe_2(CO)_6$(1,8-S_2-2-CH_2-*N*-(4-methoxyphenyl)-$C_{10}H_5$)] (**131a**)

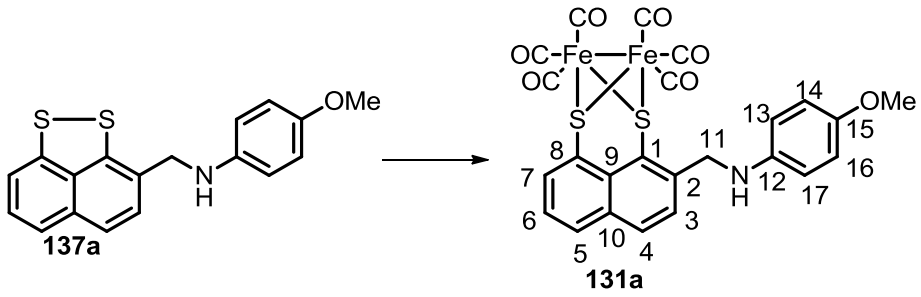

[$Fe_2(CO)_6$(1,8-S_2-2-CH_2-*N*-(-4-methoxyphenyl)-$C_{10}H_5$)] **131a** is a novel compound, prepared according to a modified literature procedure.[122]

A solution of amine **137a** (0.10 g, 0.32 mmol) and $Fe_3(CO)_{12}$ (0.16 g, 0.32 mmol) in toluene (8.2 mL) was refluxed for 4 hours under argon atmosphere. The mixture was cooled down to room temperature, filtered and concentrated under reduced pressure. The residue was purified by column chromatography (8:2, hexane:EtOAc) to afford complex **131a** as a red solid (0.08 mg, 39%). R_f: 0.35 (8:2, hexane:EtOAc); mp: decomp. above 150 °C; λ_{nm} (CH_3CN) 351 (ε = 1.7 × 10^4 M^{-1}cm^{-1}), 253 (ε = 3.0 × 10^4 M^{-1}cm^{-1}); ν_{max} (solid neat, ATR)/cm^{-1} 2064 (CO),

2026 (CO), 2005 (CO), 1988 (CO), 1963 (CO); δ_H (400 MHz, $CDCl_3$): 3.72 (3 H, s, OCH_3), 4.94 (2 H, H-11), 6.61 (2 H, d, *J* = 8.1 Hz, H-14 and H-16), 6.76 (2 H, d, *J* = 8.1 Hz, H-13 and H-17), 7.37 (1 H, t, *J* = 7.8 Hz, H-6), 7.65 (1 H, d, *J* = 8.2 Hz, H-3), 7.91 (1 H, d, *J* = 8.2 Hz, H-4), 7.95 (1 H, d, *J* = 7.8 Hz, H-7), 8.25 (1 H, d, *J* = 7.8 Hz, H-5); δ_C (101 MHz, $CDCl_3$): 49.3 (CH_2, C-11), 55.9 (CH_3, OCH_3), 114.7 (2 × CH, C-14 and C-16), 115.1 (2 × CH, C-13 and C-17), 122.8 (C, C-1), 124.7 (C, C-8), 125.0 (CH, C-6), 126.8 (CH, C-3), 127.4 (C, C-9), 131.4 (CH, C-4), 132.3 (CH, C-7), 133.2 (CH, C-5), 133.7 (C, C-10), 141.7 (C, C-12), 143.9 (C, C-2), 152.7 (C, C-15), 207.7 (6 × C, CO); *m/z* (EI^+) 604.8994 (M^+, $C_{24}H_{15}NO_7{}^{56}Fe_2S_2$ requires 604.8989), 605 (100%), 606 (14). Anal. calcd. for $C_{24}H_{15}NO_7Fe_2S_2$: C, 47.63; H, 2.50; N, 2.31; found: C, 47.75; H, 2.44; N, 2.45.

(*E*)-*N*-(4-Methoxyphenyl)-1-(naphtho[1,8-*cd*][1,2]-diselenol-3-yl)methanimine (**138b**)

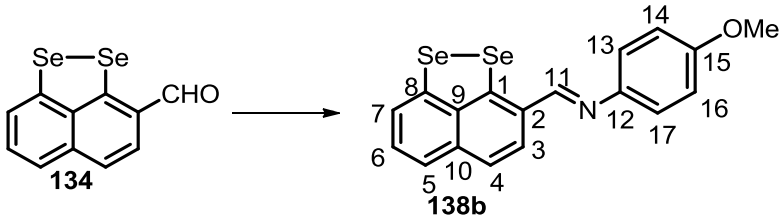

(*E*)-*N*-(4-Methoxyphenyl)-1-(naphtho[1,8-*cd*][1,2]-diselenol-3-yl)methanimine **138b** is a novel compound, prepared according to a modified literature procedure.[162]

A solution of $TiCl_4$ (0.04 mL, 0.39 mmol) in dry CH_2Cl_2 (0.9 mL) was added dropwise over 10 minutes to a solution of aldehyde **134** (0.30 mg, 0.96 mmol), 4-methoxyaniline (0.14 g, 1.15 mmol) and NEt_3 (0.27 mL, 1.92 mmol) in dry CH_2Cl_2 (7.9 mL) at 0 °C and under argon atmosphere. After 30 minutes the reaction mixture was allowed to warm to room temperature and stirred for additional 16 hours. The solvent was removed under reduced pressure and the crude product was then purified by column chromatography (8:2, hexane:EtOAc) to give imine **138b** (0.38 g, 94%) as a bright red crystalline solid. R_f: 0.71 (8:2, hexane:EtOAc); mp:

124-125 °C; λ_{nm} (CH_3CN) 307 (ε = 2.3 × 10^4 $M^{-1}cm^{-1}$), 341 (ε = 1.7 × 10^4 $M^{-1}cm^{-1}$), 492 (ε = 6.6 × 10^3 $M^{-1}cm^{-1}$); ν_{max} (solid neat, ATR)/cm^{-1} 1598, 1562, 1504, 1432, 1419, 1288, 1243, 1182, 1108, 1029, 830, 813, 796, 756, 737; δ_H (400 MHz, $CDCl_3$): 3.86 (3 H, s, OCH_3), 6.96-7.01 (2 H, m, H-14 and H-16), 7.39 (1 H, t, *J* = 7.7 Hz, H-6), 7.41-7.46 (2 H, m, H-13 and H-17), 7.57 (1 H, d, *J* = 7.7 Hz, H-7), 7.61 (1 H, d, *J* = 8.4 Hz, H-3), 7.70 (1 H, d, *J* = 8.4 Hz, H-4), 7.82 (1 H, d, *J* = 7.7 Hz, H-5), 8.93 (1 H, s, H-11); δ_C (101 MHz, $CDCl_3$): 55.7 (CH_3, OCH_3), 115.0 (2 × CH, C-14 and C-16), 121.9 (CH, C-7), 122.9 (2 × CH, C-13 and C-17), 124.6 (CH, C-5), 125.0 (CH, C-4), 127.6 (CH, C-3), 128.1 (CH, C-6), 129.9 (C, C-1), 137.0 (C, C-9), 138.5 (C, C-10), 139.8 (C, C-12), 145.8 (C, C-8), 151.4 (C, C-2), 151.8 (CH, C-11), 159.0 (C, C-15); *m/z* (ES^+) 417.9413 ($[M+H]^+$, $C_{18}H_{14}NO\ ^{78}Se^{80}Se$ requires 417.9414), 420 (100%), 413 (7), 414 (16), 415 (29), 416 (50), 417 (73), 418 (84), 419 (64), 421, (22), 422 (19).

[$Fe_2(CO)_6$(1,8-Se_2-2-CH=*N*(4-methoxyphenyl)-$C_{10}H_5$)] (**132b**)

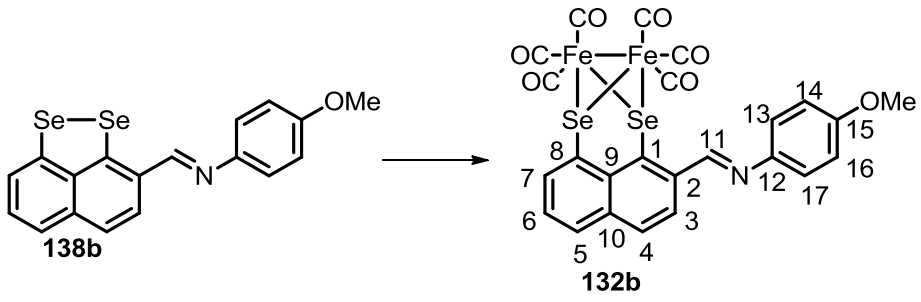

[$Fe_2(CO)_6$(1,8-Se_2-2-CH=*N*(4-methoxyphenyl)-$C_{10}H_5$)] **132b** is a novel compound, prepared according to a modified literature procedure.[122]

A solution of imine **138b** (0.10 g, 0.24 mmol) and $Fe_3(CO)_{12}$ (0.12 g, 0.24 mmol) in toluene (6.2 mL) was refluxed for 1.5 hours under argon atmosphere. The mixture was cooled down to room temperature, filtered and concentrated under reduced pressure. The residue was purified by column chromatography (8:2, hexane:EtOAc) to afford complex **132b** as a red

solid (0.10 g, 58%). R_f: 0.86 (8:2, hexane:EtOAc); mp: decomp. above 140 °C; λ_{nm} (CH_3CN) 290 ($\varepsilon = 2.5 \times 10^4$ $M^{-1}cm^{-1}$), 242 ($\varepsilon = 2.7 \times 10^4$ $M^{-1}cm^{-1}$); ν_{max} (solid neat, ATR)/cm^{-1} 2061 (CO), 2024 (CO), 1978 (CO), 1953 (CO); δ_H (400 MHz, $CDCl_3$): 3.88 (3 H, s, OCH_3), 7.03 (2 H, d, *J* = 8.0 Hz, H-14 and H-16), 7.38-7.43 (3 H, m, H-13, H-17 and H-3), 7.97 (2 H, app d, *J* = 8.5 Hz, H-6 and H-7), 8.32 (1 H, d, *J* = 6.8 Hz, H-4), 8.38 (1 H, d, *J* = 8.5 Hz, H-5), 9.77 (1 H, s, H-11); δ_C (101 MHz, $CDCl_3$): 55.6 (CH_3, OCH_3), 114.6 (2 × CH, C-14 and C-16), 119.5 (C, C-1), 121.0 (C, C-8), 122.9 (2 × CH, C-13 and C-17), 125.3 (CH, C-5), 126.0 (CH, C-3), 129.5 (C, C-9), 131.7 (CH, C-6 or C-7), 132.9 (CH, C-6 or C-7), 135.0 (CH, C-4), 135.1 (C, C-10), 140.2 (C, C-2), 144.4 (C, C-12), 157.4 (CH, C-11), 159.1 (C, C-15), 208.2 (6 × C, CO); *m/z* (EI^+) 696.7180 (M^+, $C_{24}H_{13}NO_7{}^{56}Fe_2{}^{78}Se^{80}Se$ requires 696.7149), 557 (100%), 559 (78), 611 (9), 613 (35), 615 (35). Anal. calcd. for $C_{24}H_{13}NO_7S_2Fe_2$: C, 47.79; H, 2.17; N, 2.32; found: C, 47.92; H, 2.13; N, 2.49.

4-Methoxy-*N*-(naphtho[1,8-*cd*][1,2]diselenol-3-ylmethyl)aniline (**138a**)

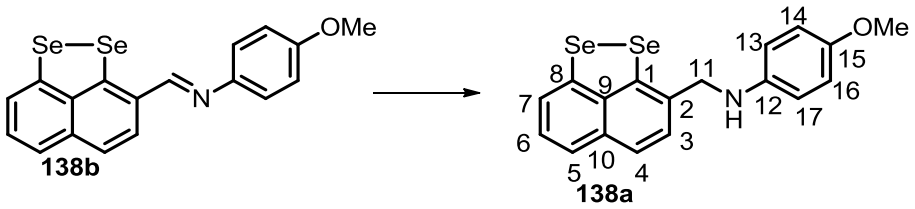

4-Methoxy-*N*-(naphtho[1,8-*cd*][1,2]diselenol-3-ylmethyl)aniline **138a** is a novel compound, prepared according to a literature procedure.[160]

$NaBH_4$ (0.18 g, 4.79 mmol) was added in one portion to a solution of imine **138b** (0.10 g, 0.24 mmol) in a mixture of MeOH:$CHCl_3$ (5:1, 11 mL) and the reaction was then stirred for 3 hours at room temperature under argon atmosphere. The resulting bright orange precipitate was poured into H_2O (51 mL) and the two layers were then separated. The aqueous layer was extracted with CH_2Cl_2 (3 × 20 mL). The combined orgamic layers were washed with brine

(20 mL), dried over $MgSO_4$ and concentrated under reduced pressure to give amine **138a** (0.10 g, 99%) as a pale orange solid, which was used without further purification. R_f: 0.54 (toluene); mp: 126-127 °C; ν_{max} (solid neat, ATR)/cm^{-1} 3382, 2828, 1536, 1508, 1492, 1477, 1439, 1358, 1325, 1292, 1251, 1233, 1209, 1180, 1117, 1034, 917, 864, 813, 773, 753, 714; δ_H (400 MHz, $CDCl_3$): 3.72 (3 H, s, OCH_3), 4.05 (1 H, br s, H-N), 4.37 (2 H, s, H-11), 6.70-6.74 (2 H, m, H-14 and H-16), 6.74-6.78 (2 H, m, H-13 and H-17), 7.17-7.22 (2 H, m, H-6 and H-7), 7.39-7.45 (2 H, m, H-3 and H-5), 7.55 (1 H, d, J = 8.2 Hz, H-4); δ_C (101 MHz, $CDCl_3$): 51.3 (CH_2, C-11), 55.7 (CH_3, OCH_3), 114.9 (2 × CH, C-14 and C-16), 116.2 (2 × CH, C-13 and C-17), 122.4 (CH, C-3 or C-5), 122.9 (CH, C-3 or C-5), 124.9 (CH, C-4), 126.6 (CH, C-6 or C-7), 127.3 (CH, C-6 or C-7), 133.2 (C, C-1), 136.8 (C, C-9), 139.3 (C, C-10), 139.8 (C, C-12), 140.3 (C, C-8), 140.9 (C, C-2), 154.3 (C, C-15); *m/z* (ES$^+$) 418.9512 ([M+H]$^+$, $C_{18}H_{15}NO^{78}Se^{80}Se$ requires 418.9492), 419 (100%), 415 (50), 417 (88), 420 (47), 421 (37), 422 (12), 434 (17), 436 (19).

[$Fe_2(CO)_6$(1,8-Se_2-2-CH_2-*N*(4-methoxyphenyl)-$C_{10}H_5$)] (**132a**)

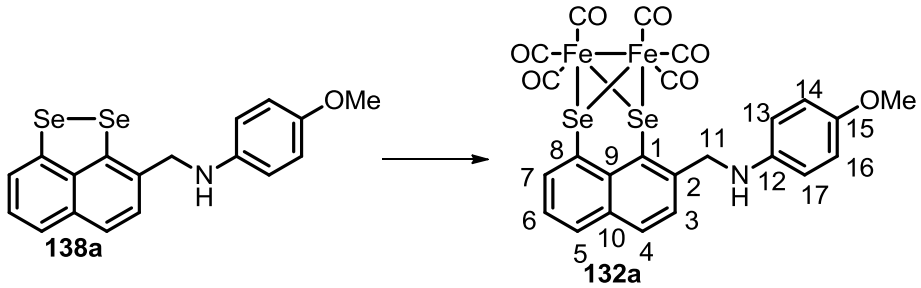

[$Fe_2(CO)_6$(1,8-Se_2-2-CH_2-*N*(4-methoxyphenyl)-$C_{10}H_5$)] **132a** is a novel compound, prepared according to a modified literature procedure.[122]

A solution of amine **138a** (0.10 g, 0.25 mmol) and $Fe_3(CO)_{12}$ (0.13 g, 0.24 mmol) in toluene (6.5 mL) was refluxed for 2.5 hours under argon atmosphere. The mixture was cooled down to room temperature, filtered and concentrated under reduced pressure. The residue was

purified by column chromatography (8:2, hexane:EtOAc) to afford complex **132a** as a red crystalline solid (0.09 g, 52%). R_f: 0.73 (8:2, hexane:EtOAc); mp: decomp. above 150 °C; λ_{nm} (CH_3CN) 346 ($\varepsilon = 1.6 \times 10^4$ $M^{-1}cm^{-1}$), 305 ($\varepsilon = 1.4 \times 10^4$ $M^{-1}cm^{-1}$), 250 ($\varepsilon = 3.4 \times 10^4$ $M^{-1}cm^{-1}$); ν_{max} (solid neat, ATR)/cm^{-1} 2057 (CO), 2020 (CO), 1997 (CO), 1981 (CO), 1958 (CO); δ_H (500 MHz, $CDCl_3$): 3.73 (3 H, s, OCH_3), 4.03 (1 H, N-H), 4.95 (2 H, H-11), 6.61 (2 H, d, *J* = 8.8 Hz, H-14 and H-16), 6.78 (2 H, d, *J* = 8.8 Hz, H-13 and H-17), 7.34 (1 H, t, *J* = 7.6 Hz, H-6), 7.66 (1 H, d, *J* = 8.4 Hz, H-3), 7.86 (1 H, d, *J* = 8.4 Hz, H-4), 7.93 (1 H, d, *J* = 7.6 Hz, H-7), 8.29 (1 H, d, *J* = 7.6 Hz, H-5); δ_C (125 MHz, $CDCl_3$): 51.3 (CH_2, C-11), 56.0 (CH_3, OCH_3), 114.6 (2 × CH, C-14 and C-16), 115.2 (2 × CH, C-13 and C-17), 118.2 (C, C-1), 118.9 (C, C-8), 124.9 (CH, C-6), 126.8 (CH, C-3), 129.7 (C, C-9), 131.9 (CH, C-4), 132.9 (CH, C-7), 133.5 (C, C-10), 134.8 (CH, C-5), 141.9 (C, C-12), 144.3 (C, C-2), 152.8 (C, C-15), 208.5 (6 × C, CO); *m/z* (ES^+) 699.7958 ($[M+H]^+$, $C_{24}H_{16}NO_7{}^{56}Fe_2{}^{78}Se^{80}Se$ requires 699.7964), 702 (100%), 696 (14), 687 (10), 698 (50), 699 (28), 700 (99), 701 (20), 703 (16), 704 (19). Anal. calcd. for $C_{24}H_{15}NO_7Fe_2Se_2$: C, 41.24; H, 2.16; N, 2.00; found: C, 39.09; H, 2.14; N, 2.11.

Naphtho[1,8-*cd*][1,2]dithiole-3-carbaldehyde oxime (**141**)

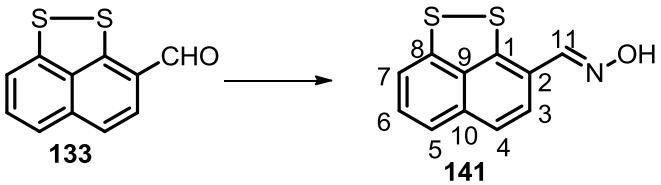

Naphtho[1,8-*cd*][1,2]dithiole-3-carbaldehyde oxime **141** is a novel compound, prepared according to a literature procedure.[170]

$NH_2OH{\cdot}HCl$ (0.03 g, 0.46 mmol) and NaOAc (0.04 g, 0.46 mmol) were added in one portion to a solution of aldehyde **133** (0.05 g, 0.23 mmol) in EtOH (2.5 mL) at room temperature. The

reaction mixture was then refluxed for 2.5 hours. The solvent was removed under reduced pressure, the residue diluted with H_2O (2 mL) and extracted with Et_2O (3 × 3 mL). The combined organic layers were washed with brine (5 mL), dried over $MgSO_4$ and concentrated under reduced pressure to give oxime **141** (0.05 g, 94%) as a bright yellow solid, which was used without further purification. R_f: 0.32 (toluene); mp: 188-189 °C; ν_{max} (solid neat, ATR)/cm^{-1} 3226, 3048, 2974, 1619, 1585, 1529, 1496, 1468, 1430, 1321, 1302, 1215, 1187, 1148, 1059, 977, 946, 908, 867, 808, 743; δ_H (400 MHz, $CDCl_3$): 7.43 (1 H, t, J = 7.7 Hz, H-6), 7.53 (2 H, m, H-7 and H-5), 7.57 (2 H, s, H-4 and H-3), 8.51 (1 H, s, H-11), 11.56 (1 H, s, O-H); δ_C (101 MHz, $CDCl_3$): 116.9 (CH, C-7), 121.0 (CH, C-5), 121.8 (CH, C-4), 128.1 (CH, C-6), 128.7 (CH, C-3), 134.5 (2 × C, C-9 and C-10), 134.8 (C, C-1), 141.1 (C, C-2), 143.9 (C, C-8), 147.0 (CH, C-11); *m/z* (ES^-) 231.9895 ($[M - H]^-$, $C_{11}H_6NOS_2$ requires 231.9891), 232 (100%), 214 (29), 233 (7).

Naphtho[1,8-*cd*][1,2]dithiole-3-carbonitrile (**142**)

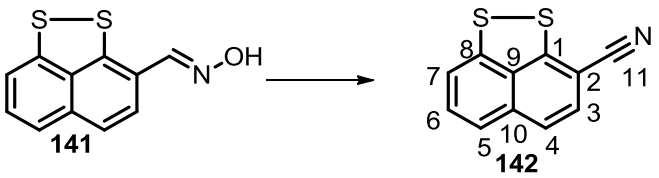

Naphtho[1,8-*cd*][1,2]dithiole-3-carbonitrile **142** is a novel compound, prepared according to a modified by modification of the literature procedure.[171]

NEt_3 (0.12 mL, 0.88 mmol) was added dropwise over 5 minutes to a solution of oxime **141** (0.10 g, 0.44 mmol) in CH_3CN (15 mL) at room temperature. After 10 minutes the reaction mixture was refluxed for 16 hours. The solvent was removed under reduced pressure and the crude product was purified by column chromatography (toluene) to give nitrile **142** (0.08 g, 84%) as a crystalline bright orange solid. R_f: 0.60 (toluene); mp: 134-136 °C; ν_{max} (solid neat,

ATR)/cm^{-1}: 2207, 1597, 1534, 1486, 1432, 1418, 1319, 1191, 1142, 1053, 916, 891, 773, 758; δ_H (400 MHz, $CDCl_3$): 7.29 (1 H, dd, J = 7.7, 0.9 Hz, H-7), 7.32 (2 H, s, H-3 and H-4), 7.39 (1 H, dd, J = 7.7, 0.9 Hz, H-5), 7.41-7.48 (1 H, m, H-6); δ_C (101 MHz, $CDCl_3$): 98.9 (C, C-11), 117.5 (C, C-1), 117.6 (CH, C-7), 121.9 (CH, C-5), 122.6 (CH, C-4), 128.9 (CH, C-3), 130.6 (CH, C-6), 134.5 (C, C-9), 136.7 (C, C-10), 145.8 (C, C-8), 153.3 (C, C-2); *m/z* (ES$^+$) 214.9859 (M^+, $C_{11}H_5NS_2$ requires 214.9863), 215 (100%), 242 (23), 298 (21), 410 (37).

Naphtho[1,8-*cd*][1,2]dithiole-3-carboxilic acid (**139**)

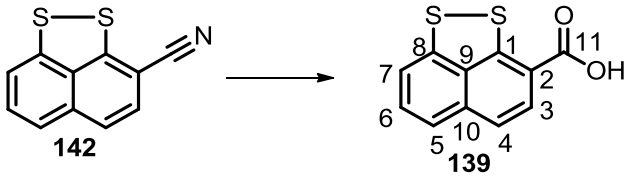

Naphtho[1,8-*cd*][1,2]dithiole-3-carboxilic acid **139** is a novel compound, prepared according to a literature procedure.[172]

To a solution of KOH (0.27 g, 4.88 mmol) in H_2O (0.19 mL) and 1,2-ethanediol (1.4 mL) nitrile **142** (0.07 g, 0.33 mmol) was added in one portion at room temperature and the mixture was then refluxed for 5.5 hours. The reaction mixture was cooled down to room temperature, diluted with H_2O (5 mL) and HCl (5 mL, 1.0 M aq. solution) was added until pH > 1. The dark yellow precipitate was extracted with EtOAc (3 × 5 mL), washed with H_2O (10 mL) and brine (10 mL), dried over $MgSO_4$, filtered and concentrated under reduced pressure. The residue was purified by column chromatography (1:1, hexane:EtOAc) to give carboxylic acid **139** (0.05 g, 63%) as a bright yellow solid. R_f: 0.38 (1:1, hexane:EtOAc); mp: 233-234 °C with decomp.; ν_{max} (solid neat, ATR)/cm^{-1}: 3394, 3319, 1745, 1653, 1623, 1573, 1529, 1495, 1442, 1321, 1221, 1201, 1176, 1163, 909, 813, 793, 745, 704; δ_H (400 MHz, DMSO-d_6): 7.46-7.57 (3 H, m, H-5, H-6 and H-7), 7.55 (1 H, d, J = 8.6 Hz, H-3), 7.76 (0.5 H, s, O-H), 7.94 (1

H, d, *J* = 8.6 Hz, H-4), 8.25 (0.5 H, s, O-H); δ_C (101 MHz, DMSO-d_6) 117.4 (CH, C-5, C-6 or C-7), 120.5 (CH, C-5, C-6 or C-7), 121.7 (C, C-1), 122.3 (CH, C-3), 125.4 (CH, C-4), 129.4 (CH, C-5, C-6 or C-7), 134.9 (C, C-9), 136.0 (C, C-10), 145.4 (C, C-8), 149.8 (C, C-2), 167.8 (C, C-11); *m/z* (ES^+) 233.9810 (M^+, $C_{11}H_6O_2S_2$ requires 233.9809), 234 (100%), 218 (34), 233 (12).

Naphtho[1,8-*cd*][1,2]diselenole-3-carbaldehyde oxime (**143**)

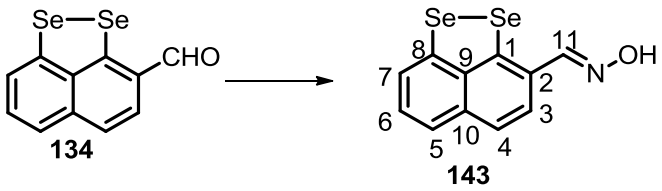

Naphtho[1,8-*cd*][1,2]diselenole-3-carbaldehyde oxime **143** is a novel compound, prepared according to a literature procedure.[170]

$NH_2OH{\cdot}HCl$ (0.07 g, 1.06 mmol) and NaOAc (0.09 g, 1.06 mmol) were added in one portion to a solution of aldehyde **134** (0.11 g, 0.35 mmol) in EtOH (3.1 mL) at room temperature. The reaction mixture was then refluxed for 2.5 hours. The solvent was removed under reduced pressure, the residue diluted with H_2O (3 mL) and extracted with Et_2O (3 × 4 mL). The combined organic layers were washed with brine (5 ml), dried over $MgSO_4$ and concentrated under reduced pressure to give oxime **143** (0.11 g, 99%) as a bright orange solid, which was used without further purification. R_f: 0.32 (toluene); mp: 149-151 °C; ν_{max} (solid neat, ATR)/cm^{-1}: 3408, 1574, 1519, 1491, 1435, 1312, 1266, 1222, 1204, 1183, 1144, 1064, 966, 954, 927, 884, 868, 817, 748; δ_H (400 MHz, $CDCl_3$): 7.36 (1 H, t, *J* = 7.7 Hz, H-6), 7.58 (1 H, d, *J* = 8.3 Hz, H-3), 7.62 (1 H, d, *J* = 7.7 Hz, H-7), 7.73 (2 H, d, *J* = 8.3 Hz, H-4 and H-5), 8.57 (1 H, s, H-11), 12.06 (1H, s, O-H); δ_C (101 MHz, $CDCl_3$): 122.4 (CH, C-7), 122.8 (CH, C-4 or C-5), 123.8 (CH, C-4 or C-5), 123.9 (C, C-1), 127.4 (CH, C-6), 128.3 (CH, C-3), 136.2

(C, C-9), 138.0 (C, C-10), 141.5 (C, C-2), 142.3 (C, C-8), 147.5 (CH, C-11); *m/z* (ES^+) 326.8867 (M^+, $C_{11}H_7NO^{78}Se^{80}Se$ requires 326.8866), 329 (100%), 322 (5), 323 (18), 324 (15), 325 (51), 326 (34), 327 (91), 328 (13), 330 (11), 331 (26).

Naphtho[1,8-*cd*][1,2]diselenole-3-carbaldehyde *O*-benzoyl oxime (**145**)

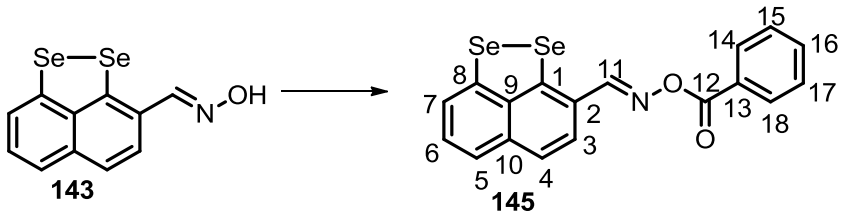

Naphtho[1,8-*cd*][1,2]diselenole-3-carbaldehyde *O*-benzoyl oxime **145** is a novel compound, prepared according to a modified literature procedure.[177]

Benzoyl chloride (0.02 mL, 0.16 mmol) was added dropwise to a solution of oxime **143** (0.05 g, 0.14 mmol) in dry pyridine (2.0 mL) and the reaction mixture was stirred at room temperature for 1 hour. H_2O (2 mL) was added and the crude product was extracted with EtOAc (3 × 4 mL). The combined organic layers were washed with brine (6 mL), dried over $MgSO_4$, concentrated under reduced pressure and purified by column chromatography (toluene) to give **145** (0.04 g, 69%) as a crystalline dark orange solid. R_f: 0.68 (toluene); mp: 122-124 °C; ν_{max} (solid neat, ATR)/cm^{-1}: 2211, 1745, 1599, 1570, 1515, 1490, 1450, 1432, 1309, 1238, 1148, 1078, 1056, 1019, 964, 918, 812, 749, 694, 680; δ_H (400 MHz, $CDCl_3$): 7.39 (1 H, t, *J* = 7.8 Hz, H-6), 7.45 (1 H, d, *J* = 8.4 Hz, H-3), 7.52 (2 H, t, *J* = 7.7 Hz, H-15 and H-17), 7.56 (1 H, d, *J* = 7.8 Hz, H-7), 7.62 (1 H, d, *J* = 8.4 Hz, H-4), 7.62-7.64 (1 H, m, H-16), 7.68 (1 H, d, *J* = 7.8 Hz, H-5), 8.17-8.19 (2 H, m, H-14 and H-18), 8.97 (1 H, s, H-11); δ_C (101 MHz, $CDCl_3$): 122.6 (CH, C-7), 122.8 (C, C-1), 123.2 (CH, C-5), 124.2 (CH, C-4), 128.2 (C, C-13), 128.4 (CH, C-6), 128.8 (2 × CH, C-14 and C-18), 129.0 (CH, C-16), 130.0 (2 × CH, C-14 and C-18), 133.8 (CH, C-3), 137.9 (C, C-9), 138.9 (C, C-10), 144.7 (C, C-8),

147.7 (C, C-2), 153.0 (CH, C-11), 162.9 (C, C-12); *m/z* (ES^+) 430.9120 (M^+, $C_{18}H_{11}NO_2{}^{78}Se^{80}Se$ requires 430.9128), 433 (100%), 427 (13), 429 (47), 431 (96), 435 (21).

Naphtho[1,8-*cd*][1,2]diselenole-3-carbaldehyde *O*-pivaloyl oxime (**146**)

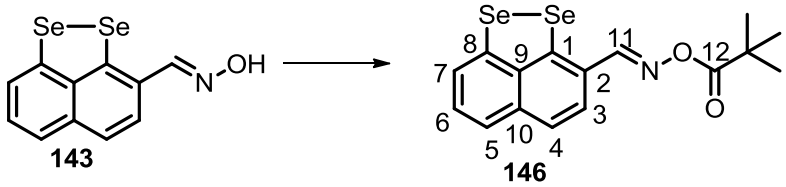

Naphtho[1,8-*cd*][1,2]diselenole-3-carbaldehyde *O*-pivaloyl oxime **146** is a novel compound, prepared according to a literature procedure.[178]

Dry NEt_3 (0.04 mL, 0.37 mmol) was added dropwise to a solution of oxime **143** (0.09 g, 0.29 mmol) in dry CH_2Cl_2 (3.6 mL) at room temperature and under argon atmosphere. The mixture was stirred for 5 minutes and pivaloyl chloride (0.05 mL, 0.37 mmol) was added dropwise over 10 minutes. After 2 hours t.l.c. analysis indicated total consumption of the starting material and CH_2Cl_2 (3 mL) was then added. The organic layer was washed with H_2O (3 × 5 mL), brine (5 mL), then dried over $MgSO_4$, concentrated under reduced pressure and purified by column chromatography (toluene) to give **146** (0.12 g, 99%) as a crystalline orange solid. R_f: 0.68 (toluene); mp: 127-129 °C; ν_{max} (solid neat, ATR)/cm^{-1}: 1757, 1570, 1515, 1477, 1459, 1432, 1397, 1364, 1309, 1265, 1223, 1210, 1185, 1148, 1097, 1022, 964, 953, 938, 916, 898, 812, 750; δ_H (400 MHz, $CDCl_3$): 1.39 (9 H, s, *t*Bu), 7.38 (1 H, t, *J* = 7.6 Hz, H-6), 7.41 (1 H, d, *J* = 8.4 Hz, H-3), 7.55 (1 H, d, *J* = 7.6 Hz, H-7), 7.61 (1 H, d, *J* = 8.4 Hz, H-4), 7.66 (1 H, d, *J* = 7.6 Hz, H-5), 8.83 (1 H, s, H-11); δ_C (101 MHz, $CDCl_3$) 27.5 (3 × CH_3, *t*Bu), 38.6 (C, *t*Bu), 122.6 (CH, C-7), 122.9 (C, C-1), 123.2 (CH, C-5), 124.2 (CH, C-4), 128.4 (CH, C-6), 129.0 (CH, C-3), 137.9 (C, C-9), 140.0 (C, C-10), 144.7 (C, C-8), 147.6 (C, C-2), 152.3

(CH, C-11), 174.3 (C, C-12); *m/z* (ES^+) 410.9439 (M^+, $C_{16}H_{15}NO_2{}^{78}Se^{80}Se$ requires 410.9441), 410.9 (100%), 410 (37), 411 (8), 412 (20).

6.4 Experimental section: Chapter 4

5,10,15,20-Tetraphenylporphyrin (**159**)

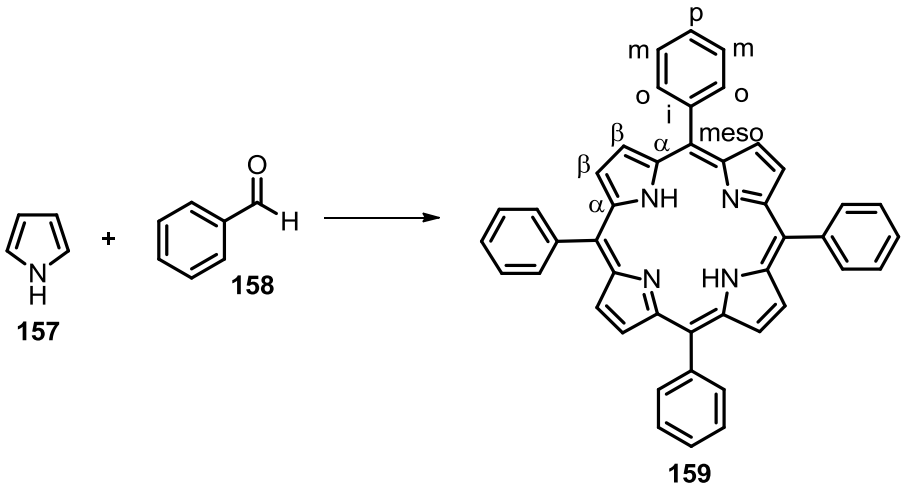

5,10,15,20-Tetraphenylporphyrin **159** was prepared according to a literature procedure.[212] Freshly distilled pyrrole **157** (4.10 mL, 59.6 mmol) and benzaldehyde **158** (6.10 mL, 59.6 mmol) were added to boiling propionic acid (225 mL). After refluxing for 1 hour, the reaction mixture was cooled down to room temperature and filtered. The remaining solid was washed first with methanol (2 × 20 mL) and then with hot H_2O (3 × 20 mL). The resulting purple crystalline solid was collected and dried *in vacuo* to yield porphyrin **159** (1.80 g, 5%). δ_H (400 MHz, $CDCl_3$): –2.79 (2 H, s, inner H-N), 7.68-7.83 (12 H, m, H-*m*,*p*), 8.22 (8 H, dd, H-*o*), 8.85 (8 H, s, H-β); δ_C (101 MHz, $CDCl_3$): 120.3 (4 × C, C-meso), 126.8 (8 × CH, C-*m*), 127.9 (4 × CH, C-*p*), 130.5-132.0 (8 × CH, br peak, C-β), 134.7 (8 × CH, C-*o*), 142.3 (4 × C, C-*i*), C-α did not appear in the recorded ^{13}C NMR spectrum; *m/z* (ES^+) 615.2540 ($[M+H]^+$, $C_{44}H_{31}N_4$ requires 615.2549), 615 (100%), 616 (55), 617 (21).

Literature data: [212,243] Anal. Calcd for $C_{44}H_{30}N_4$: C, 85.90; H, 4.92; N, 9.12. Found: C, 85.16; H, 4.99; N, 9.60. ^1H NMR (400 MHz, $CDCl_3$): 8.88 (s, 8H, pyrr-H), 8.25 (brs, 8H, *o*-

Ph), 7.77 (brs, 12H, *p* & *m*-Ph), -2.69 (s, 2H, NH). Positive-ion mode ESIMS m/z $C_{44}H_{30}N_4H^+$: 615. UV-vis (CH_2Cl_2) λ_{max} (nm): 417.

5,10,15-Triphenyl-20-(4-nitro)phenyl porphyrin (**160**)

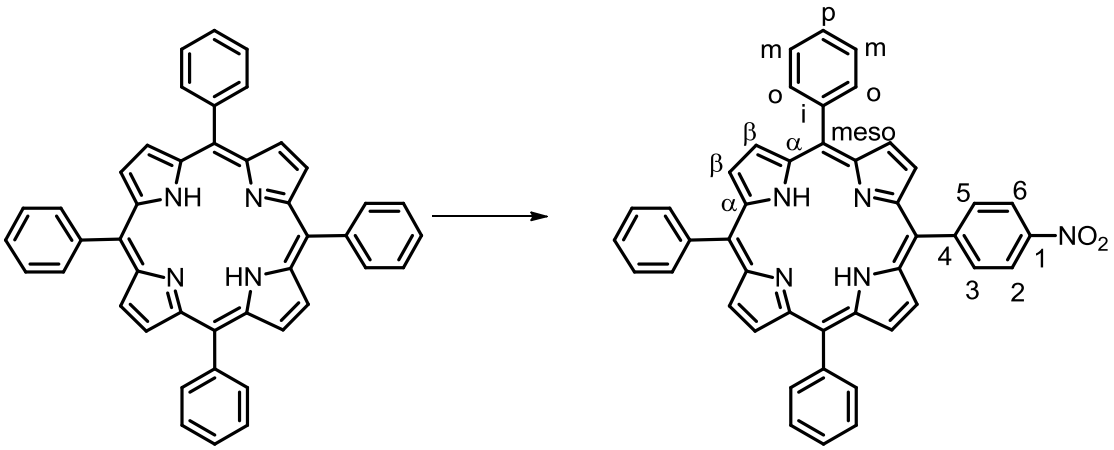

159 **160**

5,10,15-Triphenyl-20-(4-nitro)phenyl porphyrin **160** [214] was prepared according to a literature procedure.[213]

A solution $NaNO_2$ (0.11 g, 1.63 mmol) in trifluoroacetic acid (8.0 mL) was added dropwise to a solution of porphyrin **159** (1.00 g, 1.63 mmol) in TFA (41 mL) at room temperature and under argon atmosphere. The reaction mixture was stirred for additional 2 hours then poured into H_2O (300 mL) and extracted with CH_2Cl_2 (4 × 150 mL). The combined organic layers were washed with Na_2CO_3 (2 × 200 mL of a saturated aq. solution), H_2O (50 mL) and brine (50 mL), dried over Na_2SO_4, filtered and concentrated under reduced pressure. Purification by column chromatography (2:3, CH_2Cl_2:hexane) yielded nitro-substituted porphyrin **160** as a purple crystalline solid (0.61 g, 57%). δ_H (400 MHz, $CDCl_3$): –2.77 (2 H, s, inner H-N), 7.72-7.85 (9 H, m, H-*m,p*), 8.23 (6 H, dd, *J* = 7.4, 1.5 Hz, H-*o*), 8.40 (2 H, d, *J* = 8.6 Hz, H-3 and H-5), 8.63 (2 H, d, *J* = 8.6 Hz, H-2 and H-6), 8.75 (2 H, d, *J* = 4.8 Hz, H-*β*), 8.87-8.92 (6 H, m, H-β); δ_C (101 MHz, $CDCl_3$): 116.8 (C, C-meso), 120.3 (C, C-meso), 120.8 (C, C-meso),

121.2 (C, C-meso), 122.0 (2 × CH, C-3 and C-5), 126.9 (6 × CH, C-*m*), 128.0 (3 × CH, C-*p*), 131.0-132.0 (8 × CH, br peak, C-*β*), 134.7 (6 × CH, C-*o*), 135.3 (2 × CH, C-2 and C-6), 142.0 (C, C-*i*), 142.1 (C, C-*i*), 142.3 (C, C-*i*), 147.8 (C, C-4), 149.4 (C, C-1), C-*α* did not show in the recorded ^{13}C NMR spectrum; *m/z* (ES^+) 660.2409 ($[M+H]^+$, $C_{44}H_{30}N_5O_2$ requires 660.2400), 660 (100%), 661 (56), 682 (24).

Literature data: [214] mp > 250 °C; ^{1}H NMR ($CDCl_3$, 600 MHz), δ (ppm): − 2.79 (s, 2H, inner-NH), 7.75–7.81 (m, 9H, Ph-CH), 8.21 (d, *J* = 7.2 Hz, 6H, Ph-CH), 8.40 (d, *J* = 8.4 Hz, 2H, Ph-CH), 8.64 (d, *J* = 8.4 Hz, 2H, Ph-CH), 8.74 (d, *J* = 4.2 Hz, 2H, Por-CH), 8.86–8.90 (m, 6H, Por-CH); IR(KBr): υ 3446(s), 2918(w), 2850(w), 1596(w), 1517(w), 1472(w), 1392(w), 1345(m), 1073(w), 840(w), 798(m), 706(m) cm^{-1}; MS (EI): 660 (M + 1, 58%); UV–Vis (CH_2Cl_2) λmax/nm (log ε) 418 (2.28), 514 (1.28), 549 (2.98), 588 (4.85), 645 (4.18).

5,10,15-Triphenyl-20-(4-amino)phenyl porphyrin (**161**)

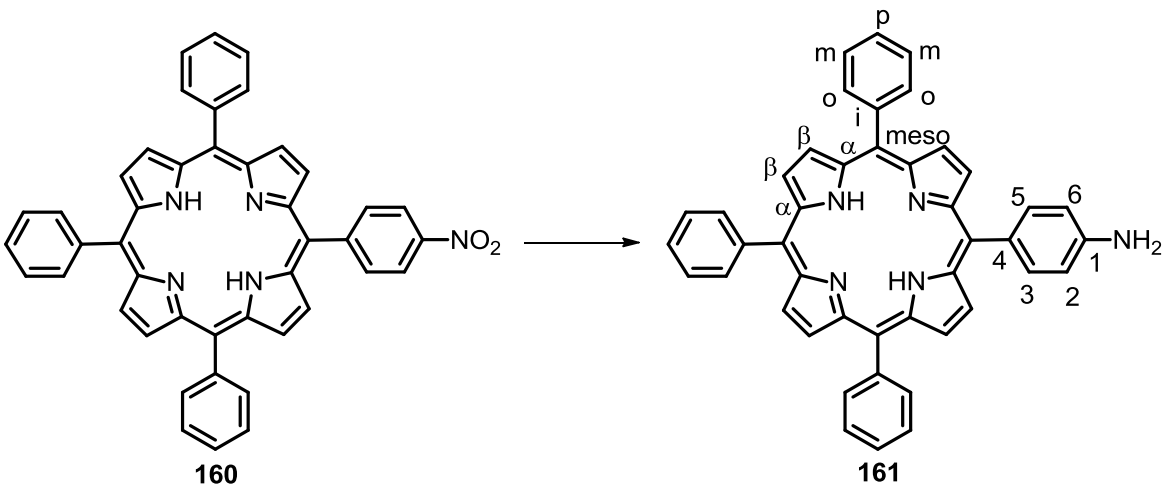

160 161

5,10,15-Triphenyl-20-(4-amino)phenyl porphyrin **161** was prepared according to a literature procedure.[214]

Nitro substituted porphyrin **160** (0.29 g, 0.44 mmol) was dissolved in conc. HCl (9.3 mL) at room temperature and under argon atmosphere. $SnCl_2$ (0.30 g, 1.33 mmol) was added in one portion to the solution, which was then heated to 65 °C and stirred for 2 hours. The reaction mixture was cooled down to room temperature and poured into ice-cold H_2O (34 mL). Conc. NH_4OH was added dropwise until pH ~ 8 and the crude product was extracted with $CHCl_3$ (4 × 50 mL) washed with H_2O (30 mL) and brine (30 mL), dried over Na_2SO_4, filtered and concentrated under reduced pressure. Purification by column chromatography (CH_2Cl_2) gave amino-substituted **161** as a purple crystalline solid (0.27 g, 97%. δ_H (400 MHz, $CDCl_3$): –2.73 (2 H, s, inner H-N), 3.98 (2 H, s, H_2-N), 7.04 (2 H, d, *J* = 8.3 Hz, H-3 and H-5), 7.69-7.84 (9 H, m, H-*m,p*), 8.01 (2 H, d, *J* = 8.3 Hz, H-2 and H-6), 8.25 (6 H, dd, *J* = 7.4, 1.7 Hz, H-*o*), 8.87 (6 H, s, H-β), 8.97 (2 H, d, *J* = 4.8 Hz, H-β); δ_C (101 MHz, $CDCl_3$): 113.6 (2 × CH, C-3 and C-5), 119.9 (C, C-meso), 120.1 (2 × C, C-meso), 121.0 (C, C-meso), 126.8 (6 × CH, C-*m*), 127.8 (3 × CH, C-*p*), 130.0-132.0 (8 × CH, br peak, C-β), 132.6 (C, C-4), 134.7 (6 × CH, C-*o*), 135.9 (2 × CH, C-2 and C-6), 142.4 (2 × C, C-*i*), 142.5 (C, C-*i*), 146.2 (C, C-1), C-α did not appear in the recorded ^{13}C NMR spectrum; *m/z* (ES^+) 630.2657 ($[M+H]^+$, $C_{44}H_{32}N_5$ requires 630.2658), 652 (100%), 630 (69), 653 (54).

Literature data: [214] ^1H NMR ($CDC1_3$) 6 8.95 (d, 2 H, J = 5.0 Hz, α-pyrrole), 8.84 (d, 2 H, J = 5.0 Hz, β-pyrrole), 8.83 (s, 2 H, α-pyrrole), 8.22 (m, 6 H, ortho triphenyl), 8.00 (d, 2 H, J = 8.2 Hz, 4-aminophenyl), 7.76 (m, 9 H, meta/para triphenyl), 7.06 (d, 2 H, J = 8.3 Hz, 4-aminophenyl), 4.02 (s, 2 H, amino), -2.73 (s, 2 H pyrrole NH); MS (70 eV, m/e 629, (5% parent), 212 (0.5), 207 (45), 149 (100). Anal. Calcd for $C_{44}H_{31}N_5$: C, 83.9; H, 4.93; N, 11.12. Found C, 84.13; H, 4.86; N, 11.20.

Zinc 5,10,15-triphenyl-20-(4-amino)phenyl porphyrin (**164**)

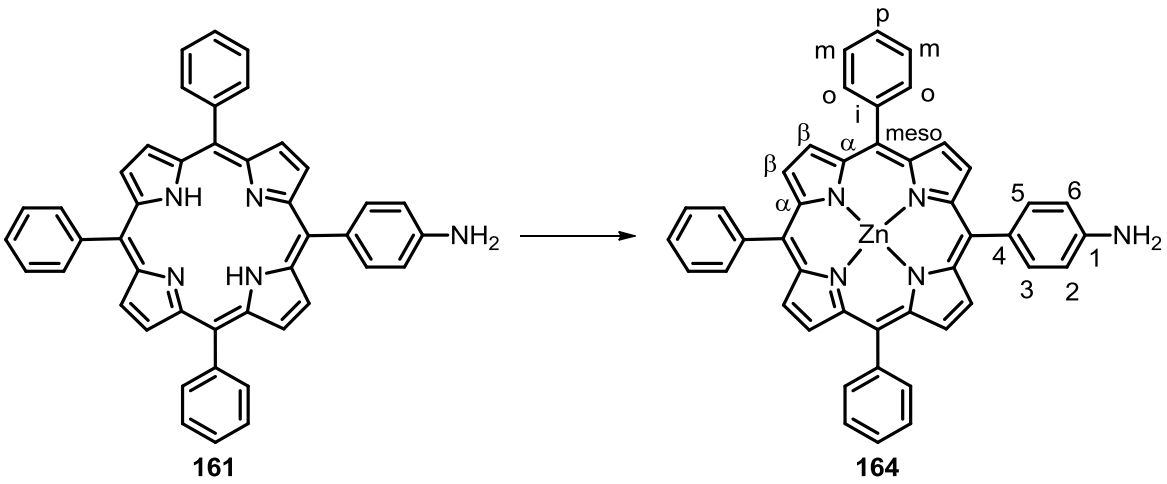

Zinc 5,10,15-triphenyl-20-(4-amino)phenyl porphyrin **164** [244] was prepared according to a modified literature procedure.[217]

$Zn(OAc)_2 \cdot 2H_2O$ (0.07 g, 0.33 mmol) was added in one portion to a solution of amino-substituted porphyrin **161** (0.19 g, 0.30 mmol) in a mixture of CH_2Cl_2:MeOH (1:5, 18 mL) at room temperature and the reaction mixture was then heated under reflux for 5.5 hours. The solvent was removed under reduced pressure and the crude product was purified by column chromatography (CH_2Cl_2) to give zinc amine-substituted porphyrin **164** as a purple crystalline solid (0.16 g, 77%). R_f: 0.67 (CH_2Cl_2); mp: >300 °C; λ_{nm} (CH_2Cl_2) 423 ($\varepsilon = 6.3 \times 10^5$ $M^{-1}cm^{-1}$), 558 ($\varepsilon = 9.2 \times 10^3$ $M^{-1}cm^{-1}$), 599 ($\varepsilon = 4.7 \times 10^3$ $M^{-1}cm^{-1}$), 593 ($\varepsilon = 1.7 \times 10^3$ $M^{-1}cm^{-1}$), 648 ($\varepsilon = 1.7 \times 10^3$ $M^{-1}cm^{-1}$); ν_{max} (solid neat, ATR)/cm^{-1} 3367, 1596, 1520, 1483, 1439, 1338, 1203, 1177, 1067, 991, 792, 750, 717, 698; δ_H (400 MHz, DMSO-d_6): 5.50 (2 H, s, H_2-N), 6.99 (2 H, d, J = 8.1 Hz, H-3 and H-5), 7.79-7.82 (9 H, m, H-*m*,*p*), 7.85 (2 H, d, J = 8.1 Hz, H-2 and H-6), 8.13-8.28 (6 H, m, H-*o*), 8.77 (6 H, s, H-*β*), 8.94 (2 H, d, J = 4.6 Hz, H-β); δ_C (101 MHz, DMSO-d_6): 112.3 (2 × CH, C-3 and C-5), 119.7 (C, C-meso), 120.1 (2 × C, C-meso), 122.1 (C, C-meso), 126.6 (6 × CH, C-*m*), 127.4 (3 × CH, C-*p*), 130.0 (C, C-4), 131.2 (2 × CH, C-*β*), 131.4 (2 × CH, C-*β*), 131.5 (2 × CH, C-*β*), 132.0 (2 × CH, C-*β*), 134.2 (6 ×

CH, C-*o*), 135.3 (2 × CH, C-2 and C-6), 142.9 (3 × C, C-*i*), 148.1 (C, C-1), 149.0 (2 × C, C-*α*), 149.2 (2 × C, C-*α*), 149.3 (2 × C, C-*α*), 150.1 (2 × C, C-*α*); *m/z* (ES^+) 692.1776 ($[M+H]^+$, $C_{44}H_{30}N_5{}^{64}Zn$ requires 692.1793), 692 (100%), 691 (45), 693 (68), 694 (69), 695 (20), 696 (44), 697 (17). To the best of our knowledge no literature data are reported.

(*E*)-*N*-(TPP)-naphtho[1,8-*cd*][1,2]dithiol-3-yl)methanimine (**162b**)

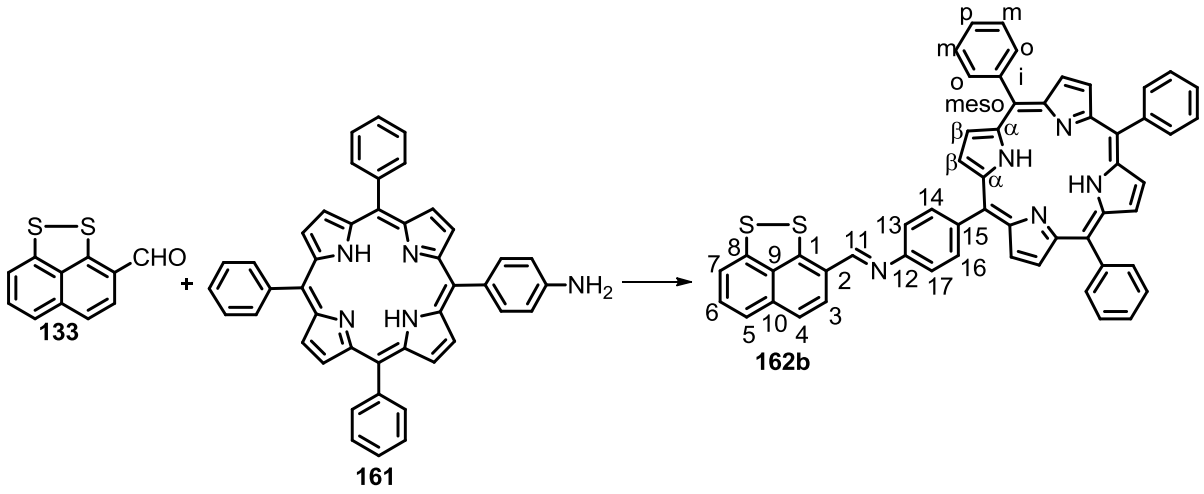

(*E*)-*N*-(TPP)-naphtho[1,8-*cd*][1,2]dithiol-3-yl)methanimine **162** is a novel compound, prepared according to a literature procedure.[216]

$La(OTf)_3$ (0.04 g, 0.06 mmol) was added in one portion to a solution of amine **161** (0.10 g, 0.16 mmol) and aldehyde **133** (0.05 g, 0.24 mmol) in dry toluene (20 mL) at room temperature and under argon atmosphere. The reaction mixture was refluxed for 8 hours. Toluene was evaporated under reduced pressure and the residue purified by column chromatography (CH_2Cl_2) to give imine **162b** as a purple crystalline solid (0.12 g, 87%). R_f: 0.96 (CH_2Cl_2); mp: >300 °C; ν_{max} (solid neat, ATR)/cm^{-1} 3315, 1595, 1568, 1517, 1471, 1435, 1401, 1348, 1315, 1209, 1185, 1169, 1155, 1145, 1072, 1058, 981, 964, 905, 876, 795, 749, 720, 698; δ_H (400 MHz, $CDCl_3$): –2.73 (2 H, s, inner H-N), 7.16-7.22 (1 H, m, Ar*H*), 7.25-7.29 (1 H, m, Ar*H*), 7.50-7.54 (3 H, m, Ar*H*), 7.56 (2 H, d, *J* = 8.4 Hz, H-14 and H-16),

7.71 (2 H, d, *J* = 8.4 Hz, H-13 and H-17), 7.73 (9 H, m, H-*m,p*), 8.22-8.27 (4 H, m, H-*o*), 8.27-8.32 (2 H, m, H-*o*), 8.87 (4 H, s, H-*β*), 8.89 (2 H, d, *J* = 4.8 Hz, H-*β*), 8.95 (2 H, d, *J* = 4.8 Hz, H-*β*), 9.15 (1 H, s, H-11); δ_C (101 MHz, $CDCl_3$): 117.5 (CH), 119.7 (C, C-meso), 120.0 (2 × CH, C-14 and C-16), 120.4 (3 × C, C-meso), 120.5 (CH), 122.5 (CH), 126.2 (C), 126.8 (6 × CH, C-*m*), 127.9 (3 × CH, C-*p*), 129.5 (CH), 129.0 (CH), 130.0-132.0 (8 × CH, br peak, C-*β*), 134.7 (6 × CH, C-*o*), 135.8 (2 × CH, C-13 and C-17), 136.0 (2 × C), 140.6 (C, C-15), 142.3 (3 × C, C-*i*), 146.9 (C), 148.0 (C, C-12), 149.5 (C), 154.3 (CH, C-11), C-*α* did not appear in the recorded ^{13}C NMR spectrum; *m/z* (ES^+) 830.2416 ($[M+H]^+$, $C_{55}H_{36}N_5S_2$ requires 830.2412), 830 (100%), 831 (64), 832 (26), 833 (9).

Zinc (*E*)-*N*-(TPP)-naphtho[1,8-*cd*][1,2]dithiol-3-yl)methanimine (**165b**)

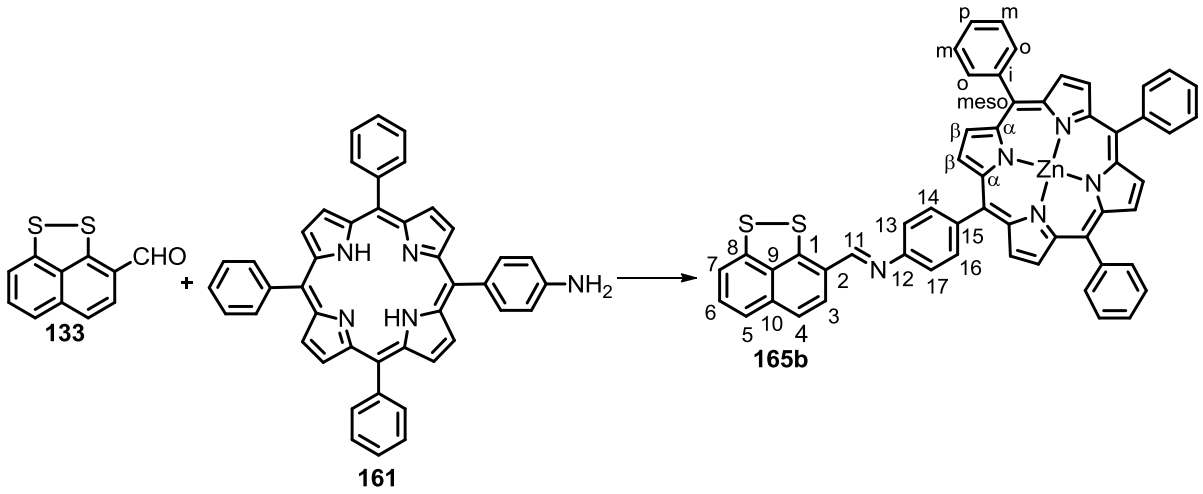

Zinc (*E*)-*N*-(TPP)-naphtho[1,8-*cd*][1,2]dithiol-3-yl)methanimine **165b** is a novel compound, prepared according to a modified literature procedure.[202]

$Zn(OAc)_2 \cdot 2H_2O$ (0.04 g, 0.17 mmol) was added in one portion to a solution of amine **161** (0.06 g, 0.09 mmol) in pyridine (13 mL) at room temperature and under argon atmosphere and the reaction mixture was refluxed for 1 hour and after this time t.l.c. analysis (CH_2Cl_2) indicated total consumption of **161** and formation of zinc amine **164**. The reaction mixture

was cooled down to room temperature, added with aldehyde **133** (0.02 g, 0.09 mmol) and more $Zn(OAc)_2 \cdot 2H_2O$ (0.08 g, 0.35 mmol) and refluxed for 2 days. Pyridine was evaporated under reduced pressure and the residue purified by column chromatography (CH_2Cl_2) to give zinc imine **165b** as a bright purple opaque solid (0.08 g, 96%). R_f: 0.93 (CH_2Cl_2); mp: decomp. above 200 °C; ν_{max} (solid neat, ATR)/cm^{-1} 3051, 3020, 2988, 2970, 2921, 1596, 1569, 1518, 1485, 1438, 1339, 1316, 1206, 1170, 1069, 994, 967, 907, 814, 750, 729, 715, 701; δ_H (400 MHz, DMSO-d_6): 7.58-7.63 (1 H, m, H-6), 7.69 (2 H, t, *J* = 7.6 Hz, H-5 and H-7), 7.77 (1 H, d, *J* = 8.4 Hz, H-3), 7.79-7.92 (9 H, m, H-*m*,*p*), 7.93 (2 H, d, *J* = 8.2 Hz, H-14 and H-16), 8.00 (1 H, *J* = 8.5 Hz, H-4), 8.17-8.23 (6 H, m, H-*o*), 8.29 (2 H, d, *J* = 8.2 Hz, H-13 and H-17), 8.78 (4 H, s, H-*β*), 8.81 (2 H, d, *J* = 4.6 Hz, H-*β*), 8.90 (2 H, d, *J* = 4.6 Hz, H-*β*), 9.55 (1 H, s, H-11); δ_C (101 MHz, DMSO-d_6) 117.7 (CH, C-7), 119.7 (2 × C, C-meso), 119.9 (2 × CH, C-14 and C-16), 120.4 (2 × C, C-meso), 120.7 (CH, H-5), 122.6 (CH, H-3), 126.4 (C, C-1), 126.6 (6 × CH, C-*m*), 127.5 (3 × CH, C-*p*), 129.1 (CH, H-4), 129.2 (CH, H-6), 131.7 (4 × CH, C-*β*), 131.7 (4 × CH, C-*β*), 134.2 (6 × CH, C-*o*), 134.9 (2 × C, C-9 and C-10), 135.4 (2 × CH, C-13 and C-17), 141.2 (C, C-15), 142.8 (3 × C, C-*i*), 145.8 (C, C-12), 146.8 (C, C-8), 147.8 (C, C-2), 149.3 (8 × C, C-*α*), 155.4 (CH, C-11); *m/z* (ES^+) 892.1575 ($[M+H]^+$, $C_{55}H_{34}N_5S_2{}^{64}Zn$ requires 892.1547), 893 (100%), 891 (84), 892 (96), 894 (87), 895 (80), 896 (63), 897 (51), 898 (30), 900 (24).

TPP-*N*-(naphtho[1,8-*cd*][1,2]dithiol-3-ylmethyl)aniline (162a)

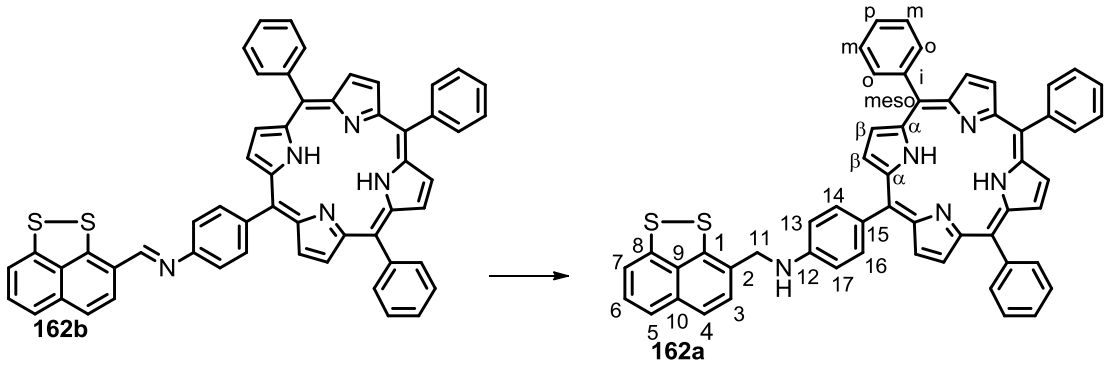

TPP-*N*-(naphtho[1,8-*cd*][1,2]dithiol-3-ylmethyl)aniline **162a** is a novel compound, prepared according to a literature procedure.[215]

$NaBH_3CN$ (0.36 mL of a 1 M solution in THF, 0.36 mmol) was added dropwise to a solution of imine **162b** (0.05 g, 0.06 mmol) in a mixture of THF:MeOH (1:1, 19 mL) at room temperature, followed by glacial AcOH (1 drop). The reaction mixture was heated under reflux for 8.5 hours under argon atmosphere. The mixture was cooled down to room temperature, the solvent evaporated under reduced pressure and the residue purified by column chromatography (8:2, CH_2Cl_2:hexane to CH_2Cl_2) to give amine **162a** as a purple crystalline solid (0.03 g, 65%). R_f: 0.95 (CH_2Cl_2); mp: 183-184 °C; λ_{nm} (CH_2Cl_2) 256 ($\varepsilon = 1.8 \times 10^4$ $M^{-1}cm^{-1}$), 421 ($\varepsilon = 1.4 \times 10^5$ $M^{-1}cm^{-1}$), 517 ($\varepsilon = 6.6 \times 10^3$ $M^{-1}cm^{-1}$), 556 ($\varepsilon = 3.8 \times 10^3$ $M^{-1}cm^{-1}$), 593 ($\varepsilon = 1.7 \times 10^3$ $M^{-1}cm^{-1}$), 648 ($\varepsilon = 1.7 \times 10^3$ $M^{-1}cm^{-1}$); ν_{max} (solid neat, ATR)/cm^{-1} 3316, 3051, 2954, 2921, 2853, 1607, 1543, 1519, 1470, 1440, 1402, 1349, 1326, 1298, 1254, 1221, 1183, 1156, 1072, 1054, 1032, 965, 877, 840, 815, 797, 723, 700; δ_H (400 MHz, $CDCl_3$): –2.74 (2 H, s, inner H-N), 4.44 (1 H, s, H-N), 4.58 (2 H, s, H-11), 7.01 (2 H, d, *J* = 8.4 Hz, H-14 and H-16), 7.23 (1 H, dd, *J* = 7.7, 0.4 Hz, H-7), 7.31 (1 H, t, *J* = 7.7 Hz, H-6), 7.40 (1 H, dd, *J* = 7.7, 0.4 Hz, H-5), 7.43 (1 H, d, *J* = 8.4 Hz, H-3), 7.46 (1 H, d, *J* = 8.4 Hz, H-4), 7.69-7.82 (9 H, m, H-*m*,*p*), 8.01 (2 H, d, *J* = 8.4 Hz, H-13 and H-17), 8.22 (6 H, dd, *J* = 7.5, 1.5 Hz, H-*o*), 8.83 (6 H, s, H-*β*), 8.93 (2 H, d, *J* = 4.4 Hz, H-*β*); δ_C (101 MHz,

$CDCl_3$): 48.5 (CH_2, C-11), 111.9 (2 × CH, C-14 and C-16), 116.3 (CH, C-7), 119.7 (C, C-meso), 120.1 (2 × C, C-meso), 120.9 (C, C-meso), 121.5 (CH, C-5), 122.7 (CH, C-4), 126.8 (9 × CH, C-*m*,*p*), 127.7 (CH, C-3), 127.8 (CH, C-6), 128.5 (C, C-1), 130.0-132.5 (8 × CH, br peak, C-β), 132.8 (C, C-15), 134.7 (6 × *C*H, C-*o*), 135.3 (C, C-9), 135.9 (2 × CH, C-13 and C-17), 136.0 (C, C-10), 142.1 (C, C-8), 142.4 (C, C-*p*), 142.4 (2 × C, *C*-*p*), 143.9 (C, C-12), 147.1 (C, C-2), C-α did not appear in the recorded ^{13}C NMR spectrum; *m/z* (ES^+) 832.2565 ($[M+H]^+$, $C_{55}H_{38}N_5S_2$ requires 832.2569), 830 (100%), 831 (70), 832 (93), 833 (47), 834 (17).

$[Fe_2(CO)_6(1,8\text{-}S_2\text{-}2\text{-}CH_2\text{-}N(ZnTPP)\text{-}C_{10}H_5)]$ (155a)

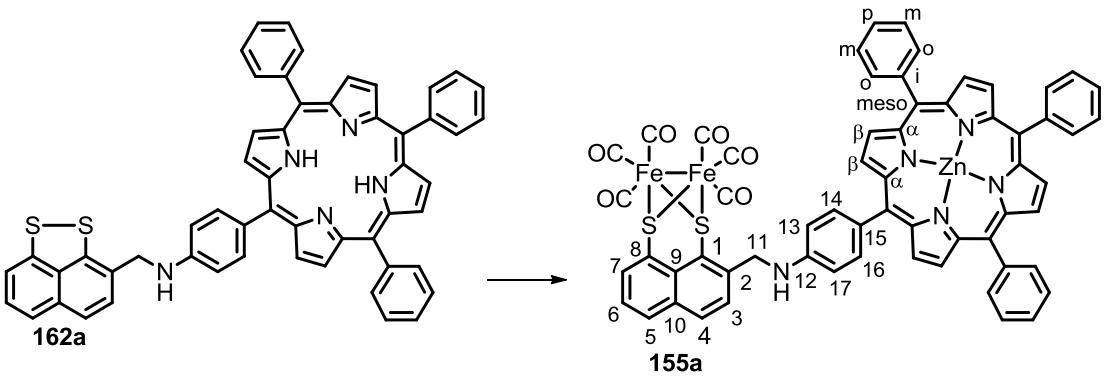

$[Fe_2(CO)_6(1,8\text{-}S_2\text{-}2\text{-}CH_2\text{-}N(ZnTPP)\text{-}C_{10}H_5)]$ **155a** is a novel compound, prepared according to a modified literature procedure.[122]

To a solution of amine **162a** (0.02 g, 0.02 mmol) in $CHCl_3$ (11 mL) $Zn(OAc)_2 \cdot 2H_2O$ (0.01 g, 0.06 mmol) was added in one portion at room temperature and the reaction mixture was heated under reflux for 1 hour. After this time t.l.c. analysis (7:3, CH_2Cl_2:hexane) indicated total consumption of **162a**. The reaction mixture was cooled down to room temperature and the solvent evaporated under reduced pressure. The residue was dissolved in toluene (11 mL) and $Fe_3(CO)_{12}$ (0.01 g, 0.03 mmol) was added in one portion at room temperature and the reaction mixture was refluxed for 3 hours under argon atmosphere. The solvent was removed

under reduced pressure and the residue purified by column chromatography to give complex **155a** as a bright purple opaque solid (0.008 g, 33%). R_f: 0.90 (CH_2Cl_2); mp: > 300 °C; λ_{nm} (CH_2Cl_2) 254 (ε = 5.8 ×10^4 $M^{-1}cm^{-1}$), 308 (ε = 3.3 × 10^4 $M^{-1}cm^{-1}$), 355 (ε = 3.5 × 10^4 $M^{-1}cm^{-1}$), 422 (ε = 4.5 × 10^5 $M^{-1}cm^{-1}$), 550 (ε = 2.6 × 10^4 $M^{-1}cm^{-1}$), 593 (ε = 7.3 × 10^3 $M^{-1}cm^{-1}$); ν_{max} (solid neat, ATR)/cm^{-1} 3413, 3051, 3021, 2922, 2852, 2072 (CO), 2032 (CO), 1982 (CO), 1596, 1519, 1485, 1440, 1339, 1205, 1179, 1069, 993, 831, 795, 749, 718, 699; δ_H (400 MHz, $CDCl_3$): 4.83 (2 H, s, H-11), 6.67 (2 H, d, *J* = 7.7 Hz, H-14 and H-16), 7.39 (1 H, t, *J* = 7.4 Hz, H-6), 7.69 (1 H, d, *J* = 8.6 Hz, H-3), 7.71-7.79 (9 H, m, H-*m*,*p*), 7.94 (2 H, d, *J* = 7.7 Hz, H-13 and H-17), 7.99 (2 H, d, *J* = 7.8, H-4 and H-7), 8.22 (6 H, d, *J* = 6.3 Hz, H-*o*), 8.27 (1 H, d, *J* = 7.4 Hz, H-5), 8.85-9.03 (8 H, m, H-*β*); δ_C (101 MHz, $CDCl_3$): 48.4 (CH_2, C-11), 111.5 (2 × CH, C-14 and C-16), 120.9 (C, C-meso), 121.1 (2 × C, C-meso), 121.9 (C, C-meso), 123.3 (C, C-1), 124.8 (C, C-8), 125.2 (CH, C-6), 126.7 (6 × CH, C-*m*), 127.1 (CH, C-3), 127.6 (3 × CH, C-*p*), 131.4 (CH, C-7), 131.9 (2 × CH, C-*β*), 132.0 (4 × CH, C-*β*), 132.0 (2 × CH, C-*β*), 132.4 (CH, C-4), 132.8 (C, C-15), 133.3 (CH, C-5), 133.9 (2 × C, C-9 and C-10), 134.6 (6 × *C*H, C-*o*), 135.6 (2 × CH, C-13 and C-17), 143.1 (3 × C, C-*i*), 143.3 (C, C-12), 146.6 (C, C-2), 150.2 (2 × C, C-*α*), 150.3 (4 × C, C-*α*), 150.9 (2 × C, C-*α*), 207.7 (6 × C, CO); *m/z* (ES^+) 1173.0010 (M^+, $C_{61}H_{35}N_5O_6S_2{}^{56}Fe_2{}^{64}Zn$ requires 1173.0019), 1175 (100%), 1171 (10), 1172 (14), 1173 (84), 1174 (98), 1176 (80), 1177 (69), 1178 (49), 1179 (26), 1180 (13), 1181 (6). Anal. calcd. for $C_{61}H_{35}N_5O_6S_2Fe_2Zn$: C, 62.34; H, 3.00; N, 5.96; found: C, 62.45; H, 3.70; N, 5.72.

(*E*)-*N*-(TPP)-naphtho[1,8-*cd*][1,2]diselenol-3-yl)methanimine (**163b**)

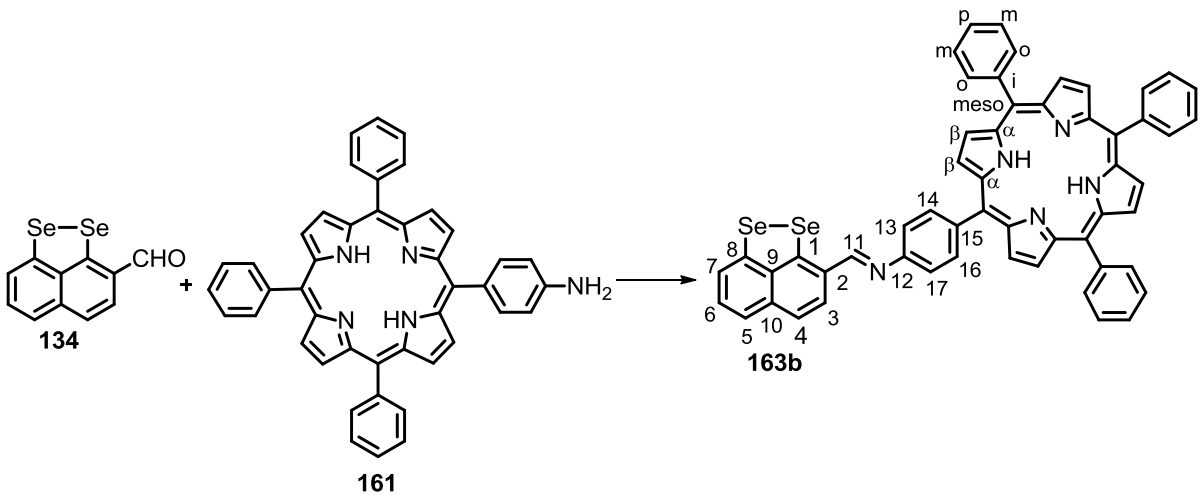

(*E*)-*N*-(TPP)-naphtho[1,8-*cd*][1,2]diselenol-3-yl)methanimine **163b** is a novel compound prepared according to a literature procedure.[216]

$La(OTf)_3$ (0.01 g, 0.01 mmol) was added in one portion to a solution of amine **161** (0.03 g, 0.05 mmol) and aldehyde **134** (0.03 g, 0.08 mmol) in toluene (6.7 mL) at room temperature and under argon atmosphere. The reaction mixture was heated under reflux and stirred for an additional 8 hours. Toluene was removed under reduced pressure and the residue purified by column chromatography (CH_2Cl_2) to give imine **163b** as a purple crystalline solid (0.04 g, 75%). R_f: 0.95 (CH_2Cl_2); mp: > 300 °C; ν_{max} (solid neat, ATR)/cm^{-1} 3318, 2921, 2852, 1561, 1509, 1472, 1418, 1348, 1319, 1205, 1185, 1171, 1000, 982, 965, 847, 794, 763, 752, 719; δ_H (400 MHz, $CDCl_3$): –2.74 (2 H, s, inner H-N), 7.48 (1 H, t, *J* = 7.7 Hz, H-6), 7.65 (1 H, d, *J* = 7.7 Hz, H-7), 7.73-7.82 (11 H, m, H-*m*,*p*, H-3 and H-4), 7.87 (2 H, d, *J* = 8.2 Hz, H-14 and H-16), 7.90 (1 H, d, *J* = 7.7 Hz, H-5), 8.20-8.26 (6 H, m, H-*o*), 8.32 (2 H, d, *J* = 8.2 Hz, H-13 and H-17), 8.86 (4 H, s, H-*β*), 8.89 (2 H, d, *J* = 4.8 Hz, H-*β*), 8.94 (2 H, d, *J* = 4.8 Hz, H-*β*), 9.33 (1 H, s, C-11); δ_C (101 MHz, $CDCl_3$): 120.3 (2 × CH, C-14 and C-16), 120.4 (4 × C, C-meso), 122.1 (CH, C-7), 124.7 (CH, C-5), 125.3 (CH, C-4), 126.9 (6 × CH, C-*m*), 127.9 (3 × CH, C-*p*), 128.0 (CH, C-3), 128.4 (C, C-1), 128.5 (CH, C-6), 129.2 (C, C-9), 130.0 (C, C-10),

131.0-132.0 (8 × CH, br peak, C-*β*), 136.7 (6 × CH, C-*o*), 136.0 (2 × CH, C-13 and C-17), 137.4 (C, C-8), 141.1 (C, C-15), 142.3 (3 × C, C-*i*), 146.2 (C, C-2), 146.3 (C, C-12), 154.0 (CH, C-11), C-*α* did not appear in the recorded ^{13}C NMR spectrum; *m/z* (ES^+) 924.1331 ($[M+H]^+$, $C_{55}H_{36}N_5{}^{78}Se^{80}Se$ requires 924.1309), 926 (100%), 920 (15), 921 (21), 922 (52), 923 (57), 924 (82), 927 (54), 928 (37), 929 (12). Anal. calcd. for $C_{55}H_{35}N_5Se_2$: C, 71.51; H, 3.82; N, 7.58; found: C, 70.38; H, 4.01; N, 7.09.

Zinc (*E*)-*N*-(TPP)-naphtho[1,8-*cd*][1,2]diselenol-3-yl)methanimine (**166b**)

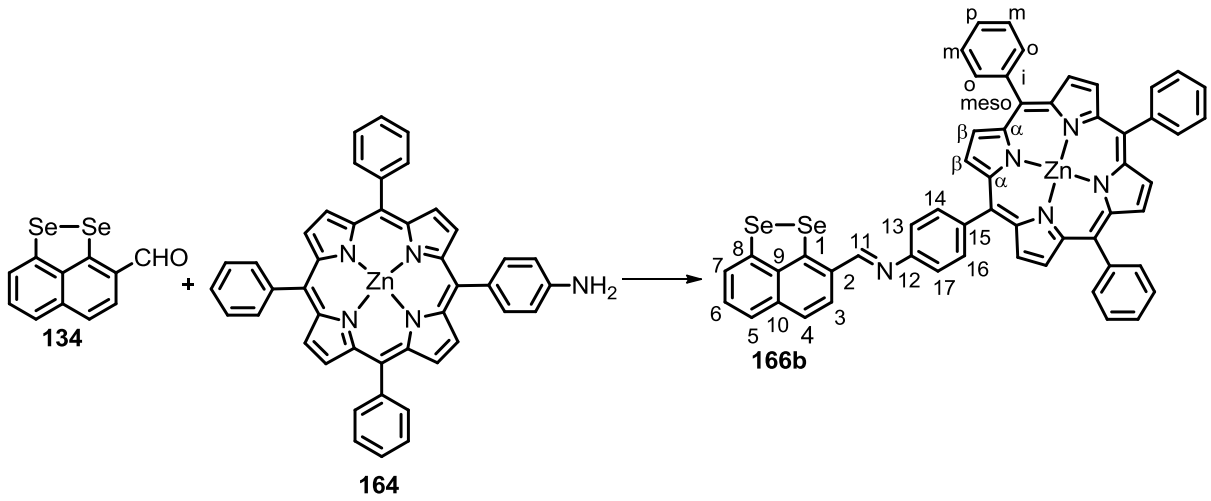

Zinc (*E*)-*N*-(TPP)-naphtho[1,8-*cd*][1,2]diselenol-3-yl)methanimine **166b** is a novel compound, prepared according to a modified literature procedure.[202]

$Zn(OAc)_2{\cdot}2H_2O$ (0.07 g, 0.33 mmol) was added in one portion to a solution of amine **164** (0.05 g, 0.07 mmol) and aldehyde **134** (0.02 g, 0.07 mmol) in pyridine (10 mL) at room temperature and under argon atmosphere and the reaction mixture was refluxed for 2 days. The reaction mixture was cooled down to room temperature and the solvent was evaporated under reduced pressure. The residue was purified by column chromatography (CH_2Cl_2) to give imine **166b** as a bright purple opaque solid (0.04 g, 61%). R_f: 0.94 (CH_2Cl_2); mp: decomp. above 230 °C; ν_{max} (solid neat, ATR)/cm^{-1} 3658, 2988, 2971, 2920, 2902, 1596,

1561, 1507, 1483, 1430, 1416, 1394, 1338, 1229, 1204, 1184, 1171, 1141, 1067, 1001, 993, 955, 814, 750, 728, 698; δ_H (400 MHz, DMSO-d_6): 7.54 (1 H, t, *J* = 8.0 Hz, H-6), 7.70 (1 H, d, *J* = 8.0 Hz, H-7), 7.80-7.82 (9 H, m, H-*m*,*p*), 7.93-7.97 (2 H, m, H-3 and H-4), 8.02 (1 H, d, *J* = 8.0 Hz, H-5), 8.05 (2 H, d, *J* = 8.2 Hz, H-14 and H-16), 8.18-8.21 (6 H, m, H-*o*), 8.32 (2 H, d, *J* = 8.2 Hz, H-13 and H-17), 8.79 (4 H, s, H-β), 8.82 (2 H, d, *J* = 4.6 Hz, H-β), 8.91 (2 H, d, *J* = 4.6 Hz, H-β), 9.81 (1 H, s, C-11); δ_C (101 MHz, DMSO-d_6): 119.5 (C, C-meso), 120.2 (2 × CH, C-14 and C-16), 120.4 (2 × C, C-meso), 122.0 (CH, C-7), 123.9 (C, C-meso), 124.3 (CH, C-3 or C-4), 124.9 (CH, C-3 or C-4), 126.6 (6 × CH, C-*m*), 127.5 (3 × CH, C-*p*), 128.5 (CH, C-6), 128.7 (CH, C-5), 130.3 (C, C-1), 131.5 (2 × CH, C-β), 131.6 (4 × CH, C-β), 131.7 (2 × CH, C-β), 134.1 (6 × CH, C-*o*), 135.6 (2 × CH, C-13 and C-17), 136.8 (C, C-9), 137.8 (C, C-10), 141.6 (C, C-15), 142.7 (3 × C, C-*i*), 145.2 (C, C-8), 145.3 (C, C-2), 149.2 (2 × C, C-α), 149.3 (4 × C, C-α), 149.5 (2 × C, C-α), 150.7 (C, C-12), 155.3 (CH, C-11); *m/z* (ES^+) 988.0437 ($[M+H]^+$, $C_{55}H_{34}N_5{}^{64}Zn\,{}^{80}Se_2$ requires 988.0436), 988 (100%), 983 (31), 984 (48), 985 (66), 986 (82), 987 (86), 989 (78), 990 (73), 991 (56), 992 (43), 993 (24).

Decachloro-1,4-dihydronaphthalene (**176**)

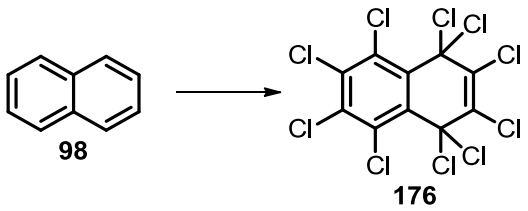

98 **176**

Decachloro-1,4-dihydronaphthalene **176** [224c)] was prepared according to a modified literature procedure.[225]

A solution of naphthalene **98** (1.00 g, 7.80 mmol) and S_2Cl_2 (0.30 mL, 3.70 mmol) in freshly distilled SO_2Cl_2 (25 mL) was added dropwise over a period of 30 minutes to a boiling

solution of $AlCl_3$ (0.25 g, 1.90 mmol) in freshly distilled SO_2Cl_2 (75 mL). The reaction mixture was then refluxed and stirred for 5 hours; during this time the volume solvent was kept constant by adding more distilled SO_2Cl_2. SO_2Cl_2 was distilled off, the residue diluted carefully with H_2O (50 mL) and solid $NaHCO_3$ was slowly added until no more gas evolution took place. The solution was then acidified with concentrated HCl, extracted with $CHCl_3$ (3 × 30 mL), washed with H_2O (50 mL) and brine (50 mL), dried over $MgSO_4$, filtered and concentrated under reduced pressure. The residue was purified by column chromatography (hexane) to give **176** as a yellow solid (2.80 g, 76%). Mp: 209-210 °C with decomp.; ν_{max} (solid neat, ATR)/cm^{-1}1644, 1520, 1356, 1287, 1245, 1222, 1142, 944, 737; δ_C (101 MHz, $CDCl_3$): 79.7 (2 × C, Ar*H*), 130.9 (2 × C, Ar*H*), 132.6 (2 × C, Ar*H*), 134.1 (2 × C, Ar*H*), 139.1 (2 × C, Ar*H*). *m/z* (EI^+) 473.6839 (M^+, $C_{10}{}^{35}Cl_8{}^{37}Cl_2$ requires 473.6826), 474 (100%), 470 (10), 472 (58), 474 (4), 476 (91), 478 (49), 480 (16).

Literature data: [224c)] M.p. 205-210 °C (decomp.). ^{13}C NMR (270 MHz, $CDCl_3$): δ 139.1, 134.2, 132.6, 131.0, 79.7. Found C 25.3; Cl 74.7. Calc. for $C_{10}Cl_{10}$: C 25.3; Cl 74.7. UV [hexane] (log ε)]: 231 (5.9), 211 (5.9) nm.

Octachloronaphthalene (**175**)

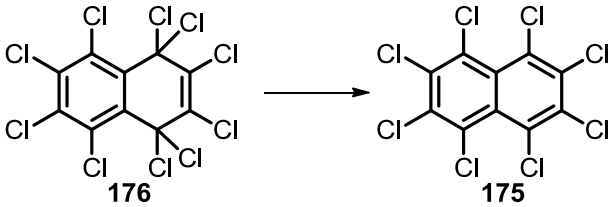

176 **175**

Octachloronaphthalene **175** was prepared according to a modified literature procedure.[224c)]

A solution of **176** (0.81 g, 1.71 mmol) in freshly distilled diisopropyl ether (102 mL) was refluxed for 2 days. After this time the solvent was evaporated under reduced pressure and the

residue purified by column chromatography (hexane) to give **175** as bright yellow solid (0.53 g, 76%). Mp: 198-200 °C; ν_{max} (solid neat, ATR)/cm^{-1} 1517, 1405, 1353, 1286, 1246, 1163, 1058, 961, 857, 782, 755; δ_C (101 MHz, $CDCl_3$): 129.1 (4 × C), 129.8 (4 × C), 136.4 (2 × C). *m/z* (EI$^+$) 403.7442 (M^+, $C_{10}{}^{35}Cl_6{}^{37}Cl_2$ requires 403.7449), 404 (100%), 400 (36), 402 (93), 403 (11), 405 (12), 406 (66), 407 (9), 408 (27).

Literature data: [224c)] M.p. 198.5-200 °C. MS; *m/z* (re lab., %): 400 (37, M^+), 402 (95), 404 (100), 406 (68), 419 (7), 330 [35, $(M-2Cl)^+$], 260 [32, $(M-4Cl)^+$], 225 [13, $(M-5Cl)^+$], 190 [39, $(M-2Cl)^+$], 155 [17, $(M-2Cl)^+$]. ^{13}C NMR (270 MHz, $CDCl_3$): δ 135.4, 129.8, 129.1 Hz. UV [hexane] (log ε)]: 276 (5.1) nm.

Chloro-heptakis(isopropylthio)naphthalene (**181**)

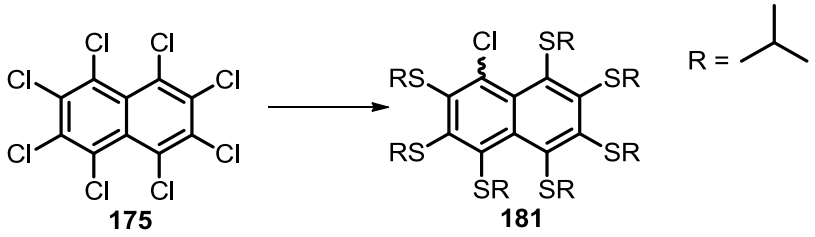

Chloro-heptakis(isopropylthio)naphthalene **181** is a novel compound prepared according to a modified literature procedure.[226]

A solution of sodium propanethiolate (0.11 g, 1.11 mmol) in dry DMF (1.2 mL) was added dropwise to a solution of **175** (0.05 g, 0.12 mmol) in dry DMF (4.0 mL) at room temperature and the reaction mixture was then stirred for 4 hours under argon atmosphere. After this time the t.l.c. analysis indicated complete consumption of the starting material, the reaction mixture was then diluted with H_2O (10 mL) and extracted with $CHCl_3$ (3 × 10 mL). The combined organic layers were washed with brine, dried over Na_2SO_4 and concentrated under reduced pressure. The residue was purified by column chromatography (hexane to 9.5:0.5,

hexane:EtOAc) to give chloro-substituted **181**, as a bright red crystalline solid (0.06 g). R_f: 0.59 (9.5:0.5, hexane:EtOAc); mp: 150-151 °C; ν_{max} (solid neat, ATR)/cm^{-1} 1444, 1379, 1362, 1243, 1221, 1152, 1048, 963, 910, 879, 766, 732; δ_H (400 MHz, $CDCl_3$): 0.76-0.99 (18 H, m, Isopropyl) 1.10-1.36 (24 H, m, *i*Pr), 2.90-3.42 (3 H, m, *i*Pr), 3.66-4.14 (4 H, m, *i*Pr); δ_C (101 MHz, $CDCl_3$) 22.6-22.9 (14 × CH_3), 40.4-42.2 (7 × CH), 133.1 (C), 134.5 (C), 134.8 (C), 135.4 (C), 137.1 (C), 138.7 (2 × C), 141.8 (C), 144.1 (C), 145.9 (C); *m/z* (ES^+) 681.1654 ($[M+H]^+$, $C_{31}H_{50}S_7{}^{35}Cl$ requires 681.1646), 681 (100%). The exact position of the chlorine on the naphthalene ring could not be verified experimentally.

Perchlorocoronene (**173**)

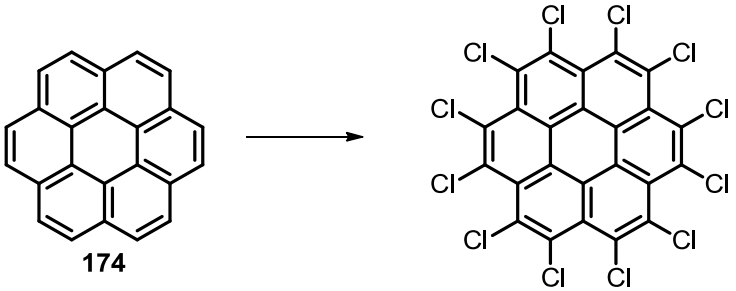

174 **173**

Perchlorocoronene **173** [224b)] was prepared according to a modified literature procedure.[225] Coronene **174** (1.00 g, 3.33 mmol) was added to a solution of S_2Cl_2 (0.13 mL, 1.86 mmol) in freshly distilled SO_2Cl_2 (30 mL). When the mixture became homogeneous, it was added dropwise over a period of 40 minutes to a refluxing solution of $AlCl_3$ (0.13 g, 0.97 mmol) in freshly distilled SO_2Cl_2 (90 mL). The reaction mixture was refluxed for 9 hours, with periodic addition of SO_2Cl_2 (every hour) to maintain the reaction volume, and then stirred overnight at room temperature.This procedure was reapeted for additional two days. SO_2Cl_2 was distilled off, the residue diluted carefully with H_2O (80 mL) and solid $NaHCO_3$ slowly added until no more gas took place. The mixture was then heated at 80 °C with stirring for 1 hour and

acidified with concentrated HCl. The solid precipitate was collected by suction filtration and washed with H_2O and MeOH. Purification by recrystallization from chlorobenzene gave **177** as a bright yellow solid (1.54 g, 65%). mp: > 300 °C; ν_{max} (solid neat, ATR)/cm^{-1}1546, 1453, 1409, 1305, 1254, 965, 924, 770, 722; *m/z* (ES^+) 736.6050 ($[M+Na]^+$, $C_{24}{}^{35}Cl_9{}^{37}Cl_3Na$ requires 736.6072), 751 (100%), 734 (20), 735 (25), 736 (32), 737 (56), 738 (26), 739 (46), 748 (32), 749 (45), 750 (67), 752 (47), 753 (84), 754 (27), 755 (21).

Literature data: [228] m.p. > 300 °C; ν_{max} (KBr, select) 1545 (s), 1452 (w), 1408 (w), 1304 (w), 1257 (s), 968 (s), 924 (w), 771 (m), 723 (m); *m/z* 714, M^+.

Dodecakis(*p*-methylphenylthio)coronene (**182**)

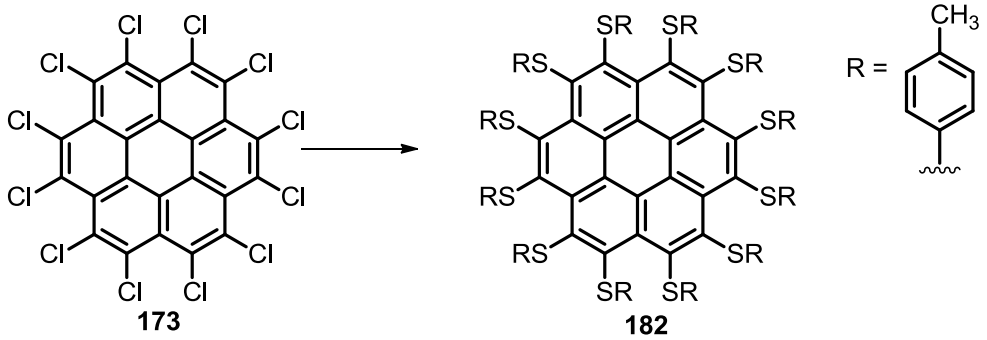

Dodecakis(*p*-methylphenylthio)coronene **182** was prepared according to a literature procedure.[224f)]

NaH (0.04 g, 1.85 mmol) was added to a vigorously stirred solution of *p*-toluenethiol (0.21 g, 19.3 mmol) in DMI (4.0 mL) at 0 °C and under argon atmosphere and the reaction mixture was then bubbled with argon for 30 minutes. Perchlorocoronene **173** (0.05 g, 0.07 mmol) was added in one portion and the resulting mixture was stirred for 4 days at room temperature and under argon atmosphere. Toluene (150 mL) and Na_2CO_3 (150 mL of a saturated aq. solution) were added. The two layers were separated and the organic layer was washed with Na_2CO_3 (2

× 50 mL of a saturated aq. solution), then with H_2O (50 mL) and brine (50 mL), dried over $MgSO_4$, filtered and concentrated under reduced pressure. The deep red crystalline residue was triturated with a mixture of toluene:hexane (4:1, 10 mL) and filtered to give **182** as dark red crystalline solid (0.05 g, 46%). δ_H (400 MHz, $CDCl_3$): 2.21 (36 H, s, CH_3), 6.46 (24 H, d, *J* = 8.0 Hz, Ar*H*), 6.74 (24 H, d, *J* = 8.0 Hz, Ar*H*); δ_C (101 MHz, $CDCl_3$): 21.2 (12 × CH_3), 124.0 (12 × C), 127.1 (12 × CH), 129.3 (12 × CH), 134.9 (24 × C), 136.6 (12 × C). *m/z* (LD^+) 1642 ($[M–(C_7H_7S)]^+$, 100%), 1765 (52).

Literature data: [224f] δ_H ($CDCl_3$) 6.74 [apparent d(AA′BB′), 24 H, ArH], 6.46 [apparent d (AA′BB′), 24 H, ArH] and 2.21 (s, 36 H, CH_3); δ_C ($CDCl_3$) 136.43, 134.74, 129.15, 127.02 and 123.90; *m*/*z* (FAB) 1766.2 (M^+, 100%).

Sodium octyldithiocarbamate (**177**)

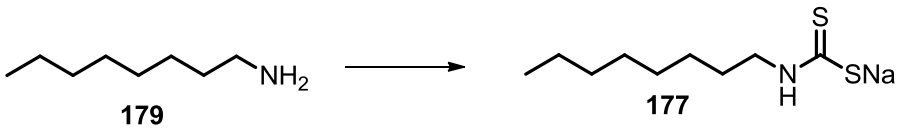

Sodium octyldithiocarbamate **177** was prepared according to a literature procedure.[227]

Octyl amine **179** (9.0 mL, 54.2 mmol) and NaOH (2.17 g, 54.2 mmol) were added to acetone (54.2 mL) and stirred for 1 hour at 0 °C. CS_2 (5.54 mL, 92.1 mmol) was then added dropwise to the reaction mixture vigorously stirred. The cloudy yellow suspension was stirred for additional 4 hours at 0 °C and then overnight at room temperature. The solvent was filtered and Et_2O (110 mL) was then added to the filtrate and kept in the refrigerator overnight. The resulting white solid was filtered and dried *in vacuo* to yield dithiocarbamate **177** as a white solid (6.00 g, 49%). δ_H (400 MHz, DMSO-d_6): 0.84 (3 H, t, *J* = 6.8 Hz, CH_3), 1.22 (10 H, br s, 5 × CH_2), 1.36-1.49 (2 H, m, CH_2), 3.31 (2 H, dd, *J* = 14.1, 6.1 Hz, CH_2); δ_C (101 MHz,

DMSO-d_6) 14.0 (CH_3), 22.1 (CH_2), 26.7 (CH_2), 28.6 (CH_2), 28.8 (CH_2), 28.9 (CH_2), 31.3 (CH_2), 46.6 (CH_2), 214.1 (C, S=*C*-SNa); *m/z* (ES^+) 227.0782 ([M^+] [$C_9H_{18}NNaS_2$] requires 227.0778), 227 (100%). To the best of our knowledge no literature data are reported.

Sodium benzyl thiolate (**191**)

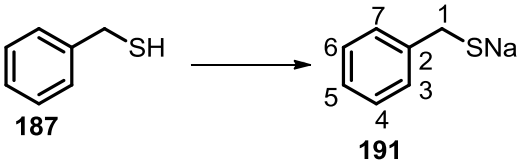

187 **191**

Sodium benzyl thiolate **191** was prepared according to a literature procedure.[230]

Na (0.68 g, 29.4 mmol) was added portionwise to a solution of benzyl mercaptan **187** (4.00 g, 29.4 mmol) in Et_2O (50 mL) at room temperature. The reaction mixture was stirred until Na was dissolved in Et_2O and then the product was filtered and dried *in vacuo* to give thiolate **191** as a white solid (3.96 g, 92%). δ_H (400 MHz, DMSO-d_6): 3.48 (2 H, s, H-1), 6.93 (1 H, t, *J* = 7.5 Hz, H-5), 7.08 (2 H, t, *J* = 7.5 Hz, H-4 and H-6), 7.22 (2 H, d, *J* = 7.5 Hz, H-3 and H-7); δ_C (101 MHz, DMSO-d_6) 32.6 (CH_2, C-1), 123.4 (CH, C-5), 127.0 (2 × CH, C-4 and C-6), 128.2 (2 × CH, C-3 and C-7), 150.8 (C, C-2). Mass spectrometry analysis for this compound could not be obtained.

Literature data: [230] 180-182 °C.

Attempt to synthesise dodecakis(pyridine-2-thio)coronene (**186**)

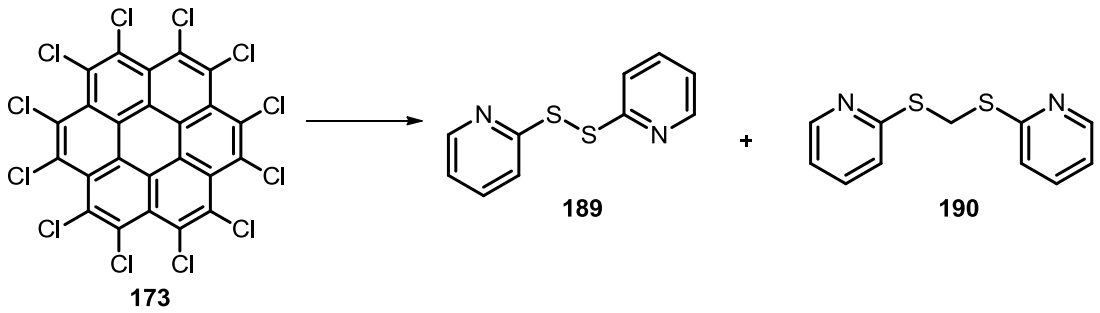

173 189 190

NaH (0.04 g, 1.85 mmol) was added to a vigorously stirred solution of pyridine-2-thiol **188** (2.15 g, 19.3 mmol) in DMI (4.0 mL) at 0 °C and under argon atmosphere. The reaction mixture was then bubbled with argon for 30 mimutes. Perchlorocoronene **177** (0.05 g, 0.07 mmol) was added in one portion and the resulting mixture was then stirred for 4 days at room temperature and under argon atmosphere. Toluene (150 mL) and Na_2CO_3 (150 ml of a saturated aq. solution) were added. The two layers were separated and the organic layer was washed with Na_2CO_3 (2 × 50 mL of a saturated aq. solution), then with H_2O (50 mL) and brine (50 mL), dried over $MgSO_4$, filtered and concentrated under reduced pressure. The residue was purified by column chromatography (hexane to 8:2, hexane:EtOAc) to give : bis(2-pyridinyl)disulfide **189** (0.09 g) as pale yellow crystalline solid and bis-(2-mercaptopyridyl)methane **190** (0.11 g) as white crystalline solid.

bis(2-pyridinyl)disulfide (**189**): δ_H (400 MHz, $CDCl_3$): 7.01-7.08 (2 H, m, Ar*H*), 7.54-7.56 (4 H, m, Ar*H*), 8.39 (2 H, d, *J* = 4.8 Hz, Ar*H*); δ_C (101 MHz, $CDCl_3$): 119.6 (2 × CH), 121.1 (2 × CH), 137.4 (2 × CH), 149.5 (2 × CH), 158.8 (2 × C); *m/z* (ES^+) 221.0206 ($[M+H]^+$, $C_{10}H_9N_2S_2$ requires 221.0207), 221 (100%).

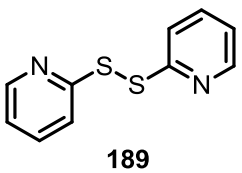

189

Literature data: [232] mp 55-57 °C (lit. 55-56 °C); R_f = 0.31 (petroleum ether / EtOAc = 5:1); δ_H (300 MHz; $CDCl_3$) 7.07-7.13 (2H, m, 5-H), 7.56-7.59 (2H, m, 4-H), 7.60-7.63 (2H, m, 3-

H) and 8.46 (2H, ddd, $^{3}J_{5\text{-H, }6\text{-H}}$ 4.8 Hz, $^{4}J_{4\text{-H, }6\text{-H}}$ 1.3 Hz or 1.8 Hz, $^{5}J_{3\text{-H, }6\text{-H}}$ 1.3 Hz or 1.8 Hz, 6-H); δ_C (75 MHz; $CDCl_3$) 119.62 (C-3), 121.05 (C-5), 137.34 (C-4), 149.51 (C-6) and 158.89 (C-2).

Bis-(2-mercaptopyridyl)methane (**190**): δ_H (400 MHz, $CDCl_3$): 5.05 (2 H, s, CH_2), 6.97 (2 H, ddd, *J* = 7.3, 5.0, 0.9 Hz, Ar*H*), 7.14 (2 H, bd, *J* = 8.1 Hz, Ar*H*), 7.44 (2 H, td, *J* = 7.9, 1.8 Hz, Ar*H*), 8.46 (2 H, *J* = 4.9 Hz, Ar*H*); δ_C (101 MHz, $CDCl_3$): 30.7 (CH_2), 119.7 (2 × CH), 122.4 (2 × CH), 136.0 (2 × CH), 149.4 (2 × CH), 157.6 (2 × C); *m/z* (ES^+) 235.0369 ($[M+H]^+$, $C_{11}H_{11}N_2S_2$ requires 235.0364), 235 (100%).

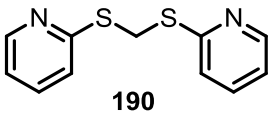

190

Literature data: [231] Anal. calcd. for $C_{11}H_{10}N_2S_2$: C, 56.38; H, 4.30; N, 11.95. Found: C, 56.23; H, 4. 25; N, 11.83%. ^{1}H NMR ($CDCl_3$): δ 8.46 (d, $^{3}J_{H–H}$ = 4.80 Hz, 2H, 6-py), 7.47~7.45 (m, 2H, 4-py), 7.16 (d, $^{3}J_{H–H}$ = 8.04 Hz, 2H, 3-py), 7.00~6.98 (m, 2H, 5-py), 5.06 (s, 2H, CH_2). ^{13}C NMR ($CDCl_3$): δ 157.72 (2-py), 149.44 (6-py), 136.02 (4-py), 122.50 (3-py), 119.71 (5-py), 30.83 (CH_2). IR (KBr; cm^{-1}): 1606 (w), 1578 (s), 1554 (s), 1467 (m), 1455 (s), 1413 (s), 1337 (m), 1286 (m), 1244 (w), 1214 (m), 1173 (w), 1145 (m), 1123 (s), 1087 (m), 1041 (m), 986 (m), 963 (w), 876 (w), 867 (w), 794 (m), 756 (s), 714 (s), 665 (w), 620 (w), 477 (m), 445 (w).

6.5 X-ray crystallography

6.5.1 X-ray crystallography for 99d and 103b

Suitable crystals were selected and datasets were measured by the EPSRC UK National Crystallography Service[245] on a Rigaku AFC12 goniometer equipped with an enhanced sensitivity (HG) Saturn724+ detector mounted at the window of an FR-E+ SuperBright molybdenum rotating anode generator ($\lambda_{Mo\text{-}K\alpha}$ = 0.71075 Å) with HF Varimax optics The instrument was equipped with an Oxford Cryosystems Cryostream device with diffraction data collected at 100 K in both cases. Absorption corrections were applied using sing CrystalClear-SM Expert[246]. The structures were solved by direct methods in SHELXS-97[247] and were refined by a full-matrix least-squares procedure on F^2 in SHELXL-97.[247] All non-hydrogen atoms were refined with anisotropic displacement parameters. The hydrogen atoms were added at calculated positions and refined by use of a riding model with isotropic displacement parameters based on the equivalent isotropic displacement parameter (U_{eq}) of the parent atom. Figures were produced and some structural analysis was carried out using OLEX2.[248] CCDC-996642-996643 contain the supplementary crystallographic data for **99d** and **103b** respectively. These data can be obtained free of charge from The Cambridge Crystallographic Data Centre via http://www.ccdc.cam.ac.uk/Community/ Requestastructure/pages/Requestastructure.aspx.

Crystal data and structure refinement for complexes **99d**.

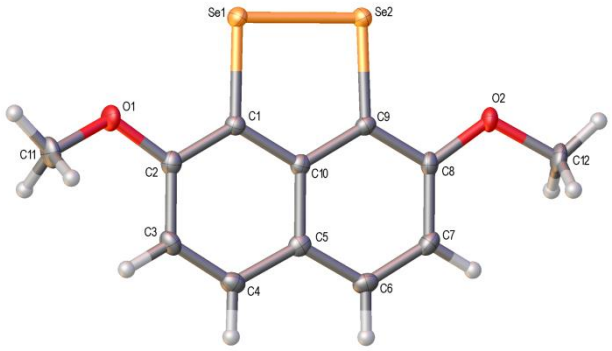

Identification code	**99d**	
Empirical formula	$C_{12}H_{10}O_2Se_2$	
Formula weight	344.12	
Temperature	100(2) K	
Wavelength	0.71075 Å	
Crystal system	Monoclinic	
Space group	*P*21/*n*	
Unit cell dimensions	*a* = 8.2528(4) Å	$\alpha = 90°$
	b = 7.8014(4) Å	$\beta = 96.989(7)°$
	c = 17.2473(12) Å	$\gamma = 90°$
Volume	1102.19(11) Å^3	
Z	4	
Density (calculated)	2.074 Mg / m^3	
Absorption coefficient	6.688 mm^{-1}	
F(000)	664	
Crystal	column; dark red	
Crystal size	0.20 × 0.08 × 0.07 mm^3	
θ range for data collection	3.53 – 27.49°	
Index ranges	$-10 \le \eta \le 10$, $-10 \le \kappa \le 10$, $-20 \le \lambda \le 22$	
Reflections collected	19486	
Independent reflections	2516 [R_{int} = 0.0399]	
Completeness to $\theta = 27.49°$	99.70%	
Absorption correction	Semi–empirical from equivalents	
Max. and min. transmission	0.6518 and 0.3481	
Refinement method	Full-matrix least-squares on F^2	
Data / restraints / parameters	2516 / 0 / 147	
Goodness-of-fit on F^2	1.046	
Final *R* indices [$F^2 > 2\sigma(F^2)$]	*R1* = 0.0220, *wR2* = 0.0556	
R indices (all data)	*R1* = 0.0251, *wR2* = 0.0567	
Largest diff. peak and hole	0.674 and –0.341 e.Å^{-3}	

Crystal data and structure refinement for complexes **103b**.

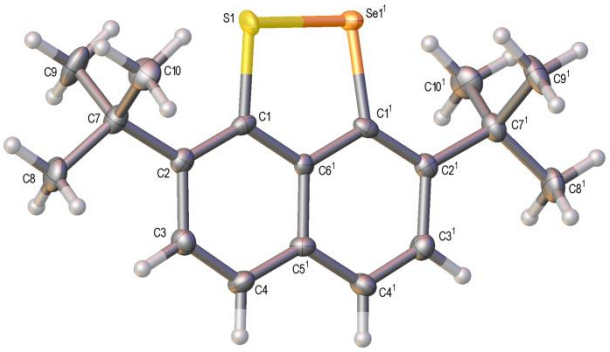

Identification code	**103b**	
Empirical formula	$C_{18}H_{22}SSe$	
Formula weight	349.38	
Temperature	100 K	
Wavelength	0.71075 Å	
Crystal system	Orthorhombic	
Space group	*P*cca	
Unit cell dimensions	a = 11.959(5) Å	α=90°
	b = 11.908(6) Å	β=90°
	c = 11.221(4) Å	γ=90°
Volume	1598.0(12) $Å^3$	
Z	4	
Density (calculated)	1.452 Mg/m^3	
Absorption coefficient	2.469 mm^{-1}	
F(000)	720	
Crystal size	0.11 × 0.07 × 0.02 mm^3	
θ range for data collection	3.02 to 25.67°	
Index ranges	−14<=h<=14,8<=k<=14,11<=l<=13	
Reflections collected	7555	
Independent reflections	1521 [R(int) = 0.0297]	
Completeness to θ = 25.67°	99.70%	
Absorption correction	Semi-empirical from equivalents	
Max. and min. transmission	1.000 and 0.760	
Refinement method	Full-matrix least-squares on F^2	
Data / restraints / parameters	1521 / 0 / 104	
Goodness-of-fit on F2	1.208	
Final R indices [I>2sigma(I)]	R1 = 0.0483, wR2 = 0.0917	
R indices (all data)	R1 = 0.0499, wR2 = 0.0923	
Largest diff. peak and hole	0.672 and -0.969 e.$Å^{-3}$	

6.5.2 X-ray crystallography for 89d, 91a-b and d, 92a-b, 93 and 94

Suitable crystals were selected and datasets were measured on an Agilent SuperNova diffractometer equipped with an Atlas detector for **91a**, **92a** and **94** ($\lambda_{Cu\text{-}K\alpha}$ = 1.5418 Å) and for **91d** (($\lambda_{Mo\text{-}K\alpha}$ = 0.71073 Å) and by the EPSRC UK National Crystallography Service[245] on a Rigaku AFC12 goniometer equipped with an enhanced sensitivity (HG) Saturn724+ detector mounted at the window of an FR-E+ SuperBright molybdenum rotating anode generator ($\lambda_{Mo\text{-}K\alpha}$ = 0.71073 Å) with HF Varimax optics for **89d**, **91b**, **92b** and **93**. Both instruments were equipped with an Oxford Cryosystems Cryostream device with diffraction data collected at 100 K in all cases. Absorption corrections were applied using CrysAlisPro[249] for **91a**, **91d**, **92a** and **94**, using a numerical absorption correction based on gaussian integration over a multifaceted crystal model for **91a**, **91d** and **94** and an empirical absorption correction using spherical harmonics implemented in SCALE3 ABSPACK scaling algorithm for **92a**. Empirical absorption corrections were applied using CrystalClear-SM Expert[250] for **89d**, **91b**, **92b** and **93**. The structures were solved by direct methods in SHELXS-97[247] for **89d**, **91a-b**, **92a** and **93**, in SHELXS-2013[247] for **92b** and **94** and in SHELXS-2014[247] for **91d** and all were refined by a full-matrix least-squares procedure on F^2 in SHELXL-2013[247] (SHELXL-2014[247] for **91d**). All non-hydrogen atoms were refined with anisotropic displacement parameters apart from disordered atoms in **92a** (see later comments). The hydrogen atoms were added at calculated positions and refined by use of a riding model with isotropic displacement parameters based on the equivalent isotropic displacement parameter (U_{eq}) of the parent atom. Figures were produced and some structural analysis was carried out using OLEX2.[248] CCDC-996634-996636, 996638-996641 and 1008312 contain the supplementary crystallographic data for **89d**, **91a-b**, **92a-b**, **93**, **94** and **91d** respectively.

These data can be obtained free of charge from The Cambridge Crystallographic Data Centre via http://www.ccdc.cam.ac.uk/Community/Requestastructure/Pages/DataRequest.aspx.

89d: Although every effort was made to grow the best possible crystals the quality of the crystals and thus corresponding diffraction data was poor. It was necessary to choose a thin platelet in order to obtain a single crystal and this did not diffract well to higher angles.

91b: The crystal was a merohedral twin with the two domains related by 180° about the direct axis [1 0 0]. The scale factor relating the two domains is 0.12.

92a: The sulphur and selenium atoms are both disordered over two positions, with the refined percentage occupancy ratio between the major and minor positions (labelled Se/S and S'/Se' respectively), being 69.8 (3) : 30.2 (3). The minor components, S' and Se', were refined isotropically due to their relatively low occupancy.

92b: The structure contains two crystallographically-independent molecules, with the corresponding geometric parameters being entirely comparable. The sulphur and selenium atoms in both molecules are both disordered over two positions, with the refined percentage occupancy ratio between the major and minor positions (labelled Se/S and S'/Se' in molecule 1 and Se1/S1 and S1'/Se1' in molecule 2 respectively), being 51.1 (8) : 48.9 (8) (molecule 1) and 53.0 (8) : 47.0 (8) (molecule 2).

93: The structure contains two crystallographically-independent molecules, with the corresponding geometric parameters being entirely comparable.

94: The structure contains two crystallographically-independent molecules, with the corresponding geometric parameters being entirely comparable.

Crystal data and structure refinement for complexes **89d**.

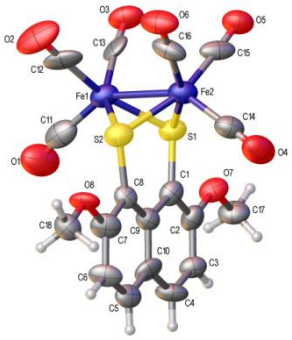

Identification code	**89d**	
Empirical formula	$C_{18}H_{10}Fe_2O_8S_2$	
Formula weight	530.08	
Temperature	100 K	
Wavelength	0.71075 Å	
Crystal system	Monoclinic	
Space group	*P*21/*c*	
Unit cell dimensions	a = 7.865(8) Å	$\alpha = 90°$
	b = 16.990(18) Å	$\beta = 103.38(3)°$
	c = 15.781(19) Å	$\gamma = 90°$
Volume	2052(4) Å^3	
Z	4	
Density (calculated)	1.716 Mg / m^3	
Absorption coefficient	1.661 mm^{-1}	
F(000)	1064	
Crystal	Plate; Orange	
Crystal size	0.25 × 0.12 × 0.01 mm^3	
θ range for data collection	2.91 – 25.00°	
Index ranges	$-9 \le \eta \le 9$, $-20 \le \kappa \le 15$, $-18 \le \lambda \le 18$	
Reflections collected	15599	
Independent reflections	3621 [R_{int} = 0.1490]	
Completeness to θ = 25.00°	99.80%	
Absorption correction	Semi–empirical from equivalents	
Max. and min. transmission	0.9836 and 0.6816	
Refinement method	Full-matrix least-squares on F^2	
Data / restraints / parameters	3621 / 0 / 273	
Goodness-of-fit on F^2	1.167	
Final R indices [$F^2 > 2\sigma(F^2)$]	$R1$ = 0.1379, $wR2$ = 0.3195	
R indices (all data)	$R1$ = 0.2106, $wR2$ = 0.3686	
Largest diff. peak and hole	2.130 and –0.776 e.Å^{-3}	

Crystal data and structure refinement for complexes **91a**.

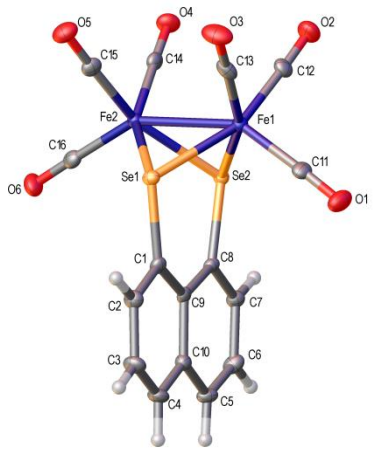

Identification code	**91a**	
Empirical formula	$C_{16}H_6Fe_2O_6Se_2$	
Formula weight	563.83	
Temperature	100.00(10) K	
Wavelength	1.5418 Å	
Crystal system	Triclinic	
Space group	P -1	
Unit cell dimensions	a = 7.5339(4) Å	α =99.559(4)°
	b = 10.2894(6) Å	β=101.362(4)°
	c = 11.7529(6) Å	γ =92.799(4)°
Volume	877.68(8) $Å^3$	
Z	2	
Density (calculated)	2.133 Mg/m^3	
Absorption coefficient	18.291 mm^{-1}	
F(000)	540	
Crystal size	0.234 × 0.088 × 0.022 mm^3	
θ range for data collection	6.452 to 70.063°	
Index ranges	−8<=h<=9, -12<=k<=12, −14<=l<=7	
Reflections collected	5729	
Independent reflections	3301 [R(int) = 0.0414]	
Completeness to θ = 67.680°	99.60%	
Absorption correction	Gaussian	
Max. and min. transmission	0.986 and 0.930	
Refinement method	Full-matrix least-squares on F^2	
Data / restraints / parameters	3301 / 0 / 235	
Goodness-of-fit on F2	1.064	
Final R indices [I>2sigma(I)]	R1 = 0.0358, wR2 = 0.0933	
R indices (all data)	R1 = 0.0387, wR2 = 0.0977	
Extinction coefficient	n/a	
Largest diff. peak and hole	1.030 and -0.824 e.$Å^{-3}$	

Crystal data and structure refinement for complexes **91b**.

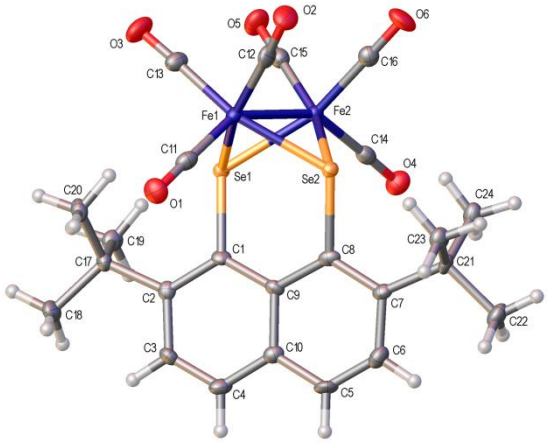

Identification code	**91b**	
Empirical formula	$C_{24}H_{22}Fe_2O_6Se_2$	
Formula weight	676.03	
Temperature	100(2) K	
Wavelength	0.71075 Å	
Crystal system	Monoclinic	
Space group	P 2_1/n	
Unit cell dimensions	a = 7.4151(5) Å	α = 90°
	b = 17.8152(13) Å	β=90.795(12)°
	c = 18.9707(13) Å	γ =90°
Volume	2505.8(3) $Å^3$	
Z	4	
Density (calculated)	1.792 Mg/m^3	
Absorption coefficient	4.100 mm^{-1}	
F(000)	1336	
Crystal size	0.140 × 0.030 × 0.010 mm^3	
Theta range for data collection	2.936 to 27.483°	
Index ranges	−8<=h<=9,−23<=k<=22,−24<=l<=24	
Reflections collected	21056	
Independent reflections	5687 [R(int) = 0.0672]	
Completeness to θ = 25.242°	100.60%	
Absorption correction	Semi-empirical from equivalents	
Max. and min. transmission	1.000 and 0.434	
Refinement method	Full-matrix least-squares on F^2	
Data / restraints / parameters	5687 / 0 / 314	
Goodness-of-fit on F2	1.035	
Final R indices [I>2sigma(I)]	R1 = 0.0494, wR2 = 0.1072	
R indices (all data)	R1 = 0.0876, wR2 = 0.1293	
Extinction coefficient	n/a	
Largest diff. peak and hole	0.919 and -1.025 e.$Å^{-3}$	

Crystal data and structure refinement for complexes **91d**.

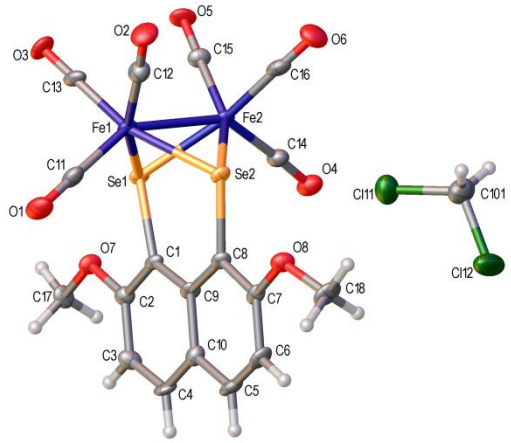

Identification code	**91d**	
Empirical formula	$C_{18}H_{10}Fe_2O_8Se_2$, CH_2Cl_2	
Formula weight	708.81	
Temperature	100.01(10) K	
Wavelength	0.71073 Å	
Crystal system	Triclinic	
Space group	P -1	
Unit cell dimensions	a = 7.9081(5) Å	α=93.216(6)°
	b = 12.2704(11) Å	β=99.886(5)°
	c = 12.3025(7) Å	γ=97.232(6)°
Volume	1163.00(15) $Å^3$	
Z	2	
Density (calculated)	2.024 Mg/m^3	
Absorption coefficient	4.650 mm^{-1}	
F(000)	688	
Crystal size	0.197 × 0.110 × 0.039 mm^3	
θ range for data collection	2.927 to 25.350°	
Index ranges	−9<=h<=8,−14<=k<=14,−14<=l<=14	
Reflections collected	8966	
Independent reflections	4266 [R(int) = 0.0340]	
Completeness to θ = 25.242°	99.80%	
Absorption correction	Gaussian	
Max. and min. transmission	0.846 and 0.547	
Refinement method	Full-matrix least-squares on F^2	
Data / restraints / parameters	4266 / 0 / 300	
Goodness-of-fit on F2	1.133	
Final R indices [I>2sigma(I)]	R1 = 0.0643, wR2 = 0.1674	
R indices (all data)	R1 = 0.0755, wR2 = 0.1745	
Extinction coefficient	n/a	
Largest diff. peak and hole	2.389 and -1.511 e.$Å^{-3}$	

Crystal data and structure refinement for complexes **92a**.

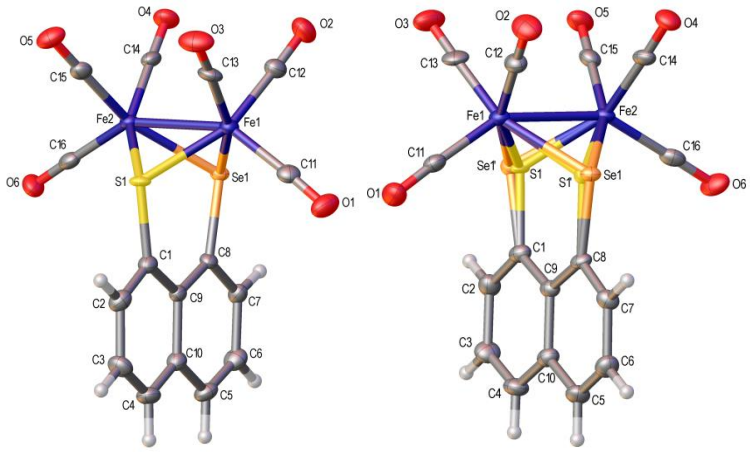

Identification code	**92a**	
Empirical formula	$C_{16}H_6Fe_2O_6SSe$	
Formula weight	516.93	
Temperature	100.00(10) K	
Wavelength	1.5418 Å	
Crystal system	Triclinic	
Space group	P −1	
Unit cell dimensions	a = 7.5023(4) Å	α=99.672(5)°
	b = 10.2906(7) Å	β=100.494(5)°
	c = 11.6461(6) Å	γ=91.992(5)°
Volume	869.53(9) $Å^3$	
Z	2	
Density (calculated)	1.974 Mg/m^3	
Absorption coefficient	17.190 mm^{-1}	
F(000)	504	
Crystal size	0.150 × 0.070 × 0.020 mm^3	
θ range for data collection	6.375 to 70.075°	
Index ranges	−9<=h<=8,−12<=k<=12,−12<=l<=14	
Reflections collected	5636	
Independent reflections	3255 [R(int) = 0.0487]	
Completeness to θ = 67.684°	99.60%	
Absorption correction	Semi-empirical from equivalents	
Max. and min. transmission	1.00000 and 0.20592	
Refinement method	Full-matrix least-squares on F^2	
Data / restraints / parameters	3255 / 0 / 244	
Goodness-of-fit on F2	1.071	
Final R indices [I>2sigma(I)]	R1 = 0.0445, wR2 = 0.1129	
R indices (all data)	R1 = 0.0539, wR2 = 0.1215	
Extinction coefficient	n/a	
Largest diff. peak and hole	0.962 and -0.699 e.$Å^{-3}$	

Crystal data and structure refinement for complexes **92b**.

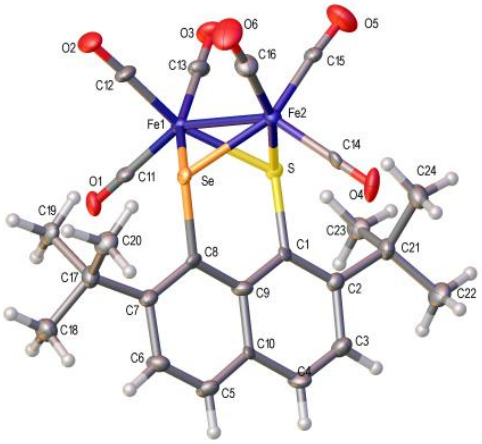

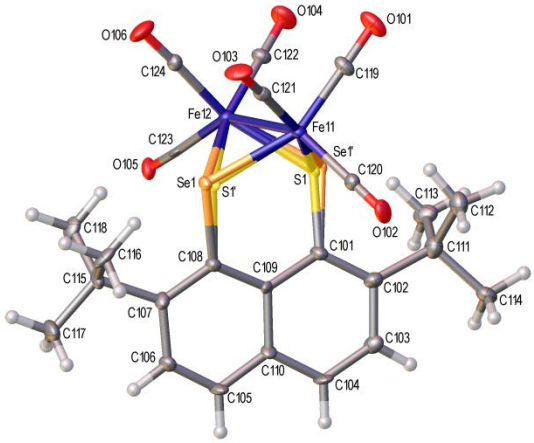

Identification code	**92b**	
Empirical formula	$C_{24}H_{22}Fe_2O_6SSe$	
Formula weight	629.13	
Temperature	100(2) K	
Wavelength	0.71073 Å	
Crystal system	Triclinic	
Space group	P −1	
Unit cell dimensions	a = 7.4178(5) Å	α=79.877(8)°
	b = 14.1007(10) Å	β=87.581(9)°
	c = 24.3025(17) Å	γ=87.026(9)°
Volume	2497.6(3) $Å^3$	
Z	4	
Density (calculated)	1.673 Mg/m^3	
Absorption coefficient	2.740 mm^{-1}	
F(000)	1264	
Crystal size	0.07 × 0.02 × 0.01 mm^3	
θ range for data collection	2.435 to 25.027°	
Index ranges	−8<=h<=8,−16<=k<=16,28<=l<=28	
Reflections collected	23769	
Independent reflections	8494 [R(int) = 0.1070]	
Completeness to θ = 25.242°	94.10%	
Absorption correction	Semi-empirical from equivalents	
Max. and min. transmission	1.000 and 0.813	
Refinement method	Full-matrix least-squares on F^2	
Data / restraints / parameters	8494 / 260 / 633	
Goodness-of-fit on F2	1.099	
Final R indices [I>2sigma(I)]	R1 = 0.1000, wR2 = 0.2357	
R indices (all data)	R1 = 0.1723, wR2 = 0.2862	
Extinction coefficient	n/a	
Largest diff. peak and hole	2.573 and -0.896 e.$Å^{-3}$	

Crystal data and structure refinement for complexes **93**.

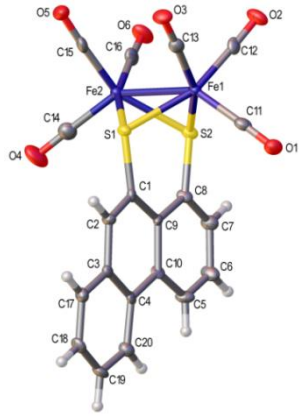

Identification code	**93**	
Empirical formula	$C_{20}H_8Fe_2O_6S_2$	
Formula weight	520.08	
Temperature	100 K	
Wavelength	0.71075 Å	
Crystal system	Monoclinic	
Space group	*P*21/*n*	
Unit cell dimensions	a = 7.718(3) Å	$\alpha = 90°$
	b = 18.033(8) Å	$\beta = 97.057(7)°$
	c = 28.234(12) Å	$\gamma = 90°$
Volume	3900(3) Å^3	
Z	8	
Density (calculated)	1.772 Mg / m^3	
Absorption coefficient	1.738 mm^{-1}	
F(000)	2080	
Crystal	lath; orange	
Crystal size	0.20 × 0.08 × 0.03 mm^3	
θ range for data collection	3.06 – 27.48°	
Index ranges	$-7 \le \eta \le 9$, $-23 \le \kappa \le 14$, $-31 \le \lambda \le 36$	
Reflections collected	19011	
Independent reflections	8774 [R_{int} = 0.0692]	
Completeness to θ = 27.48°	98.20%	
Absorption correction	Semi–empirical from equivalents	
Max. and min. transmission	0.9497 and 0.7225	
Refinement method	Full-matrix least-squares on F^2	
Data / restraints / parameters	8774 / 0 / 541	
Goodness-of-fit on F^2	1.194	
Final R indices [$F^2 > 2\sigma(F^2)$]	*R1* = 0.0903, *wR2* = 0.1606	
R indices (all data)	*R1* = 0.1202, *wR2* = 0.1747	
Largest diff. peak and hole	0.677 and –0.976 e.Å^{-3}	

Crystal data and structure refinement for complexes **94**.

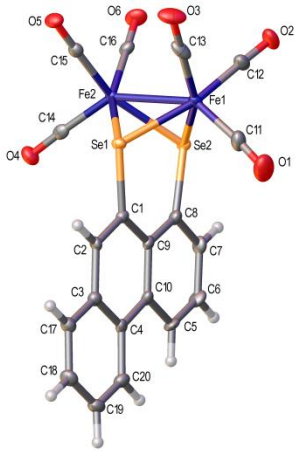

Identification code	**94**	
Empirical formula	$C_{20}H_8Fe_2O_6Se_2$	
Formula weight	613.88	
Temperature	100(2) K	
Wavelength	1.5418 Å	
Crystal system	Monoclinic	
Space group	P 21/n	
Unit cell dimensions	a = 7.73650(10) Å	α= 90°
	b = 18.2484(3) Å	β=97.198(2)°
	c = 28.3551(4) Å	γ = 90°
Volume	3971.59(10) $Å^3$	
Z	8	
Density (calculated)	2.053 Mg/m^3	
Absorption coefficient	16.241 mm^{-1}	
F(000)	2368	
Crystal size	0.2077 × 0.1419 × 0.0441 mm^3	
θ range for data collection	2.886 to 74.530°	
Index ranges	−9<=h<=8,−21<=k<=22,−32<=l<=35	
Reflections collected	16024	
Independent reflections	7810 [R(int) = 0.0316]	
Completeness to θ = 67.684°	99.60%	
Absorption correction	Gaussian	
Max. and min. transmission	0.958 and 0.878	
Refinement method	Full-matrix least-squares on F2	
Data / restraints / parameters	7810 / 0 / 554	
Goodness-of-fit on F2	1.044	
Final R indices [I>2sigma(I)]	R1 = 0.0388, wR2 = 0.0948	
R indices (all data)	R1 = 0.0475, wR2 = 0.1000	
Extinction coefficient	n/a	
Largest diff. peak and hole	2.360 and -0.557 e.$Å^{-3}$	

6.5.3 X-ray crystallography for 131a-b and 132a

Suitable crystals were selected and datasets were measured on an Agilent SuperNova diffractometer equipped with an Atlas detector for **131b** and **132a** ($\lambda_{Mo\text{-}K\alpha}$ = 0.71073 Å) and by the EPSRC UK National Crystallography Service[245] on a Rigaku AFC12 goniometer equipped with an enhanced sensitivity (HG) Saturn724+ detector mounted at the window of an FR-E+ SuperBright molybdenum rotating anode generator ($\lambda_{Mo\text{-}K\alpha}$ = 0.71075 Å) with HF Varimax optics for **131a**. Both instruments were equipped with an Oxford Cryosystems Cryostream device with diffraction data collected at 100 K in all cases. Absorption corrections were applied using CrysAlisPro[249] using a numerical absorption correction based on gaussian integration over a multifaceted crystal model for **131b** and **132a**. An empirical absorption correction was applied using CrystalClear-SM Expert[250] for **131a**. All three structures were solved by direct methods in SHELXS-2014[247] and were refined by a full-matrix least-squares procedure on F^2 in SHELXL-2014.[247] All non-hydrogen atoms were refined with anisotropic displacement parameters. The hydrogen atoms were added at calculated positions and refined by use of a riding model with isotropic displacement parameters based on the equivalent isotropic displacement parameter (U_{eq}) of the parent atom. Figures were produced and some structural analysis was carried out using OLEX2.[248]

131a: The crystal was the best quality that could be grown but the diffraction pattern was subject to streaking and as such the refinement is somewhat poor.

132a: The structure contains a significant amount of highly disordered solvent and the diffraction data were extremely weak, especially at higher angles. Thus the refinement is poor quality. The SQUEEZE Algorithm[251] was employed to remove the contribution of the solvent from the diffraction data as it was not possible to model the solvent. As a result of these serious problems the structure is intended for use for compound ID only.

Crystal data and structure refinement for complexes **131a**.

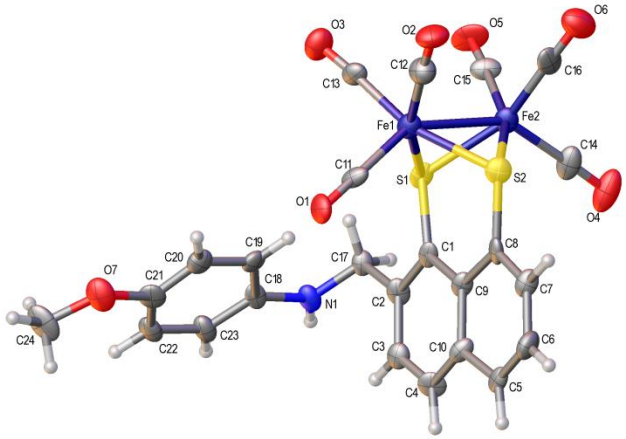

Identification code	**131a**	
Empirical formula	$C_{24}H_{15}Fe_2NO_7S_2$	
Formula weight	605.19	
Temperature	100(2) K	
Wavelength	0.71075 Å	
Crystal system	Triclinic	
Space group	P −1	
Unit cell dimensions	a = 7.4381(6) Å	α=96.12(3)°
	b = 12.1808(9) Å	β=101.11(3)°
	c = 13.5281(10) Å	γ =91.80(3)°
Volume	1194.1(2) $Å^3$	
Z	2	
Density (calculated)	1.683 Mg/m^3	
Absorption coefficient	1.436 mm^{-1}	
F(000)	612	
Crystal size	0.090 × 0.010 × 0.010 mm^3	
θ range for data collection	2.915 to 25.028°	
Index ranges	−8<=h<=8,−14<=k<=14,16<=l<=16	
Reflections collected	8368	
Independent reflections	4050 [R(int) = 0.1722]	
Completeness to θ = 25.242°	94.10%	
Absorption correction	Semi-empirical from equivalents	
Max. and min. transmission	1.000 and 0.545	
Refinement method	Full-matrix least-squares on F2	
Data / restraints / parameters	4050 / 361 / 325	
Goodness-of-fit on F2	1.061	
Final R indices [I>2sigma(I)]	R1 = 0.1459, wR2 = 0.3132	
R indices (all data)	R1 = 0.2913, wR2 = 0.4021	
Extinction coefficient	n/a	
Largest diff. peak and hole	2.386 and -0.805 e.$Å^{-3}$	

Crystal data and structure refinement for complexes **131b**.

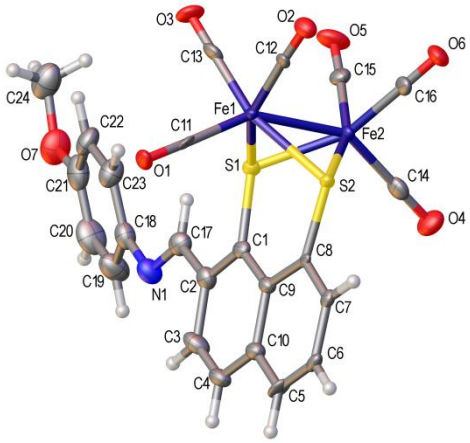

Identification code	**131b**	
Empirical formula	$C_{24}H_{13}Fe_2NO_7S_2$	
Formula weight	603.17	
Temperature	99.95(18) K	
Wavelength	0.71073 Å	
Crystal system	Triclinic	
Space group	P −1	
Unit cell dimensions	a = 7.5048(3) Å	α=92.017(5)°
	b = 16.4362(8) Å	β=94.220(5)°
	c = 20.4236(14) Å	γ=95.982(4)°
Volume	2496.4(2) $Å^3$	
Z	4	
Density (calculated)	1.605 Mg/m^3	
Absorption coefficient	1.374 mm^{-1}	
F(000)	1216	
Crystal size	0.234 × 0.067 × 0.020 mm^3	
θ range for data collection	2.987 to 25.350°	
Index ranges	−9<=h<=8,−19<=k<=19,24<=l<=24	
Reflections collected	23664	
Independent reflections	9108 [R(int) = 0.0674]	
Completeness to θ = 25.242°	99.90%	
Absorption correction	Gaussian	
Max. and min. transmission	0.993 and 0.963	
Refinement method	Full-matrix least-squares on F2	
Data / restraints / parameters	9108 / 0 / 651	
Goodness-of-fit on F2	1.059	
Final R indices [I>2sigma(I)]	R1 = 0.0834, wR2 = 0.2123	
R indices (all data)	R1 = 0.1315, wR2 = 0.2490	
Extinction coefficient	n/a	
Largest diff. peak and hole	1.189 and -1.349 e.$Å^{-3}$	

Crystal data and structure refinement for complexes **132a**.

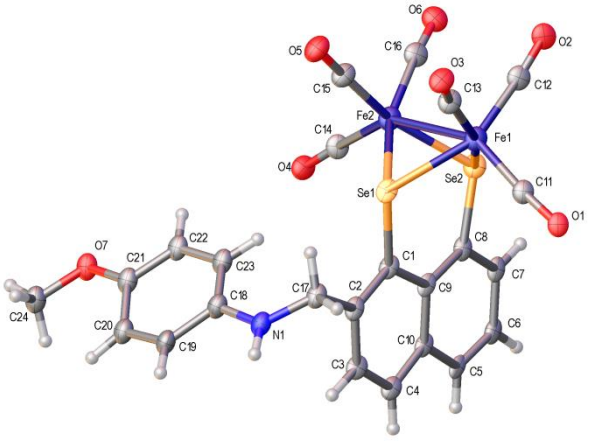

Identification code	**132a**	
Empirical formula	$C_{24}H_{15}Fe_2NO_7Se_2$	
Formula weight	698.99	
Temperature	99.9(2) K	
Wavelength	0.71073 Å	
Crystal system	Triclinic	
Space group	P −1	
Unit cell dimensions	a = 7.4917(9) Å	α= 99.415(14)°
	b = 13.316(2) Å	β= 90.744(12)°
	c = 26.816(5) Å	γ=100.357(11)°
Volume	2593.7(7) $Å^3$	
Z	4	
Density (calculated)	1.790 Mg/m^3	
Absorption coefficient	3.968 mm^{-1}	
F(000)	1368	
Crystal size	0.137 × 0.065 × 0.017 mm^3	
θ range for data collection	2.921 to 25.026°	
Index ranges	−8<=h<=8,−15<=k<=15,−31<=l<=27	
Reflections collected	14857	
Independent reflections	9089 [R(int) = 0.1621]	
Completeness to θ = 25.242°	97.20%	
Absorption correction	Gaussian	
Max. and min. transmission	0.937 and 0.713	
Refinement method	Full-matrix least-squares on F2	
Data / restraints / parameters	9089 / 1022 / 625	
Goodness-of-fit on F2	1.111	
Final R indices [I>2sigma(I)]	R1 = 0.2298, wR2 = 0.4451	
R indices (all data)	R1 = 0.3444, wR2 = 0.5046	
Extinction coefficient	n/a	
Largest diff. peak and hole	2.794 and -3.516 $e.Å^{-3}$	

Chapter 7: References

[1] a) Energy Information Administration (EIA), (August 2013). International Energy Outlook 2013, DOE/EIA-0484. Available: http://www.eia.gov/forecasts/ieo/pdf/0484(2013).pdf.

b) BP press office. (London, 2014). *BP Energy Outlook 2035.* Available: http://www.bp.com/en/global/corporate/about-bp/energy-economics/energy-outlook/outlook-to-2035.html.

c) International Energy Agency. (November 2013). *World Energy Outlook 2013: Renewable Energy Outlook.* Available: http://www.powermag.com/ieas-world-energy-outlook-2013-renewables-and-natural-gas-to-surge-through-2035/.

[2] Audus, H.; Kaarstad, O.; Kowal, M. *Decarbonisation of fuels: hydrogen as an energy carrier*, Proceedings of the 11th World Hydrogen Energy Conference, Stuttgart; June 23–28,1996; 525–534.

[3] Häussinger, P.; Lohmüller, R.; Watson, A. M. Hydrogen, 1. Properties and Occurance. In *Ulmann's Encyclopedia of Industrial Chemistry;* John Wiley & Son, 2011, 235-248.

[4] Gandía, L. M.; Arzamendi, G.; Diéguez, P. M. Renewable Hydrogen Energy: An Overview. In *Renweable Hydrogen Technologies*; Elsevier, 2013; 1-17.

[5] a) Veziroglu, T. N. *Int. J. Hydrogen Energy* **2000**, *25*, 1143-1150.

b) Momirlan, M.; Veziroglu, T. N. *Renew. Sust. Energ. Rev.* **2002**, *6*, 141-179.

[6] Da Rosa, A. Hydrogen Production. In *Fundamentals of renewable Energy Processes*; Elsevier, 3rd ed., 2012; 371-428.

[7] Bartels, J. R.; Pate, M. B.; Olson, N. K. *Int. J. Hydrogen Energy* **2010**, *37*, 8371-8384.

[8] Holladay, J. D.; Hu, J.; King, D. L.; Wang, Y. *Catal. Today* **2009**, *139*, 244-260.

[9] a) Palo, D. R.; Dagle, R. A.; Holladay, J. D. *Chem. Rev.* **2007**, *107*, 3992-4021.

b) Haryanto, A.; Fernando, S.; Murali, N.; Adhikari, S. *Energy Fuels* **2005**, *19*, 2098-2106.

[10] Da Rosa, A. Biomass. In *Fondamentals of renewable Energy Processes*; Elsevier, 3rd ed., 2012; 533-590.

[11] Hemshemeier, A.; Melis, A.; Happe, T. *Photosynth. Res.* **2009**, *102*, 523-540.

[12] Baebprasert, W.; Jantaro, S.; Khetkorn, W.; Lindblad, P.; Incharoensakdi, A. *Metab. Eng.* **2011**, *13*, 610-616.

[13] Vignais, P. M.; Billoud, B. *Chem. Rev.* **2007**, *107*, 4206-4272.

[14] Corr, M. J.; Murphy, J. A. *Chem. Soc. Rev.* **2011**, *40*, 2279-2292.

[15] a) Buurman, G.; Shima, S.; Thauer, R. K. *FEBS Lett.* **2000**, *485*, 200-204.

b) Shima, S.; Lyon, E. J.; Sordel-Klippert, M. S.; Kauss, M.; Kahnt, J.; Thauer, R. K.; Steinbach, K.; Xie, X. L.; Verdier, L.; Griesinger, C. *Angew. Chem. Int. Ed.* **2004**, *43*, 2547-2551.

c) Lyon, E. J.; Shima, S.; Boecher, R.; Thauer, R. K.; Grevels, F. W.; Bill, E.; Roseboom, W.; Albracht, S. P. J. *J. Am. Chem. Soc.* **2004**, *126*, 14239-14248.

d) Shima, S.; Pilak, O.; Vogt, S.; Schick, M.; Stagni, M. S.; Meyer-Klaucke, W.; Warkentin, E.; Thauer, R. K.; Ermler, U. *Science* **2008**, *321*, 572-575.

e) Pilak, O.; Mamat, B.;Vogt, S.; Hagemeier, C. H.; Thauer, R. K.; Shima, S.; Vonrhein, C.; Warkentin, E.; Ermler, U. *J. Mol. Biol.* **2006**, *358*, 798-809.

f) Hiromoto, T.; Ataka, K.; Pilak, O.; Vogt, S.; Stagni, M. S.; Meyer-Klaucke, W.; Warkentin, E.; Thauer, R. K.; Shima, S.; Ermler, U. *FEBS Lett.* **2009**, *583*, 585-590.

g) Shima, S.; Ataka, K. *FEBS Lett.* **2011**, *585*, 353-356.

h) Tamura, H.; Salomone-Stagni, M.; Fujishiro, T.; Warkentin, E.; Meyer-Klaucke, W.; Ermler, U.; Shima, S. *Angew. Chem. Int. Ed.* **2013**, *52*, 9656-9659.

[16] Simmons, T. R.; Berggren, G.; Bacchi, M.; Fontecave, M.; Artero, V. *Coord. Chem. Rev.* **2014**, 270-271, 127-150.

[17] Tard, C.; Pickett, C. J. *Chem. Rev.* **2009**, *109*, 2245-2274.

[18] Wright, J. A.; Turrell, P. J.; Pickett, C. J. *Organometallics* **2010**, *29*, 6146-6156.

[19] Dey, S.; Das, P. K.; Dey, A. *Coord. Chem. Rev.* **2013**, *257*, 42-63.

[20] a) Chen, D.; Scopelliti, R.; Hu, X. *Angew. Chem. Int. Ed.* **2010**, *49*, 7512-7513.

b) Chen, D.; Scopelliti, R.; Hu, X. *J. Am. Chem. Soc.* **2010**, *132*, 928-929.

c) Chen, D.; Ahrens-Botzong, A.; Schünemann, V.; Scopelliti, R.; Hu, X. *Inorg. Chem.* **2011**, *50*, 5249-5257.

d) Chen, D.; Scopelliti, R.; Hu, X. *Angew. Chem. Int. Ed.* **2011**, *50*, 5671-5673.

e) Chen, D.; Scopelliti, R.; Hu, X. *Angew. Chem. Int. Ed.* **2012**, *124*, 1955-1957.

f) Hu, B.; Chen, D.; Hu, X. *Chem. Eur. J.* **2012**, *18*, 11528-11530.

g) Hu, B.; Chen, D.; Hu, X. *Chem. Eur. J.* **2013**, *19*, 6221-6224.

[21] a) Turrel, P. J.; Wright, J. A.; Peck, J. N. T.; Oganesyan, V. S.; Pickett, C. J. *Angew. Chem. Int. Ed.* **2010**, *49*, 7508-7511.

b) Turrell, P. J.; Hill, A. D.; Ibrahim, S. K.; Wright, J. A.; Pickett, C. J. *Dalton Trans.* **2013**, *42*, 8140-8146.

[22] Royer, A. M.; Salomone-Stagni, M.; Rauchfuss, T. B.; Meyer-Klaucke, W. *J. Am. Chem. Soc.* **2010**, *132*, 16997-17003.

[23] Liu, T.; Li, B.; Popescu, C. V.; Bilko, A.; Perez, L.M.; Hall, M. B.; Darensbourg, M. Y. *Chem. Eur. J.* **2010**, *16*, 3083-3089.

[24] a) Song, L.-C.; Xie, Z.-J.; Wang, M.-H.; Zhao, G.-Y.; Song, H.-B. *Inorg. Chem.* **2012**, *51*, 7466-7468.

b) Song, L.-C.; Zhao, G.-Y.; Xie, Z.-J.; Zhang, J.-W. *Organometallics* **2013**, *32*, 2509-2512.

[25] Volbeda, A.; Charon, M.; Piras, C.; Hatchikian, E. C.; Frey, M.; Fontecilla-Camps, J.-C. *Nature* **1995**, *373*, 580-587.

[26] a) Volbeda, A.; Garcin, E.; Piras, C.; de Lacey, A. L.; Fernandez, V. M.; Hatchikian, E. C.; Frey, M.; Fontecilla-Camps, J.-C. *J. Am. Chem. Soc.* **1996**, *118*, 12989-12996.

b) Ogata, H.; Mizoguchi, Y.; Mizuno, N.; Miki, K.; Adachi, S.; Yasuoka, N.; Yagi, T.; Yamauchi, O.; Hirota, S.; Higuchi, Y. *J. Am. Chem. Soc.* **2002**, *124*, 11628-11635.

c) Volbeda, A.; Martin, L.; Cavazza, C.; Matho, M.; Faber, B. W.; Roseboom, W.; Albracht, S. P. J.; Garcin, E.; Rousset, M.; Fontecilla-Camps, J.-C. *J. Biol. Inorg. Chem.* **2005**, *10*, 239-249.

d) Ogata, H.; Hirota, S.; Nakahara, A.; Komori, H.; Shibata, N.; Kato, T.; Kano, K.; Higuchi, Y. *Structure* **2005**, *13*, 1635-1642.

e) Fontecilla-Camps, J.-C.; Volbeda, A.; Cavazza, C.; Nicolet, Y. *Chem. Rev.* **2007**, *107*, 4273-4303.

f) Leroux, F.; Dementin, S.; Burlatt, B.; Cournac, L.; Volbeda, A.; Champ, S.; Martin, L.; Guigliarelli, B.; Bertrand, P.; Fontecilla-Camps, J.-C.; Rousset, M.; Leger, C. *Proc. Natl. Acad. Sci. U. S. A.* **2008**, *105*, 11188-11193.

g) Shafaat, H. S.; Rüdiger, O.; Ogata, H.; Lubitz, W. *Biochim. Biophys. Acta* **2013**, *1827*, 986-1002.

[27] a) Garcin, E.; Vernede, X.; Hatchikian, E. C.; Volbeda, A.; Frey, M.; Fontecilla-Camps, J.-C. *Structure* **1999**, *7*, 557-566.

b) Valente, F. M.; Oliveira, A. S.; Gnadt, N.; Pacheco, I.; Coelho, A.V.; Xavier, A. V.; Teixeira, M.; Soares, C. M.; Pereira, I. A. *J. Biol. Inorg. Chem.* **2005**, *10*, 667-682.

c) Valente, F. M.; Pereira, P. M.; Venceslau, S. S.; Regalla, M.; Coelho, A. V.; Pereira, I. A. *FEBS Lett.* **2007**, *581*, 3341-3344.

[28] de Lacey, A.; Férnandez, V. M.; Rousset, M.; Cammack, R. *Chem. Rev.* **2007**, *107*, 4304-4330.

[29] Darensbourg, M. Y.; Lyon E. J.; Smee, J. J. *Coord. Chem. Rev.* **2000**, *206-207*, 533-561.

[30] a) Crabtree, R. H. *Acc. Chem. Res.* **1990**, *23*, 95-101.

b) Kubas, G. J. *Acc. Chem. Res.* **1988**, *21*, 128-134.

c) Cotton, F. A.; Wilkinson, G.; Murill, C. A.; Bochmann, M. In *Advanced Inorganic Chemistry*; John Wiley and Sons, New York, 6th ed., 1999.

[31] Stenson, P. A.; Marin-Becerra, A.; Wilson, C.; Blake, A. J.; McMaster, J.; Schroder, M. *Chem. Commun.* **2006**, 317-319.

b) Song, L.-C.; Sun, X.-J.; Zhao, P.-H.; Li, J.-P.; Song, H.-B. *Dalton Trans.* **2012**, *41*, 8941-8950.

[32] a) Duff, S. E.; Hitchcock, P. B.; Davies, S. C.; Barclay, J. E.; Evans, D. J. *Acta Crystallogr.* **2005**, *61*, 1316-1319.

b) Song, L.-C.; Li, Y.-I.; Li, L.; Gu, Z.-C.; Hu, Q.-M. *Inorg. Chem.* **2010**, *49*, 10174-10182.

c) Song, L.-C.; Li, J.-P.; Xie, Z.-J.; Song, H.-B. *Inorg. Chem.* **2013**, 11618-11626.

[33] Ogo, S.; Ichikawa, K.; Kishima, T.; Matsumoto, T.; Nakai, H.; Kusaka, K.; Ohhara, T. *Science* **2013**, *339*, 682-684.

[34] Manor, B. C.; Rauchfuss, T. B. *J. Am. Chem. Soc.* **2013**, *135*, 11895-11900.

[35] a) Ohki, Y.; Yasumura, K.; Kuge, K.; Tanino, S.; Ando, M.; Li, Z.; Tatsumi, K. *Proc. Natl. Acad. Sci. U. S. A.* **2008**, *105*, 7652-7657.

b) Ohki, Y.; Yasumura, K.; Ando, M.; Shimokata, S.; Tatsumi, K. *Proc. Natl. Acad. Sci USA* **2010**, *107*, 3994-3997.

c) Weber, K.; Krämer, T.; Shafaat, H. S.; Weyhermüller, T.; Bill, E.; van Gastel, M.; Neese, F.; Lubitz, W. *J. Am. Chem. Soc.* **2012**, *134*, 20745-20755.

d) Canaguier, S.; Fontecave, M.; Artero, V. *Eur. J. Inorg. Chem.* **2011**, 1094-1099.

e) Weber, K.; Heise, I.; Weyhermüller, T.; Lubitz, W. *Eur. J. Inorg. Chem.* **2014**, 148-155.

[36] Ohki, Y.; Sakamoto, M.; Tatsumi, K. *J. Am. Chem. Soc.* **2008**, *130*, 11610-11611.

[37] Frey, M. *ChemBioChem* **2002**, *3*, 153-160.

[38] Fournier, M.; Dermoun, Z.; Durand, M.; Dolla, A. *J. Biol. Chem.* **2004**, *279*, 1787-1793.

[39] a) Peters, J. W.; Lanzillotta, W. N.; Lemon, B. J.; Seefeldt, L. C. *Science* **1998**, *282*, 1853-1858.

b) Nicolet, Y.; Piras, C.; Legrand, P.; Hatchikian, C. E.; Fontecilla-Camps, J.-C. *Structure* **1999**, *7*, 13-23.

[40] a) Lemon, B. J.; Peters, J. W. *Biochemistry* **1999**, *38*, 12969-12973.

b) Bennett, B.; Lemon, B. J.; Peters, J. W. *Biochemistry* **2000**, *39*, 7455-7460.

c) Lemon, B. J.; Peters, J. W. *J. Am. Chem. Soc.* **2000**, *122*, 3793-3794.

d) Chen, Z.; Lemon, B. J.; Huang, S.; Swartz, D. J.; Peters, J. W.; Bagley, K. A. *Biochemistry* **2002**, *41*, 2036-2043.

[41] a) Nicolet, Y.; de Lacey, A. L.; Vernede, X.; Fernandez, V. M.; Hatchikian, E. C.; Fontecilla-Camps, J.-C. *J. Am. Chem. Soc.* **2001**, *123*, 1596-1601.

b) Nicolet, Y.; Lemon, B. J.; Fontecilla-Camps, J.-C.; Peters, J. W. *Trends Biochem. Sci.* **2000**, *25*, 138-143.

c) Nicolet, Y.; Cavazza, C.; Fontecilla-Camps, J.-C. *J. Inorg. Biochem.* **2002**, *91*, 1-8.

d) Lubitz, W.; Reijerse, E.; van Gastel, M. *Chem. Rev.* **2007**, *107*, 4331-4365.

e) Silakov, A.; Wenk, B.; Reijerse, E.; Lubitz, W.; *Phys. Chem. Chem. Phys.* **2009**, *11*, 6592-6599.

f) Erdem, O. F.; Schwartz, L.; Stein, M.; Silakov, A.; Kaur-Ghumaan, S.; Huang, P.; Ott, S.; Reijerse, E. J.; Lubitz, W. *Angew. Chem. Int. Ed.* **2011**, *50*, 1439-1443.

[42] Pandey, A. S.; Harris, T. V.; Giles, L. J.; Peters, J. W.; Szilagyi, R. K. *J. Am. Chem. Soc.* **2008**, *130*, 4533-4540.

[43] a) Berggren, G.; Adamska, A.; Lambertz, C.; Simmons, T. R.; Esselborn, J.; Atta, M.; Gambarelli, S.; Mouesca, J. M.; Reijerse, E.; Lubits, W.; Happe, T.; Artero, V.; Fontecave, M. *Nature* **2013**, *499*, 66-69.

b) Esselborn, J.; Lambertz, C.; Adamska-Venkatesh, A.; Simmons, T. R.; Berggren, G.; Noth, J.; Siebel, J.; Hemschemeier, A.; Artero, V.; Reijerse, E.; Fontecave, M.; Lubitz, W.; Happe, T. *Nat. Chem. Biol.* **2013**, *9*, 607-609.

[44] Capon, J.-F.; Gloaguen, F.; Pétillion, F. Y.; Schollhammer, P.; Talarmin, J. *Coord. Chem. Rev.* **2009**, *253*, 1476-1494.

[45] a) Adamska, A.; Silakov, A.; Lambertz, C.; Rüdiger, O.; Happe, T.; Lubitz, W. *Angew. Chem. Int. Ed.* **2012**, *51*, 11458-11462.

b) Mulder, D. W.; Ratzloff, M. W.; Shepard, E. M.; Byer, A. S.; Noone, S. M.; Peters, J. W.; Broderick, J. B.; King, P. W. *J. Am. Chem. Soc.* **2013**, *135*, 6921-6929.

[46] a) van der Vlugt, J. I.; Rauchfuss, T. B.; Whaley, C. M.; Wilson, S. R. *J. Am. Chem. Soc.* **2005**, *127*, 16012-16013.

b) Carroll, M. E.; Barton, B. E.; Rauchfuss, T. B.; Carroll, P. J. *J. Am. Chem. Soc.* **2012**, *134*, 18843-18852.

[47] Gloaguen, F.; Rauchfuss, T. B. *Chem. Soc. Rev.* **2009**, *38*, 100-108.

[48] Tschierlei, S.; Ott. S.; Lomoth, R. *Energy Environ. Sci.* **2011**, *4*, 2340-2352.

[49] Reihlen, H.; Gruhl, A.; Hessling, G. *Liebigs Ann. Chem.* **1929**, *472*, 268-287.

[50] Seyferth, D.; Womack, G. B.; Gallagher, M. K.; Cowie, M.; Hames, B. W.; Fackler, J. P.; Mazzany, A. M. *Organometallics* **1987**, *6*, 283-294.

[51] a) Lyon, E. J.; Georgakaki, I. P.; Reibespies, J. H.; Darensbourg, M. Y. *Angew. Chem. Int. Ed.* **1999**, *38*, 3178-3180.

b) Schimdt, M.; Contakes, S. M.; Rauchfuss, T. B. *J. Am. Chem. Soc.* **1999**, *121*, 9736-9737.

c) Le Cloirec, A.; Best, S. P.; Borg, S.; Davies, S. C.; Evans, D. J.; Hughes, D. L.; Pickett, C. J. *Chem. Commun.* **1999**, 2285-2286.

[52] a) Borg, S. J.; Behrsing, T.; Best, S P.; Razavet, M.; Liu, X.; Pickett, C. J. *J. Am. Chem. Soc.* **2004**, *126*, 16988-16999.

b) Borg, S. J.; Ibrahim, S. K.; Pickett, C. J.; Best, S. P. *C. R. Chimie* **2008**, *11*, 852-860.

[53] Seyferth, D.; Henderson, R. S.; Song, L.-C. *Organometallics* **1982**, *1*, 125-133.

[54] a) Lawrence, J. D.; Li, H.; Rauchfuss, T. B.; Bénard, M.; Rohmer, M. *Angew. Chem. Int. Ed.* **2001**, *40*, 1768-1771.

b) Li, H.; Rauchfuss, T. B. *J. Am. Chem. Soc.* **2002**, *124*, 726-727.

[55] a) Ott, S.; Kritikos, M.; Åkermark, B.; Sun, L.; Lomoth, R. *Angew. Chem. Int. Ed.* **2004**, *43*, 1006-1009.

[56] a) Song, L.-C.; Yang, Z.-Y.; Bian, H.-Z.; Hu, Q.-M. *Organometallics* **2004**, *23*, 3082-3084.

b) Song, L.-C.; Yang, Z.-Y; Bian, H.-Z.; Liu, Y.; Wang, H.-T.; Liu, X.-F.; Hu, Q.-M. *Organometallics* **2005**, *24*, 6126-6135.

[57] Song, L.-C.; Yang, Z.-Y.; Hua, Y.-J.; Wang, H.-T.; Liu, Y.; Hu, Q.-M. *Organometallics* **2007**, *26*, 2106-2110.

[58] Windhager, J.; Rudolph, M.; Brautigam, S.; Görls, H.; Weigand, W. *Eur. J. Inorg. Chem.* **2007**, 2748-2760.

[59] Glass, R. S.; Gruhn, N. E.; Lorance, E.; Singh, M. S.; Stessman, N. Y. T.; Zakai, U. I. *Inorg. Chem.* **2005**, *44*, 5728-5737.

[60] a) Apfel, U.-P.; Troegel, D.; Halpin, Y.; Tschierlei, S.; Uhlemann, U.; Görls, H.; Schmitt, M.; Popp, J.; Dunne, P.; Venkatesan, M.; Coey, M.; Rudolph, M.; Vos, J. G.; Tacke, R.; Weigand, W. *Inorg. Chem.* **2010**, *49*, 10117-10132.

b) Apfel, U.-P.; Halpin, Y.; Görls, H.; Vos, J. G.; Weigand, W. *Eur. J. Inorg. Chem.* **2011**, 581-588.

[61] Harb, M. K.; Niksch, T.; Windhager, J.; Görls, H.; Holza, R.; Lockett, L. T.; Okumura, N.; Evans, D. H.; Glass, R. S.; Lichtenberger, D. L.; El-khateeb, M.; Weigand, W. *Organometallics* **2009**, *28*, 1039-1048.

[62] Almazahreh, L. R.; Apfel, U.-P.; Imhof, W.; Rudolph, M.; Görls, H.; Talarmin, J.; Schollhammer, P.; El-khateeb, M.; Weigand, W. *Organometallics* **2013**, *32*, 4523-4530.

[63] Zhao, X.; Georgakaki, I. P.; Miller, M. L.; Yarbrough, J. C.; Darensbourg, M. Y. *J. Am. Chem. Soc.* **2001**, *123*, 9710-9711.

[64] Gloaguen, F.; Lawrence, J. D.; Rauchfuss, T. B. *J. Am. Chem. Soc.* **2001**, *123*, 9476-9477.

[65] Gloaguen, F.; Lawrence, J. D.; Rauchfuss, T. B.; Bénard, M.; Rohmer, M.-M. *Inorg. Chem.* **2002**, *41*, 6573-6582.

[66] a) Liu, T.; Darensbourg, M. Y. *J. Am. Chem. Soc.* **2007**, *129*, 7008-7009.

b) Singleton, M. L.; Bhuvanesh, N.; Reibenspies, J. H.; Darensbourg, M. Y. *Angew. Chem. Int. Ed.* **2008**, *47*, 9492-9495.

c) Thomas, C. M.; Liu, T.; Hall, M. B.; Darensbourg, M. Y. *Inorg. Chem.* **2008**, *47*, 7009-7024.

d) Thomas, C. M.; Liu, T.; Hall, M. B.; Darensbourg, M. Y. *Chem. Commun.* **2008**, 1563-1565.

e) Thomas, C. M.; Darensbourg, M. Y.; Hall, M. B. *J. Inorg. Biochem.* **2007**, *101*, 1752-1757.

[67] a) Justice, A. K.; Rauchfuss, T. B.; Wilson, S. R. *Angew. Chem. Int. Ed.* **2007**, *46*, 6152−6154.

b) Justice, A. K.; De Gioia, L.; Nilges, M. J.; Rauchfuss, T. B.; Wilson, S. R.; Zampella, G. *Inorg. Chem.* **2008**, *47*, 7405-7414.

c) Justice, A. K.; Nilges, M. J.; Rauchfuss, T. B.; Wilson, S. R.; De Gioia, L.; Zampella, G. *J. Am. Chem. Soc.* **2008**, *130*, 5293-5301.

[68] Chouffai, D.; Zampella, G.; Capon, J.-F.; De Gioia, L.; Le Goff, A.; Pétillon, F. Y.; Schollhammer, P.; Talarmin, J. *Organometallics* **2012**, *31*, 1082-1091.

[69] Karnahl, M.; Tschierlei, S.; Erdem, Ö. F.; Pullen, S.; Santoni, M.; Reijerse, E. J.; Lubitz, W.; Ott, S. *Dalton Trans.* **2012**, *41*, 12468-12477.

[70] Capon, J.-F.; Gloaguen, F.; Schollhammer, P.; Talarmin, J. *Coord. Chem. Rev.* **2005**, *249*, 1664-1676.

[71] Chong, D.; Georgakaki, I. P.; Mejia-Rodriguez, R.; Sanabria-Chinchilla, J.; Soriaga, M. P.; Darensbourg, M. Y. *Dalton Trans.* **2003**, 4158-4163.

[72] Liu, Y.-C.; Chu, K.-T.; Jhang, R.-L.; Lee, G.-M.; Chiang, M.-H. *Chem. Commun.* **2013**, *49*, 4743-4745.

[73] a) Rakowski DuBois, M.; DuBois, D. L. *C. R. Chimie* **2008**, *11*, 805-817.

b) Wilson, A. D.; Shoemaker, R. K.; Miedaner, A.; Muckerman, J. T.; DuBois, D. L.; Rakowski DuBois, M. *Proc. Natl. Acad. Sci. U.S.A.* **2007**, *104*, 6951-6958.

c) Curtis, C. J.; Miedaner, A.; Ciancanelli, R.; Ellis, W. W.; Noll, B. C.; Rakowski DuBois, M.; DuBois, D. L. *Inorg. Chem.* **2003**, *42*, 216-227.

[74] a) Adam, F. I.; Hogarth, G.; Richards, I.; Sanchez, B. E. *Dalton Trans.* **2007**, 2495-2498.

b) Wang, N.; Wang, M.; Liu, T.; Zhang, T.; Darensbourg, M. Y.; Sun, L. *Inorg. Chem.* **2008**, *47*, 6948-6955.

c) Xu, F.; Tard, C.; Wang, X.; Ibrahim, S. K.; Hughes, D. L.; Zhong, W.; Zeng, X.; Luo, Q.; Liu, X.; Pickett, C. J. *Chem. Commun.* **2008**, 606-608.

d) Wang, Z.; Jiang, W.; Liu, J.; Jiang, W.; Wang, Y.; Åkermark, B.; Sun, L. *J. Organomet. Chem.* **2008**, *693*, 2828-2834.

e) Wang, N.; Wang, M.; Zhang, T.; Li, P.; Liu, J.; Sun, C. *Chem. Commun.* **2008**, 5800-5802.

f) Ezzalher, S.; Capon, J.-F.; Gloaguen, F.; Pétillon, F. Y.; Schollhammer, P.; Talarmin, J. *Inorg. Chem.* **2009**, *48*, 2-4.

g) Wang, N.; Wang, M.; Liu, J.; Jin, K.; Chen, L.; Sun, L. *Inorg. Chem.* **2009**, *48*, 11551-11558.

h) Wang, N.; Wang, M.; Wang, Y.; Zheng, D.; Han, H.; Ahlquist, M. S. G.; Sun, L. *J. Am. Chem. Soc.* **2013**, *135*, 13688-13691.

[75] Ezzaher, S.; Gogoll, A.; Bruhn, C.; Ott, S. *Chem. Commun.* **2010**, *46*, 5775-5777.

[76] a) Thomas, C.M.; Rüdiger, O.; Liu, T.; Carson, C. E.; Hall, M. B.; Darensbourg, M. Y. *Organometallics* **2007**, *26*, 3976-3984.

b) Vijaikanth, V.; Capon, J.-F.; Gloaguen, F.; Pétillon, F. Y.; Schollhammer, P.; Talarmin, J. *J. Organomet. Chem.* **2007**, *692*, 4177-4181.

[77] Gao, W.; Sun, J.; Åkermark, T.; Li, M.; Eriksson, L.; Sun, L.; Åkermark, B. *Chem. Eur. J.* **2010**, *16*, 2537-2546.

[78] Wang, N.; Wang, M.; Chen, L.; Sun, L. *Dalton Trans.* **2013**, *42*, 12059-12071.

[79] a) Fauvel, K.; Mathieu, R.; Poilblanc, R. *Inorg. Chem.* **1976**, *15*, 976-978.

b) Arabi. M. S.; Mathieu, R.; Poilblanc, R. *J. Organomet. Chem.* **1979**, *177*, 199-209.

[80] van der Vlugt, J. I.; Rauchfuss, T. B.; Whaley, C. M.; Wilson, S. R. *J. Am. Chem. Soc.* **2005**, *127*, 16012-16013.

[81] a) Ezzaher, S.; Capon, J.-F.; Gloaguen, F.; Pétillon, F. Y.; Schollhammer, P.; Talarmin, J. *Inorg. Chem.* **2007**, *46*, 3426-3428.

b) Adam, F. I.; Hogarth, G.; Kabir, S. E.; Richards, D. *C. R. Chim.* **2008**, *11*, 890-905.

[82] Barton, B. E.; Rauchfuss, T. B. *Inorg. Chem.* **2008**, *47*, 2261-2263.

[83] Wang, W.; Rauchfuss, T. B.; Zhu, L.; Zampella, G. *J. Am. Chem. Soc.* **2014**, *136*, 5773-5782.

[84] Carroll, M. E.; Barton, B. R.; Rauchfuss, T. B. *J. Am. Chem. Soc.* **2012**, *134*, 18843-18852.

[85] Jacob, C.; Giles, G. I.; Giles, N. M.; Sies, H. *Angew. Chem. Int. Ed.* **2003**, *42*, 4742-4758.

[86] Gao, S.; Fan, J.; Sun, S.; Peng, X.; Zhao, X.; Hou, J. *Dalton Trans.* **2008**, 2128-2135.

[87] Song, L.-C.; Gai, B.; Wang, H.-T.; Hu, Q.-M. *J. Inorg. Biochem.* **2009**, *103*, 805-812.

[88] Apfel, U.-P.; Halpin, Y.; Gottschaldt, M.; Görls, H.; Vos, J. G.; Weigand, W. *Eur. J. Inorg. Chem.* **2008**, 5112-5118.

[89] a) Harb, M. K.; Windhager, J.; Daraosheh, A.; Görls, H.; Lockett, L. T.; Okumura, N.; Evans, D. H.; Glass, R. S.; Lichtenberger, D. L.; El-khateeb, M.; Weigand, W. *Eur. J. Inorg. Chem.* **2009**, 3414-3420.

b) Song, L.-S; Gao, W.; Feng, C.-P.; Wang, D.-F.; Hu, Q.-M. *Organometallics* **2009**, *28*, 6121-6130.

c) Harb, M. K.; Apfel, U.-P.; Kübel, J.; Görls, H.; Felton, G. A. N.; Sakamoto, T.; Evans, D. H.; Glass, R. S.; Lichtenberger, D. L.; El-khateeb, M.; Weigang, W. *Organometallics* **2009**, *28*, 6666-6675.

d) Gao, W.; Song, L.-C.; Yin, B.-S.; Zan, H.-N.; Wang, D.-F.; Song, H.-B. *Organometallics* **2011**, *30*, 4097-4107.

e) Harb, M. K.; Windhager, J.; Niksch, T.; Görls, H.; Sakamoto, T.; Smith, E. R.; Glass, R. S.; Lichtenberger, D. L.; Evans, D. H.; El-khateeb, M.; Weigand, W. *Tetrahedron*, **2012**, *68*, 10592-10599.

f) Trautwein, R.; Almazahreh, L. R.; Görls, H.; Weigand, W. *Z. Anorg. Allg. Chem.* **2013**, *639*, 1512-1519.

g) El-khateeb, M.; Harb, M.; Abu-Salem, Q.; Görls, H.; Weigand, W. *Polyhedron* **2013**, *61*, 1-5.

h) Song, L.-C.; Gai, B.; Feng, Z.-H.; Du, Z.-Q.; Xie, Z.-Q.; Sun, X.-J.; Song, H.-B. *Organometallics* **2013**, *32*, 3673-3684.

[90] a) Harb, M. K.; Görls, H.; Sakamoto, T.; Felton, G. A. N.; Evans, D. H.; Glass, R. S.; Lichtenberger, D. L.; El-khateeb, M.; Weigand, W. *Eur. J. Inorg. Chem.* **2010**, 3976-3985.

b) Harb. M. K.; Apfel, U.-P.; Sakamoto, T.; El-khateeb, M.; Weigand, W. *Eur. J. Inorg. Chem.* **2011**, 986-993.

c) Apfel, U.-P.; Görls, H.; Felton, G. A.; Evans, D. H.; Glass, R. S.; Lichtenberger, D. L.; Weigand. W. *Helv. Chim. Acta* **2012**, *95*, 2168-2175.

d) Song, L.-C.; Li, Q.-L.; Feng, Z.-H.; Sun, X.-J.; Xie, Z.-Q.; Song, H.-B. *Dalton Trans.* **2013**, *42*, 1612-1626.

[91] a) Cheah, M. H.; Borg, S. J.; Bondin, M. I.; Best, S. P. *Inorg. Chem.* **2004**, *43*, 5635-5644.

b) Das, P.; Capon, J.; Gloaguen, F.; Pétillon, F. Y.; Schollhammer, P.; Talarmin, J. *Inorg. Chem.* **2004**, *43*, 8203-8205.

c) Song, L.-C.; Zeng, G.-H.; Hu, Q.-M.; Ge, J.-H.; Lou, S.-X. *Organometallics* **2005**, *24*, 16-19.

d) Song, L.-C.; Zeng, G.-H.; Lou, S.-X.; Zan, H.-N.; Ming, J.-B.; Hu, Q.-M. *Organometallics* **2008**, *27*, 3714-3721.

[92] Volkers, P. I.; Rauchfuss, T. B. *Inorg. Biochem.* **2007**, *101*, 1748-1751.

[93] a) Razavet, M.; Davies, S. C.; Hughes, D. L.; Pickett, C. J. *Chem. Commun.* **2001**, 847-848.

b) Ravazet, M.; Davies, S. C.; Hughes, D. L.; Barclay, J. E.; Evans, D. J.; Fairhurst, S. A.; Liu, X.; Pickett, C. J. *Dalton Trans.* **2003**, 586-595.

[94] Tard, C.; Liu, X.; Ibrahim, S. K.; Bruschi, M.; De Gioia, L.; Davies, S. C.; Yang, X.; Wang, L.; Sawers, G.; Pickett, C. J. *Nature* **2005**, *433*, 610-613.

[95] Lawrence, J. D.; Li, H.; Rauchfuss, T. B. *Chem. Commun.* **2001**, 1482-1483.

[96] a) Zeng, X.; Li, Z.; Xiao, Z.; Wang, Y.; Liu, X. *Electrochem. Commun.* **2010**, *12*, 342-345.

b) Zhao, J.; Wei, Z.; Zeng, X.; Liu, X. *Dalton Trans.* **2012**, *41*, 11125-11133.

c) Gimbert-Suriñach, C.; Bhadbhade, M.; Colbran, S. B. *Organometallics* **2012**, *31*, 3480-3491.

d) Liu, Y.-C.; Lee, C.-H.; Lee, G.-H.; Chiang, M.-H. *Eur. J. Inorg. Chem.* **2011**, 1155-1162.

[97] Si, Y.; Charreteur, K.; Capon, J.-F.; Gloaguen, F.; Pétillon, F. Y.; Schollhammer, P.; Talarmin, J. *J. Inorg. Biochem.* **2010**, *104*, 1038-1042.

[98] Roy, S.; Groy, T. L.; Jones, A. K. *Dalton Trans.* **2013**, *42*, 3843-3853.

[99] Liu, Y.-C.; Yen, T.-H.; Tseng, Y.-J.; Hu, C.-H.; Lee, G.-H.; Chiang, M.-H. *Inorg. Chem.* **2012**, *51*, 5997-5999.

[100] Camara, J. M.; Rauchfuss, T. B. *Nat. Chem.* **2012**, *4*, 26-30.

[101] He, C.; Wang, M.; Zhang, X.; Wang, Z.; Chen, C.; Liu, J.; Åkermark, B.; Sun, L. *Angew. Chem. Int. Ed.* **2004**, *43*, 3571-3574.

[102] de Hatten, X.; Bothe, E.; Merz, K.; Huc, I.; Metzler-Nolte, N. *Eur. J. Inorg. Chem.* **2008**, 4530-4537.

[103] Liu, Z.-P.; Hu, P. *J. Chem. Phys.* **2002**, *117*, 8177-8180.

[104] a) Apfel, U.-P.; Kowol, C. R.; Halpin, Y.; Kloss, F.; Kübel, J.; Görls, H.; Vos, J. G.; Keppler, B. K.; Morera, E.; Lucente, G.; Weigand, W. *J. Inorg. Biochem.* **2009**, *103*, 1236-1244.

b) Apfel, U.-P.; Kowol, C. R.; Morera, E.; Görls, H.; Lucente, G.; Keppler, B. K.; Weigand, W. *Eur. J. Inorg. Chem.* **2010**, 5079-5086.

[105] a) Jones, A. K.; Lichtenstein, B. R.; Dutta, A.; Gordon, G.; Dutton, P. L. *J. Am. Chem. Soc.* **2007**, *129*, 14844-14845.

b) Roy, S.; Shinde, S.; Hamilton, G. A.; Hartnett, H. E.; Jones, A. K. *Eur. J. Inorg. Chem.* **2011**, 1050-1055.

[106] Vijaikanth, V.; Capon, J.-F.; Gloaguen, F.; Schollhammer, P.; Talarmin, J. *Electrochem. Commun.* **2005**, *7*, 427-430.

[107] Ibrahim, S. K.; Liu, X.; Tard, C.; Pickett, C. J. *Chem. Commun.* **2007**, 1535-1537.

[108] Thomas, C. M.; Rüdiger, O.; Liu, T.; Carson, C. E.; Hall, M. B.; Darensbourg, M. Y. *Organometallics* **2007**, *26*, 3976-3984.

[109] Green, K. N.; Hess, J. L.; Thomas, C. M.; Darensbourg, M. Y. *Dalton Trans.* **2009**, 4344-4350.

[110] Frederix, P. W. J. M.; Kania, R.; Wright, J. A.; Lamprou, D. A.; Ulijn, R. V.; Pickett, C. J.; Hunt, N. T. *Dalton Trans.* **2012**, *41*, 13112-13119.

[111] a) Singleton, M. L.; Reibenspies, J. H.; Darensbourg, M. Y. *J. Am. Chem. Soc.* **2010**, *132*, 8870-8871.

b) Singleton, M. L.; Crouthers, D. J.; Duttweiler, III, R. P.; Reibenspies, J. H.; Darensbourg, M. Y. *Inorg. Chem.* **2011**, *50*, 5015-5026.

c) Li, X.; Wang, M.; Zheng, D.; Han, K.; Dong, J.; Sun, L. *Energy Environ. Sci.* **2012**, *5*, 8220-8224.

[112] a) Capon, J.-F.; Gloaguen, F.; Schollhammer, P.; Talarmin, J. *J. Electroanal. Chem.* **2004**, *566*, 241-247.

b) Capon, J.-F.; Gloaguen, F.; Schollhammer, P.; Talarmin, J. *J. Electroanal. Chem.* **2006**, *595*, 47-52.

[113] Felton, G. A. N.; Vannucci, A. K.; Chen, J.; Lockett, L. T.; Okumura, N.; Petro, B. J.; Zakai, U. I.; Evans, D. H.; Glass, R. S.; Lichtenberger, D. L. *J. Am. Chem. Soc.* **2007**, *129*, 12521-12530.

[114] Wright, R. J.; Zhang, W.; Yang, X.; Fasulo, M.; Tilley, T. D. *Dalton Trans.* **2012**, *41*, 73-82.

[115] Liu, Y.; Chu, K.; Jhang, R.; Lee, G.; Chiang, M. *Chem. Commun.* **2013**, *49*, 4743-4745.

[116] a) Schwartz, L.; Singh, P. S.; Eriksson, L.; Lomoth, R.; Ott, S. *C. R. Chimie* **2008**, *11*, 875-889.

b) Streich, D.; Karnahl, M.; Astuti, Y.; Cady, C. W.; Hammarström, L.; Lomoth, R.; Ott, S. *Eur. J. Inorg. Chem.* **2011**, 1106-1111.

[117] Donovan, E. S.; McCormick, J. J.; Nichol, G. S.; Felton, G. A. N. *Organometallics* **2012**, *31*, 8067-8070.

[118] Chen, J.; Vanucci, A. K.; Mebi, C. A.; Okumura, N.; Borowski, S. C.; Swenson, M.; Lockett, L. T.; Evans, D. H.; Glass, R. S.; Lichtenberger, D. L. *Organometallics* **2010**, *29*, 5330-5340.

[119] Schwartz, L.; Eriksson, L.; Lomoth, R.; Teixidor, F.; Viñas, C.; Ott, S. *Dalton Trans.* **2008**, 2379-2381.

[120] Singh, P. S.; Rudbeck, H. C.; Huang, P.; Ezzaher, S.; Eriksson, L.; Stein, M.; Ott, S.; Lomoth, R. *Inorg. Chem.* **2009**, *48*, 10883-10885.

[121] Kilian, P.; Knight, F. R.; Woollins, J. D. *Coord. Chem. Rev.* **2011**, *255*, 1387-1413.

[122] Wright, R. J.; Lim, C.; Tilley, T. D. *Chem. Eur. J.* **2009**, *15*, 8518-8525.

[123] Topf, C.; Monkowius, U.; Knör, G. *Inorg. Chem. Commun.* **2012**, *21*, 147-150.

[124] Teramoto, Y.; Kubo, K.; Kume, S.; Mizuta, T. *Organometallics* **2013**, *32*, 7014-7024.

[125] Mebi, C. A.; Noll, B. C.; Gao, R.; Karr, D. *Z. Anorg. Allg. Chem.* **2010**, *636*, 2550-2554.

[126] Fuller, A. L.; Knight, F. R.; Slawin, A. M.; Woollins, J. D. *Eur. J. Inorg. Chem.* **2010**, *25*, 4034-4043.

[127] Meinwald, J.; Dauplaise, D.; Wudl, F.; Hauser, F. F. *J. Am. Chem. Soc.* **1977**, *99*, 255-257.

[128] Tesmer, M.; Vahrenkamp, H. *Eur. J. Inorg. Chem.* **2001**, 1183-1188.

[129] Aucott, S. M.; Milton, H. L.; Robertson, S. D.; Slawin, A. M. Z.; Woollins, J. D. *Dalton Trans.* **2004**, 3347-3352.

[130] Grainger, R. S.; Patel, B.; Kariuki, B. M. *Angew. Chem. Int. Ed.* **2009**, *48*, 4832-4835.

[131] Testaferri, C.; Tiecco, M.; Tingoli, M.; Chianelli, D.; Montanucci, M. *Synthesis* **1983**, 751-755.

[132] Alam, A.; Ogawa, S.; Muraoka, H.; Kon-on, M.; Nakajo, S.; Sato, R. *Eur. J. Org. Chem.* **2007**, 6097-6105.

[133] a) Blair, P. A.; Chang, S. J.; Shechter, H. *J. Org. Chem.* **2004**, *69*, 7123-7133.

b) Kihnert, N.; Burzlaff, N.; Patel, C.; Lopez-Periago, A. *Org. Biomol. Chem.* **2005**, *3*, 1911-1921.

[134] Grainger, R. S.; Patel, B.; Kariuki, B. M.; Male, L.; Spencer, N. *J. Am. Chem. Soc.* **2011**, *133*, 5843-5852.

[135] Press, D. J.; Back, T. G. *Org. Lett.* **2011**, *13*, 4104-4107.

[136] Look, K.; Norris, R. K. *Aus. J. Chem.* **1999**, *52*, 1077-1083.

[137] Kienle, M.; Unsinn, A.; Knochel, P. *Angew. Chem. Int. Ed.* **2010**, *49*, 4751-4754.

[138] Sasaki, T.; Sato, N.; Takahashi, T.; Mizutani, T. Nouveau derive de benzoxathiine. EP1944301 A1, July 16, 2008.

[139] Chery, F.; Pillard, C.; Tatibouët, A.; De Lucchi, O.; Rollin, P. *Tetrahedron* **2006**, *62*, 5141-5151.

[140] Krishnamurthy, S.; Aimino, D. *J. Org. Chem.* **1989**, *54*, 4458-4462.

[141] Kulka, M. *Can. J. Chem.* **1956**, *34*, 1093-1100.

[142] Ashe, A. J.; Kampf, J. W.: Savla, P. M. *Heteroat. Chem.* **1994**, *5*, 113-119.

[143] Bonifàcio, V. D. B.; Morgado, J.; Scherf, U. *Synlett* **2010**, 1333-1336.

[144] Works, C. F. *J. Chem. Educ.* **2007**, *84*, 836-838.

[145] Izutsu, K. *Acid-Base Dissociation Constants in Dipolar Aprotic Solvents* 1990, Blackwell Scientific Publications, Oxford.

[146] Felton, G. A. N.; Mebi, C. A.; Petro, B. J.; Vanucci, A. K.; Evans, D. H.; Glass, R. S.; Lichtenberger, D. L. *J. Organomet. Chem.* **2009**, *694*, 2681-2699.

[147] b) Andrieux, C. P.; Blocman, C.; Dumas-Bouchiat, J.; M'Halla, F.; Savéant, J. *J. Electroanal. Chem.* **1980**, *113*, 19-40.

c) Savéant, J.; Su, K. B. *J. Electroanal. Chem.* **1984**, *171*, 341-349.

[148] Felton, G. A. N.; Glass, R. S. ; Lichtenberger, D. L.; Evans, D. H. *Inorg. Chem.* **2006**, *45*, 9181-9184.

[149] Darensbourg, M. Y.; Weigand, W. *Eur. J. Inorg. Chem.* **2011**, 994-1004.

[150] Ogata, H.; Lubitz, W.; Higuchi, Y. *Dalton Trans.* **2009**, 7577-7587.

[151] Vincent, K. A.; Parkin, A.; Lenz, O.; Albracht, S. P. J.; Fontecilla-Camps, J.-C.; Cammack, R.; Friederich, B.; Armstrong, F. A. *J. Am. Chem. Soc.* **2005**, *127*, 18179-18189.

[152] Liu, T.; Li, B.; Singleton, M. L.; Hall, M. B.; Darensbourg, M. Y. *J. Am. Chem. Soc.* **2009**, *131*, 8296-8307.

[153] a) Windhager, J.; Rudolph, M.; Bräutigam, S.; Görls, H.; Weigand, W. *Eur. J. Inorg. Chem.* **2007**, 2748-2760.

b) Windhager, J.; Seidel, R. A.; Apfel, U.-P.; Görls, H,; Linti, G.; Weigand, W. *Chem. Biodiversity* **2008**, *5*, 2023-2041.

c) Windhager, J.; Apfel, U.-P.; Yoshino, T.; Nakata, N.; Görls, H.; Rudolph, M.; Ishii, A.; Weigand, W. *Chem. Asian J.* **2010**, *5*, 1600-1610.

[154] Amouyal, A. *Sol. Energy Mater. Sol. Cells* **1995**, *8*, 249-276.

[155] Sun, L.; Åkermark, B.; Ott, S. *Coord. Chem. Rev.* **2005**, *249*, 1653-1663.

[156] Wang, M.; Na, Y.; Gorlov, M.; Sun, L. *Dalton Trans.* **2009**, 6458-6467.

[157] Lomoth, R.; Ott, S. *Dalton Trans.* **2009**, 9952-9959.

[158] Wang, M.; Chen, L.; Li, X.; Sun, L. *Dalton Trans.* **2011**, *40*, 12793-12800.

[159] Miller, E. W.; Bian, S. X.; Chang, C. J. *J. Am. Chem. Soc.* **2007**, *129a*, 3458-3459.

[160] Manna, D.; Mugesh, G. *J. Am. Chem. Soc.* **2012**, *134*, 4269-4279.

[161] Vatmurge, N. S.; Hazra, B. G.; Pore, V. S.; Shirazi, F.; Chavan, P. S.; Deshpande, M. V. *Bioorg. Med. Chem. Lett.* **2008**, *18*, 2043-2047.

[162] Periasamy, M.; Srinivas, G.; Bharathi, P. *J. Org. Chem.* **1999**, *64*, 4204-4205.

[163] Kataoka, T.; Iwamura, T.; Tsutsui, H.; Kato, Y.; Banno, Y.; Aoyama, Y.; Shimizu, H. *Heteroat. Chem.* **2001**, *12*, 317-326.

[164] Liu, G.; Link, J. T.; Pei, Z.; Reilly, E. B.; Leitza, S.; Nguyen, B.; Marsh, K. C.; Okasinski, G. F.; von Geldern, T. W.; Ormes, M.; Fowler, K.; Gallatin, M. *J. Med. Chem.* **2000**, *43*, 4025-4040.

[165] Campaigne, E.; LeSuer, W. M. *Org. Synth.* **1963**, *4*, 919.

[166] Bal, B. S.; Childers, W. E., Jr.; Pinnick, H. W. *Tetrahedron* **1981**, *37*, 2091-2096.

[167] Mohamed, M. A.; Yamada, K.-I.; Tomioka, K. *Tetrahedron Lett.* **2009**, *50*, 3436-3438.

[168] Bringmann, G.; Holenz, J.; Weirich, R.; Rübenacker, M.; Funke, C.; Boyd, M. R.; Gulakowski, R. J.; François, G. *Tetrahedron* **1998**, *54*, 497-512.

[169] Goh, K. S.; Tan, C.-H. *RSC Adv.* **2012**, *2*, 5536-5538.

[170] Huang, N.-K.; Chern, H.; Fang, J.-M.; Lin, C.-I.; Chen, W.-P.; Lin, Y.-L. *J. Nat. Prod.* **2007**, *70*, 571-574.

[171] Coskun, N. *Synth. Commun.* **2004**, *34*, 1625-1630.

[172] Eastmond, G. C.; Paprotny, J.; Steiner, A.; Swanson, L. *New J. Chem.* **2001**, *25*, 379-384.

[173] Du, Y.; Hyster, T. K.; Rovis, T. *Chem. Commun.* **2011**, *47*, 12074-12076.

[174] Tang, Q.; Xia, D.; Jin, X.; Zhang, Q.; Sun, X.-Q.; Wang, C. *J. Am. Chem. Soc.* **2013**, *135*, 4628-4631.

[175] Parson, T. B.; Spencer, N.; Tsang, C. W.; Grainger, R. S. *Chem. Commun.* **2013**, *49*, 2296-2298.

[176] Myers, A. G.; Yang, B. H.; Chen, H. *Org. Synth.* **2004**, *10*, 509-516.

[177] Cho, B. R.; Chung, H. S.; Cho, N. S. *J. Org. Chem.* **1998**, *63*, 4685-4690.

[178] Salerno, C. P.; Magde, D.; Patron, A. P. *J. Org. Chem.* **2000**, *65*, 3971-3981.

[179] Cho, B. R.; Chung, H. S.; Pyun, S. Y. *J. Org. Chem.* **1998**, *64*, 8375-8378.

[180] Cho, B. R.; Jang, W. J.; Je, J. T.; Bartsch, R. A. *J. Org. Chem.* **1993**, *58*, 3901-3904.

[181] Denton, R. M.; An, J.; Lindovska, P.; Lewis, W. *Tetrahedron* **2012**, *68*, 2899-2905.

[182] Hou, J.; Peng, X.; Liu, J.; Gao, Y.; Zhao, X.; Gao, S.; Han, K. *Eur. J. Inorg. Chem.* **2006**, 4679-4686.

[183] Liu, T.; Wang, M.; Shi, Z.; Cui, H.; Dong, W.; Chen, J.; Åkermark, B.; Sun, L. *Chem. Eur. J.* **2004**, *10*, 4474-4479.

[184] Hou, J.; Peng, X.; Liu, J.; Gao, Y.; Zhao, X.; Gao, S.; Han, K. *Eur. J. Inorg. Chem.* **2006**, 4679-4686.

[185] Liu, T.; Wang, M.; Shi, Z.; Cui, H.; Dong, W.; Chen, J.; Åkermark, B.; Sun, L. *Chem. Eur. J.* **2004**, *10*, 4474-4479.

[186] Wang, F.; Wang, W.-G.; Wang, H.-Y.; Si, G.; Tung, C.-H.; Wu, L.-Z. *ACS Catal.* **2012**, *2*, 407-416.

[187] Boudart, M. *Chem. Rev.* **1995**, *95*, 661-666.

[188] a) Salyi, S.; Kritikos, M.; Åkermark, B.; Sun, L. *Chem. J. Eur.* **2003**, *9*, 557-560.

b) Ott, S.; Kritikos, M.; Åkermark, B.; Sun, L. *Angew. Chem. Int. Ed.* **2003**, *42*, 3285-3288.

d) Wolpher, H.; Borgström, M.; Hammarström, L.; Bergquist, J.; Sundström, V.; Styring, S.; Sun, L.; Åkermark, B. *Inorg. Chem. Commun.* **2003**, *6*, 989-991.

c) Ott, S.; Borgström, M.; Kritikos, M.; Lomoth, R.; Bergquist, J.; Åkermark, B.; Hammarström, L.; Sun, L. *Inorg. Chem.* **2004**, *43*, 4683-4692.

[189] Ekström, J.; Abrahamsson, M.; Olson, C.; Bergquist, J.; Kaynak, F. B.; Eriksson, L.; Sun, L.; Becker, H.-C.; Åkermark, B.; Hammarström, L.; Ott, S. *Dalton Trans.* **2006**, 4599-4606.

[190] Na, Y.; Pan, J.; Wang, M.; Sun, L. *Inorg. Chem.* **2007**, *46*, 3813-3815.

[191] Na, Y.; Wang, M.; Pan, J.; Zhang, P.; Åkermark, B.; Sun, L. *Inorg. Chem.* **2008**, *47*, 2805-2810.

[192] Steich, D.; Astuti, Y.; Orlandi, M.; Schwartz, L.; Lomoth, R.; Hammarström, L.; Ott, S. *Chem. Eur. J.* **2010**, *16*, 60-63.

[193] Zhang, P.; Wang, M.; Na, Y.; Li, X.; Jiang, Y.; Sun, L. *Dalton Trans.* **2010**, *39*, 1204-1206.

[194] Cui, H.-H.; Hu, M.-Q.; Wen, H.-M.; Chai, G.-L.; Ma, C.-B.; Chen, H.; Chen, C.-N. *Dalton Trans.* **2012**, *41*, 13899-13907.

[195] Gao, W.; Liu, J.; Jiang, W.; Wang, M.; Weng, L.; Åkermark, B.; Sun, L. *C. R. Chimie* **2008**, *11*, 915-921.

[196] Wang, W.-G.; Wang, F.; Wang, H.-Y.; Si, G.; Tung, C.-H.; Wu, L.-Z. *Chem.-Asian J.* **2010**, *5*, 1796-1803.

[197] a) Jiang, W.; Liu, J.; Li, C. *Inorg. Chem. Commun.* **2011**, *16*, 81-85.

b) Liu, J.; Jiang, W. *Dalton Trans.* **2012**, *41*, 9700-9707.

[198] a) Song, L.-C.; Tang, M.-T.; Su, F.-H.; Hu, Q.-M. *Angew. Chem. Int. Ed.* **2006**, *45*, 1130-1133.

b) Song, L.-C.; Tang, M.-T.; Mei, S.-Z.; Huang, J.-H.; Hu, Q.-M. *Organometallics* **2007**, *26*, 1575-1577.

c) Song, L.-C.; Wang, L.-X.; Yin, B.-S.; Li, Y.-L.; Zhang, X.-G.; Zhang, Y.-W.; Luo, X.; Hu, Q.-M. *Eur. J. Inorg. Chem.* **2008**, 291-297.

d) Song, L.-C.; Wang, L.-X.; Li, C.-G.; Li, F.; Chen, Z. *J. Organomet. Chem.* **2014**, *749*, 120-128.

[199] Li, X.; Wang, M.; Zhang, S.; Pan, J.; Na, Y.; Liu, J.; Åkermark, B.; Sun, L. *J. Phys. Chem. B.* **2008**, *112*, 8198-8202.

[200] Kluwer, A. M.; Kapre, R.; Hartl, F.; Lutz, M.; Spek, A. L.; Brouwer, A. M.; van Leeuwen, P. W. N. M.; Reek, J. N. H. *Proc. Natl. Acad. Sci. U. S. A.* **2009**, *106*, 10460-10465.

[201] Song, L.-C.; Wang, L.-X.; Tang, M.-Y.; Li, C.-G.; Song, H.-B.; Hu, Q.-M. *Organometallics* **2009**, *28*, 3834-3841.

[202] Samuel, A. P. S.; Co, D. T.; Stern, C. L.; Wasielewski, M. R. *J. Am. Chem. Soc.* **2010**, *132*, 8813-8815.

[203] Wang, H.-Y.; Si, G.; Cao, W.-N.; Wang, W.-G.; Li, Z.-J.; Wang, F.; Tung, C.-H.; Wu, L.-Z. *Chem. Commun.* **2011**, *47*, 8406-8408.

[204] Poddutoori, P.; Co, D. T.; Samuel, A. P. S.; Kim, C. H.; Vagnini, M. T.; Wasielewski, M. R. *Energy Environ. Sci.* **2011**, *4*, 2441-2450.

[205] Yu, T.; Zeng, Y.; Chen, J.; Li, Y.-Y.; Yang, G.; Li, Y. *Angew. Chem. Int. Ed.* **2013**, *52*, 5631-5635.

[206] Rossetti, R.; Nakahara, S.; Brus, L. E. *J. Chem. Phys.* **1983**, *79*, 1086-1087.

[207] a) Wang. F.; Wang, W.-G.; Wang, X.-J.; Wang, H.-Y.; Tung, C.-H.; Wu, L.-Z. *Angew. Chem. Int. Ed.* **2011**, *50*, 3193-3197.

b) Wang, F.; Liang, W.-J.; Jian, J.-X.; Li, C.-B.; Chen, B.; Tung, C.-H.; Wu, L.-Z. *Angew. Chem. Int. Ed.* **2013**, *52*, 8134-8138.

c) Li, C.-B.; Li, Z.-J.; Yu, S.; Wang, G.-X.; Wang, F.; Meng, Q.-Y.; Chen, B.; Feng, K.; Tung, C.-H.; Wu, L.-Z. *Energy Environ. Sci.* **2013**, *6*, 2597-2602.

[208] a) Wen, F.; Wang, X.; Huang, L.; Ma, G.; Yang, J.; Li, C. *ChemSusChem* **2012**, *5*, 849-853.

b) Yang, J.; Wang, D.; Han, H.; Li, C. *Acc. Chem. Res.* **2013**, *46*, 1900-1909.

[209] Song, X.-W.; Wen, H.-M.; Ma, C.-B.; Hu, M.-Q.; Chen, H.; Cui, H.-H.; Chen, C.-N. *Appl. Organometal. Chem.* **2014**, *28*, 267-273.

[210] a) Sano, Y.; Onoda, A.; Hayashi, T. *Chem. Commun.* **2011**, *47*, 8229-8231.

b) Sano, Y.; Onoda, A.; Hayashi, T. *J. Inorg. Biochem.* **2012**, *108*, 159-162.

[211] Roy, A.; Madden, C.; Ghirlanda, G. *Chem. Commun.* **2012**, *48*, 9816-9818.

[212] Adler, A.; Longo, F. R.; Finarelli, J. D.; Goldmacher, J.; Assour, J.; Korsakoff, L. *J. Org. Chem.* **1967**, *32*, 476-476.

[213] Sun, L.; Chen, H.; Zhang, Z.; Yang, Q.; Tong, H.; Xu, A.; Wang, C. *J. Inorg. Biochem.* **2012**, *108*, 47-52.

[214] Kruper, Jr, W. J.; Chamberlin, T. A.; Kochanny, M. *J. Org. Chem.* **1989**, *54*, 2753-2756.

[215] Cho, Y.-J.; Ahn, T. K.; Song, H.; Kim, K. S.; Lee, C. Y.; Seo, W. S.; Lee, K.; Kim, S. K.; Kim, D.; Park, J. T. *J. Am. Chem. Soc.* **2005**, *127*, 2380-2381.

[216] Sharma, S.; Nath, M. *Beilstein J. Org. Chem.* **2013**, *9*, 496-502.

[217] Rothemund, P.; Menotti, A. R. *J. Am. Chem. Soc.* **1948**, *70*, 1808-1808.

[218] Tan, Q.; Zhang, X.; Mao, L.; Xin, G.; Zhang, S. *J. Mol. Struct.* **2013**, *1035*, 400-406.

[219] Visher, H. F.; Hulshof, J. W.; Hulscher, S.; Fratantoni, S. A.; Verheij, M. H. P.; Victorina, J.; Smit, M. J.; de Esch, I. J. P.; Leurs, R. *Bioorg. Med. Chem.* **2010**, *18*, 675-688.

[220] Hernández-Juárez, M.; Vaquero, M.; Álvarez, E.; Salazar, V.; Suárez, A. *Dalton Trans.* **2013**, *42*, 351-354.

[221] Hodge, J. A.; Hill, M. G.; Gray, H. B. *Inorg. Chem.* **1995**, *34*, 809-812.

[222] Gingras, M.; Raimundo, J.-M.; Chabre, Y. M. *Angew. Chem. Int. Ed.* **2006**, *45*, 1686-1712.

[223] a) Ballester, M.; Riera, J.; Castañer, J.; Badía, C.; Monsó, J. M. *J. Am. Chem. Soc.* **1971**, *93*, 2215-2225.

b) Juliá, L.; Ballester, M.; Riera, J.; Castañer, J.; Ortin, J. L.; Onrubia, C. *J. Org. Chem.* **1988**, *53*, 1267-1273.

c) Ballaster, M.; Castañer, J.; Riera, J.; Pujadas, J.; Armet, O.; Onrubia, C.; Rio, J. A. *J. Org. Chem.* **1984**, *49*, 770-778.

[224] a) Deinzer, M.; Miller, T.; Lamberton, J.; Arbogast, B. *J. Org. Chem.* **1981**, *46*, 4800-4802.

b) Baird, T.; Gall, J. H.; MacNicol, D. D.; Mallinson, P. R.; Michie, R. *J. Chem. Soc., Chem. Commun.* **1988**, 1471-1473.

c) Jakobsson, E.; Eriksson, L.; Bergman, Å. *Acta Chem. Scand.* **1992**, *46*, 527-532.

d) Downing, G. A.; Frampton, C. S.; MacNicol, D. D.; Mallinson, P. R. *Angew. Chem. Int. Ed. Engl.* **1994**, *33*, 1587-1589.

e) Yip, H. K.; Schier, A.; Riede, J.; Schmidbaur, H. *J. Chem. Soc. Dalton Trans.* **1994**, 2333-2334.

f) Tucker, J. H. R.; Gingras, M.; Brand, H.; Lehn, J.-M. *J. Chem. Soc., Perkin Trans. 2* **1997**, 1303-1307.

g) Ruiz-Molina, D.; Veciana, J.; Palacio, F.; Rovira, C. *J. Org. Chem.* **1997**, *62*, 9009-9017.

h) o) Chen, Z.; Sutton, L. R.; Moran, D.; Hirsch, A.; Thiel, W.; von Ragué Schleyer, P. *J. Org. Chem.* **2003**, *68*, 8808-8814.

g) Gingras, M.; Pinchart, A.; Dallaire, C.; Mallah, T.; Levillain, E. *Chem. Eur. J.* **2004**, *10*, 2895-2904.

l) Bergamini, G.; Ceroni, P.; Balzani, V.; Gingras, M.; Raimundo, J.-M.; Morandi, V.; Merli, P. *Chem. Commun.* **2007**, 4167-4169.

m) Gao, Z.-Y.; Jiang, W.-S.; Sun, D.; Xie, Y.; Chen, Z.-L.; Yu, L.-J.; Xie, S.-Y.; Huang, R.-B.; Zheng, L.-S. *Talanta* **2010**, *81*, 48-54.

[225] Bellester, M.; Molinet, C.; Castaňer, J. *J. Am. Chem. Soc.* **1960**, *82*, 4252-4254.

[226] Mayer, B.; Decker, D.; Knieß, T.; Lang. R. *Z. Chem.* **1990**, *30*, 404-405.

[227] Mansouri-Torshizi, H.; I-Moghaddam, M.; Divsalar, A.; Saboury, A. *Bioorg. Med. Chem.* **2008**, *16*, 9616-9625.

[228] Downing, G. A. *Design and synthesis of coronene-based and other novel inclusion compounds*, PhD Dissertation, University of Glasgow, 1993.

[229] a) Nakamura, S.; Furutani, A.; Toru, T. *Eur. J. Org. Chem.* **2002**, 1690-1695.

b) Richter, H.; Beckendorf, S.; Mancheňo, O. G. *Adv. Synth. Catal.* **2011**, *353*, 295-302.

c) García-Rubia, A.; Fernández-Ibáňez, M. Á.; Arrayás, R. G.; Carretero, J. C. *Chem. Eur. J.* **2011**, *17*, 3567-3570.

d) Zhang, X.; Yu, M.; Yao, J.; Zhang, Y. *Synlett.* **2012**, *23*, 463-467.

[230] Bulanov, M. N.; Sosonyuk, S. E.; Zyck, N. V.; Zefirov, N. S. *Russ. J. Org. Chem.* **2003**, *29*, 415-421.

[231] Kinoshita, I.; Wright, L. J.; Kubo, S.; Kimura, K.; Sakata, A.; Yano, T.; Miyamoto, R.; Nishioka, T.; Isobe, K. *Dalton Trans.* **2003**, 1993-2003.

[232] Abdel-Mohsen, H. T.; Sudheendran, K.; Conrad, J.; Beifuss, U. *Green Chem.* **2013**, *15*, 1490-1495.

[233] Orain, C.; Quentel, F.; Gloaguen, F. *ChemSusChem* **2014**, *7*, 638-643.

[234] Armarego, W. L.; Perrin, D. D. *Purification of Laboratory Chemicals*, Butterworth-Heinemann, Oxford, 4th ed., 1998.

[235] Patel, B. *Peri-substituted dithianaphthalenes as sources of reactive intermediates in organic chemistry*, PhD Dissertation, University of Birmingham, 2009.

[236] Fulmer, G. R.; Miller, A. J. M.; Sherden, N. H.; Gottlieb, H. E.; Nudelman, A. N.; Stoltz, B. M.; Bercaw, J. E.; Goldberg, K. I. *Organometallics* **2010**, *29*, 2176-2179.

[237] Meinwald, J.; Dauplaise, D.; Wudl, F.; Hauser, J. J. *J. Am. Chem. Soc.* **1977**, *99*, 255-257.

[238] Wilson, R. D. *Tetrahedron* **1959**, *3*, 236-242.

[239] a) Kondolff, I.; Doucet, H.; Santelli, M. *Tetrahedron* **2004**, *60*, 3813-3818.

b) Susanto, W.; Chu, C; Ang, W. J.; Chou, L.; Lam, Y. *J. Org. Chem.* **2012**, *77*, 2729-2742.

[240] a) Smith, A. R.; Watson, D. F. *Chem. Mater.* **2010**, *22*, 294-303.

b) Conway, W; Tarbell, D. S. *J. Am. Chem. Soc.* **1956**, *78*, 2228-2233

[241] Zweig, A.; Hoffmann, A. K. *J. Org. Chem.* **1965**, *30*, 3997-4001.

[242] Tesmer, M.; Vahrenkamp, H. *Eur. J. Inorg. Chem.* **2001**, 1183-1188.

[243] Ló, S. M. S.; Ducatti, D. R. B.; Duarte, M. E. R.; Barreira, S. M. W.; Noseda, M. D.; Gonçalves, A. G. *Tetrahedron Lett.* **2011**, *52*, 1441-1443.

[244] Takahashi, K.; Katsurada, H.; Komura, T.; Imanaga, H. *Bull. Chem. Soc. Jpn.* **1990**, *63*, 3315-3316.

[245] Coles, S. J.; Gale, P. A. *Chem. Sci.*, **2012**, *3*, 683-689.

[246] *CrystalClear-SM Expert 2.0 r7*, **2011**, *2.0 r11*, **2011**, Rigaku.

[247] Sheldrick, G. M. *Acta Cryst.*, **2008**, *A64*, 112-122.

[248] Dolomanov, O. V.; Bourhis, L. J.; Gildea, R. J.; Howard J. A. K.; Puschmann, H. *J. Appl. Crystallogr., 2009, 42,* 339.

[249] *CrysAlisPro,* Version 1.171.36.28, Agilent Technologies, **2013**.

[250] *CrystalClear-SM Expert 2.0 r7*, **2011**, 3.1 b21, **2012**, 3.1 b13a, **2012**, 3.1 b27, **2012**, Rigaku.

[251] Sluis, P. v.d.; Spek, A. L. *Acta Crystallogr., Sect. A*, **1990**, *46*, 194-201.